NUMERICAL MODELING OF PIPE–SOIL AND ANCHOR–SOIL INTERACTIONS IN DENSE SAND

by

© Kshama Roy

A Thesis submitted to the

School of Graduate Studies

in partial fulfillment of the requirements for the degree of

Doctor of Philosophy

Faculty of Engineering and Applied Science

Memorial University of Newfoundland

May 2018

St. John's Newfoundland Canada

ABSTRACT

Buried pipelines are one of the most efficient modes for transportation of hydrocarbons, in both onshore and offshore environments. While traversing large distances through a wide variety of soil, buried pipelines might be subjected to lateral or upward loading. Pipelines are generally installed in a trench and then backfilled with loose to medium dense sand. However, in many situations, the backfill sand might be densified even after installation due to natural phenomena, such as wave action in offshore environments. Proper estimation of force/resistance due to relative displacement between soil and pipe during lateral or upward movement is an important engineering consideration for safe and economic design of pipelines. In the development of design guidelines for pipelines, theoretical and experimental studies on anchor behaviour are also used, assuming that a geometrically similar pipe and anchor behave in a similar fashion. Pipelines and anchors buried in dense sand are the focus of the present study.

Improved methods for analysis of complex pipe– and anchor–soil interactions are developed in the present study through finite element (FE) analysis using Abaqus FE software. Recognizing the limitations of the classical Mohr–Coulomb (MC) model, which is typically used for modelling sand in FE modeling of pipe–soil interaction, a modified Mohr–Coulomb (MMC) model is proposed, which considers nonlinear variation of angles of internal friction and dilation with plastic shear strain, loading condition, density and confining pressure, as observed in laboratory tests on dense sand. The proposed MMC model is implemented in Abaqus using a user-defined subroutine. The response of buried pipelines subjected to lateral ground movement is investigated using FE analysis with the MC and MMC models. The FE results (e.g. force–displacement behaviour including the peak and post-peak lateral resistances) are consistent with the results of physical model tests and numerical analysis available in the literature.

The uplift resistance against upheaval buckling is a key design parameter, which is investigated for a shallow buried pipeline across a range of pipe displacements. An uplift force–displacement curve can be divided into three segments: pre-peak, post-peak softening and gradual reduction of resistance at large displacement. A set of simplified equations is proposed to obtain the force–displacement curve for a shallow buried pipe.

Although many pipelines are embedded at shallow burial depths, deep burial conditions are also evident in many scenarios (e.g. ice gouging prone regions). The uplift resistance and its relation to progressive formation of shear bands (i.e. zones of localized plastic shear strain) are also investigated for deep buried pipes across a range of burial depths and pipe diameters. A simplified method to calculate the peak and post-peak uplift resistances, using an equivalent angle of internal friction, is proposed for practical applications.

A comparative study is conducted to explain the similarities and differences between the lateral response of buried pipes and strip anchors, which shows that the anchor gives approximately 10% higher peak resistance than does a pipe of diameter equal to the height of the anchor. The lateral resistance increases with burial depth and becomes almost constant at large burial depths. The transition from shallow to deep failure mechanisms occurs at a larger burial depth for anchors than pipes. Finally, a set of simplified equations is proposed to estimate the lateral resistances for a wide range of burial depths.

This thesis is dedicated to my late father,

who always encouraged me to become a scholar and was a driving force in my decision to pursue a Ph.D. He always had confidence in me and is perpetually present in spirit to light my life's path.

ACKNOWLEDGMENTS

Being a part of a talented and diverse geotechnical engineering research group at Memorial University of Newfoundland is a privilege. The time spent during my PhD study has been an incredible journey in which I have learned so many things and matured in so many ways. I am taking this opportunity to acknowledge the help and support of a number of individuals who have contributed in many different ways to the work described in this dissertation.

In all my years of experience, some people stand out for their great leadership and supervisory qualities and my supervisor, Dr. Bipul Hawlader, Professor and Research Chair in Seafloor Mechanics, is one of those people. His time and attention devoted to the countless hours of advice, including the philosophy of life, discussion, thorough review and constructive criticism have contributed immeasurably to my personal and professional growth. I still remember the very first time when we talked over phone and how he encouraged me to follow my dream of pursuing higher studies. In working with him, I immediately sensed that his values and ethics are in the right place. He never compromised the quality of my research work even in the case of meeting deadlines. I have been very fortunate that Dr. Hawlader is my supervisor, and I have learnt many lessons in working under his guidance that I will remember for rest of my life. Thank you very much for being my guide, mentor and role model.

I would also like to thank to my co-supervisor and supervisory committee member, Dr. Shawn Kenny, Associate Professor, Carleton University and Dr. Ian Moore, Professor and Canada Research Chair in Infrastructure Engineering at Queen's University, for their invaluable suggestions, insightful guidance and continuous encouragement throughout my PhD program. I could not have expected a better combination of mentors for my research and this dissertation would not have been possible without their unconditional support and guidance.

I would not have been able to undertake this work without the financial support of the Research and Development Corporation (RDC), Chevron Canada Limited, NSERC, the Faculty of Engineering and Applied Science and the School of Graduate Studies. The funding contributions allowed me not only to maintain a comfortable lifestyle but also to stay focused on my research.

I owe a debt of gratitude to Dr. Leonard Lye, Associate Dean (Graduate studies), for encouraging me to hone my leadership skills by involving and volunteering in different societies. He assisted me with every aspect of my graduate student life and also with any kind of help that I needed. His enlightening and constructive ideas especially during the first few years of my Ph.D., have helped me to improve myself and this research. I also want to express my sincere admiration to Dr. Greg Naterer, the Dean of the Faculty of Engineering and Applied Science, who always encourages me to become a leader of the future and provides valuable suggestions for my future career. I would be remiss if I did not thank Ms. Moya Crocker and Ms. Colleen Mahoney, who deserve credit for providing much needed assistance with administrative tasks, reminding us of impending deadlines, and keeping our work running smoothly.

I cannot express with words my gratitude towards my lovely sister, mother and late father, who always trusted me and had confidence in my decision. The patience and willingness of my wife, Nabanita, to share with me the hurdles of this journey, allowed me to navigate safely through the ocean of knowledge. Her love and care during all these years were really the true motor of my life. The support of my brothers-in-law and parents-in-law has been tremendous. I am so lucky to have such amazing people in my life. I strongly believe this is not just an end of a journey for me; this is the start of a new journey, a journey of dreams.

Table of Contents

List of Figures

List of Tables

List of Symbols

As the thesis is written in manuscript format, the symbols used in this study are listed in each chapter (Chapters 3–6).

CHAPTER 1

Introduction

1.1 Background and Motivation

Buried pipelines play a significant role in the economy and human life in many countries because of the transportation of hydrocarbons in onshore and offshore environments. According to the Canadian Energy Pipeline Association (CEPA), Canada has a network of approximately 115,000 km of underground energy transmission pipelines that operates every day, to transport oil and natural gas (http://www.cepa.com/). The United States of America has a network of more than 185,000 miles (~298,000 km) of liquid petroleum pipelines, nearly 320,000 miles (~515,000 km) of gas transmission pipelines, and more than 2 million miles of gas distribution pipelines (http://www.pipeline101.com/). Because pipelines travel large distances through a wide variety of soils, geohazards and the associated ground movement might pose a significant threat to pipeline integrity that may result in pipeline damage and potential failure. According to the report of the European Gas pipeline Incident data Group (EGIG), ground movement represents the fourth major cause of gas pipeline failures; almost half of these incidents resulted in pipe rupture (EGIG 2005). Enhanced understanding of pipe–soil interaction will, therefore, lead to improved engineering design of pipeline resistance against geohazards and thereby, ensure safe, economic and reliable operation of pipeline systems. In this thesis, unless stated otherwise, pipelines refer to oil and gas pipelines.

Buried pipelines might be subjected to different forms of loading. For example, lateral loading could be caused by relative movement between soil and pipe due to permanent ground deformations (Fig. 1.1(a)). On the other hand, an upward loading might be caused by temperature induced expansion during operation, together with vertical out-of-straightness (Fig. 1.1(b)). In both cases, a section of pipeline might be displaced a significantly large distance through the surrounding soil. For example, Nielsen et al. (1990) reported that a 219-mm diameter (D) pipeline in the North Sea displaced vertically ~1.5 m (i.e. 6.8D) through the soil and then protruded a maximum vertical distance of 1.1 m (i.e. 5D) above the seabed due to upheaval buckling during the first 7 months after being brought into service. Similarly, during the 1971 San Fernando earthquake, one of the most severe damages to the steel pipeline system was caused by lateral spreading, where the pipe was deformed by a differential lateral movement up to 1.7 m (SYNER-G 2010). The performance of buried pipelines under lateral or upward loading is, therefore, an important engineering consideration.

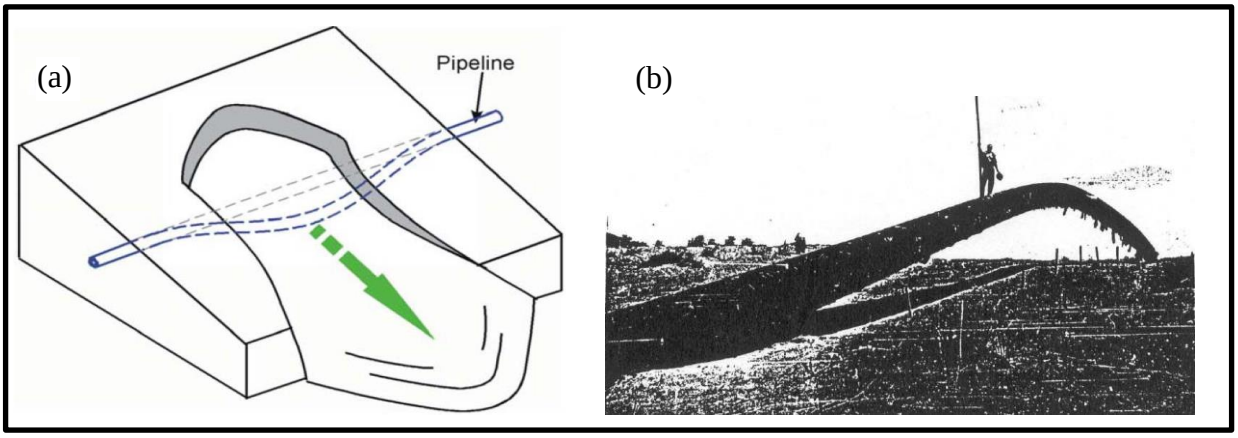

Figure 1.1: (a) Lateral loading on pipe (Dash et al. 2007), (b) Upheaval buckling of pipe (Palmer and Williams 2003)

A number of design guidelines have been developed for estimation of soil resistance for buried pipelines (ASCE 1984; PRCI 2003, 2009; ALA 2005; DNV 2007). To develop the force–displacement relationships, in addition to the research on buried pipelines, studies on strip anchors have been utilized, assuming that a geometrically similar (e.g. pipe diameter is equal to anchor height) pipe and anchor essentially behave in a similar fashion (Dickin 1994; Ng 1994). However, comparing the behaviour of buried pipes and anchors, some contradictory results have been reported. Reanalyzing 61 tests on model pipes and 54 on anchors, White et al. (2008) found a considerable difference between uplift resistances of pipes and anchors, and inferred that this discrepancy might be due to the inherent difference between the behaviour of pipes and anchors. Although there are a few studies on the comparison of the uplift behaviour of pipes and strip anchors (Dickin 1994; White et al. 2008), very limited research comparing the lateral resistance of pipes and anchors is available.

One of the most common construction practices for buried pipelines is the installation of the pipeline into a trench. When the trench is backfilled with sand, the backfill material might be in a loose to medium dense state. However, during the lifetime of an onshore pipeline, the backfill sand might be densified due to traffic loads, nearby machine vibrations or seismic wave propagation (Kouretzis et al. 2013). Furthermore, Clukey et al. (2005) showed that the relative density of sandy backfill of an offshore pipe section increased from less than ~57% to ~85–90% in 5 months after construction, which has been attributed to wave action at the test site in the Gulf of Mexico. Pipelines and strip anchors buried in dense sand are the focus of the present study.

Pipelines and anchors might be buried at a wide range of burial depths, which is typically expressed by embedment ratio $\widetilde{H}=H/D$, where H is the distance of the pipe centre from the ground

surface. As the burial is a major source of pipeline construction cost, the embedment ratio needs to be minimized while maintaining adequate design requirements. Onshore pipelines are generally embedded at $2 \leq \widetilde{H} \leq 10$ (O'Rourke and Liu 2012). For example, according to the Association of Oil Pipe Liners (AOPL), the minimum cover requirement over a newly installed pipe varies from 762 mm to 1219 mm (i.e. $\widetilde{H}$=3.3~5.5 for D=200 mm) depending on the location of pipe. However, if a pipeline passes under an embankment, the embedment ratio could be as large as ~40 to ~80 (Yimsiri et al. 2004). Offshore pipelines are generally embedded at $\widetilde{H} \leq 4$. However, in many special scenarios, the embedment ratio could be higher than 4. For example, for a 254-mm diameter oil pipeline constructed by Chevron in the South Pass Block 38 of the Gulf of Mexico, the embedment ratio changed from ~4 in 1980 to ~24 in 1998 due to sediment deposition (Liu and O'Rourke 2010). Similarly, in the regions where ice gouging is expected, a large embedment is maintained to protect the pipeline from ice gouging effects (Palmer 1990; Hequette et al. 1995; Kenny et al. 2007; Been et al. 2008; Barrette 2011). Furthermore, anchoring operations might cause significant damage to submarine pipelines and therefore they should be buried at a sufficiently large depth.

In most of the design guidelines, the soil resistance on a pipeline is represented by discrete nonlinear springs for each orthogonal loading axis, as shown in Fig. 1.2. Although physical model tests of pipes buried in dense sand show a reduction of resistance after the peak, both for lateral and upward loading (Trautmann 1983; Chin et al. 2006; Cheuk et al. 2008; Burnett 2015), most of the existing design guidelines recommend the use of peak resistance, even at displacements greater than required to mobilize the peak value, as shown by the dashed lines in Fig. 1.2 (ALA 2005; PRCI 2003). When the force–displacement relation is used to calculate force on the pipe due to ground movement (e.g. landslide), the use of the peak resistance is conservative because it

calculates a higher force on the pipe. However, in some practical situations, the available soil resistance is the design requirement: for example, for the design of lateral or upheaval buckling of high pressure and high temperature buried oil pipelines, where post-peak soil resistance might be conservative. The importance of post-peak reduction of soil resistance in the design has been recognized for upheaval buckling of buried pipelines (DNV 2007) and lateral buckling of as-laid offshore pipelines (Randolph 2012).

A number of researchers have studied the behaviour of pipelines and anchors buried in dense sand using physical modeling. In recent years, the particle image velocimetry (PIV) technique (White et al. 2003) has been used in physical modeling to obtain the movement of soil particles during pipeline displacement. The PIV results provide very useful information on soil deformation, which could be used to interpret the progressive formation of failure planes with loading. The formation of a failure plane is governed by nonlinear stress–strain behaviour of soil including strain-softening. Numerical modeling could be used to investigate the role of soil behaviour on pipeline response.

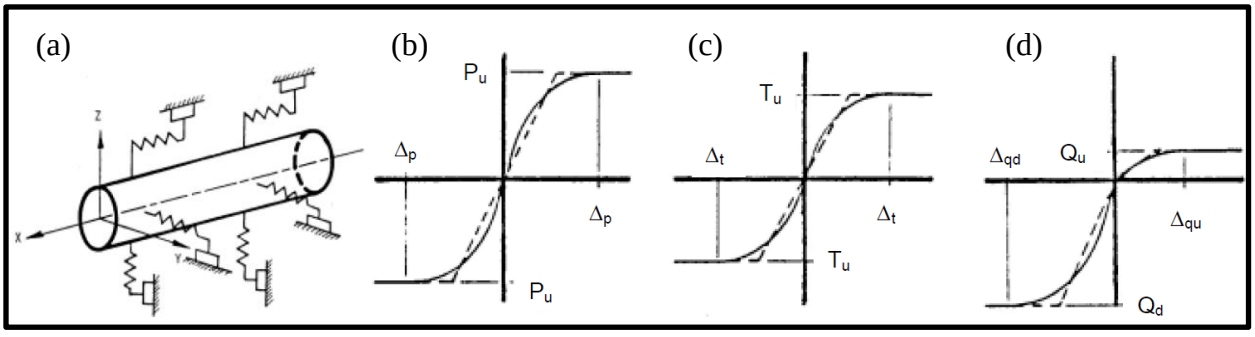

Figure 1.2: (a) Idealized pipe–soil interaction with discrete springs, (b) Lateral loading, (c) Axial loading, and (d) Upward loading (ALA 2005)

The Mohr–Coulomb (MC) model has been widely used in numerical simulations to model the behaviour of sand. The MC model considers constant values of angles of internal friction (ϕ') and dilation (ψ). However, laboratory tests show than ϕ' and ψ are not constant but varies with mean effective stress and level of shear strain. Moreover, the variation of ϕ' and ψ with plastic shear strain is nonlinear having a pre-peak hardening followed by a post-peak softening. (Hsu and Liao 1998). The mode of shearing (e.g. triaxial versus plane-strain) also significantly influences the behaviour of dense sand (Bolton 1986). All these features of the stress–strain behaviour of dense sand have not been considered in previous numerical models or existing design guidelines.

1.2 Rationale

Despite the large number of previous studies on pipeline–soil interaction, there are a number of issues that have not been resolved and incorporated properly in design guidelines for pipelines buried in dense sand.

a) Most of the design guidelines have recommended procedures for estimation of the peak resistance (e.g. ALA 2005), although the importance of post-peak degradation of resistance in dense sand has been recognized in at least one guideline (DNV 2007).

b) The post-peak reduction of resistance, as observed in physical model tests, can result from strain-softening behaviour of dense sand, together with reduction of burial depth when the pipe moves up significantly from its initial position during uplift, and also when pulled laterally. Finite element analysis, employing an appropriate soil constitutive model, that can simulate sufficiently large displacements of the pipe without numerical issues, is required to investigate this response.

c) All the failure planes through dense sand, especially at large burial depths, do not develop at the same time; rather they develop progressively, as reported from analysis using PIV of images collected during physical experiments (Cheuk et al. 2005; Burnett 2015; Huang et al. 2015). In addition, the location of the failure planes changes with displacement of the pipe, especially in uplift tests. Therefore, the simple limit equilibrium method with constant soil strength parameters, commonly used to calculate uplift resistance, cannot explain this process. Further investigation is needed to understand the mechanism through modelling of progressive formation of failure planes that can accommodate the variation of mobilized shear resistance along these planes.

d) The soil failure mechanisms due to displacement of the pipe vary with burial depth. The failure mechanisms, especially in the transition zone where the failure mechanism changes from the shallow to the deep mechanism, need further investigation.

e) Although the studies on anchor response have also been used in the development of design guidelines for pipelines, a close examination is required to compare the response of these two types of structures buried in dense sand. While some previous studies (e.g. Dickin 1994) showed a similar response, other studies (e.g. White et al. 2008) suggested that there might be a systematic difference between the response of similar-sized anchors and pipes.

1.3 Objectives

The main objective of the present study is to develop numerical and analytical tools for estimation of lateral and uplift resistances of pipelines and anchors buried in dense sand, addressing the key issues listed in Section 1.2. For numerical modeling, two-dimensional FE

analyses for the plane-strain condition are performed using Abaqus/Explicit FE software. Recognizing the importance of the soil model in pipe– and anchor–soil interactions, the MMC model that can capture most of the important features of stress–strain behaviour of dense sand is proposed. In addition to the peak resistance, the post-peak lateral and uplift resistances and their relation to the progressive formation of shear bands (i.e. the zones of plastic shear strain localization) are investigated.

1.4 Methodology

The steps taken to achieve the objectives of this study can be summarized as follows:

1) Develop a soil model that can simulate the strain-softening behaviour of dense sand and also can accommodate the effects of density, mean stress and loading conditions on stress–strain behaviour.
2) Implement the new soil model in Abaqus FE software using a user-defined subroutine and compare its performance with the built-in Mohr-Coulomb model and laboratory test results.
3) Conduct FE analysis of a buried pipe in dense sand under lateral loading, for varying burial depths and soil properties, and identify the role of soil model, especially strain-softening, on lateral force–displacement behaviour, including the peak and post-peak resistances.
4) Conduct FE analysis for uplift resistance of buried pipes and identify the role of the soil failure mechanisms and progressive formation of slip planes on mobilized pipe uplift resistances including both peak and post-peak, for shallow to deep burial conditions.

5) Conduct FE analysis for similar-sized pipes and vertical strip anchors buried in dense sand, subjected to lateral loading, and identify the similarities and differences between the responses of these two types of structure to evaluate the use of studies on vertical strip anchors for estimation of lateral resistance on pipelines.
6) Develop a set of simplified equations for lateral and uplift resistances (both peak and post-peak conditions) for practical applications.

1.5 Thesis Organization

This thesis is prepared in manuscript format. The outcome of the study is presented in seven chapters and six appendices (A–F). Additional details on the FE modelling and modelling of soil behaviour is presented in Appendix G. This first chapter describes the background, motivations, scope, objectives and contributions of the present study.

Chapter 2 presents a general literature review. As the thesis is prepared in manuscript format, the problem-specific literature reviews are provided in Chapters 3–6 and Appendices A–F.

Chapter 3 presents the details of the proposed MMC model, including its calibration against laboratory test data. The FE analysis of lateral pipe–soil interactions in dense sand is presented in this chapter. This chapter has been published as a technical paper in the Canadian Geotechnical Journal. A part of this study has been published as a technical paper in the 33rd International Conference on Ocean, Offshore and Arctic Engineering (OMAE 2014), San Francisco, California, USA, 2014 (Appendix A).

Chapter 4 presents the FE analysis of upward pipe–soil interaction for shallowly buried pipelines in dense sand. This chapter has been submitted to a journal as a technical paper for

review. The effects of strain-softening behaviour of dense sand on both lateral and upward pipe−soil interaction have also been investigated and the outcome of this study has been published as two conference papers: one in the 6th Canadian Geohazards Conference (Geohazards6), Kingston, Ontario, Canada, 2014 (Appendix B), and the other one in the 34th International Conference on Ocean, Offshore and Arctic Engineering (OMAE 2015), St. John's, Newfoundland and Labrador, Canada, 2015 (Appendix C).

Chapter 5 presents the uplift failure mechanisms of pipes buried in dense sand for a wide range of burial depths and diameters. This chapter has been submitted to a journal as a technical paper for review. A part of this study has been published in the 68th Canadian Geotechnical Conference (GeoQuebec 2015), Quebec City, Quebec, Canada, 2015 (Appendix D).

Chapter 6 presents a comparative study of similar-sized pipes and anchors buried in dense sand and subjected to lateral loading. This chapter has been submitted to a journal as a technical paper for review. Parts of this study have been published as two conference papers: one in the 26th International Ocean and Polar Engineering Conference (ISOPE 2016), Rhodes, Greece, 2016 (Appendix E), and the other one in the 11th International Pipeline Conference (IPC 2016), Calgary, Alberta, Canada, 2016 (Appendix F).

Chapter 7 presents the general conclusions of the thesis and recommendations for future studies. However, problem specific conclusions are provided at the end of each chapter (Chapters 3–6) and appendices (Appendices A–G).

As the thesis is prepared in manuscript format, the references cited in Chapters 3–6 and Appendices A–F are listed at the end of each chapter and appendix. The references cited in Chapters 1, 2 and Appendix G are listed in the "Reference" section at the end of the thesis.

1.6 Significant Contributions

The following technical papers have been produced from the research presented in this thesis.

Journal papers

1) **Roy, K.**, Hawlader, B.C., Kenny, S. and Moore, I. (2017). Lateral resistance of pipes and strip anchors buried in dense sand. (Under review).

2) **Roy, K.**, Hawlader, B.C., Kenny, S. and Moore, I. (2017). Uplift failure mechanism of pipes buried in dense sand. (Under review).

3) **Roy, K.**, Hawlader, B.C., Kenny, S. and Moore, I. (2017). Upward pipe–soil interaction for shallowly buried pipelines in dense sand. (Under review).

4) **Roy, K.**, Hawlader, B.C., Kenny, S. and Moore, I. (2016). Finite element modeling of lateral pipeline−soil interactions in dense sand. Canadian Geotechnical Journal, 53(3): 490–504, DOI: 10.1139/cgj-2015-0171

Conference papers

1) **Roy, K.**, Hawlader, B.C., Kenny, S. and Moore, I. (2016). A comparative study between lateral and upward pipe–soil and anchor–soil interaction in dense sand. 11th International Pipeline Conference (IPC 2016), Calgary, Alberta, Canada, September 26–30.

2) **Roy, K.**, Hawlader, B.C., Kenny, S. and Moore, I. (2016). Finite element analysis of strip anchors buried in dense sand subjected to lateral loading. 26th International Ocean and Polar Engineering Conference (ISOPE 2016), Rhodes, Greece, June 26–July 2.

3) **Roy, K.**, Hawlader, B.C. and Kenny, S. (2015). Soil failure mechanism for lateral and upward pipeline–soil interaction analysis in dense sand. GeoQuebec 2015, Quebec City, Quebec, Canada, September 20–23.

4) **Roy, K.**, Hawlader, B.C., Kenny, S. and Moore, I. (2015). Effects of post-peak softening behaviour of dense sand on lateral and upward displacement of buried pipelines. 34th International Conference on Ocean, Offshore and Arctic Engineering (OMAE 2015), St. John's, Newfoundland and Labrador, Canada, May 31–June 5.

5) **Roy, K.**, Hawlader, B.C. and Kenny, S. (2014). Influence of low confining pressure on lateral soil/pipeline interaction in dense sand. 33rd International Conference on Ocean, Offshore and Arctic Engineering (OMAE 2014), San Francisco, California, USA, June 8–13.

6) **Roy, K.**, Hawlader, B.C., Kenny, S. and Moore, I. (2014). Finite element modeling of uplift pipeline/soil interaction in dense sand. 6th Canadian Geohazards Conference (Geohazards6), Kingston, Ontario, Canada, June 15–18.

Co-Authorship: Most of the research presented in journal papers 1–4 and conference papers 1–6 has been performed by the author of this thesis, Mr. Kshama Roy under the supervision of Dr. Bipul Hawlader. Mr. Roy also prepared the draft manuscripts. The other authors, Dr. Shawn Kenny and Dr. Ian Moore co-supervised the research and reviewed the manuscripts.

CHAPTER 2

Literature Review

2.1 Introduction

As the thesis is written in manuscript format, a problem specific literature review is presented in Chapters 3–6 and Appendices A–F. The primary purpose of adding this chapter is to present additional critical review of available studies relevant to the present research. Where needed, a number of tables and figures is prepared for a better comparison and to provide further information about previous studies, which could not be included in the manuscripts because of space limitation. The literature review presented in this chapter covers the behaviour of anchors and pipes buried in dense sand for lateral and upward loading. In this thesis, unless otherwise mentioned, an 'anchor' refers to a 'strip anchor' having length to width ratio greater than 6 (Das and Shukla 2013).

2.2 Terminologies and Definitions

Typical load–displacement behaviour of pipelines buried in dense sand and subjected to lateral and upward loading is shown schematically in Figs. 2.1(a) and 2.1(b), respectively. The shape of the force–displacement curves for the deep burial condition is similar for both lateral and upward loading. However, for the shallow burial condition, the decrease in uplift resistance continues even after initial softening (i.e. immediately after the peak resistance) during upward displacement, which is primarily because of the reduction of burial depth; however, for lateral loading the resistance remains almost constant at large displacements (residual resistance).

In this thesis, unless otherwise mentioned, the lateral and uplift force–displacement behaviours are expressed in normalized form using $N_h=F_h/(\gamma HD)$, $\tilde{u}=u/D$ and $N_v=F_v/(\gamma HD)$, $\tilde{v}=v/D$ respectively. Here, D is the diameter of the pipe (replace D with height of the anchor (B) for anchor–soil interaction); γ is the unit weight of the soil; F_h and F_v are the lateral and uplift forces, respectively; H is the depth of the centre of the pipe/anchor; u and v are the lateral and upward displacements, respectively. The burial depth is also expressed in normalized form using "embedment ratio, $\tilde{H}=H/D$". For lateral loading, the values of N_h at the peak and residual are defined as N_{hp} and N_{hr}, respectively, and the magnitudes of $\tilde{u}$ required to mobilize N_{hp} and N_{hr}, are defined as $\tilde{u}_p$ and $\tilde{u}_r$, respectively. For uplift, the values of N_v at the peak and after softening are defined as N_{vp} and N_{vs}, respectively; and the $\tilde{v}$ values required to mobilize N_{vp} and N_{vs}, are defined as $\tilde{v}_p$ and $\tilde{v}_s$, respectively.

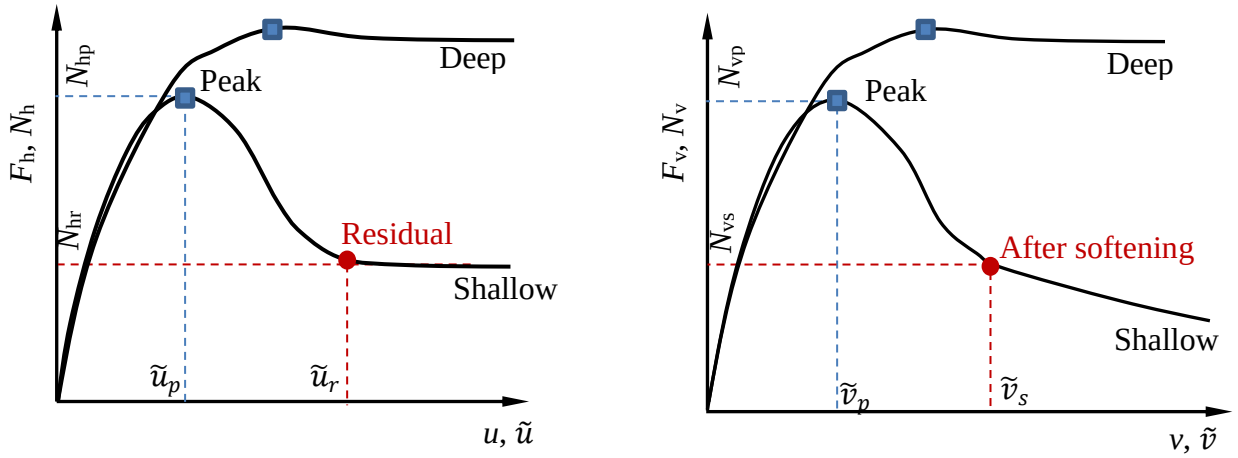

a) Lateral b) uplift

Figure 2.1 Typical force–displacement curves: (a) lateral loading (b) upward loading

2.3 Lateral Pipe–Soil Interaction

A considerable number of physical model tests has been conducted to understand lateral resistance of pipes buried in dense sand (Audibert and Nyman 1977; Trautmann 1983; Daiyan et al. 2011; Almahakeri et al. 2012; Burnett 2015). From the test results, the force–displacement curves can be obtained and the failure mechanisms can be interpreted. The displacement of soil particles with lateral movement of the pipe can be visualized using the particle image velocimetry (PIV) technique (Burnett 2015). A critical review of past experimental works has been presented by Guo and Stolle (2005). They compiled the results of eleven experimental studies and showed a wide variation in the non-dimensional peak lateral force, which depends on sand properties, diameter of the pipe, embedment ratio, test procedure and type of structure (pipes/anchors). For shallow to moderate embedment ratios, the physical model test results show that N_h increases with $\tilde{u}$, reaches the peak (N_{hp}) and then quickly decreases to a residual value (N_{hr}), which is primarily due to the strain-softening behaviour of dense sand. After N_{hr}, N_h remains almost constant (Fig. 2.1(a)). A summary of available full- and reduced-scale tests in dense sand for lateral loading is presented in Table 2.1.

In addition to physical model tests, a large number of numerical studies on lateral pipe–soil interaction in dense sand are also available in the literature (e.g. Yimsiri et al. 2004; Guo and Stolle 2005; Yimsiri and Soga 2006; Xie et al. 2013; Daiyan et al. 2011; Jung et al. 2013a). A wide variety of commercial software packages (e.g. Abaqus, DEM, FLAC) and soil constitutive models (e.g. Mohr-Coulomb, modified form of Mohr-Coulomb, NorSand, and Hardening soil model) has been used in these analyses. A summary of available numerical studies on lateral pipe–soil interaction in dense sand is presented in Table 2.2.

2.4 Upward Pipe–Soil Interaction

A large number of physical experiments on upward movement of pipes in dense sand have been conducted (Dickin and Leung 1983; Trautmann 1983; Dickin 1994; White et al. 2001; Cheuk et al. 2008; Wang et al. 2010). The experimental conditions have been varied in terms of the diameter of the pipe, embedment ratio, soil type, and test procedure (i.e. full-scale or centrifuge model tests). Most of the physical experiments were conducted for $\widetilde{H} \leq 4$; however, a limited number of tests at large embedment ratios is also available (Trautmann 1983; Dickin 1994). Experimental results show that N_v increases with $\widetilde{H}$ and relative density (D_r) (Trautmann 1983; Bransby et al. 2002; Chin et al. 2006; Cheuk et al. 2008). The model tests on dense sand show that N_v increases quickly with $\tilde{v}$, reaches the peak (N_{vp}), quickly decreases to N_{vs} and then decreases further with an increase in $\tilde{v}$ (Fig. 2.1(b)) (Trautmann 1983; White et al. 2001; Cheuk et al. 2008). A summary of available experimental studies on upward pipe–soil interaction in dense sand is presented in Table 2.3.

The mobilized uplift resistance depends on upward displacement of the pipe and is generally comprised of three components: (i) the submerged weight of soil being lifted; (ii) the vertical component of shearing resistance offered by the soil; and (iii) suction under the pipe. The suction component under the pipe can be neglected for a drained loading condition at low uplift velocities (Bransby and Ireland 2009; Wang et al. 2010). When the peak uplift resistance mobilizes in medium to dense sand, two inclined symmetric slip planes form in the backfill soil, starting from the pipe waist (White et al. 2001). The inclination of the slip planes with the vertical (θ) is approximately equal to the peak dilation angle (ψ_p) (White et al. 2001; Cheuk et al. 2005). The vertical inclination of slip planes decreases with $\tilde{v}$, and they become almost vertical at large $\tilde{v}$. A model test conducted by Huang et al. (2015) shows that θ gradually increases in the pre-peak,

reaches ~ψ_p at the N_{vp} and then decreases in the post-peak zone. Further discussion is provided in Section 2.7.2. Although the post-peak degradation of N_v is very common in physical tests, most of the FE analyses conducted in the past did not properly model the post-peak degradation of the uplift resistance, except for the reduction due to change in cover depth (Yimsiri et al. 2004; Farhadi and Wong 2014). A summary of the available FE analyses on upward pipe–soil interaction in dense sand is presented in Table 2.4.

In addition to physical and numerical modeling, the limit equilibrium method and plasticity solutions have also been proposed to calculate the peak uplift resistance, N_{vp} (Merifield et al. 2001; White et al. 2008). The plasticity solutions, which rely on normality (i.e. $\theta=\psi=\phi'$) give an increased non-conservative uplift resistance compared to the limit equilibrium method with $\theta=\psi_p$ ($<\phi'$), as normality is rarely observed during the drained failure of soil (White et al. 2008). The limit equilibrium method can be used to calculate the uplift resistance; however, the location of the inclined shear bands and mobilized shear strength parameters along these bands need to be known, especially for calculating the uplift resistance at large displacements.

In the field, pipelines might also be subjected to combined loading (i.e. lateral and upward loading at the same time) during a ground movement incident. Several experimental and numerical studies have been conducted on the response of buried pipelines to combined loading (e.g. Guo 2005; Hsu et al. 2006; Daiyan et al. 2011; Roy 2012; Jung et al. 2016). However, the present study focuses only on pure lateral and upward loading, and therefore, detailed review of the literature on combined loading is not presented.

Table 2.1. Summary of previous experimental studies on lateral pipe–soil interaction

Reference	Test Type	*H*/*D*	Pipe Diameter (mm)	Relative Density, D_R (%)	Remarks
Audibert and Nyman (1977)	Experimental tank	1–24	25, 60, 111	–	Cast iron pipe, Dry dense Carver sand
Trautmann (1983)	Large-scale	1.5–11	102	80	Steel pipe, Dry Cornell Filter sand
Paulin et al. (1997)	Full-scale	1.5–3.5	–	100	Well graded sand
C-CORE (1999)	Full-scale	2.3	201	–	Dry sand with density of 1984 kg/m^3
Scarpelli et al. (1999)	Full-scale	3.5–5	203.2, 609.6	–	Coal tar and polyethylene coated pipe; Dry to moist uniform sand with a trace of silt
O'Rourke and Turner (2006)	Full-scale	2–12	–	–	Partially saturated sand
Hsu et al. (2006)	Large-scale	1–3	152.4, 228.6, 304.8	94	Da-du river bed sand of Taiwan
Karimian et al. (2006)	Full-scale	1.92	457	75	Steel pipe; Dry and moist Fraser river sand
Di Prisco and Galli (2006)	Small-scale experimental	1.5–3.5	50	100	Dry Ticino sand
Ha et al. (2008)	Centrifuge	2.8	407.5	–	Flexible HDPE pipe
Sakanoue (2008)	Full-scale	6	100	–	Dry Chiba sand

Reference	Test Type	*H*/*D*	Pipe Diameter (mm)	Relative Density, D_R (%)	Remarks
Daiyan et al. (2011)	Centrifuge	2	504	83	Steel pipe; Dry sand
Almahakeri et al. (2012)	Full-scale	3–7	102	–	Steel and GFRP laminate pipe; Synthetic Olivine sand
Burnett (2015)	Full-scale	1–7	254, 610	–	Steel pipe; Dry synthetic Olivine sand

Table 2.2. Summary of previous numerical studies on lateral pipe–soil interaction

Reference	Software	*H*/*D*	Pipe Diameter (mm)	Relative Density, D_R (%)	Remarks
C-CORE (2003)	Abaqus/Standard	2.3	203	95	MC model (ϕ'=44°, ψ=12°)
Yimsiri et al. (2004)	Abaqus/Standard	2–100	102	80	MC model (ϕ'=44°, ψ=16°) and NorSand
Yoshizaki and Sakanoue (2004)	Abaqus/Standard	9.5	100	–	MC model (ϕ'=46.5°); Dry sand (γ=16kN/m^3)
Guo and Stolle (2005)	Abaqus/Standard	1.03–10	33–3300	82	MC model (variable ϕ' with equivalent plastic shear strain and mean effective stress, ψ=10°)
di Prisco and Galli (2006)	Tochnog	1.5	750	100	MC model (ϕ'=30°, ψ=20°)

Reference	Software	*H*/*D*	Pipe Diameter (mm)	Relative Density, D_R (%)	Remarks
Yimsiri and Soga (2006)	Discrete element method (DEM)	2–60	102	–	
Karimian et al. (2006)	FLAC 2D	1.92	460	75	MC model (ϕ'=43–45.5°, ψ=11–17°); Hyperbolic model
Sakanoue (2008)	DEM	6	100	100	
Badv and Daryani (2010)	FLAC 2D	2–60	102–2000	80	MMC model
Cheong et al. (2011)	Abaqus/Standard	2–11.5	102	–	MC model (ϕ'=45°, ψ=16.3°) and NorSand
Daiyan et al. (2011)	Abaqus/Standard	2	504	83	MC model (ϕ'=43°, ψ=20°)
Almahakeri et al. (2012)	Abaqus/Standard	1.92, 2.75	324, 457	–	MC model (ϕ'=53°, ψ=16°)
Xie et al. (2013)	Abaqus/Standard	2.8	400	–	MC model (ϕ'=40°, ψ=10°)
Jung et al. (2013)	Abaqus/Standard	3.5–11	102, 124	–	Dry and partially saturated sand; MMC model
Pike et al. (2014)	Abaqus/Explicit	3.5–8	102	45	MMC model
Farhadi and Wong (2014)	Abaqus/Standard	1.5–6	950	–	MC model (ϕ'=30–40°, ψ=5–30°)

Note: MMC in this table represents a modified form of Mohr-Coulomb models where ϕ' and ψ have been varied with a combination of plastic shear strain, mean stress and/or test configuration. The method of variation may be different in different studies, including the present study.

Table 2.3. Summary of previous experimental studies on upward pipe–soil interaction

Reference	Test Type	*H*/*D*	Pipe Diameter (mm)	Relative Density, D_R (%)	Remarks
Trautmann (1983)	Large scale	1.5–13	102	80	Steel pipe; Dry Cornell Filter sand
Matyas and Davis (1983)	Laboratory test	1.7–8.8	47.6	–	Dry angular silica sand
Schaminee et al. (1990)	Laboratory test	4–12	101.6	–	Saturated sand and rock
Dickin (1994)	Centrifuge	1.5–7.5	250, 500, 1000, 2000	76	Steel pipe; Dry Erith sand
Barefoot (1998)	Centrifuge	4.6–6.2	–	70	Aluminium pipe; Saturated sand
White et al. (2001)	Centrifuge	3.14	220	67	Brass pipe; Dry Fraction D silica sand
Mohri et al. (2001)	Laboratory test	0.3–1.96	260	–	Dry Toyoura sand
Bransby et al. (2001)	Laboratory test and Centrifuge	2.75-3.6	48, 240	100	Dry and saturated silica sand
Palmer et al. (2003)	Laboratory test and Centrifuge	2.63, 3.14	220	–	PVC pipe; Fraction D silica sand
Chin et al. (2006)	Centrifuge	3–7.7	190	85	Dry Congleton sand
Cheuk et al. (2008)	Laboratory test	3	100	92	Hollow brass tube; Dry Leighton Buzzard silica sand

Reference	Test Type	*H*/*D*	Pipe Diameter (mm)	Relative Density, D_R (%)	Remarks
Choobbasti et al. (2012)	Laboratory test	1	110	–	Saturated Babolsar shore soil
Wang et al. (2010)	Full scale and Centrifuge	0.1–4	100, 258	85	PTFE pipe; Dry Fraction E silica sand
Saboya et al. (2012)	Centrifuge	0.5–3	500	70	Aerospace aluminum alloy pipe, Dry industrial grade sand of Brazil
Huang et al. (2014)	Centrifuge	0.5, 2	40	60	Aluminum pipe; Fujin standard sand

Table 2.4. Summary of previous numerical studies on upward pipe–soil interaction

Reference	Software	*H*/*D*	Pipe Diameter (mm)	Relative Density, D_R (%)	Remarks
Mohri et al. (2001)	Discrete element method (DEM)	0.3–2	260	–	
Yimsiri et al. (2004)	Abaqus/Standard	1.5–100	102	80	MC model (ϕ'=44°, ψ=16°) and NorSand
Yimsiri and Soga (2006)	Discrete element method (DEM)	2–60	102	–	
Badv and Daryani (2010)	FLAC 2D	4–13	102–2000	80	MMC model
Jung et al. (2013)	Abaqus/Standard	1.5–13	102	–	Dry and partially saturated sand, MMC model
Chakraborty and Kumar (2014)	Lower bound FE limit analysis	1–10	20, 2000	75	MC model (ϕ'=44.2–58.7°)
Fahadi and Wong (2014)	Abaqus/Standard	1.5–6	950	–	MC model (ϕ'=30–40°, ψ=5–30°)
Robert and Thusyanthan (2014)	Abaqus/Standard	2–15	114, 200	80	MMC model and NorSand

Note: MMC in this table represents a modified form of Mohr-Coulomb models where ϕ' and ψ have been varied with a combination of plastic shear strain, mean stress and/or test configuration. The method of variation may be different in different studies, including the present study.
'–' refers to missing data/information.

2.5 Lateral Anchor–Soil Interaction

A limited number of experimental studies on lateral anchor–soil interaction is available in the literature (Neely et al. 1973; Das et al. 1977; Akinmusuru 1978; Dickin and Leung 1983; Hoshiya and Mandal 1984; Choudhary and Das 2017). Similar to pipelines, physical model tests on buried anchors in dense sand show a post-peak degradation of lateral resistance for shallow to moderate burial depths (Neely et al 1973; Dickin and Leung 1983). A summary of the available experimental studies on lateral anchor–soil interaction in dense sand is presented in Table 2.5.

The majority of the past works on buried anchors in dense sand have been based on experimental and analytical studies and, as a result, current design practices are largely empirical (Merifield and Sloan 2006). Most of the theoretical studies are based on the rigid plastic behaviour of soil (Chattopadhyay and Pise 1986; Murray and Geddes 1989). Very few numerical studies have been performed to determine the ultimate pullout capacity of strip anchors buried in dense sand. FE (Rowe and Davis 1982; Dickin and King 1993) and FE limit (Murray and Geddes 1989; Merifield and Sloan 2006; Kumar and Sahoo 2012; Bhattacharya and Kumar 2013) analyses have been conducted in the past using the classical Mohr–Coulomb model. The force–displacement curves obtained from physical model tests show a post-peak degradation of resistance. However, only the peak lateral resistance can be obtained using the analytical solution with a rigid plastic soil model and with numerical analysis using the MC model with constant values of friction and dilation angles, if the representative values for these two soil parameters are carefully selected. The use of a resistance after post-peak reduction (e.g. the residual resistance) might be safe for anchors buried in dense sand because the anchor might undergo much larger displacement in the field. A summary of the available numerical studies on lateral anchor–soil interaction in dense sand is presented in Table 2.6.

Table 2.5. Summary of previous experimental studies on lateral anchor–soil interaction

Reference	Test Type	*H*/*D*	Anchor Height (mm)	Relative Density, D_R (%)	Remarks
Neely et al. (1973)	Small-scale	1–5	50.8	–	Medium grained; Well graded sand with ρ_{max}=1780 kg/m^3 and ρ_{min}=1550 kg/m^3
Das et al. (1977)	Small-scale	1–5	51	–	Bulk density of sand=1610 kg/m^3
Akinmusuru (1978)	Small-scale	1–10	50	–	76 mm long steel pins were used to simulate the sand
Rowe and Davis (1982)	Small-scale	1–8	51	–	Dry medium grained quartz Sydney sand with γ_{max}=17.3 kN/m^3 and γ_{min}=14.3 kN/m^3
Dickin and Leung (1983)	Centrifuge	1–13	1000	78	Dense dry Erith sand with γ=16 kN/m^3
Hoshiya and Mandal (1984)	Small-scale	1–6	25.4	–	Dry sand with ρ_{max}=1.60 g/cm^3 and ρ_{min}=1.31 g/cm^3
Choudhary and Dash (2017)	Small-scale	1–9	100	75	Locally available dry sand with γ_{max}=17.87 kN/m^3 and γ_{min}=14.90 kN/m^3

Table 2.6. Summary of previous numerical studies on lateral anchor–soil interaction

Reference	Software	H/D	Anchor Height (mm)	Relative Density, D_R (%)	Remarks
Rowe and Davis (1982)	–	1–8	51	–	MC model
Dickin and King (1993)	SOSTV & FEPL1	2–12	1000	78	Variable elastic model and elastic plastic soil model; Plane-strain condition
Merifield and Sloan (2006)	SNAC	1–10	–	–	MC model; Upper bound limit analysis and FE method; $E/\gamma B$=500
Kumar and Sahoo (2012)	–	0–7	–	–	Upper bound limit analysis and FE analysis with ϕ'=20°–45°
Bhattacharya and Kumar (2013)	–	1–7	–	–	Lower bound limit analysis with the MC model, ϕ'=20°–45°

Note: '–' refers to missing data/information.

2.6 Comparative Study of Anchors and Pipes

As listed in Tables 2.1–2.6, a significant number of experimental and numerical studies have been conducted for lateral and upward loading of buried pipelines and anchors. However, a very limited number of comparative studies between similar sized pipes and anchors are available in the literature, which are discussed in the following subsections.

2.6.1 Physical model test data

While some previous studies showed similar responses for buried pipes and anchors, some suggested that there might be a systematic difference between the response of similar-sized anchors and pipes. For example, based on centrifuge tests, Dickin (1994) showed there was no significant difference between the peak uplift resistance of pipes and anchors; however, the displacement required to mobilize this resistance is different for these two structures. On the other hand, White et al. (2008) showed that the same limit equilibrium method overpredicts the maximum uplift resistance (mean value) of pipes by 11%, while it underpredicts the peak anchor resistance by 14%. In a limited number of centrifuge tests, Dickin (1988) found no significant difference between the lateral force–displacement curves for pipes and anchors up to the peak resistance; however, the anchors show more resistance than pipes after the peak.

The physical model test results for lateral loading of buried pipes and anchors available in the literature (Tables 2.1 and 2.5) are compiled and the peak lateral resistance (N_{hp}) is plotted against burial depth (H/D or H/B), as shown in Figs. 2.2(a) and 2.2(b) for pipes and anchors, respectively. For clarity, physical model tests conducted only on steel pipes buried in dry sand are shown in Fig. 2.2.

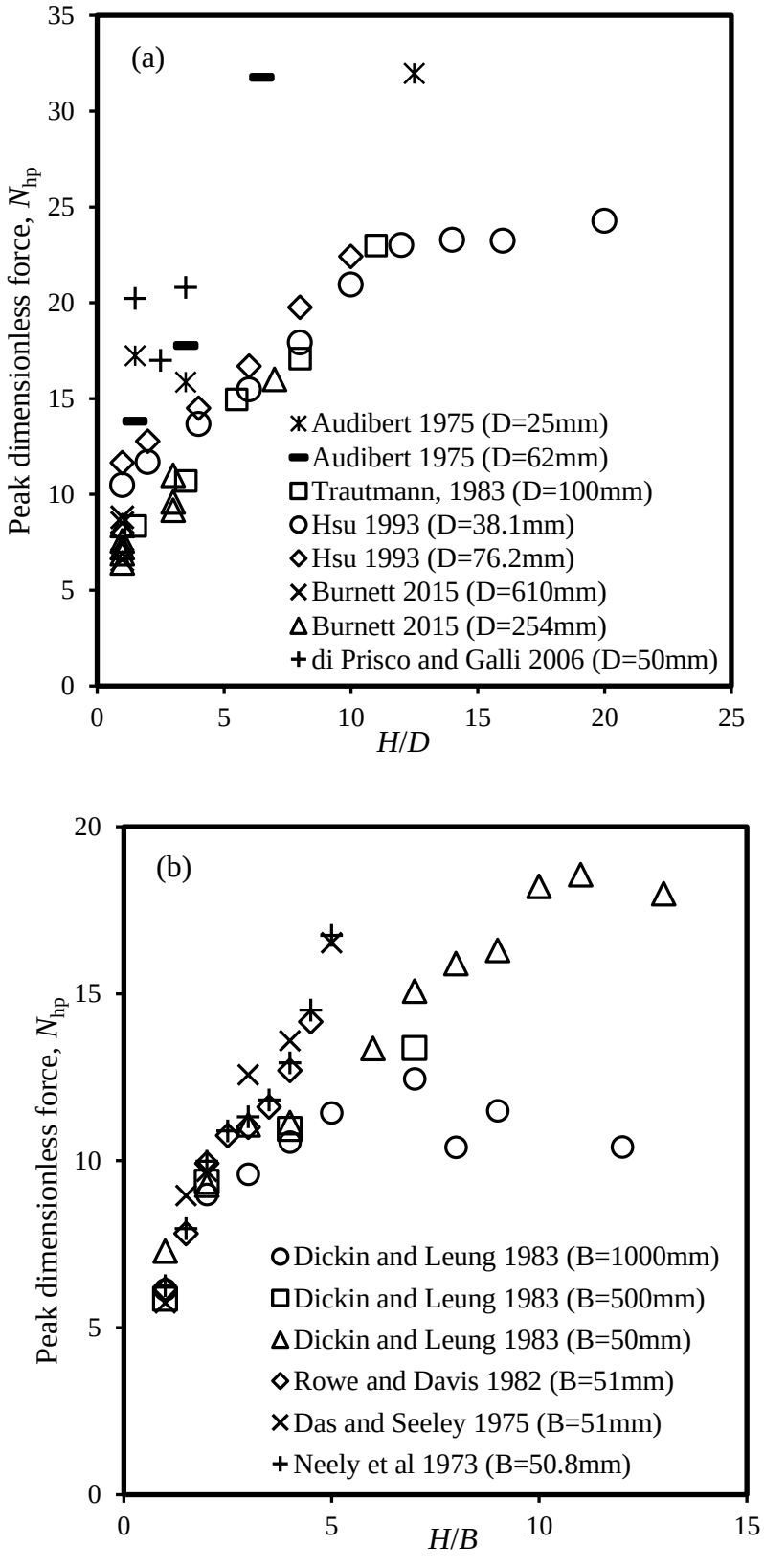

Figure 2.2: Peak dimensionless force with burial depth (a) for pipes, (b) for anchors

The following conclusions can be drawn from Figs. 2.2(a) and 2.2(b):

(i) The peak lateral resistances (N_{hp}) increases with embedment ratio ($\widetilde{H}$) for both pipes (Fig. 2.2(a)) and anchors (Fig. 2.2(b)). However, after a critical $\widetilde{H}$, N_{hp} remains almost constant for both pipes (Fig. 2.2(a)) and anchors (Fig. 2.2(b)).

(ii) The critical $\widetilde{H}$ varies with pipe diameter (D) ((Fig. 2.2 (a)) and anchor height (B) ((Fig. 2.2(b)). For example, in Fig. 2.2(b), the critical $\widetilde{H}$ for a 50-mm anchor is higher than that of a 1,000-mm anchor. However, further investigation is needed to calculate the critical $\widetilde{H}$ for a wide range of D and B.

(iii) A significant difference between N_{hp} for different pipe diameters (D) ((Fig. 2.2 (a)) and anchor heights (B) (Fig. 2.2 (b)) is evident in these physical model tests, which indicates that there is a size effect on the peak lateral resistance. However, further investigation is required to examine the effect of pipe/anchor size on N_{hp} for a wide range of D and B.

(iv) A very limited number of physical model tests for large diameters, especially at large $\widetilde{H}$, is available (Fig. 2.2). Therefore, more physical modeling and comprehensive numerical analyses are required for deep burial conditions.

Finally, care must be taken when comparing N_{hp} for the pipes and anchors shown in Fig. 2.2, because N_{hp} depends not only on $\widetilde{H}$ but also on other factors such as B or D and soil properties. Evaluation of the performance of similar-sized pipes and anchors buried in similar soil, as performed by Dickin (1994) for upward loading, would provide a better comparison. This issue has been discussed further in Chapter 6.

2.6.2 Empirical equations and design guidelines for peak resistance

Early studies on lateral pipe–soil interaction events sought analogous behaviour with other buried structures, such as vertical anchors and piles. For example, Trautmann (1983) showed that Ovesen's (1964) approach for vertical anchor slabs provides a good correspondence with his large-scale test data. On the other hand, ALA (2005) design guidelines adopted Hansen's (1961) relationships for lateral loading of rigid piles, which have been shown to be conservative compared to the physical test results of Trautmann (1983) (O'Rourke and Liu 2012). Although some discrepancies exist, Dickin (1988) suggested that the design approaches for vertical anchor plates may be applicable to laterally loaded buried pipes. The lateral bearing factors recommended by the PRCI (2009) are based on the verified numerical simulation results by Yimsiri et al. (2004) against the physical tests conducted by Trautmann (1983).

For structural analysis of the pipeline, the force–displacement relationship is generally given by a set of independent springs in the three orthogonal axes (e.g. ALA 2005), as shown in Fig. 1.2, where the spring's behaviour is defined by bilinear or hyperbolic functions (ALA 2005; PRCI 2009). However, a large discrepancy exists in the recommendations provided by different design guidelines for calculating the peak (maximum) lateral resistance (N_{hp}). Figure 2.3 shows N_{hp} versus $\widetilde{H}$ curves recommended by different design guidelines and empirical equations proposed in some previous studies (Trautmann and O'Rourke 1985; ALA 2005; PRCI 2009; Rajah 2014; Pike 2016). To calculate N_{hp}, in addition to H/D, only the representative value of the angle of internal friction is required, except in the work of Pike (2016), who proposed the equation only for dense sand and only as a function of H/D. The lines in Fig. 2.3 are drawn using $\phi'=45°$ for dense sand.

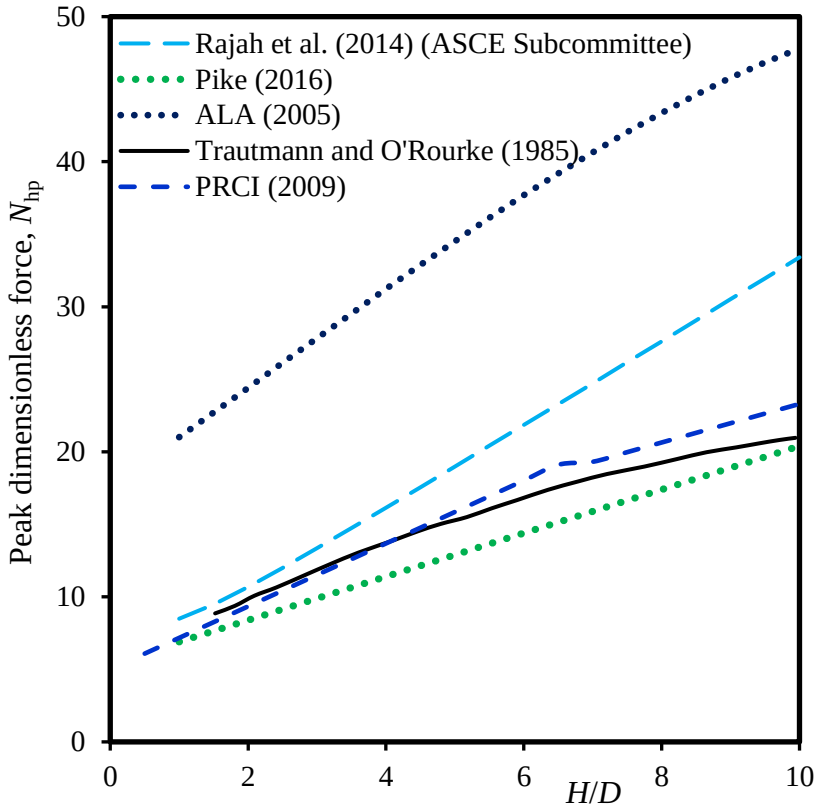

Figure 2.3: Comparison of design guidelines and empirical equations for peak lateral resistance of pipeline

The following conclusions can be drawn from Fig. 2.3:

(i) The ALA (2005) gives a significantly high lateral resistance compared to other guidelines and empirical equations (Fig. 2.3). Note, however, the use of a higher resistance is generally conservative in terms of structural response of a pipeline, because the force on pipeline is higher for a given lateral displacement (O'Rourke and Liu 2012).

(ii) The N_{hp} versus $\widetilde{H}$ curve proposed by the PRCI (2009) is very close to Trautmann and O'Rourkes' (1985), because the PRCI (2009) recommendations are based on FE results presented by Yimsiri et al. (2004), which have been calibrated against Trautmann's (1983) physical test data.

(iii) The N_{hp} versus $\widetilde{H}$ curve recommended by the ASCE task committee on the thrust restraint design of buried pipelines (Rajah 2014) shows higher N_{hp}, especially at large $\widetilde{H}$, compared to Trautmann and O'Rourkes' (1985) physical model test results. Note that this method has been developed based on the analogy of passive wedge formation in front of a pile.

(iv) The linear approximation of Pike (2016), $N_{hp}=1.5(\widetilde{H}+3.6)$, gives N_{hp} similar to that of Trautmann and O'Rourke (1985) and PRCI (2009). Note that this equation has been proposed from physical model tests of pipes buried in dense sand having D>75 mm.

(v) None of the available design guidelines consider the effects of pipe diameter on N_{hp}, although it might be significant, as shown in Fig. 2.2.

For shallow to moderate embedment ratios, the physical model tests on dense sand show a post-peak degradation of resistance in the force–displacement curve (Fig. 2.1). However, most of the current design guidelines for buried pipelines do not consider this reduction of resistance (cf. Fig. 1.2); instead, the soil resistance is assumed to be constant with displacement after the peak. As mentioned in Section 1.1, the use of higher resistance might lead to an unconservative design when soil provides resistance to the movement of the pipe (e.g. lateral buckling). Note that the importance of post-peak reduction of uplift resistance in the design has been recognized for the upheaval buckling of buried pipelines (DNV 2007) and lateral buckling of as-laid offshore pipelines (e.g. Randolph 2012), considering the fact that a better representation of the force–displacement curve up to a sufficiently large displacement will improve structural modeling of pipelines.

2.7 Failure Mechanisms

The lateral and upward resistances of buried pipelines and anchors, as discussed in previous sections, are closely related to failure mechanisms of soil, including progressive development of shear bands. The failure mechanisms observed in experimental studies are discussed in the following sections.

2.7.1 Lateral Loading

Audibert and Nyman (1977) described the soil failure mechanisms based on observation of the failure pattern through a plexiglass wall during lateral movement of the pipe in physical model tests having cover depths ≤6*D*. Figure 2.4(a) shows that, for shallow burial depths, a well-defined soil wedge formed during loading, which is comprised of three distinct zones. This type of failure is known as "wedge" type failure. However, for deep burial conditions, a punching failure mechanism, which extended approximately one pipe diameter in front of the pipe, was observed (Fig. 2.4(b)). This type of failure mechanism is known as the "flow-around" mechanism.

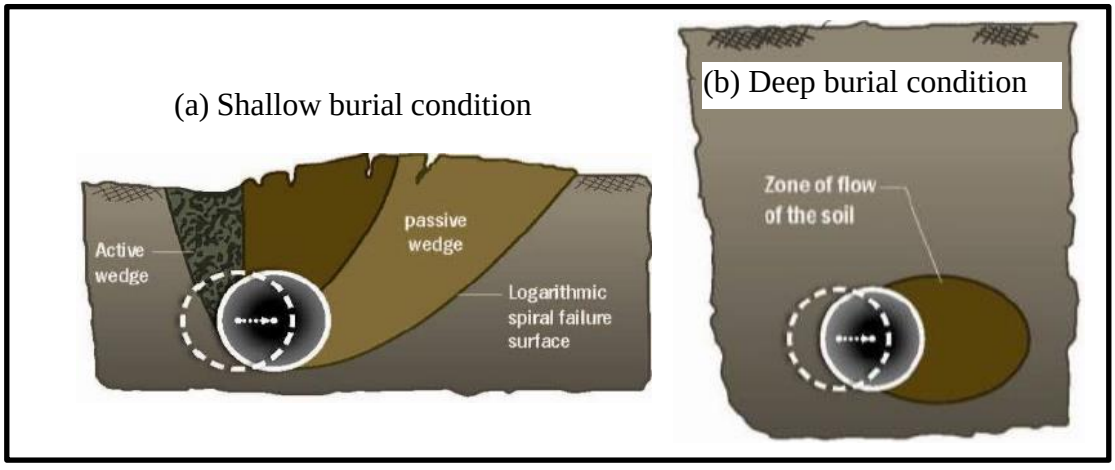

Figure 2.4: Soil failure mechanisms for lateral pipe–soil interaction (Audibert and Nyman 1977)

Noticeable surface heave was observed for shallow burial cases (Fig. 2.4(a)). Similar failure mechanisms were also observed by Trautmann (1983) in their experimental study. Figure 2.5 shows that the soil failure mechanisms for anchors are very similar to those of pipes (e.g. Dickin and Leung 1985): wedge type failure for shallow and flow-around in deep burial conditions.

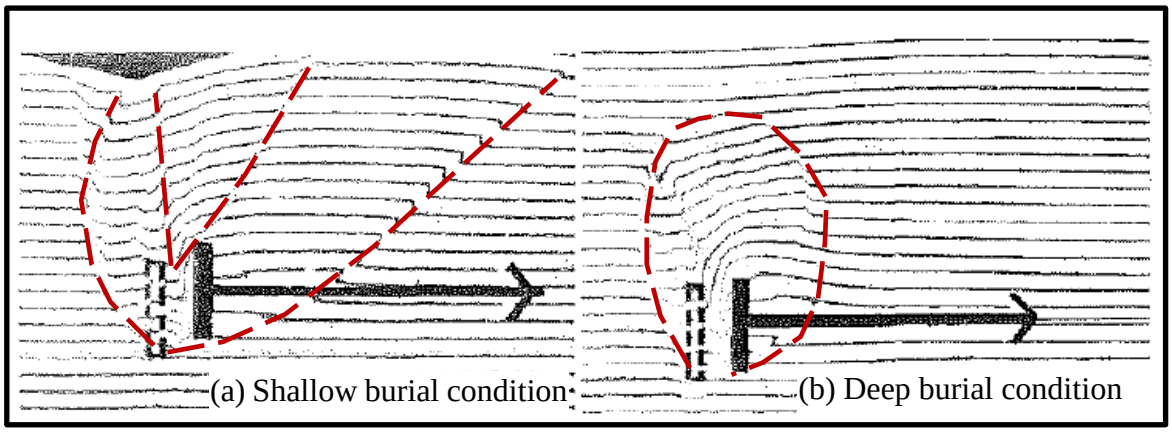

Figure 2.5: Soil failure mechanisms for lateral anchor–soil interaction (after Dickin and Leung 1985)

Through a joint research project of Memorial University of Newfoundland and Queen's University, Canada, Burnett (2015) conducted a number of full-scale physical model tests for lateral pipe–soil interaction. Figure 2.6 shows that the slip planes developed progressively with lateral loading. For example, Fig. 2.6(a) shows that the active wedge develops at $\tilde{u}$=0.025. The peak resistance mobilized $\tilde{u}$~0.1 (Fig. 2.6(b)). As shown in this figure, the incremental shear strain is not uniform along the shear band. As the mobilized shear resistance of dense sand depends on accumulated shear strain, especially in the strain-softening stage, the shear strength of the soil elements along these planes is different, which could be simulated using FE modeling with an appropriate soil model. Figure 2.6(c) shows a considerable settlement of the ground surface in the active zone at large lateral displacements.

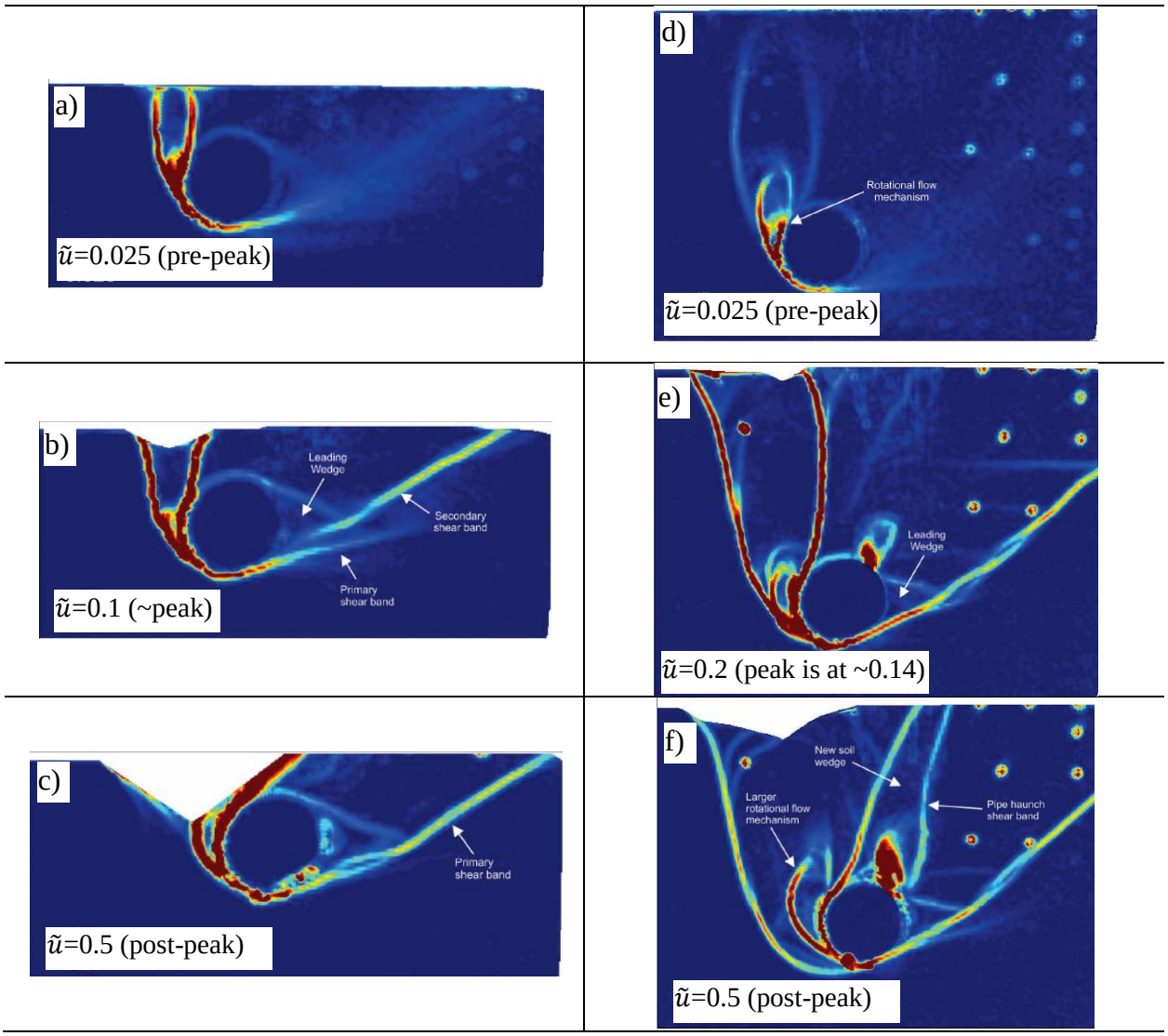

Figure 2.6: Progressive formation of failure planes during lateral loading: a–c are for $\tilde{H}$=1 and d–f are for $\tilde{H}$=3 (Burnett 2015)

For a larger burial depth ($\tilde{H}$=3), shear band formation up to the peak is very similar to the formation in the $\tilde{H}$=1 test (Figs. 2.6(d) & 2.6(e)). However, at large $\tilde{u}$, a number of additional shear bands form (Fig. 2.6(f)). This implies that the force–displacement response obtained from physical model tests evolves from a complex displacement of soil blocks that develop due to progressive formation of the number of shear bands, where a varying level of shear strain develops.

2.7.2 Upward Loading

Three types of simplified failure mechanisms have been proposed for upward loading of pipes and anchors buried in sand (Fig. 2.7). The vertical slip surface type failure mechanisms (Fig. 2.7(a)) are mainly observed in shallowly buried pipes in loose sand (Wang et al. 2010). For dense sand, which is the focus of the present study, inclined slip surface (Fig. 2.7(b)) or flow-around (Fig. 2.7(c)) mechanisms are developed for shallow and deep burial conditions, respectively.

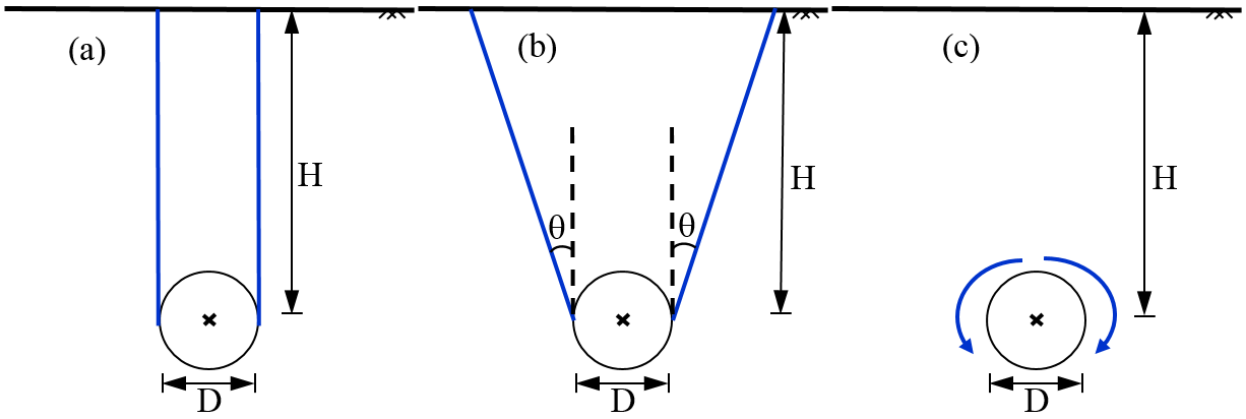

Figure 2.7: Simplified failure mechanisms: (a) vertical slip surface; (b) inclined slip surface (White et al. 2001); (c) flow-around mechanisms (redrawn from Williams et al. 2013)

White et al. (2001) showed that when the peak uplift resistance mobilizes in medium to dense sand, two inclined symmetric slip planes form in the soil originating from the pipe waist (Fig. 2.7(b)). Although the slip planes are slightly curved outward, their inclination with the vertical (θ) is approximately equal to the peak dilation angle (ψ_p).

Depending upon the level of upward displacement and burial depth, both an inclined slip surface and flow-around mechanisms might be observed in the same test. White et al. (2001) observed an inclined slip surface mechanism at $\tilde{v} = 0.23$ (Fig. 2.8(a)), while it changed to a

flow-around mechanism at large displacements (e.g. $\tilde{v} = 1.0$), as shown in Fig. 2.8(b)). At a very large displacement, the cavity that formed beneath the pipe is filled by slumping of the surrounding soil (Fig. 2.8 (c)).

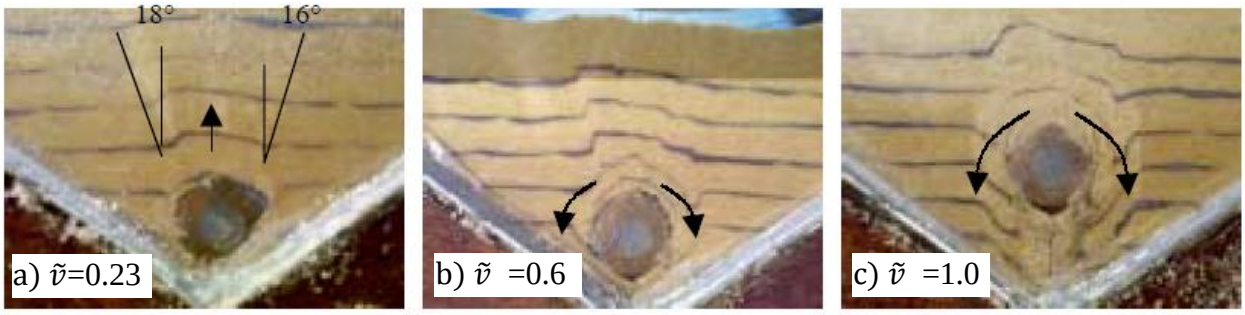

Figure 2.8: Soil failure mechanism during a pipe uplift test (White et al. 2001)

Using the PIV technique, Huang et al. (2015) showed that θ is less than ψ_p at a small $\tilde{v}$, which gradually increases with $\tilde{v}$ to the maximum value (θ~ψ_p) when the peak resistance is mobilized (Figs. 2.9 (a–c)). The vertical inclination of the slip plane (θ) then decreases with a further a decrease in $\tilde{v}$, and θ~0 at large $\tilde{v}$, at least for shallow burial conditions (Figs. 2.9 (d–f)).

In summary, although two inclined slip planes are used to calculate the uplift resistance (Fig. 2.7(b), the inclination of the slip plane changes with loading (Fig. 2.9). The uplift soil resistance depends on the inclination of these slip planes (Fig. 2.7(b)). In addition, for dense sand, the shear resistance of the soil elements along the slip plane depends on plastic shear strain. If the values of θ and shear resistance are known, the uplift resistance can be calculated using the limit equilibrium method (White et al. 2008). To obtain these values, the soil failure mechanisms and progressive development of shear bands need to be critically examined. Although the PIV technique provides useful information on soil deformation, the progressive formation of shear bands in dense sand

due to strain-softening behaviour of soil can be better explained by numerical modeling with an advanced soil constitutive model. A detailed discussion on modeling of dense sand using the proposed MMC model is provided in Chapter 3.

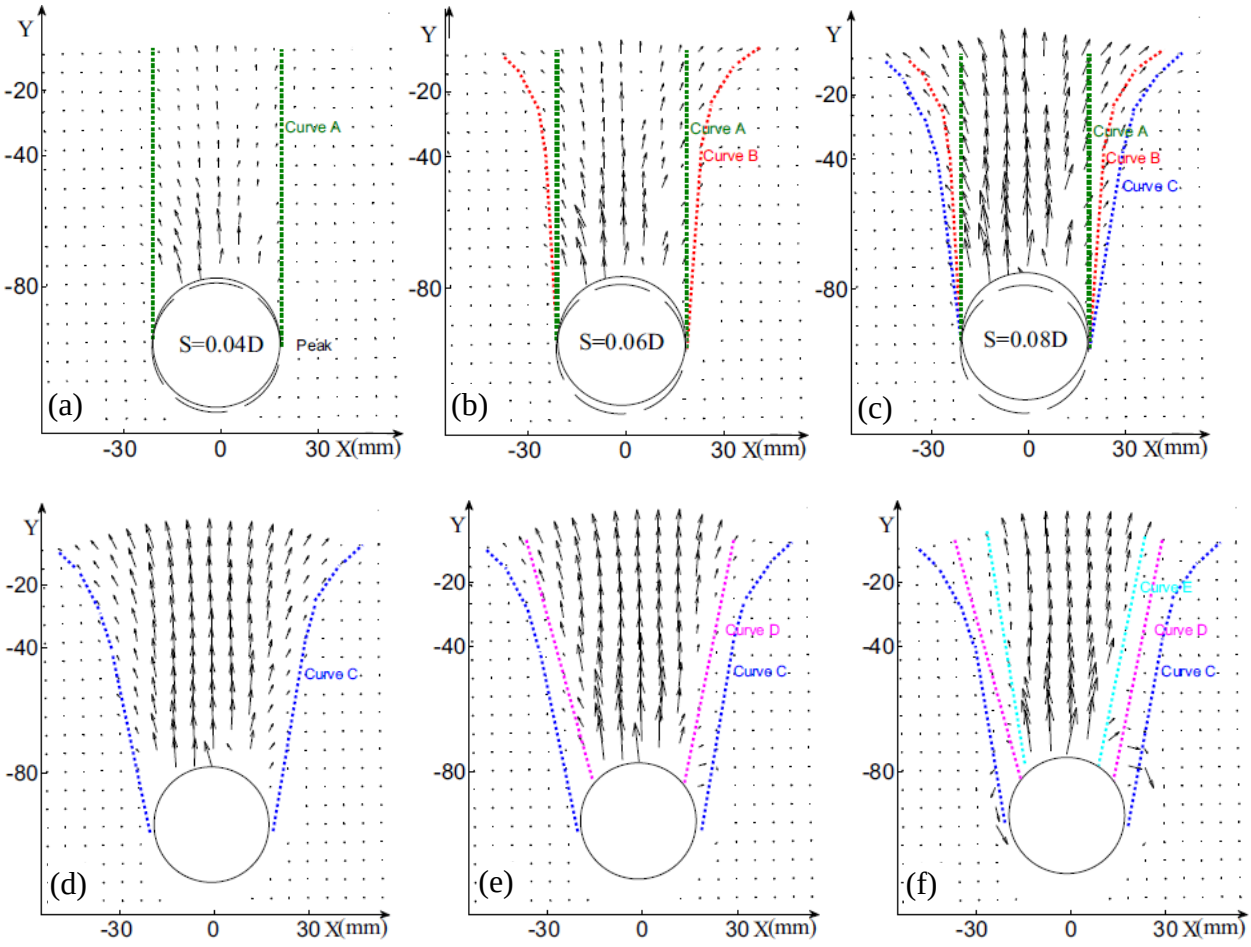

Figure 2.9: Uplift soil failure mechanism in both pre-peak (a–c) and post-peak conditions (d–f) (Huang et al. 2015)

2.8 Summary

Soil resistance is one of the critical parameters in the design of buried pipelines. The literature review presented in this chapter, and also in the following chapters, shows that there

exists a wide difference among soil resistances obtained from physical model tests and in the recommendations provided in the design guidelines. A number of factors might cause this difference, such as stress–strain behaviour of soil, pipe diameter, and the shape of the buried structures (pipes versus anchors).

Most of the design guidelines focus on the peak resistance, both for lateral and upward loading. However, physical model tests in dense sand at low to moderate embedment ratios show the reduction of resistance after mobilization of the peak resistance. At least the following two factors might cause this reduction: (i) strain-softening behaviour of dense sand, and (ii) reduction of embedment ratio with loading, especially for upward loading. The effects of the former factor can be investigated by implementing an appropriate soil model that can capture the features observed in laboratory tests on dense sand, including strain-softening behaviour. However, the present literature review shows that most of the previous numerical studies are based on the MC model for soil, which cannot capture strain-softening behaviour. A considerable degradation of resistance due to the reduction of the embedment ratio occurs when the pipe displaces a sufficiently large distance. Therefore, this effect can be investigated if the FE simulation can be continued over a large distance without numerical issues due to mesh distortion. The present literature review shows that most of the numerical studies have been conducted using Lagrangian-based FE modeling, which often suffers from numerical issues at large displacements.

Physical model tests for upward loading at low to moderate embedment ratios show that the vertical inclination of the slip planes changes with upward displacement. In addition, similar to lateral loading events, these slip planes form progressively with displacement of the pipe and the mobilized shear resistance of the soil elements along these planes might vary as the accumulated shear strains are different. These effects cannot be captured using the limit equilibrium methods

or plasticity solutions, which are commonly used to calculate the uplift resistance. Numerical analysis with the MC model for soil also cannot simulate this effect properly. Moreover, the failure mechanisms change with burial depth, which could be modeled better using an advanced soil model.

Finally, although the studies on strip anchors have also been used to develop design guidelines for pipeline resistance, the literature review shows that there are discrepancies between the responses of pipes and anchors. A systematic comparison of the responses of similar-sized pipes and anchors will provide further insights, and could identify the potential reasons for these discrepancies.

CHAPTER 3

Finite Element Modeling of Lateral Pipeline–Soil Interactions in Dense Sand

Co–Authorship: This chapter has been published in the Canadian Geotechnical Journal as: Roy, K., Hawlader, B.C., Kenny, S. and Moore, I. (2016), 'Finite Element Modeling of Lateral Pipeline−Soil Interactions in Dense Sand.' Most of the research presented in this chapter has been conducted by the first author. He also prepared the draft manuscript. The other authors mainly supervised the research and reviewed the manuscript.

3.1 Abstract

Finite element (FE) analyses of pipeline–soil interaction for pipelines buried in dense sand subjected to lateral ground displacements are presented in this paper. Analysis is performed using the Arbitrary Lagrangian-Eulerian (ALE) method available in Abaqus/Explicit FE software. The pipeline–soil interaction analysis is performed in the plane strain condition using the Mohr-Coulomb (MC) and a modified Mohr-Coulomb (MMC) models. The MMC model considers a number of important features of stress–strain and volume change behaviour of dense sand including the nonlinear pre- and post-peak behaviour with a smooth transition and the variation of the angle of internal friction and dilation angle with plastic shear strain, loading conditions (triaxial or plane strain), density and mean effective stress. Comparing FE and experimental results, it is shown that the MMC model can better simulate the force–displacement response for a wide range of lateral displacements of the pipe for different burial depths, although the peak force on the pipe could be matched using the MC model. Examining the progressive development of zones of large

inelastic shear deformation (shear bands), it is shown that the mobilized angle of internal friction and dilation angle vary along the length of the shear band, however constant values are used in the MC model. A comprehensive parametric study is also performed to investigate the effects of pipeline diameter, burial depth and soil properties. Many important aspects in the force–displacement curves and failure mechanisms are explained using the present FE analyses.

3.2 Introduction

Pipelines are extensively used for transporting water and hydrocarbons. Any relative displacement (e.g. during slope movement) between pipeline and soil exert forces on pipelines. The pipeline–soil interaction analyses are generally performed defining the force–displacement curves in the lateral, vertical and axial directions based on available guidelines (American Lifelines Alliance 2005; Honegger and Nymann 2004). Pipelines might be buried in a wide variety of soils and subjected to loading from different directions. Pipelines buried in dense sand subjected to large lateral displacement are the focus of the present study, since nonuniform lateral displacement leads to longitudinal bending and other structural demands that can exceed the structural capacity. Experimental studies have been conducted in the past to understand lateral pipeline–soil interaction in sand (e.g. Audibert and Nyman 1977; Trautmann 1983; Scarpelli et al. 1999; Turner 2004; Wijewickreme et al. 2009; Daiyan 2013; Almahakeri et al. 2013, 2014). From the test results, the force–displacement curves could be obtained and the failure mechanisms could be interpreted. The displacements of soil particles with lateral movement of the pipe could be visualized using the advanced particle image velocimetry (PIV) techniques (Burnett 2014). Guo and Stolle (2005) compiled the data from experimental studies and showed a wide variation in the non-dimensional peak force, which depends upon sand properties, diameter of the pipe, burial depth, and test

procedure. In addition to the peak force, the shape of the force–displacement curve is also influenced by these factors. In structural modeling, the force–displacement curves as elastoplastic soil springs are given as input, which is valid up to mobilization of the peak force. However, a section of pipeline might experience large displacements where post-peak soil resistance governs the response. Recognizing this, design guidelines (e.g. DNV 2007) suggested that the post-peak response of dense sand should be considered in uplift resistance calculation as the sand moves to a looser state at displacements beyond the peak displacement. As shown later, the mobilization of angles of internal friction (ϕ') and dilation (ψ) both in pre- and post-peak levels is equally important for calculation of lateral resistance. Moreover, a better representation of force–displacement curves up to sufficiently large displacements will improve structural modeling of pipeline.

Continuum finite element (FE) analyses have been performed in the past to simulate lateral pipeline–soil interaction in sand (e.g. Yimsiri et al. 2004; Guo and Stolle 2005; Xie 2008; Daiyan et al. 2011; Jung et al. 2013). The soil constitutive model used in the analysis influences FE simulation results (Yimsiri et al. 2004). Figure 3.1 shows the typical stress–strain and volume change behaviour of dense sand in consolidated isotropically drained (CID) triaxial compression tests. The stress ratio (q/p'), (where p' is the mean effective stress and q is deviatoric stress) increases gradually (hardening) up to the peak and then decreases (softening) to the critical state at large axial strains (Fig. 3.1a). The axial strain at the peak stress ratio (ε_a^p) decreases with confining pressure (σ_c). Experimental evidence also shows that ε_a^p decreases with relative density (Lee 1965; Kolymbas and Wu 1990; Lancelot et al. 2006). Figure 3.1(b) shows higher dilation in tests with low σ_c. Moreover, the volumetric expansion starts at lower axial strains for low confining pressures. These characteristics observed not only in the triaxial stress condition; the results from

direct shear tests also show similar behaviour for different vertical normal stresses (Lings and Dietz 2004).

Another important experimental observation is that the behaviour of dense sand in triaxial and simple shear conditions is different. For example, Ahmed (1973) conducted tests on crushed silica sand in drained triaxial (TX) and plane strain (PS) loading conditions. The peak friction angles (ϕ'_p) from his test results are shown in Fig. 3.2. Three key features of these test results need to be mentioned: (i) ϕ'_p for the plane strain condition (ϕ'^{PS}_p) is higher than ϕ'_p for the triaxial condition (ϕ'^{TX}_p), and the value of $\phi'^{PS}_p - \phi'^{TX}_p$ is higher at low stress levels, (ii) both ϕ'^{PS}_p and ϕ'^{TX}_p increase with D_r, and (iii) ϕ'_p for both TX and PS configurations decrease with of confining pressure.

In summary, pre-peak hardening, post-peak softening, density and confining pressure dependent ε^p_a, angle of internal friction and dilation angle are the common features of the stress–strain behaviour of dense sand. The mode of shearing (TX or PS) also significantly influences the behaviour. All these features of the stress–strain behaviour of dense sand have not been considered in the available FE modeling of pipeline–soil interaction. For example, Yimsiri et al. (2004) used the Mohr-Coulomb model with constant angles of internal friction and dilation (MC). They also conducted FE analyses using the Nor-Sand soil constitutive models. Guo and Stolle (2005) and Daiyan et al. (2011) considered the effects of p' and plastic shear strain on ϕ' and ψ but did not incorporate the effects of density on the plastic strain required to mobilize the peak value. Robert (2010) and Jung et al. (2013) incorporated the post-peak softening using a linear variation of angles of internal friction and dilation with plastic strain, but did not consider the pre-peak hardening. However, Jung et al. (2013) conducted the simulation using plane strain strength parameters.

From a numerical point of view, the softening of soil causes strain localization into shear bands resulting in significant mesh distortion in typical FE formulations expressed in the Lagrangian framework (Qiu et al. 2009; Pike et al. 2013). It is preferable to avoid such mesh distortion issues in FE simulation. The distinct element method has also been used in the past to accommodate large soil movement around the pipe and to continue the analysis for a large displacement of the pipe (Yimsiri and Soga 2006).

The main objective of the present study is to simulate lateral pipeline–soil interaction using Abaqus/Explicit (taking the advantages of better modeling capability of strength degradation in shear bands over Abaqus/Standard) implementing a modified Mohr-Coulomb (MMC) model that can capture the features of dense sand behaviour discussed above. The paper has been organized in the following way. First, the development of the MMC model is presented. The key model parameters and their relations to experimental results are discussed. Second, the FE simulations of triaxial test results are performed to show the performance of the proposed MMC model. Third, the FE simulations are performed for lateral pipeline–soil interaction and compared with test results. Finally, a comprehensive parametric study is performed.

3.3 Modeling of Soil Behaviour

The elastic perfectly plastic Mohr-Coulomb (MC) model, in its original form and also after some modifications, has been used by a number of researchers in the past for pipeline–soil interaction analysis (e.g. Moore and Booker 1987; Taleb and Moore 1999; Ellis and Springman 2001; Yimsiri et al. 2004; Guo and Stolle 2005; Daiyan et al. 2011; Almahakeri et al. 2012; Kouretzis et al. 2013). In MC model, the soil behaviour is elastic until the stress state reaches the yield surface which is defined by the Mohr-Coulomb failure criterion. This model is available in

commercial software packages including Abaqus FE program. The modification of MC model has been performed by implementing some additional features of dense sand behaviour (Guo and Stolle 2005; Daiyan et al. 2011; Jung et al. 2013). The present FE analyses are performed using a MMC model incorporating all of the features of dense sand behaviour discussed in the following sections.

3.3.1 Angle of internal friction in triaxial compression (TX) and plane strain (PS) conditions

The strength of sand is characterized by mobilized angle of internal friction (ϕ') and dilation angle (ψ). First, two limiting values of ϕ' are examined: (i) at the peak (ϕ'_p) and (ii) the critical state (ϕ'_c).

Experimental results show that ϕ'_p depends on density of sand and also on the direction of shearing (e.g. Bolton 1986; Houlsby 1991; Schanz and Vermeer 1996). Kulhawy and Mayne (1990) compiled a large volume of test data and showed that, for dense sand, ϕ'^{PS}_p is approximately 10 to 20% higher than ϕ'^{TX}_p. Furthermore, experimental evidence also shows that ϕ'_p decreases with confining pressure (σ_c) (Fig. 3.1) or p' at failure (Bolton 1986).

Assuming unique ϕ'_c for both TX and PS conditions, Bolton (1986) proposed the following relationships from test results for 17 sands.

$$\phi'_p - \phi'_c = A_\psi I_R \quad (3.1)$$

where A_ψ=3 for TX and 5 for PS conditions. I_R is the relative density index defined as $I_R=I_D(Q-\ln p')-R$ in which I_D=relative density (=D_r(%)/100), Q=10 and R=1. Bolton (1986) also recognized that stress and strain non-uniformity could be strong at very low p'. Moreover, at that time, accurate measurement of small stresses and strains was difficult. As such Bolton (1986) set

the maximum limit of I_R=4. White et al. (2008) also used I_R=0–4 as a permissible range for modeling pipelines buried in sand. Therefore, according to Eq. (3.1), the maximum value of $\phi'_p - \phi'_c$ of 12° and 20° for the TX and PS conditions, respectively, are used in the present study.

Equation (3.1) has been verified with additional test data and used by many researchers. For example, Houlsby (1991) developed a relationship similar to Eq. (3.1) based on the critical state theory. Similarly, based on Eq. (3.1), Schanz and Vermeer (1996) showed that $\phi_p'^{PS} = \left(5\phi_p'^{TX} - 2\phi'_c\right)/3$ is valid for a wide range of test results on Hostun dense sand. In other words, for dense sand at low stress levels, $\phi_p'^{PS}$ is higher than $\phi_p'^{TX}$. Attempts have also been made in the past to develop relationships between ϕ'^{PS} and ϕ' obtained from direct shear tests (ϕ'^{DS}) (Taylor 1948; Davis 1968; Rowe 1969). Lings and Dietz (2004) provided a detailed discussion of these relationships. From comparisons with test results, they showed that $\phi_p'^{PS} \approx \phi_p'^{DS} + 5°$, where $\phi_p'^{DS}$ is the peak friction angle from a direct shear test. In summary, although triaxial and direct shear tests are widely used to determine ϕ', it should be properly adjusted if the analysis is performed for plane strain conditions where $\phi'^{PS}$is required.

The value of A_ψ in Eq. (3.1) might vary with type of sand and fine contents. For example, Chakraborty and Salgado (2010) found A_ψ=3.8 for Toyoura sand for both TX and PS conditions, while Xiao et al. (2014) showed A_ψ=3.0–5.53 for Ottawa sand with 0–20% fine contents for triaxial condition. Xiao et al. (2014) also proposed an empirical relationship for A_ψ as a function of fine content. Moreover, Q is also varied using an empirical function of σ_c (Chakraborty and Salgado 2010; Xiao et al. 2014), instead of a constant value as proposed by Bolton (1986). Although these empirical functions of A_ψ and Q might fit the test results better, a constant value of Q (=10) and

A_ψ=5 with the limiting maximum value of $\phi'_p - \phi'_c$ of 12° and 20° for TX and PS configurations, respectively, are used in the present study.

Experimental evidence shows that $\phi_c'^{PS}$ is a few degrees higher than $\phi_c'^{TX}$. Bishop (1961) and Cornforth (1964) conducted laboratory tests over the full range of relative densities at a wide range of σ_c and showed that $\phi_c'^{PS}$ is approximately 4° greater than $\phi_c'^{TX}$. A similar trend was found from laboratory tests on Toyoura sand, and it has been shown that $\phi_c'^{PS}$ ≈34.5°–38° while $\phi_c'^{TX}$≈33° (Tatsuoka et al. 1986; Pradhan et al. 1988; Yoshimine 2005).

In this study, $\phi_c'^{TX}$=31° and $\phi_c'^{PS}$=35° are used. The authors also aware of the fact that ϕ'_c might slightly increase with decrease in p' (Lings and Dietz 2004); however, such variation is not considered in this study.

Bolton (1986) also showed that the maximum dilation angle (ψ_p) is related to the peak and critical state friction angle as:

$$\phi'_p - \phi'_c = k_\psi \psi_p \quad (3.2)$$

where k_ψ=0.8 for PS and 0.5 for TX configurations (Bolton 1906). Note that k_ψ might be also dependent on type of sand, fines content and/or gravel fraction (Simoni and Houlsby 2006; Chakraborty and Salgado 2010; Xiao et al. 2014).

3.3.2 Stress–strain behaviour of dense sand

Generally in the widely used MC model it is assumed that: (i) plastic strains develop only when the stress state is on the failure (yield) surface, (ii) any change in stresses inside the yield surface results in only elastic strain, and (iii) soil deforms at a constant dilation angle once the stress state reaches the yield surface. However, experimental evidence shows that plastic strains

usually develop well before failure. In order to capture this behaviour, constitutive models of different forms have been proposed in the past (Prevost 1985; Gajo and Wood 1999; Dafalias and Manzari 2004). Similar to these works, it is assumed that the plastic deformation occurs only for changes of q/p'. The development of plastic strain for loading under constant stress ratio is neglected because the soil considered in this study is not loose and crushing of sand particles is not expected due to stress increase around the pipeline.

Following the conceptual frameworks developed in previous studies (e.g. Jardine 1992; Mitchell and Soga 2005), the stress–strain behaviour of dense sand is divided into three zones as shown in Fig. 3.3.

Zone-I: In this zone, elastic (linear and/or nonlinear) deformation occurs. In the pure linear elastic zone the soil particles do not slide relative to each other. However, in nonlinear elastic deformation small slide or rolling between particles might occur but the deformation is recoverable during unloading. The deformation behaviour in this zone can be defined by elastic properties namely Young's modulus (E), and Poisson's ratio (ν).

Zone-II: If the shearing is continued, the soil element will move to zone-II (Fig. 3.3) which can be considered as the "pre-peak plastic zone" (Mitchell and Soga 2005). The mobilized ϕ' (Fig. 3.3) is used to define the yield surface using the Mohr-Coulomb model. When the stress state approaches the initial yield surface (i.e. yield surface with ϕ'_{in} at point A in Fig. 3.3), plastic strains occur upon further loading. The initial yield surface of dense sand is inside the failure envelope defined by the peak friction angle. The pre-peak plastic deformation of geomaterials has been recognized by many researchers from experimental data, and multiple yield surfaces are used to simulate this; for example, the multi-yield surface model (Mroz 1967), the nested surface plasticity model (e.g. Prévost 1985), the bounding surface plasticity model (Dafalias and Herrman 1982),

and the subloading surface model (Hashiguchi and Ueno 1977). These complex models can simulate many important features including the stress–strain behaviour during cyclic loading. However, in the present MMC model the mobilized ϕ' and ψ are varied with accumulated engineering plastic shear strain (γ^p) as shown in Fig. 3.3. A set of equations (Eq. 3.3–3.8) are proposed to model this behaviour after some modifications of similar type of models proposed in previous studies (Vermeer and de Borst 1984; Tatsuoka et al. 1993; Hsu and Liao 1998).

In the pre-peak zone-II, ϕ' and ψ increase from ϕ'_{in} and ψ_{in} to the peak values ϕ'_p and ψ_p at strain, γ_p^P. Based on Rowe (1969), Mitchell and Soga (2005) suggested that the mobilized ϕ' of sand is the sum of the contributions of four components: interparticle friction, rearrangement of particles (fabric), crushing, and dilation. As p' is not very high in the pipeline–soil interaction analysis being undertaken here, the crushing effect is negligible. At the beginning of plastic deformation ψ_{in}=0 is assumed. Therefore, interparticle friction and soil fabric are the main contributors to ϕ'_{in} (point A in Fig. 3.4). Based on typical contributions of each component of ϕ' (Mitchell and Soga, 2005), ϕ'_{in}=29° is assumed in this study.

The values of ϕ'_p and ψ_p are obtained from Eqs. (3.1 and 3.2). As discussed in the introduction, the shear strain or displacement required to mobilize ϕ'_p decreases with density and increases with confining pressure (Lee et al. 1965; Tatsuoka et al. 1986; Hsu and Liao 1998; Lings and Dietz 2004). The effects of density and stress level are incorporated in γ_p^P as:

$$\gamma_p^P = \gamma_c^P \left(\frac{p'}{p'_a}\right)^m \quad (3.3)$$

$$\gamma_c^P = C_1 - C_2 I_D \quad (3.4)$$

where γ_c^p= strain softening parameter; p'_a= reference pressure which is considered as the atmospheric pressure (=100 kPa); *m*, C_1 and C_2 are soil parameters, which could be obtained from a set of triaxial or simple shear tests at different confining pressures and densities. Further explanation of these parameters are provided in the following sections.

The following sine functions are then used to model the variation of mobilized ϕ' and ψ in zone-II.

$$\phi' = \phi'_{in} + \sin^{-1}\left[\left(\frac{2\sqrt{\gamma^p \gamma_p^p}}{\gamma^p + \gamma_p^p}\right)\sin(\phi'_p - \phi'_{in})\right] \quad (3.5)$$

$$\psi = \sin^{-1}\left[\left(\frac{2\sqrt{\gamma^p \gamma_p^p}}{\gamma^p + \gamma_p^p}\right)\sin(\psi_p)\right] \quad (3.6)$$

The lines AB and DE in Fig. 3.3 demonstrate the variation of ϕ' and ψ, respectively, in the pre-peak zone for D_r=80% and p'=40 kPa.

Zone-III: If the shearing is continued, both ϕ' and ψ will decrease with γ^p in Zone-III (Fig. 3.3). This zone is referred as the "post-peak softening zone". The following exponential functions are used to define the curves *BC* and *EF* to model the variation of ϕ' and ψ with plastic strain, respectively.

$$\phi' = \phi'_c + \left(\phi'_p - \phi'_c\right)\exp\left[-\left(\frac{\gamma^p - \gamma_p^p}{\gamma_c^p}\right)^2\right] \quad \text{curve } BC \quad (3.7)$$

$$\psi = \psi_p \exp\left[-\left(\frac{\gamma^p - \gamma_p^p}{\gamma_c^p}\right)^2\right] \quad \text{curve } EF \quad (3.8)$$

The strain softening parameter γ_c^p controls the shape of the post-peak curves. The lower the value of γ_c^p, the faster the decrease of ϕ' from ϕ'_p to ϕ'_c. After some algebraic calculation, it can be shown from Eqs. (3.7) and (3.8) that the point of inflection of the post-peak softening curve occurs

at $\gamma_c^P/\sqrt{2}$ from γ_p^P as shown by the open circles in Fig. 3.3. The shapes of the curves defined by Eqs. (3.6–3.8) are very similar to the observed behaviour of dense sand.

The novel aspects that the present MMC model adds to the existing models of similar type for pipeline–soil interaction analysis (e.g. Guo and Stolle 2005; Robert 2010; Daiyan et al. 2011; Jung et al. 2013a,b; Pike et al. 2013) are primarily twofold. Firstly, nonlinear pre- and post-peak behaviour with a smooth transition is incorporated. Secondly, the mobilization of ϕ' and ψ with plastic strain, including the peak values, depends on density and mean effective stress.

3.3.3 Elastic properties

Poisson's ratio (ν) and Young's modulus (E) of the soil are the two elastic parameters. The Poisson's ratio of 0.2 is used, which has been considered as the best representative value for dense sand (Jefferies and Been 2006). E is varied with p' using the following power function (Hardin and Black 1966; Janbu 1963).

$$E = Kp'_a \left(\frac{p'}{p'_a}\right)^n \tag{3.9}$$

where K is a material constant, p'_a is the atmospheric pressure (=100 kPa) and n is an exponent. A number of authors used Eq. (3.9) in FE modeling of pipeline–soil interaction (Taleb and Moore 1999; Yimsiri et al. 2004; Guo and Stolle 2005; Daiyan et al. 2011; Jung et al. 2013). Further discussion on the selection of elastic parameters can be found in those studies and is not repeated here.

3.4 FE Modeling of Pipeline–soil Interaction

Two-dimensional pipeline–soil interaction analyses are conducted using the Abaqus/Explicit FE software. The main advantages of using Abaqus/Explicit over Abaqus/Standard is that the pipe

can be moved relatively large distances while still largely avoiding numerical issues associated with mesh distortion as encountered when employing Abaqus/Standard, especially in the zones of shear strain localization. Therefore, the large strains that concentrate in the shear bands can be better simulated using Abaqus/Explicit.

A typical FE mesh for 300 mm outer pipe diameter (D) is shown in Fig. 3.4. For FE modeling of soil, the 4-node bilinear plane strain quadrilateral element (CPE4R) is used. The pipe is modeled as a rigid body. Abaqus/cae is used to generate the FE mesh. The structured mesh (Fig. 3.4) is generated by zoning the soil domain. A denser mesh is used near the pipe. The bottom of the FE domain is restrained from any movements, while all the vertical faces are restrained from any lateral movement using roller supports (Fig. 3.4). No displacement boundary condition is applied on the top face. The pipe is placed at the desired location (i.e. wished-in-place configuration). The depth of the pipe is measured in terms of H/D ratio, where H is the depth from the top of the soil to the centre of the pipe. The locations of the bottom and right boundaries with respect to the location of the pipe are sufficiently large and therefore boundary effects on calculated lateral resistance, displacement and soil failure mechanisms are not found. This has been verified by a number of FE analyses setting these boundaries at larger distances than those shown in Fig. 3.4. The pipe is pulled laterally, without any rotation, applying a displacement boundary condition at the reference point (center of the pipe). No additional boundary condition is applied in the vertical direction such that the pipe could displace in the vertical direction during lateral movement. The horizontal component of the reaction force at the reference point of the rigid pipe gives the lateral resistance.

The interface between pipe and soil is simulated using the contact surface approach available in Abaqus/Explicit. The Coulomb friction model is used for the frictional interface between the

outer surface of the pipe and sand. In this method, the friction coefficient (μ) is defined as $\mu=\tan(\phi_\mu)$, where ϕ_μ is the friction angle of the pipe-soil interface. The value of ϕ_μ depends on the interface characteristics and relative movement between the pipe and soil. The larger values of ϕ_μ represent the characteristics of rough uncoated pipes with rusty or corroded surfaces, while the lower values would correspond to pipes with smooth coating. The value of ϕ_μ lies between 50 and 100% of the peak friction angle (Yimsiri et al, 2004). A value of μ equal to 0.32 is used in this study.

The numerical analysis is conducted in two steps. In the first step, geostatic stress is applied under K_0=1 condition. The value of K_0 might be smaller than 1; however, a parametric study shows that K_0 does not have significant effects on lateral resistance (Jung et al. 2013). In the second step, the pipe is displaced in the lateral direction specifying a displacement boundary condition at the reference point of the pipe.

Abaqus does not have any direct option for modeling stress–strain behaviour using the proposed MMC model; therefore, in this study it is implemented by developing a user subroutine VUSDFLD written in FORTRAN. The stress and strain components are called in the subroutine in each time increment. From the stress components, p' is calculated. The strain components are transferred to the principal strain components and stored as state variables. The plastic strain increment ($\Delta\gamma^p$) in each time increment is calculated as $\Delta\gamma^p = (\Delta\varepsilon_1^p - \Delta\varepsilon_3^p)$, where $\Delta\varepsilon_1^p$and $\Delta\varepsilon_3^p$ are the major and minor principal plastic strain components, respectively. The value of γ^p is calculated as the sum of incremental $\Delta\gamma^p$ over the period of analysis. In the subroutine, γ^p and $p'$are defined as two field variables FV1 and FV2, respectively. In the input file, using Eqs. (3.1–3.8), the mobilized ϕ' and ψ are defined in tabular form as a function of γ^p and p'. During the analysis, the program accesses the subroutine and updates the values of ϕ' and ψ with field variables.

Two sets of FE analyses in the plane strain condition are performed for lateral displacement of the pipe. In the first set, analyses are performed for D=102 mm pipes and compared with Trautmann (1983) model test results, which is denoted the "model test simulation". In the second set, a parametric study is performed varying pipe diameter, burial depth and soil properties. In addition, triaxial test results are simulated for soil parameter estimation and also to examine the performance of the proposed MMC model.

3.5 FE simulation of triaxial test

Trautmann (1983) conducted a series of model tests to understand the mechanisms involved in lateral displacement of pipes buried in sand. The tests in dry dense sand are simulated in the present study. Cornell filter sand was used in these tests. These test results have been used by previous researchers to validate the performance of numerical modeling. For example, Yimsiri et al. (2004) simulated these tests using the MC and Nor-Sand models. For the Mohr-Coulomb model, they obtained the values of ϕ' and ψ from direct shear test results, assuming that the plane strain nature of pipeline–soil interaction problem is more consistent with direct shear than triaxial compression. However, ϕ'_p in PS could be approximately 5° higher than ϕ'_p in the direct shear condition (Pradhan et al. 1998; Lings and Dietz 2004). Yimsiri et al. (2004) also estimated the Nor-Sand model parameters by fitting FE simulation against the triaxial test results for Cornell filter sand (Turner and Kulhawy 1987).

To show the performance of the proposed MMC model, consider the same triaxial test on dense sand used by Yimsiri et al. (2004). Figure 3.5 shows the comparison between test results and FE simulations using three models: MC, Nor-Sand, and MMC. A CAX4 element in Abaqus is used in the FE modeling. The Young's modulus is calculated using Eq. (3.9) substituting p' for

confining pressure. As estimated by Yimsiri et al. (2004) for dense Cornell filter sand, constant ϕ'(=44°) and ψ(=16°) are used in the MC model. The FE simulation with Nor-Sand model is plotted from Yimsiri et al. (2004). The FE analysis with the present MMC model is performed using the VUSDFLD subroutine, as discussed in previous section, with triaxial condition in Eqs. (3.1) and (3.2). All other parameters used in the analysis are listed in Table 3.1.

Figure 3.5(a) shows that for the MC model q/p' increases with ε_a to the peak value and then remains constant because a constant ϕ' is used in the analysis. Figure 3.5(b) shows that volumetric compression occurs initially and then the soil dilates linearly, because a constant ψ is used. In other words, the constant strength and dilatancy criteria take over the stress–strain behaviour once it reaches the maximum stress ratio. As stated by Wood (2007), the MC model is sufficient if the failure is the only concern; however, its ability to match the complete mechanical response of a soil element is poor. Both strength and deformation behaviour of soil are equally important in the pipeline–soil interaction analysis. Therefore, an advanced model that considers the variation of strength of dense sand with shear deformation could give improved simulation results.

Unlike the simulation with the MC model, the shape of q/p'–ε_a and ε_v–ε_a curves using the Nor-Sand model is very similar to test results (Fig. 3.5). However, a complex VUMAT subroutine needs to be developed for the Nor-Sand model while the MMC can be implemented through a relatively simple user subroutine VUSDFLD as discussed above. As shown later, most of the features involved in pipeline–soil interaction could be simulated using the proposed MMC model. In addition, the pre-peak hardening behaviour is considered in the present MMC model.

The simulations with the MMC model are performed for two sets of A_ψ and k_ψ values in Eqs. 3.1 and 3.2, respectively. First, A_ψ=3 and k_ψ=0.5 (Bolton 1986) is used. Chakraborty and Salgado (2010) showed that A_ψ=3.8 and k_ψ=0.6 match better the triaxial test results on Toyoura sand at low

stresses. Therefore, FE simulation is performed also with A_ψ=3.8 and k_ψ=0.6 to show their effects. As shown in Fig. 3.5(a), the proposed MMC model can successfully simulate the stress–strain behaviour. Calculated q/p' nonlinearly increases with ε_a, reaches the peak, and then decreases in the post-peak region. Volumetric compression occurs initially and then the specimen expands nonlinearly with ε_a (Fig. 3.5b). At large ε_a, $\Delta\varepsilon_v/\Delta\varepsilon_a$=0, which is different from the simulation with the MC model that calculates constant $\Delta\varepsilon_v/\Delta\varepsilon_a$ when the soil element is at the plastic state. As shown Fig. 3.5, the simulated results with the MMC model match well with the test results not only the peak (like the MC model) but also for a wide range of strains encountered in the pipeline–soil interaction analysis as presented in the following sections. It can be also concluded that the parameters listed in Table 3.1 can simulate the stress–strain behaviour of this sand. Adjustments to the values of A_ψ and k_ψ could improve matching between FE simulations and test results; however, that is not the aim of the present study.

The effects of σ_c and D_r on stress–strain behaviour are also investigated. Figure 3.6(a) shows the variation of q/p' with ε_a for 4 different confining pressures (σ_c=20, 40, 80 and 120 kPa) for D_r=80%. The maximum stress ratio $(q/p')_{max}$ decreases with σ_c because dilation is suppressed by confining pressure. The magnitude of ε_a at $(q/p')_{max}$ increases with σ_c. Under lower confining pressures, the post-peak degradation of q/p' occurs quickly. Figure 3.6(b) shows that the magnitude and rate of development of ε_v depend on confining pressure. The soil specimens compress initially (i.e. positive ε_v) and then dilate after reaching the maximum ε_v. For lower σ_c, dilation starts at smaller value of ε_a. Moreover, the rate of dilation and maximum volumetric expansion decrease with σ_c. The variations of q/p' and ε_v obtained from FE simulations using the proposed MMC model (Figs. 3.6a and 3.6b) are very similar to typical triaxial test results on dense sand as shown in Fig. 3.1(a) and 3.1(b).

Figure 3.7 shows the results of FE simulations for 4 relative densities (D_r=70%, 80%, 90% and 100%) under the same σ_c (=40 kPa). Figure 3.7(a) shows that $(q/p')_{max}$ increases and ε_a at $(q/p')_{max}$ decreases with D_r. As expected, higher dilation is calculated for higher relative densities. Similar effects of D_r on stress–strain behaviour were obtained in laboratory tests reported by previous researchers (e.g. Lee 1965).

It is also to be noted here that the simulation of drained triaxial tests with the MMC model gives a nonlinear critical state line in the e–lnp' space.

In summary, the above simulations show that the proposed MMC model can successfully simulate both pre- and post-peak behaviour of dense sand including the effects of confining pressure and relative density. This model is primarily used for pipeline–soil interaction analyses presented in the following sections, although some analyses with the MC model are performed for comparison.

3.6 Model test simulation results

Figure 3.8 shows the variation of dimensionless lateral force N_h (=$F/\gamma HD$) with dimensionless lateral displacement u/D for two burial depths (H/D=1.5 and 5.5). Here F is the lateral force on the pipe per metre length, H is the depth of the centre of the pipe, γ is the unit weight of sand and u is the lateral displacement. The peak value of N_h is defined as N_{hp} and the lateral displacement required to mobilize N_{hp} is defined as u_p. Analyses are performed for the plane strain condition (A_ψ=5 and k_ψ=0.8 in Eq. 3.1 and 3.2, respectively) using the user subroutine VUSDFLD. Using the initial mean effective stress at the centre of the pipe the Young's modulus (E) is calculated from Eq. (3.9), which implies that E increases with D_r and H. The results of two model tests of similar conditions (Test-22 and 24) from Trautmann (1983) are also plotted in this

figure. The force–displacement curves obtained from the FE analysis with the MMC model match very well for a wide range of lateral displacements. For H/D=1.5, the dimensionless force reaches the peak and then remains almost constant. However, for H/D=5.5, the dimensionless force reaches the peak and then decreases with further lateral displacement. The model tests conducted by Audibert and Nyman (1977) using a 25 mm diameter pipe buried in dense Carver sand also show similar response—no post-peak degradation of N_h for shallow depths (H=1.5D and 3.5D) but significant post-peak degradation for deep burial conditions (H=6.5D and 12.5D).

The difference between the shape of the force–displacement curves could be explained further using mobilized ϕ' and ψ along the shear bands and their formation. The role of ϕ' is easily understood—the higher the ϕ' the higher the force, provided all other conditions remain same. Figure 3.9(a) shows γ^p at u/D=0.12 (i.e. after the peak) for simulation with the MMC model. The solid lines through the highly concentrated γ^p zone are drawn for further investigation of the location of the shear bands for various conditions. To explain the role of ψ, two more analyses are performed using the MC model for two values of ψ (=16° and 25°) but constant ϕ' (=44°) for H/D=1.5. The force–displacement curve for ψ=16° in Fig. 3.8 shows that N_h increases with displacement and reaches the peak of N_{hp}=8.4. For ψ=25°, N_{hp}=8.8 (not plotted in Fig. 3.8). Similar to Fig. 3.9(a), the locations of the shear bands are obtained for u/D=0.12 and plotted in Fig. 3.9(b). The shear bands for ψ=25° are located outside the shear bands with ψ=16°, which implies that with increase in ψ the size of the failure wedge increases and that in turn produces higher N_{hp}.

In the MMC model, ψ is not constant but varies with plastic shear strain (Fig. 3.3). Therefore, in the simulations with the MMC, shear band formation due to post-peak reduction of shear strength initiates when γ^p exceeds γ_p^P. With increase in lateral displacement of the pipe, strain concentration further increases in the previously formed shear band; however, no significant

change in the location and orientation of the shear band is found in this case although ψ gradually reduces to zero at large γ^p. To verify this, analyses have been performed with ψ=0 and $\phi'=\phi'_c=35°$ and a smaller failure wedge is found as shown in Fig. 3.9(b) and this gives N_{hp}=6.45. In other words, the mobilized dilation angle during the initiation of the shear band influences the shape of the failure wedge and thereby the reaction force.

Figure 3.9(a) also shows that the shear band reaches the ground surface at a displacement near the peak. At this stage, the γ^p in the major portion of the shear band is sufficiently high to reduce ϕ' almost to ϕ'_c and ψ to 0. Because ϕ' and ψ do not decrease with further increase in γ^p, the N_h remains almost constant between u/D=0.1 and 0.4. However, if analysis is simplified by using $\phi'=\phi'_c$ and ψ=0, a smaller failure wedge forms which gives lower reaction force.

The shear band formation for H/D=5.5 is different from that of H/D=1.5. The calculated γ^p using the MMC model at u/D=0.12 is shown in Fig. 3.10(a). The mobilized ϕ' and ψ at this stage are shown in Figs. 3.10(b) and 3.10(c), respectively. As shown in Fig. 3.3, the maximum values of ϕ' and ψ are mobilized at γ^p_p, and therefore $\phi' < \phi'_p$ and $\psi < \psi_p$ in the pre-peak ($\gamma^p < \gamma^p_p$) and also in the post-peak ($\gamma^p > \gamma^p_p$) conditions. In Figs. 3.10a–c, the post-peak condition ($\gamma^p > \gamma^p_p$) is developed in the shear bands near the pipe (colored zone), while in the potential shear band above this (gray zone) some plastic shear strains develop ($\gamma^p < \gamma^p_p$) but these remain in the pre-peak shear zone. In the colored segments of the shear bands in Figs. 3.10(b) and 10(c), the mobilized ϕ' and ψ are in the post-peak while in the gray segments they are in the pre-peak zone. Unlike the simulation for H/D=1.5 (Fig. 3.9a), large segments of the plastic shear zone are in the pre-peak condition (gray) which will gradually change to the post-peak condition with increasing γ^p due to lateral displacement of the pipe. As the strength of the soil is reduced with γ^p, the post-peak

degradation of N_h is calculated for this H/D (Fig. 3.8). As the post-peak softening of stress–strain behaviour is not considered, the MC model cannot simulate the degradation of N_h after the peak as shown in Fig. 3.8.

In summary, the above analyses with the proposed MMC model show not only superior simulation of the force–displacement response but also explain the possible mechanisms involved through close examination of the roles of model parameters and burial depth. The peak force could be matched using representative values of ϕ' and ψ in the MC model. However, if the variation of mobilized ϕ' and ψ with plastic shear strain and mean effective stress is considered the insight into the mechanisms of pipeline–soil interaction could be better explained.

However, it is to be noted here that FE mesh size influences the results when the analyses involve with post-peak softening behavior of soil. Gylland (2012) presented a summary of regularization techniques available in the literature to reduce mesh dependent effects. Robert (2010) used a simple element size scaling rule for pipeline–soil interaction analysis. An improved regularization technique, considering the orientation of the curved shear bands, might give better results. This has not been studied in detail, which is the limitation of the present study.

3.7 Parametric study

Guo and Stolle (2005) compiled a large number of test results from 11 experimental studies and showed that various factors (e.g. H, D, D_r, ϕ') influence the dimensionless force N_h. A parametric study is presented in this section in which only one parameter is varied while the other parameters are kept constant as listed in Table 3.1, unless otherwise mentioned.

3.7.1 Effect of *H*/*D*

The *H*/*D* ratio could be varied by changing the value of *H* or *D* or both. To show the effects of *H*/*D*, a total of 10 FE analyses are conducted with the MMC model for the following configurations: (i) *D*=102 mm, *H*/*D*=1.5, 5.5, 6, 10; (ii) *D*=150 mm, *H*/*D*=4, 6; (iii) *D*=300 mm, *H*/*D*=2, 4, 6, 10.

Figure 3.11 shows the force–displacement curves for a given *H*/*D* (=6) but for three different diameters. At u_p, the mean effective stress p' around the pipe is higher for larger diameter pipe. The higher p' has two effects: (i) lower mobilized ϕ' and ψ, and (ii) higher γ_p^p required to mobilize ϕ_p' and ψ_p (cf. Fig. 3.3 and 3.6a). Because of these two reasons, the N_{hp} reduces and u_p/D increases with diameter. Compiling the results of model tests in dense sand, Guo and Stolle (2005) showed the trend of decreasing N_{hp} with increase in *D*. This implies that the present FE analyses could successfully simulate this trend.

Figures 3.12 and 3.13 show the effects of *H* and *D* on force–displacement curves when one of them is varied keeping the other one fixed. The increase of *H* or reduction of *D*, increases the *H*/*D* ratio. In both cases (Figs. 3.12 and 3.13) N_{hp} and u_p/D increase with *H*/*D*, which is consistent with model tests and FE results (Audibert and Nyman 1977; Trautmann 1983; Guo and Stolle 2005).

The peak dimensionless force N_{hp} is one of the main parameters used in current pipeline design practice. The calculated values of N_{hp} with the MMC model are plotted with *H*/*D* ratio on Fig. 3.14. For comparison, the results of physical model tests and some FE analyses available in the literature are also plotted on this figure. The N_{hp} increases with *H*/*D*. The present FE analyses calculate lower rate of increase of N_{hp} at higher *H*/*D* ratio. This trend is similar to the model tests of Dickin and Leung (1985). As discussed before, p' around the pipe increases with depth of burial,

and that reduces the mobilized ϕ' and ψ which in turn results in lower N_{hp}. If ϕ' and ψ are independent of p', higher values of N_{hp} could be obtained especially for larger H/D as shown in Fig. 3.14 calculated by Yimsiri et al. (2004) with the MC model and Jung et al. (2013) who used the MC model with post-peak softening. It is to be noted here that Guo and Stolle (2005) also investigated the effects of pressure dependency and showed a significant increase in N_{hp} at low H/D when ϕ'_p increases with p' and ψ remains constant. However, with the present MMC model, such increase of N_{hp} at low H/D is not found because the maximum limit of I_R=4 is used (Bolton 1986; White et al. 2008) and in all the analyses with the MMC model ψ varies with plastic shear strain. A comparison between the results for D=102 mm and 300 mm shows that a lower pipe diameter gives consistently higher N_{hp} at a given H/D, which is consistent with the model test results compiled by Guo and Stolle (2005) and Dickin and Leung (1985) as shown in Fig. 3.14. The possible reasons behind this are explained in previous sections.

3.7.2 Effect of model parameters A_ψ and k_ψ

As discussed in Section 3.3.1, for the PS condition Bolton (1986) recommended A_ψ=5.0 for use in Eq. (3.1). Analyzing test results on Toyoura sand, Chakraborty and Salgado (2010) recommended A_ψ=3.8 for both TX and PS conditions. Figure 3.15 shows the force–displacement curves for A_ψ=3.8 and 5.0 for different H/D but the same pipe diameter (D=300 mm). For a given I_R, ϕ'_c and k_ψ, the peak friction angle ϕ'_p and dilation angle ψ_p increase with A_ψ as defined in Eqs. (3.1) and (3.2), which increase the mobilized ϕ' and ψ (Eqs. 3.5–3.8). Because of this, N_{hp} increases with A_ψ. Moreover, u_p/D also increases with A_ψ.

The soil failure due to lateral displacement of a buried pipe is generally categorized into two simple modes, namely the “wedge” mode in shallow burial conditions and the “plow through”

mode in deep burial conditions (e.g. O'Rourke and Liu, 2012). For shallow burial in dense sand, the drained lateral displacement of the pipe results in upward and lateral movement of a soil wedge that is assumed to slide along either a straight (triangular wedge) or curved (log-spiral wedge) line. On the other hand, for deep burial conditions, the lateral movement of the pipe results in soil flow around the pipe with negligible deformation at the ground surface. Further discussion on failure mechanisms is provided in the following sections.

A close examination of progressive development of shear bands shows that for H/D=2 and 4 the wedge while for H/D=10 the plow through mode governs the response. For H/D=6, wedge type of failure occurs when A_ψ=3.8 is used, while the failure is very similar to plow through mode for A_ψ=5.0. In other words, in the transition zone (from shallow to deep) the failure mechanism is influenced by this parameter, and therefore a significant difference between calculated N_h is found for H/D=6.

Similar to A_ψ, different values of k_ψ were obtained from test results on different sands (Bolton 1986; Chakraborty and Salgado 2010; Xiao 2014). Figure 3.16 shows the force–displacement curves for three different values of k_ψ. For a given $\phi'_p - \phi'_c$, the value of ψ_p increases with decrease in k_ψ (Eq. 3.2), which increases mobilized ψ (Eqs. 3.6 and 3.8). As discussed before, the size of the failure wedge increases with ψ, therefore the dimensionless force is higher for lower value of ψ as shown in Fig. 3.16.

3.7.3 Effect of relative density of sand

As the focus of the present study is to model the response of pipelines in dense sand, the effects of relative density are examined for D_r between 70% and 90% (Fig. 3.17). In the analyses, I_R in Eq. (3.1) is calculated for given D_r. In addition, the unit weight of sand for a given D_r is

calculated using specific gravity of sand G_s=2.74 and maximum and minimum densities of 15.5 and 18.3 kN/m^3 (Trautmann 1983). Figure 3.17 shows that N_{hp} increases with D_r. However, there is no significant difference between calculated N_h at large displacements for different D_r.

3.8 Failure Pattern

The soil failure mechanisms are explained using the formation of shear bands with lateral displacements. Figures 3.18(a–c) show the plastic shear strain (field variable FV1 in Abaqus) for three lateral displacements, shown by the points A, B and C in Fig. 3.13: (i) at N_{hp} (u/D=0.12) (ii) at moderate displacement (u/D=0.17), and (iii) at large displacement (u/D=0.4). At u/D=0.12, large plastic shear strains accumulate in narrow zones and two shear bands f_1 and f_2 are formed (Fig. 3.18a). With increase in displacement (e.g. u/D=0.17) the shear bands f_1 and f_2 propagate further upward and also an additional shear band f_3 is formed (Fig. 3.18b). At very large displacements (e.g. u/D=0.4) all the shear bands reach to the ground surface (Fig. 3.18c). In other words, the failure surfaces develop progressively and mobilized ϕ' and ψ in the shear band are not constant until large displacements when the soil reaches the critical state. The plastic shear strains in the soil elements outside the shear bands are negligible. Therefore, the soil elements bounded by f_1 and f_3 displace upward and left as a wedge while another wedge formed by the shear bands f_2 and f_3 sinks downward, which is shown by the instantaneous velocity vectors in the right column of Fig. 3.18. The shear bands in Fig. 3.18(c) are very similar to model tests of Turner (2004) in dense sand. Shear bands of almost similar pattern are also found in the FE simulations with the MMC model for $H/D \leq 6$. Moreover, as shown in Figs. 3.18(a)–(c), significant plastic strains develop in the shear band which could be successfully simulated using Abaqus/Explicit without numerical issues due to significant mesh distortion.

The soil failure mechanisms at large displacements for H/D=10 (Fig. 3.19) are different from Fig. 3.18. The plastic shear strain concentration mainly occurs near the pipe instead of reaching the ground surface. The shear bands are not symmetric above and below the centre of the pipe rather the shear bands propagate more above the pipe. Behind the pipe, the plastic shear strains develop in a relatively large zone and sand moves into the gap created by pipe displacements. The instantaneous velocity vectors show that the soil element flow mainly occurs above the pipe. Jung et al. (2013) suggested that burial depths of 15–23D are required for the symmetric flow of soil around the pipe. As the burial depth considered in this study is not sufficient for flow around mechanism, N_{hp} increases monotonically with H/D even at H/D=10 (Fig. 3.14), which should approach a horizontal asymptote at large H/D (Jung et al. 2013).

3.9 Conclusions

The response of buried pipelines subjected to lateral ground movement is critical for safe and reliable design of pipelines. In this study, the lateral pipeline–soil interaction is investigated using comprehensive FE analyses. One of the key components that significantly influences the success of FE analyses of pipeline–soil interaction is the constitutive behaviour used for modeling the soil. In this study, a modified Mohr-Coulomb (MMC) model is proposed which has limited complexity but sufficient to capture most of the important features of stress–strain behaviour of dense sand such as the nonlinear pre- and post-peak variation of the angle of internal friction and dilation angle with plastic shear strain, loading conditions, density and mean effective stress. A method to implement the MMC in Abaqus using a user subroutine is presented. The FE results with the MMC are compared with FE results obtained with the conventional Mohr-Coulomb (MC) model and experimental results. The following conclusions can be drawn from this study.

a) The failure surfaces develop progressively with lateral displacement of the pipe. The mobilized ϕ' and ψ are not constant along the shear bands although constant values are used in the conventional MC model.

b) The shear band formation and the mobilized values of ϕ' and ψ along the shear band significantly influence the shape of the force–displacement curves. For the same sand, post-peak degradation of N_h is observed at intermediate burial depth (e.g. H/D=5.5 in Fig. 3.8), while N_h remains almost constant for shallow depths (e.g. H/D=1.5). The present MMC model is shown capable of simulating this.

c) The mobilized dilation angle ψ significantly influences the shape of the failure wedge and thus the reaction force on the pipeline.

d) The variation of calculated peak dimensionless force (N_{hp}) with H/D using the present MMC model is consistent with previous experimental results and numerical analyses; however, the pressure and plastic shear strain dependency of ϕ' and ψ in the MMC model gives better simulation of lateral resistance (N_h) for a wide range of lateral displacements including the post-peak reduction of N_h.

e) The depth of embedment for transition from shallow to deep failure mechanisms is influenced by the soil parameters A_ψ. For a higher value of A_ψ, the plow through mechanism develops at shallower depths resulting in higher lateral resistance.

Acknowledgements

The works presented in this paper have been supported by the Research and Development Corporation of Newfoundland and Labrador and the Natural Sciences and Engineering Research Council of Canada (NSERC).

List of symbols

The following abbreviations and symbols are used in this paper:

TX	Triaxial
PS	Plane strain
DS	Direct shear
MC	Mohr-Coulomb model with constant ϕ' and ψ
MMC	Modified Mohr-Coulomb model with mobilized ϕ' and ψ as Fig. 3.3
A_ψ	Slope of $(\phi'_p - \phi'_c)$ vs. I_R in Eq.(1)
m,C_1,C_2	Soil parameter (Eqs. 3 and 4)
D	Pipeline diameter
E	Young's modulus
H	Distance from ground surface to the centre of pipe
I_R	Relative density index
K	Material constant
K_0	Earth pressure coefficient at rest
N_h	Lateral dimensionless force
N_{hp}	Peak lateral dimensionless force
Q, R	Material constant (Bolton 1986)
k_ψ	Slope of $(\phi'_p - \phi'_c)$ vs. ψ_p in Eq. (2)
p'	Mean effective stress
q	Deviatoric stress
u	Lateral displacement of pipe
u_p	Lateral displacement at N_{hp}

μ	Friction coefficient between pipeline and soil
ν	Poisson's ratio
ε_a^p	Axial strain at the peak stress ratio
ε_1^p	Major principal plastic strain
ε_3^p	Minor principal plastic strain
σ_c	Confining pressure
ϕ'	Mobilized angle of internal friction
ϕ'_{in}	ϕ' at the start of plastic deformation
ϕ'_p	Peak friction angle
ϕ'_c	Critical state friction angle
ϕ'^{PS}_p	Peak friction angle in plane strain condition
ϕ'^{TX}_p	Peak friction angle in triaxial condition
ϕ'^{DS}	Angle of internal friction in direct shear test
ϕ'^{DS}_p	Peak friction angle in direct shear condition
ϕ_μ	Pipe-soil interface friction angle
ψ	Mobilized dilation angle
ψ_p	Peak dilation angle
ψ_{in}	ψ at the start of plastic deformation (=0)
γ^p	Engineering plastic shear strain
γ_p^p	γ^p required to mobilize ϕ'_p
γ_c^p	Strain softening parameter

References

Ahmed, S.M.U. 1973. A study of the influence of confining pressure on the behaviour of sands. M.Sc. Thesis, McGill University, Montreal, Canada.

Almahakeri, M., Fam, A., and Moore, I.D. 2012. The flexural behaviour of buried steel and composite pipes pulled relative to dense sand: experimental and numerical investigation. 9th Int. Conf. on Pipelines IPC2012, September 24−28, Calgary, AB, Canada. IPC 2012-90158. pp. 9.

Almahakeri, M., Fam, A., and Moore, I.D. 2014. Experimental investigation of longitudinal bending of buried steel pipes pulled through dense sand. Journal of Pipeline Systems Engineering and Management, ASCE, **5**(2). doi: 10.1061/(ASCE)PS.1949-1204.0000141.

Almahakeri, M., Fam, A., and Moore, I.D. 2013. Longitudinal bending and failure of GFRP pipes buried in dense sand under relative ground movement. Journal of Composites for Construction, ASCE, **17**(5):702−710.

American Lifelines Alliance. 2005. Seismic design guidelines for water pipelines. American Lifelines Alliance in partnership with the Federal Emergency Management Agency, Washington, D.C. Available from www.americanlifelinesalliance.org [accessed 4 April 2015].

Audibert, J.M.E., and Nyman, K.J. 1978. Soil restraint against horizontal motion of pipes. International Journal of Rock Mechanics and Mining Sciences and Geomechanics Abstracts, **15**(2): A29−A29.

Bishop, A. W. 1961. Discussion on soil properties and their measurement. Proceedings of 5th Int. Conf. on Soil mechanics and Foundation engineering, vol. III.

Bolton, M. D. 1986. The strength and dilatancy of sands. Geotechnique, **36**(1):65−78.

Burnett, A. J. 2015. Investigation of full scale horizontal pipe–soil interaction and large strain behaviour of sand. MASc. thesis, Queen's University, Kingston, Ontario, Canada.

Chakraborty, T., and Salgado, R. 2010. Dilatancy and shear strength of sand at low confining pressures. Journal of Geotechnical and Geoenvironmental Engineering, **136**(3):527−532.

Conforth, D.H. 1964. Some experiments on the influence of strain conditions on the strength of sand. Geotechnique, **14**:143−167.

Dafalias, Y. F., and Herrmann, L. R. 1982. Bounding surface formulation of soil plasticity. Soil Mechanics–Transient and Cyclic Loads. Pande, G. N. and Zienkiewicz, O. C., Eds., John Wiley and Sons, New York, NY.

Dafalias, Y. F., and Manzari, M. 2004. Simple plasticity sand model accounting for fabric change effects. ASCE Journal of Engineering Mechanics, **130**(6): 622−634.

Daiyan, N., Kenny, S., Phillips, R., and Popescu, R. 2011. Investigating pipeline–soil interaction under axial–lateral relative movements in sand. Canadian Geotechnical Journal, **48**(11):1683−1695.

Davis, E. H. 1968. Theories of plasticity and the failure of soil masses. In Soil mechanics: Selected topics (ed. I. K. Lee), London: Butterworth. pp. 341–380.

Dickin, E.A., and Leung, C.F. 1983. Centrifugal model tests on vertical anchor plates. Journal of Geotechnical Engineering, **109**(12):1503−1525.

DNV 2007 (Det Norske Veritas). DNV-OS-F101. Available from: https://exchange.dnv.com/servicedocuments/dnv/ [accessed 4 April 2015].

Ellis, E.A., and Springman, S.M. 2001. Modelling of soil-structure interaction for a piled bridge abutment in plane strain FEM analyses. Computers and Geotechnics, **28**(2):79–98. doi:10.1016/S0266-352X(00)00025-2.

Gajo, A., and Muir Wood, D. 1999. A kinematic hardening constitutive model for sands: the multiaxial formulation. International Journal for Numerical and Analytical Methods in Geomechanics, **23**(9): 925–965.

Guo, P., and Stolle, D. 2005. Lateral pipe-soil interaction in sand with reference to scale effect. Journal of Geotechnical and Geoenvironmental Engineering, **131**(3):338−349.

Gylland AS. 2012. Material and slope failure in sensitive clays. PhD thesis, Norwegian University of Science and Technology.

Hardin, B .O., and Black, W. L. 1966. Sand stiffness under various triaxial stress. Journal of the Soil Mechanics and Foundations Division, ASCE, **92**(SM2):27−42.

Hashiguchi, K., and Ueno, M. 1977. Elastoplastic constitutive laws of granular materials, Constitutive Equations of Soils. Proc. 9th Int. Con5 Soil Mech. Found. Eng., Spec. Session S, eds. Murayama, S. and Schofield, A. N., JSSMFE, Tokyo. pp. 73−82.

Honegger, D., and Nyman, D.J. 2004. Guidelines for the seismic design and assessment of natural gas and liquid hydrocarbon pipelines. Pipeline Research Council International, Catalog No. L51927, October.

Houlsby, G.T. 1991. How the dilatancy of soils affects their behaviour. Invited Theme Lecture, Proceedings of the Tenth European Conference on Soil Mechanics and Foundation Engineering, Florence, May 27-30, Vol. 4, ISBN 90-5410-005-2. pp. 1189−1202.

Hsu, S.T., and Liao, H.J. 1998. Uplift behaviour of cylindrical anchors in sand. Canadian Geotechnical Journal, **35**(1):70–80.

Janbu, N. 1963. Soil compressibility as determined by oedometer and triaxial tests. Proceedings, European Conference on Soil Mechanics and Foundations Engineering, Wiesbaden, Germany, Vol. 1. pp.19−25.

Jardine, R. J. 1992. Nonlinear stiffness parameters from undrained pressuremeter Tests. Canadian Geotechnical Journal, **29**(3):436−447. doi: 10.1139/t92-048.

Jefferies, M., and Been, K. 2000. Soil liquefaction: a critical state approach. Taylor & Francis, New York.

Jung, J., O'Rourke, T., and Olson, N. 2013. Lateral soil-pipe interaction in dry and partially saturated sand. Journal of Geotechnical and Geoenvironmental Engineering, **139**(12): 2028−2036.

Jung, J., O'Rourke, T., and Olson, N. 2013. Uplift soil–pipe interaction in granular soil. Canadian Geotechnical Journal, **50**(7):744−753. doi: 10.1139/cgj-2012-0357.

Kolymbas, D, and Wu, W. 1990. Recent results of triaxial tests with granular materials. Powder Technology, **60**(2):99–119.

Kouretzis, G.P., Sheng, D., and Sloan, S.W. 2013. Sand-pipeline-trench lateral interaction effects for shallow buried pipelines. Computers and Geotechnics, **54**:53-59.

Kulhawy, F.H., and Mayne, P.W. 1990. Manual on estimating soil properties for foundation design. Report EPRI-EL 6800, Electric Power Research Institute, Palo Alto. pp. 306.

Lancelot, L, Shahrour, I, and Mahmoud, MA. 2006. Failure and dilatancy properties of sand at relatively low stresses. J. Eng. Mech, ASCE, **132**(12):1396 –1399.

Lee, K. L., and Seed, H. B. 1965. Drained strength characteristics of sands. Journal of the Soil Mechanics and Foundations Division, ASCE, **93**(6):117−141.

Lings, M. L., and Dietz, M. S. 2004. An improved direct shear apparatus for sand. Geotechnique, **54**(4):245−256.

Mitchell, J.K., and Soga, K., 2005. Fundamentals of soil behavior. 3rd Edition. John Wiley & Sons, Hoboken.

Moore, I.D. and Booker, J.R., 1987. Ground failure around buried tubes. International Journal of Rock Mechanics and Rock Engineering, **20**(4):243−260.

Mroz, Z. 1967. On the description of anisotropic work hardening. J. Mech. Phys. Solids. **15**:163−175.

O'Rourke, and M.J., Liu, X. 2012. Seismic design of buried and offshore pipelines. MCEER Monograph, MCEER-12-MN04.

Pike, K., Kenny, S., and Hawlader, B. 2013. Advanced analysis of pipe/soil interaction accounting for strain localization. Proceeding, GéoMontréal 2013, the 66th Canadian Geotechnical Conference and the 11th Joint CGS/IAH-CNC Groundwater Conference, Montreal, Canada.

Pradhan, T.B.S., Tatsuoka, F., and Horii, N. 1988. Strength and deformation characteristics of sand in torsional simple shear. Soils and Foundations, **28**(3):131−148.

Prevost, J.H. 1985. A simple plasticity theory for frictional cohesionless soils. Soil Dynamics and Earthquake Engineering, **4**(1): 9−17.

Qiu G, Henke S, and Grabe J. 2009. Applications of coupled Eulerian–Lagrangian method to geotechnical problems with large deformations. Proceeding of SIMULIA customer conference 2009, London, UK. pp. 420–435.

Robert, D. J. 2010. Soil-pipeline interaction in unsaturated soils. PhD thesis, University of Cambridge, United Kingdom.

Rowe, P. W. 1969. The relation between the shear strength of sands in triaxial compression, plane strain and direct shear. Geotechnique, **19**(1):75–86.

Scarpelli, G., Sakellariadi, E., and Furlani, G. 1999. Longitudinal pipeline–soil interaction: results from field full scale and laboratory testing. Twelfth European Conference on Soil Mechanics and Geotechnical Engineering. pp. 511.

Schanz, T., and Vermeer, P. A. 1996. Angles of friction and dilatancy of sand. Geotechnique, **46**(1):145–151.

Simoni, A., and Houlsby, G. T. 2006. The direct shear strength and dilatancy of sand-gravel mixtures. Geotechnical & Geological Engineering, **24**(3):523–549.

Taleb, B. and Moore, I.D., 1999. Metal culvert response to earth loading – Performance of two−dimensional analysis. Transportation Research Record No. 1656, Underground and Other Structural Design Issues. National Research Council, Washington. pp. 25−36.

Tatsuoka, F., Sakamoto, M., Kawamura, T., and Fukushima, S. 1986. Strength and deformation characteristics of sand in plane strain compression at extremely low pressures. Soils and Foundations, **26**(1):65–84.

Tatsuoka, F., Siddiquee, M. S. A., Park, C-S, Sakamoto, M. and Abe, F. 1993. Modeling stress–strain relations of sand. Soils and Foundations, **33**(2):60−81.

Taylor, D. W. 1948. Fundamentals of soil mechanics. New York: Wiley.

Trautmann, C. 1983. Behavior of pipe in dry sand under lateral and uplift loading. PhD thesis, Cornell University, Ithaca, NY.

Turner, J. P., and Kulhawy, F. H. 1987. Experimental analysis of drilled shaft foundations subjected to repeated axial loads under drained conditions. Rep. to Electric Power Research Institute, Cornell University, Ithaca, NY.

Turner, J.E. 2004. Lateral force–displacement behavior of pipes in partially saturated sand. M.S. Thesis, Cornell University, Ithaca, NY.

Vermeer, P. A. and de Borst, R. 1984. Non-associated plasticity for soils, concrete and rock. HERON, **29**(3):1−64.

White, D. J., Cheuk, C. Y., and Bolton, M. D. 2008. The uplift resistance of pipes and plate anchors buried in sand. Geotechnique, **58**(10), 771–777.

Wijewickreme, D., Karimian, H., and Honegger, D. 2009. Response of buried steel pipelines subjected to relative axial soil movement. Canadian Geotechnical Journal, **46**(7):735−735.

Wood, D. M. 2007. The magic of sands — The 20th Bjerrum Lecture presented in Oslo, 25 November 2005. Canadian Geotechnical Journal, **44**(11):1329−1350. doi: 10.1139/T07-060.

Xie, X. 2008. Numerical analysis and evaluation of buried pipeline response to earthquake-induced ground fault rupture. PhD thesis, Rensselaer Polytechnic Institute, New York.

Xiao, Y., Liu, H., Chen, Y., and Chu, J. 2014. Strength and dilatancy of silty sand. ASCE Journal of Geotechnical and Geoenvironmental Engineering, **140**(7).

Yimsiri, S., Soga, K., Yoshizaki, K., Dasari, G., and O'Rourke, T. 2004. Lateral and upward soil-pipeline interactions in sand for deep embedment conditions. Journal of Geotechnical and Geoenvironmental Engineering, **130**(8):830−842.

Yimsiri, S. and Soga, K. 2006. DEM analysis of soil–pipeline interaction in sand under lateral and upward movements at deep embedment. Journal of Southeast Asian Geotechnical Society, **37**:83−94.

Yoshimine, M. 2005. Archives–soil mechanics laboratory. Tokyo Metropolitan University, Retrieved from http://geot.civil.ues.tmu.ac.jp/archives/ [accessed 4 April 2015]

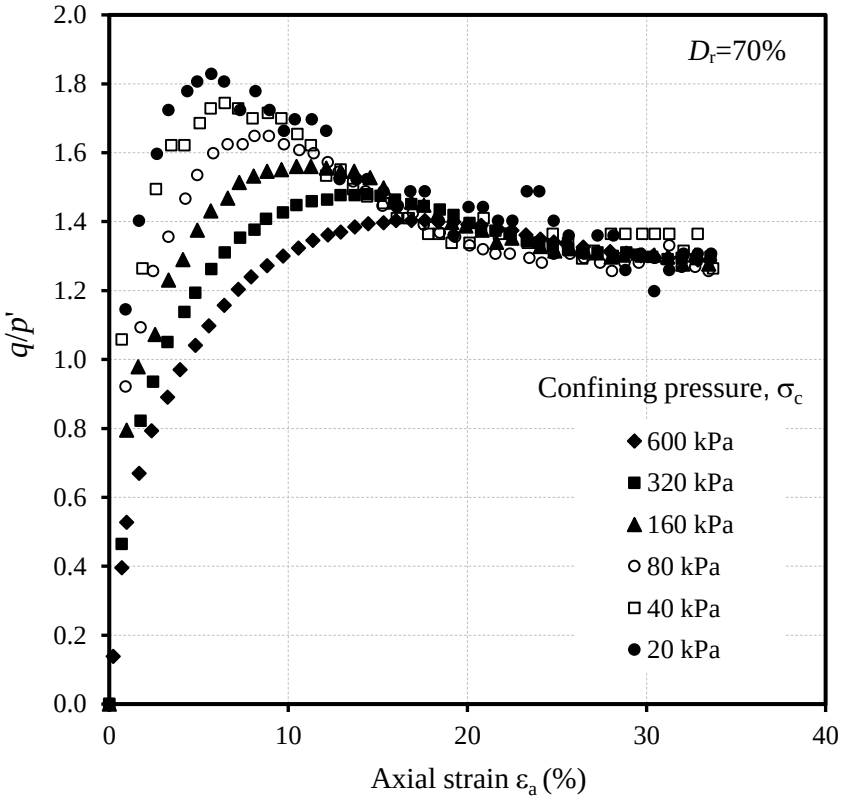

Fig. 3.1: Consolidated isotropically drained triaxial test results on dense sand (after Hsu and Liao 1998): (a) stress-strain behaviour

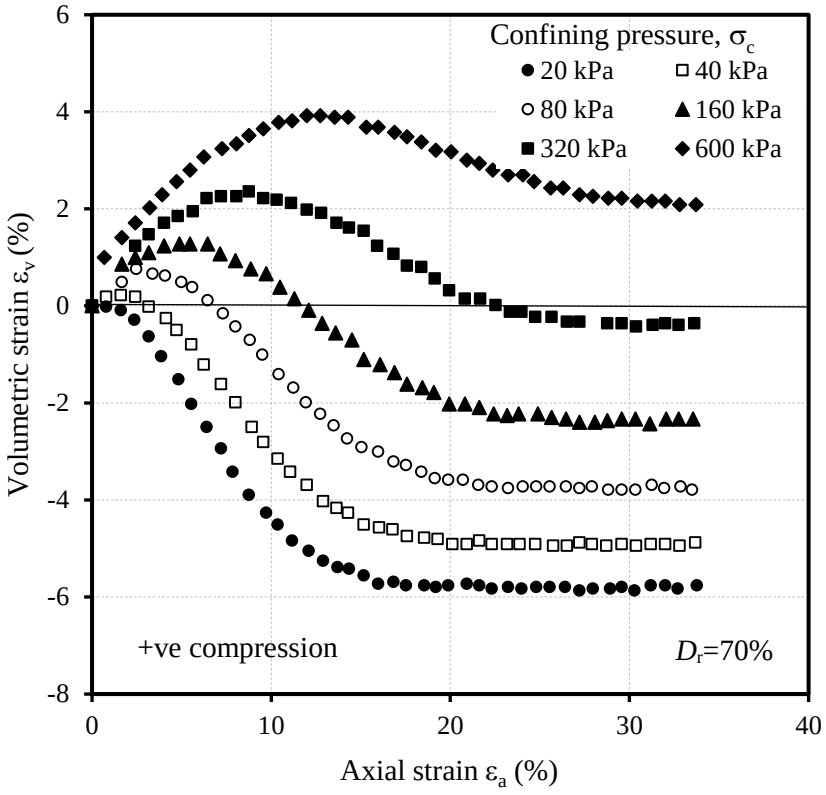

Fig. 3.1: Consolidated isotropically drained triaxial test results on dense sand (after Hsu and Liao 1998): (b) volume change behaviour

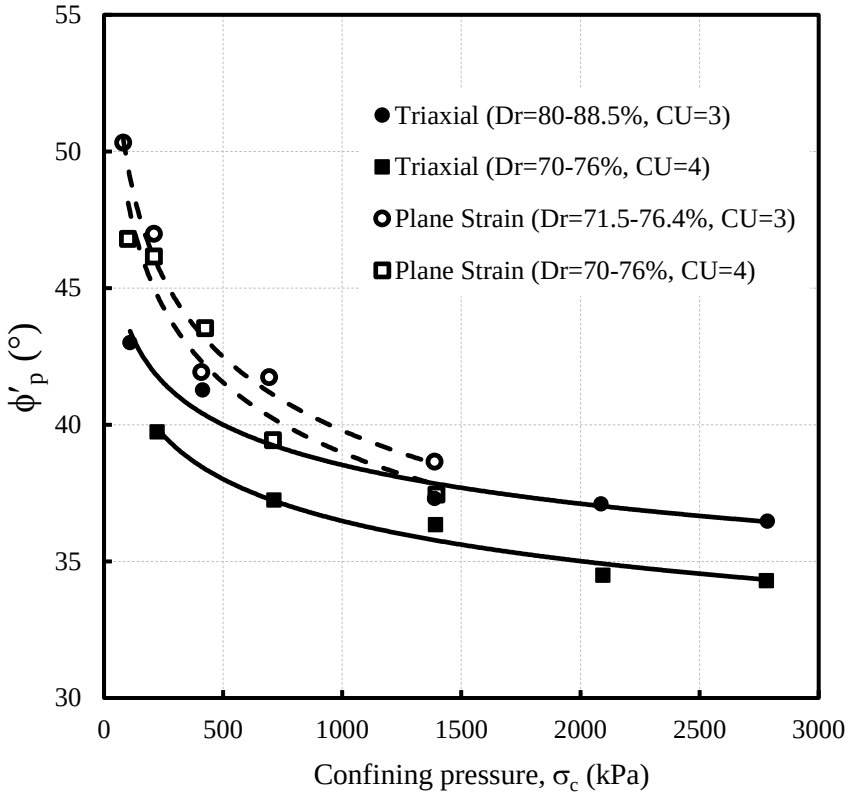

Fig. 3.2: Peak friction angle of crushed silica sand from triaxial and simple shear tests (after Ahmed 1973)

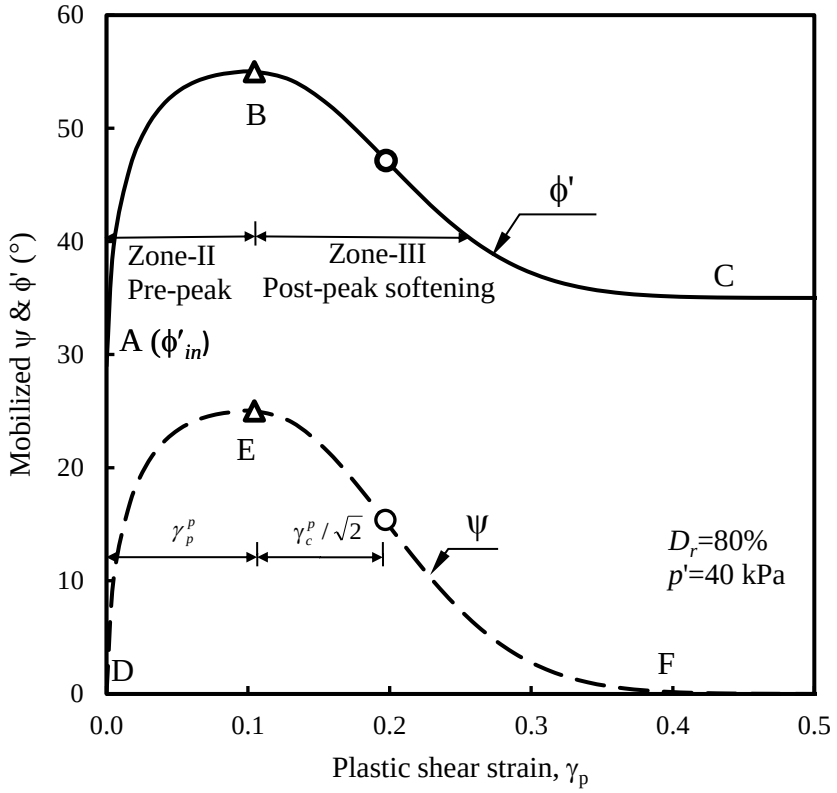

Fig. 3.3: Modeling of stress-strain behavior of dense sand using modified Mohr-Coulomb (MMC) model (plane strain condition)

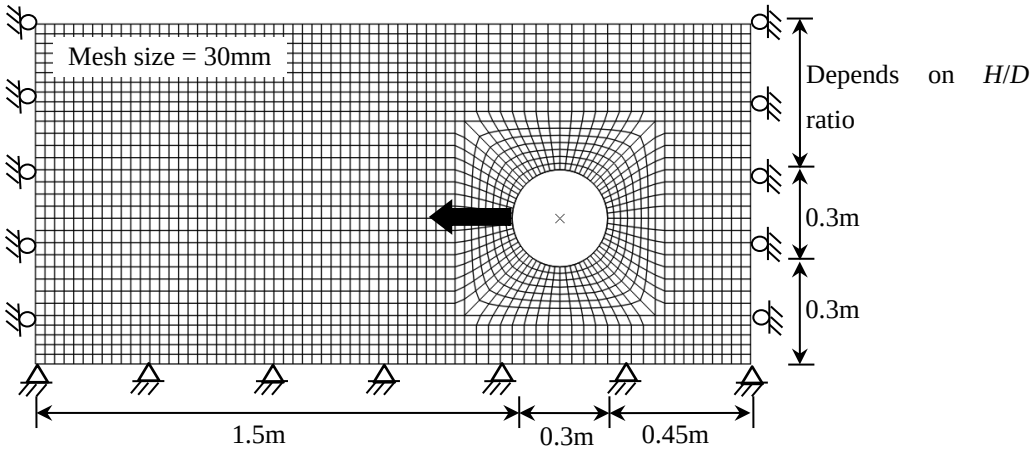

Fig. 3.4: Typical finite element mesh for H/D=2 and D=300 mm

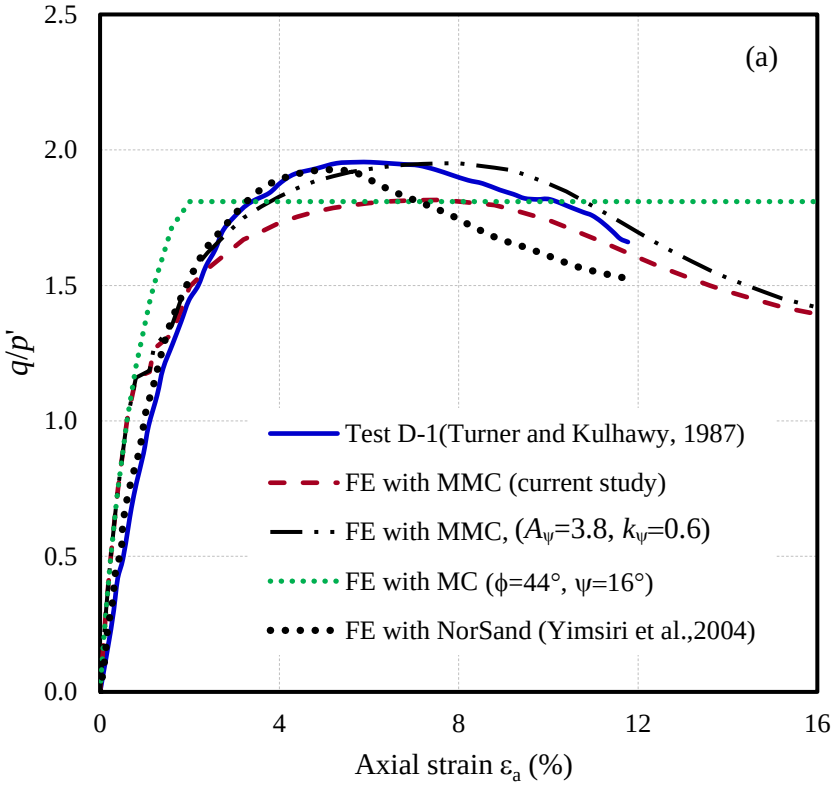

Fig. 3.5: Comparison of FE and triaxial compression tests results (σ_c=39 kPa, D_r=80%): (a) stress-strain behaviour

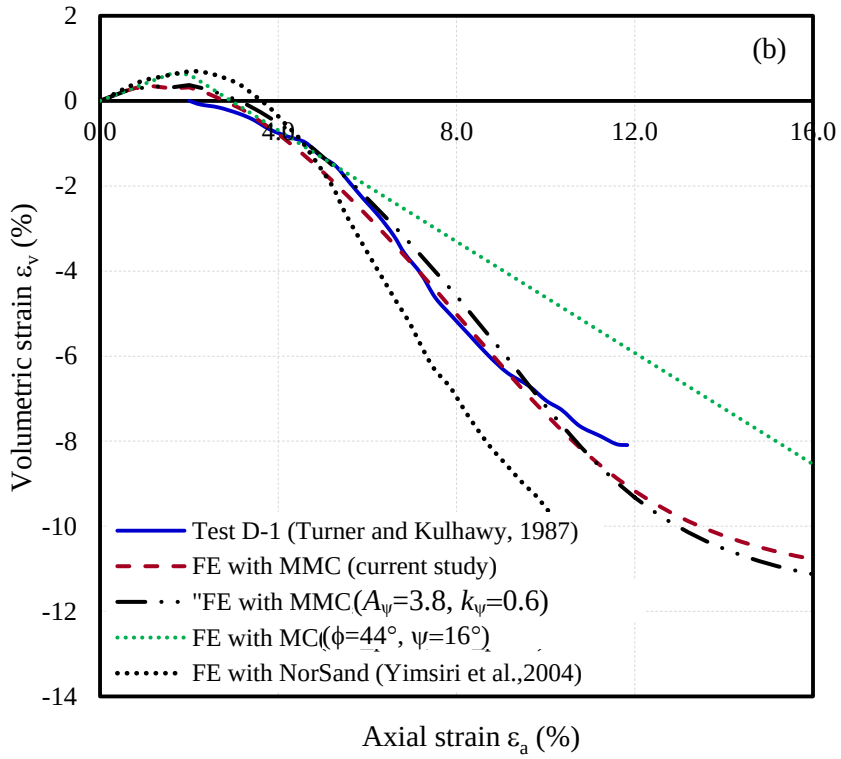

Fig. 3.5: Comparison of FE and triaxial compression tests results (σ_c=39 kPa, D_r=80%): (b) volume change behaviour

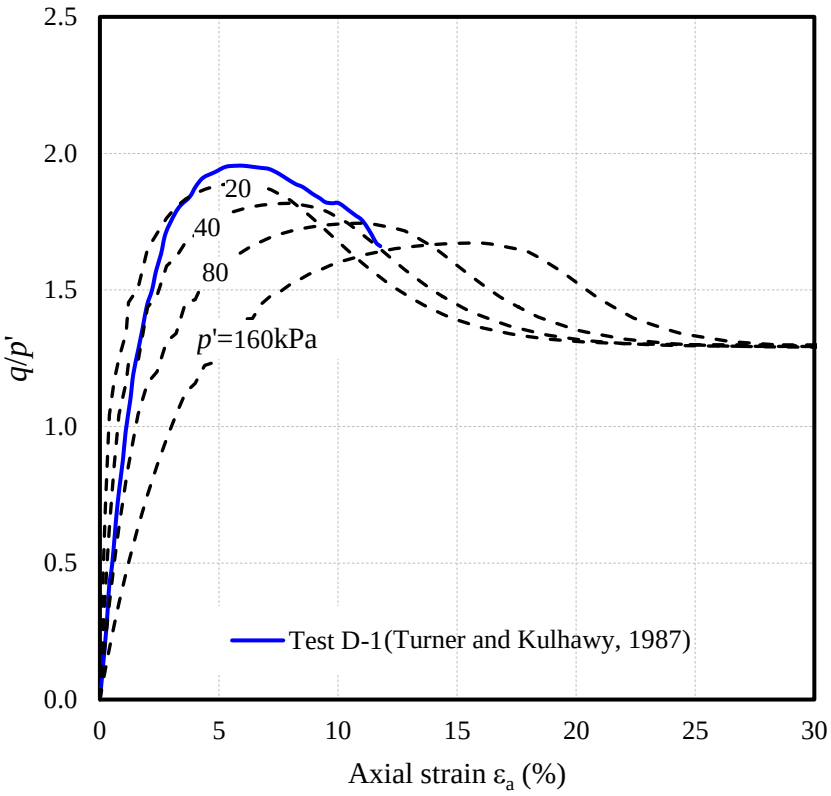

Fig. 3.6: Effect of confining pressure on triaxial tests (D_r=80%): (a) stress-strain behaviour

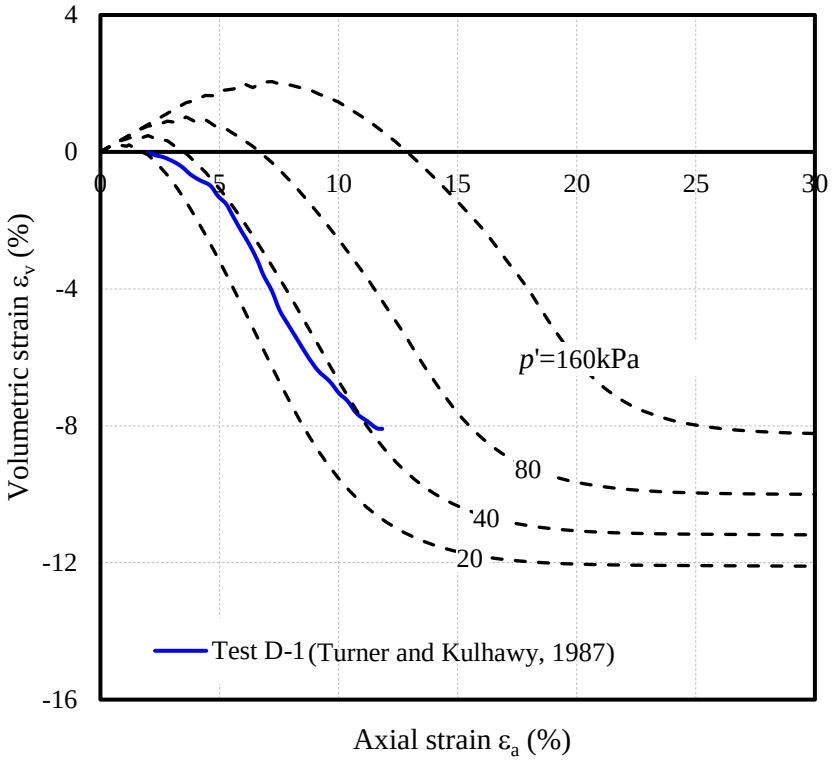

Fig. 3.6: Effect of confining pressure on triaxial tests (D_r=80%): (b) volume change behaviour

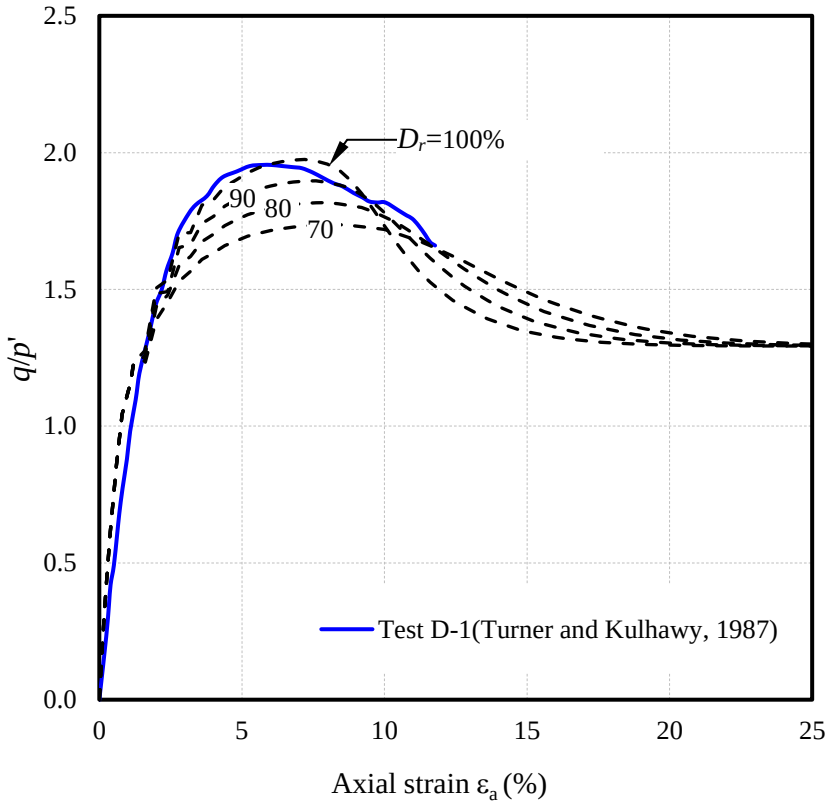

Fig. 3.7: Effect of relative density: (a) stress-strain behaviour

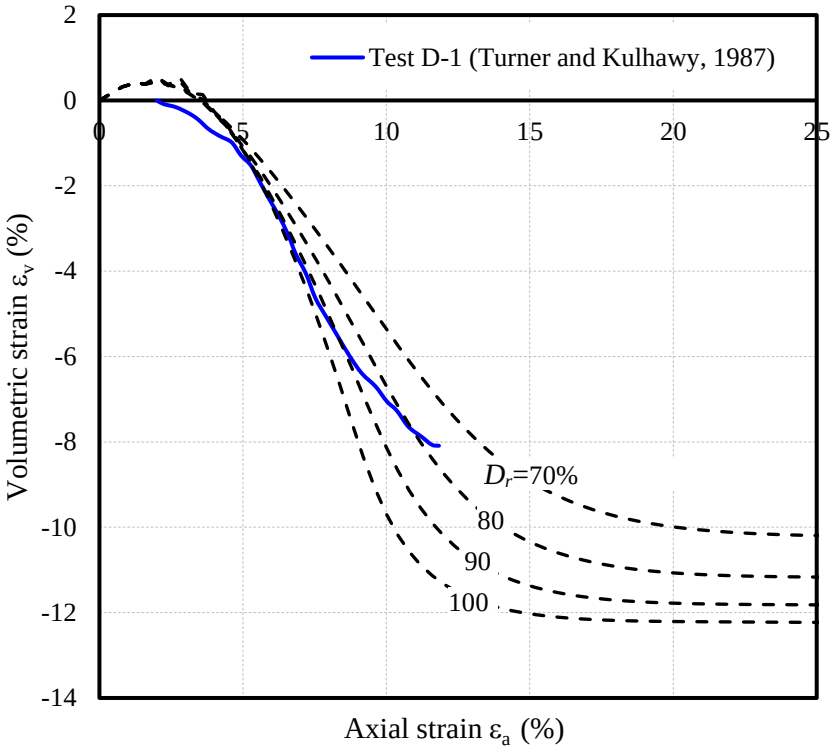

Fig. 3.7: Effect of relative density: (b) volume change behaviour

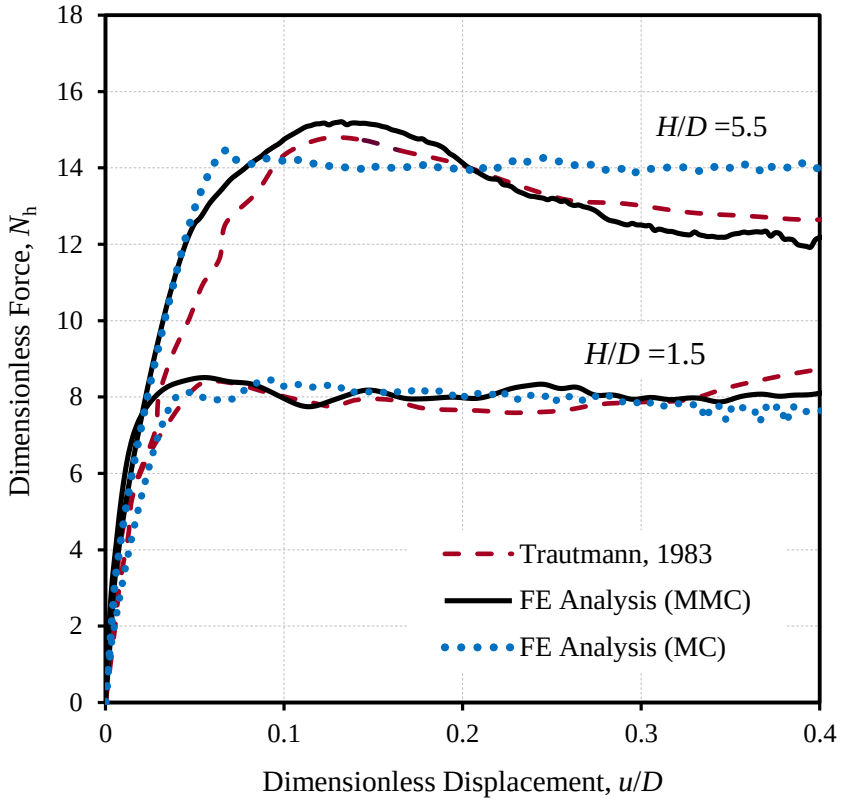

Fig. 3.8: Comparison of FE results with the large scale test results (Trautmann, 1983)

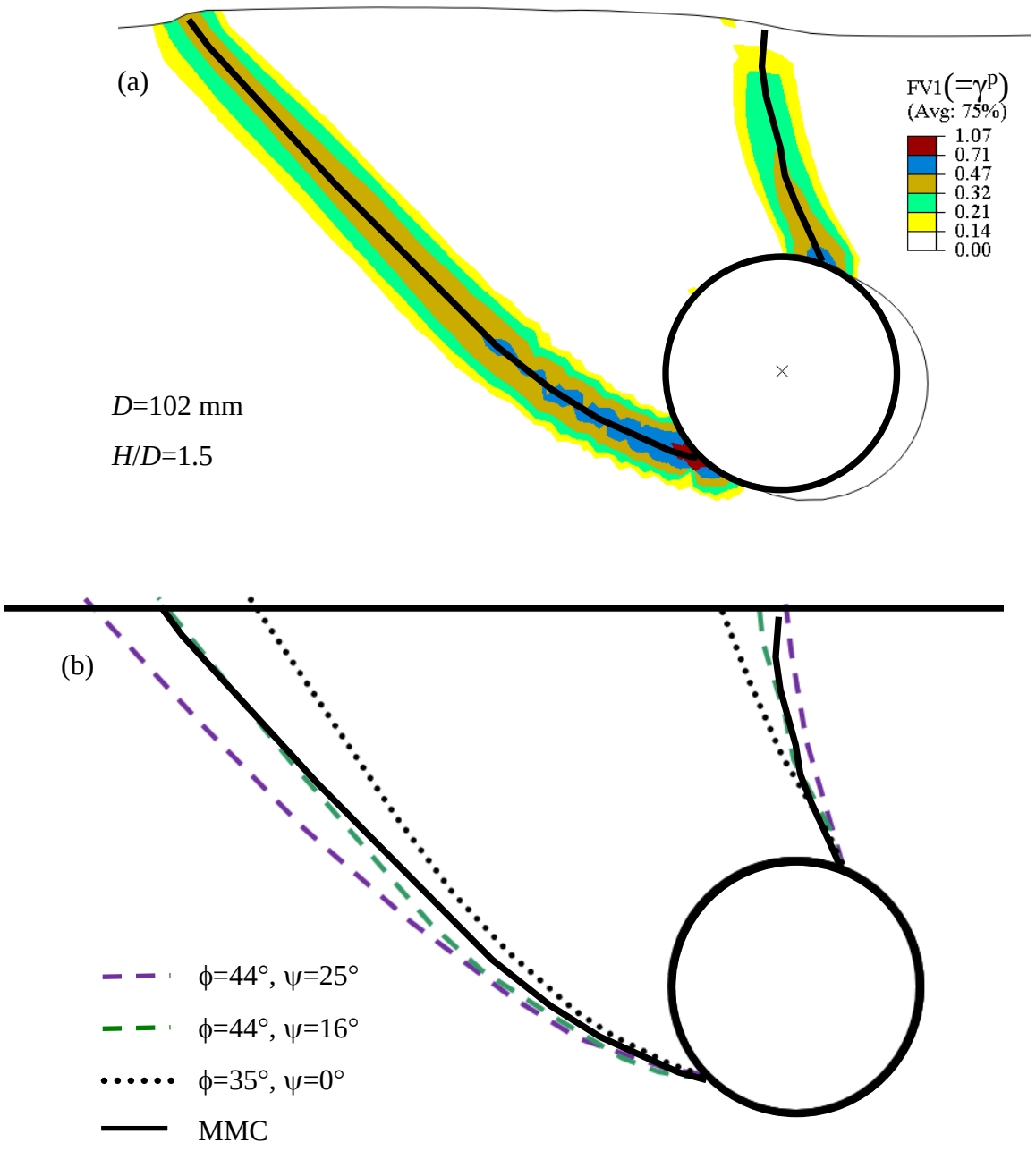

Fig. 3.9: Location of shear band at u/D=0.12: (a) using MMC (b) using MC and MMC model

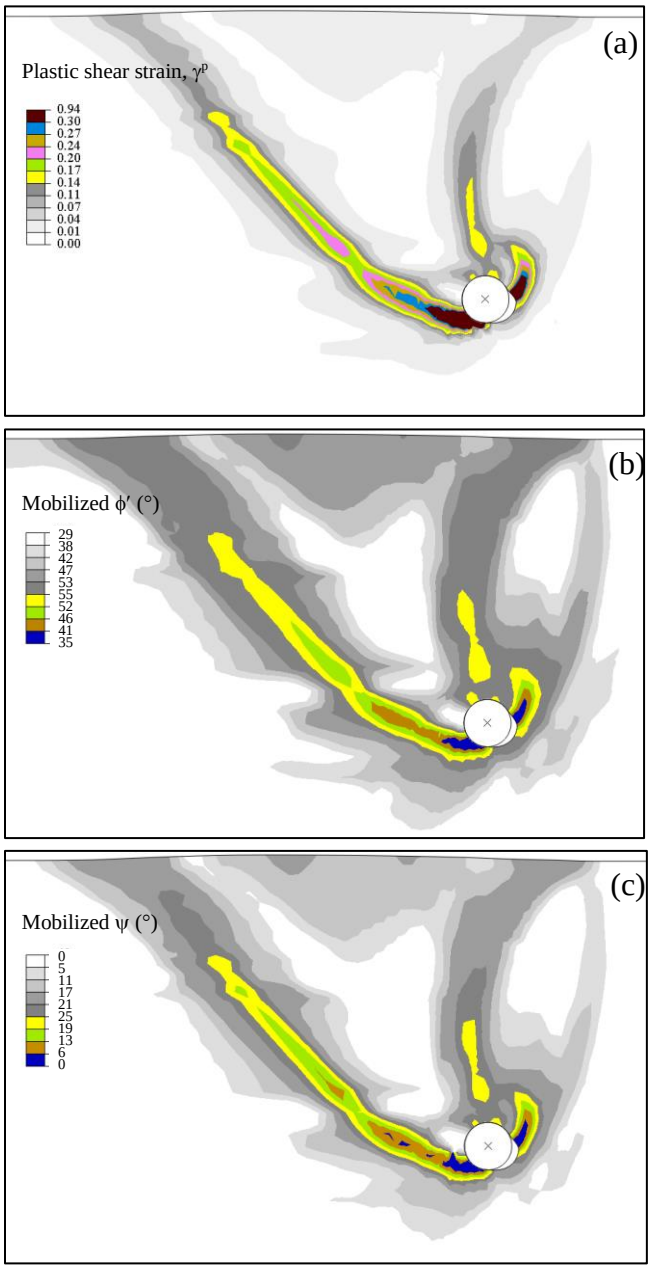

Fig. 3.10: Shear band formation and strength mobilization for H/D=5.5 and D=102 mm at u/D=0.12 with MMC model: (a) plastic shear strain γ^p, (b) mobilized ϕ', (c) mobilized ψ

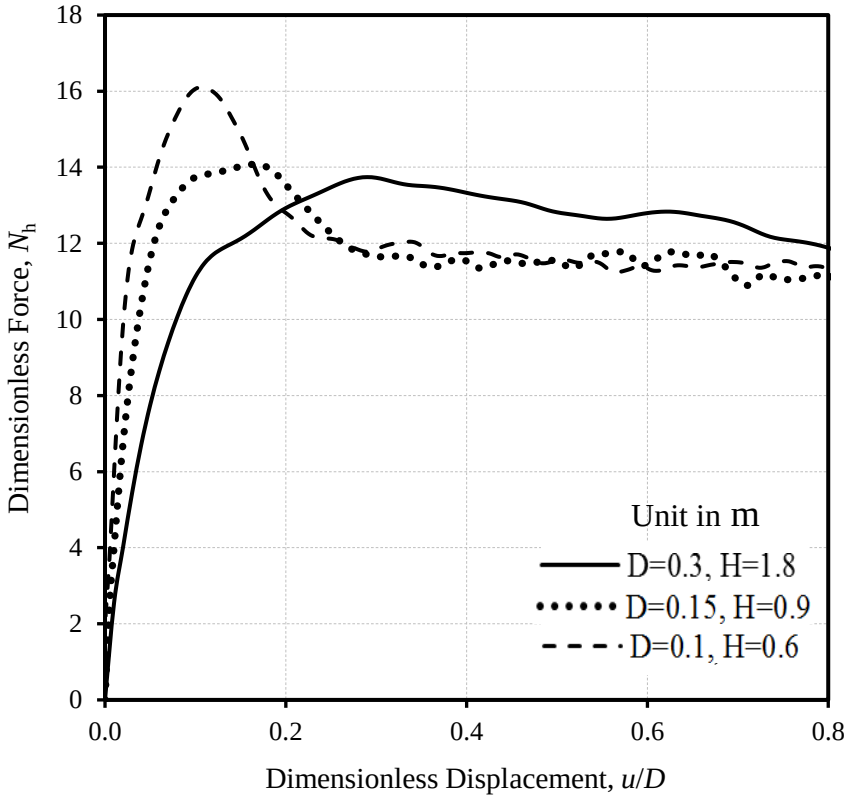

Fig. 3.11: Effects of diameter on force-displacement curve for H/D=6

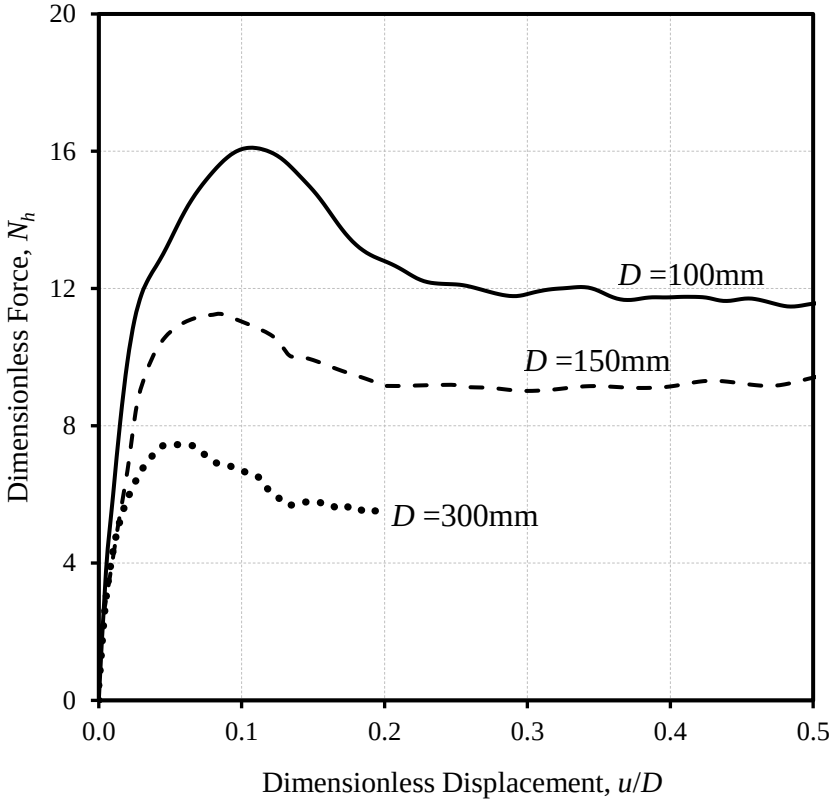

Fig. 3.12: Effect of pipe diameter on N_h for H=600 mm

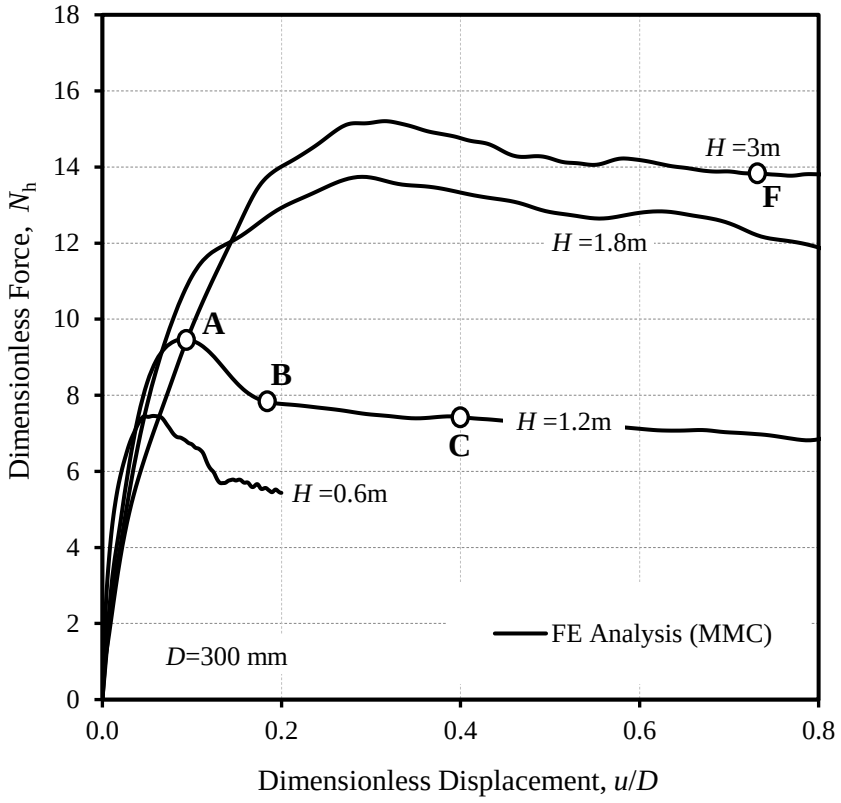

Fig. 3.13: Effects of burial depth on N_h for D=300 mm

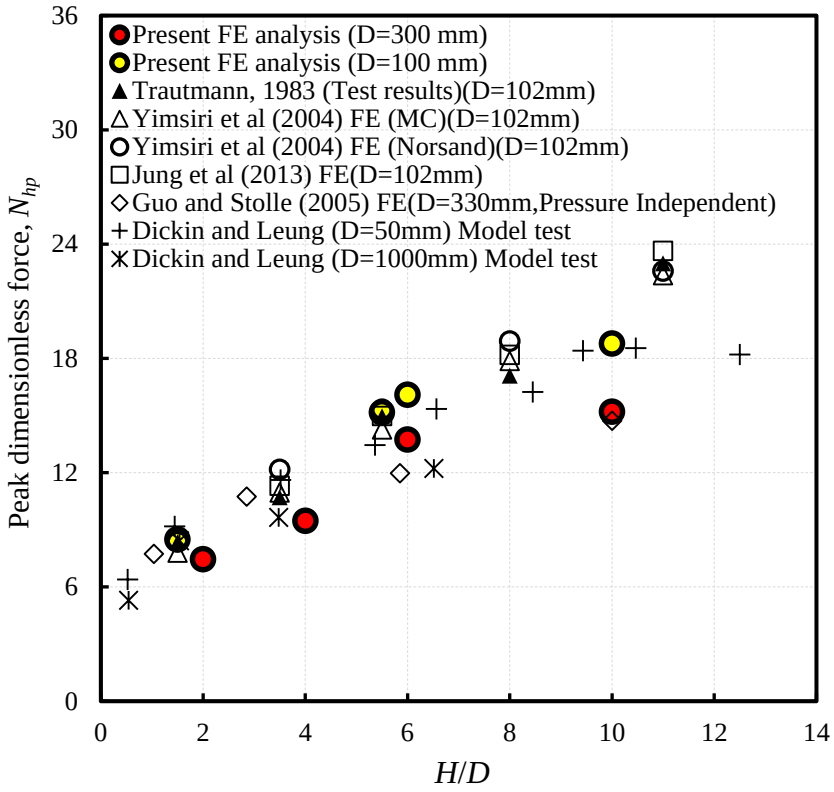

Fig. 3.14: Comparison of peak resistance N_{hp} with previous studies

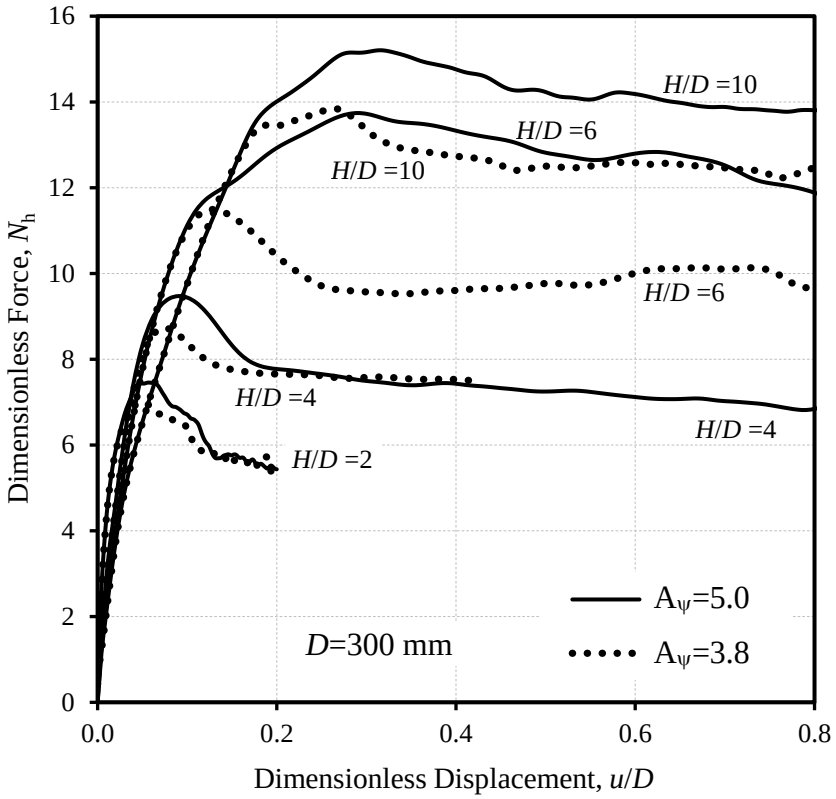

Fig. 3.15: Effect of A_ψ on dimensionless force N_h for D=300 mm

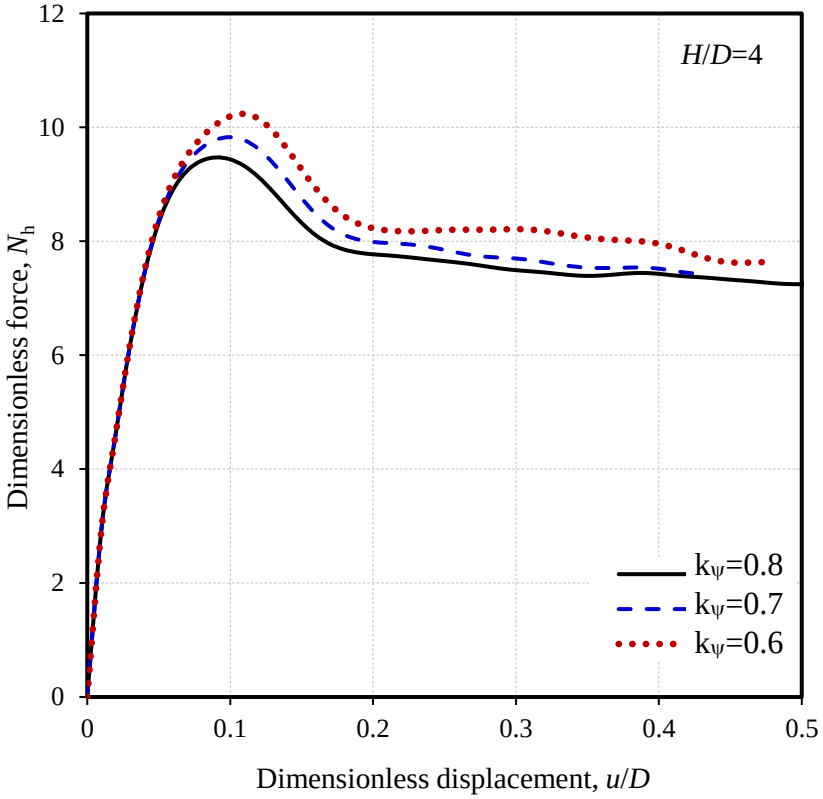

Fig. 3.16: Effect of k_ψ on dimensionless force N_h for H/D=4 and D=300 mm

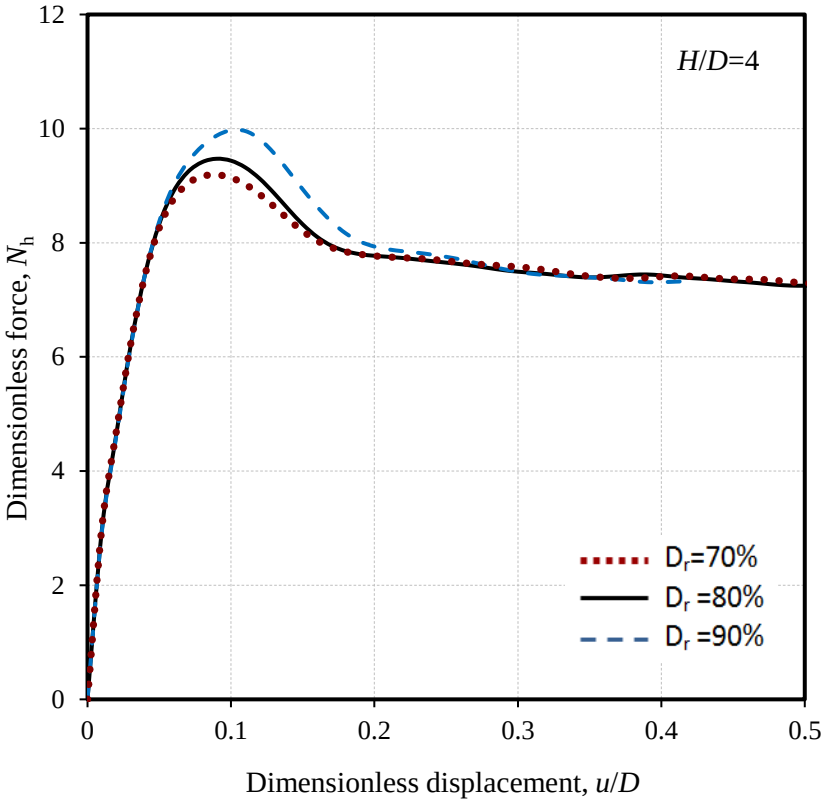

Fig. 3.17: Effect of relative density on dimensionless force N_h for H/D=4 and D=300 mm

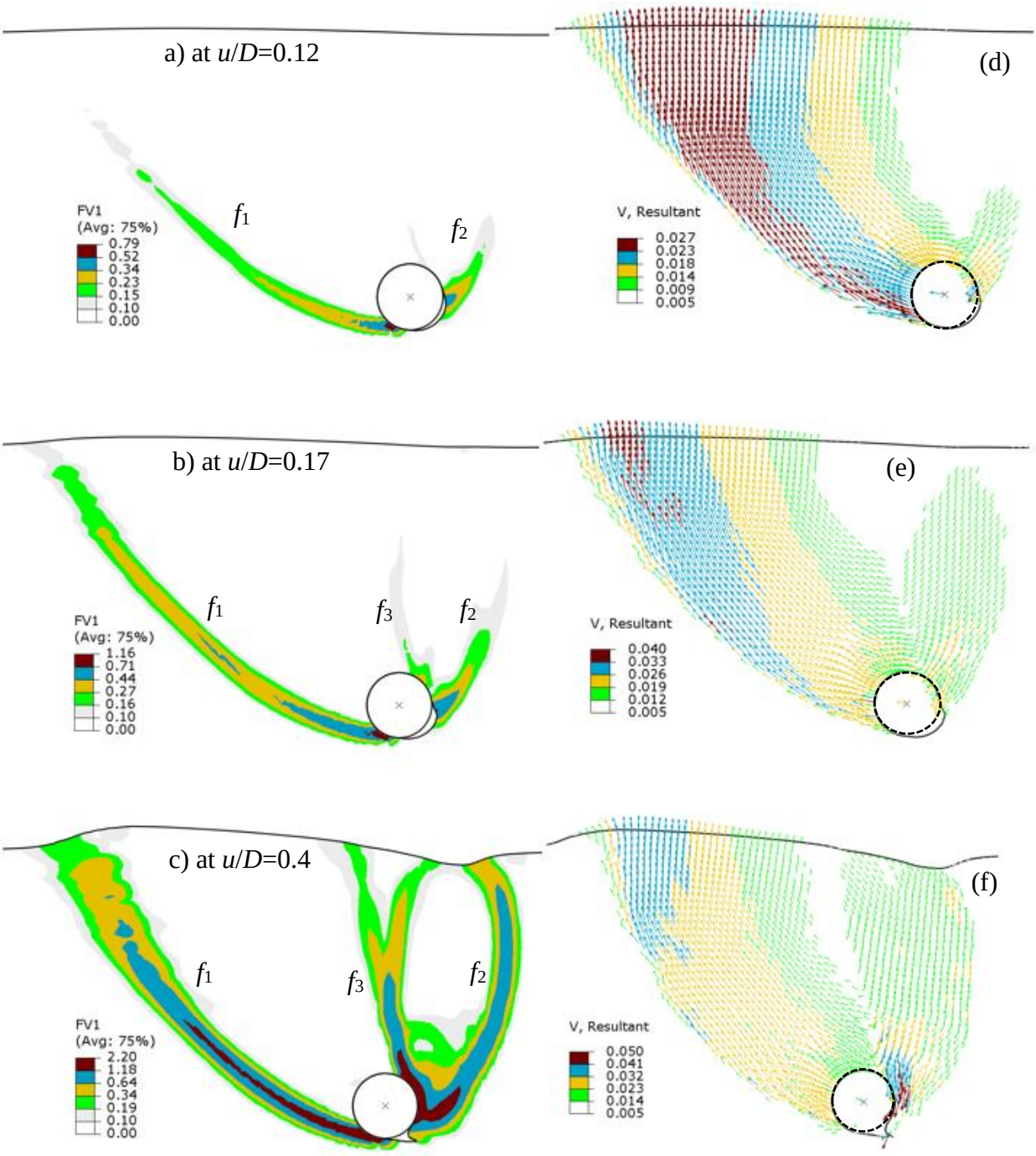

Fig. 3.18: Strain localization and instantaneous velocity vectors for H/D=4 and D=300 mm

(g) Model test (after Turner 2004)

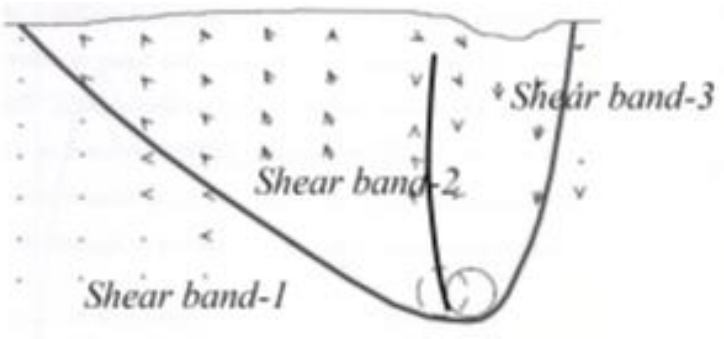

Fig. 3.18: Strain localization and instantaneous velocity vectors for *H*/*D*=4 and *D*=300 mm (cont.)

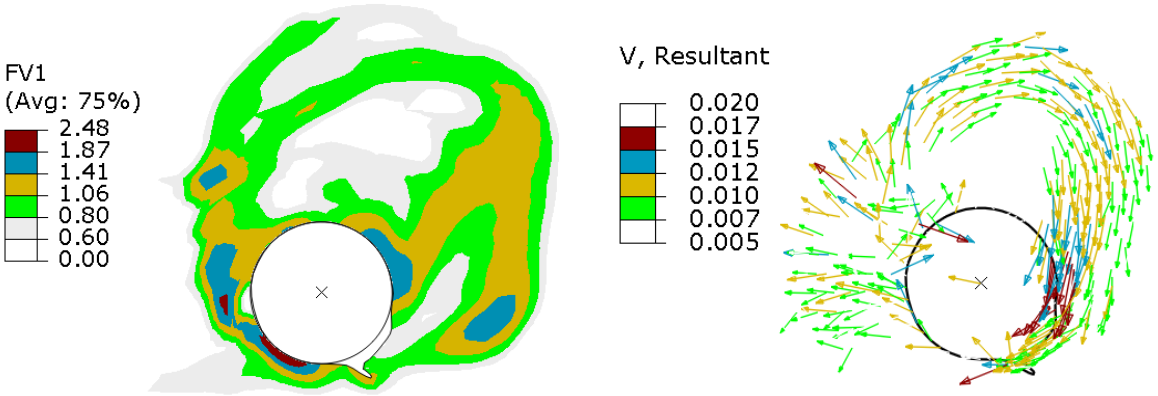

Fig. 3.19: Plastic shear strain and velocity vectors for H/D=10 and D=300 mm at u/D=0.72

Table 3.1: Geometry and soil parameters used in the FE analyses

Parameter	Triaxial test	Model test (Parametric Study)
External diameter of pipe, D (mm)	-	102 (100, 150, 300)
K	150	150
n	0.5	0.5
p_a (kN/m^2)	100	100
ν_{soil}	0.2	0.2
A_ψ	3	5 (3, 3.8, 5)
k_ψ	0.5	0.8 (0.6, 0.7, 0.8)
ϕ'_{in}	29°	29°
C_1	0.22	0.22
C_2	0.11	0.11
m	0.25	0.25
Critical state friction angle, ϕ'_c	31°	35°
Relative density, D_r (%)	70, 80, 90, 100	80 (70, 80, 90)
Unit weight, γ (kN/m^3)	-	17.7 (17.31, 17.7, 18.12)
Interface friction coefficient, μ	-	0.32
Depth of pipe, H/D	-	1.5 & 5.5 (2, 4, 6, 10)

Note: Numbers in parenthesis in right column show the values used in the parametric study

CHAPTER 4

Upward Pipe–Soil Interaction for Shallowly Buried Pipelines in Dense Sand

Co-Authorship: This chapter has been submitted to a journal as a technical paper for review as: Roy, K., Hawlader, B.C., Kenny, S. and Moore, I. (2017), 'Upward Pipe–Soil Interaction for Shallowly Buried Pipelines in Dense Sand.' Most of the research in this chapter has been conducted by the first author. He also prepared the draft manuscript. The other authors mainly supervised the research and reviewed the manuscript.

4.1 Abstract

The uplift resistance is a key parameter against upheaval buckling in the design of a buried pipeline. In addition to the peak, the importance of post-peak resistance has been recognized in some design guidelines. The mobilization of uplift resistance in dense sand is investigated in the present study based on finite element (FE) analysis. The pre-peak hardening, post-peak softening, density and confining pressure dependent soil behaviour are implemented in FE analysis. The uplift resistance mobilizes with progressive formation of shear bands. The vertical inclination of the shear band is approximately equal to the maximum dilation angle at the peak and then decreases with upward displacement. The uplift force–displacement curves can be divided into different segments including pre-peak, quick post-peak softening, and gradual reduction of resistance at large displacements. Simplified equations are proposed for mobilization of uplift resistance. The results of FE analysis, simplified equations and model tests are compared.

4.2 Introduction

Buried pipelines used for transporting oil usually operate at high temperature and pressure. Temperature induced expansion, together with vertical out-of-straightness, might cause global upheaval buckling (UHB). Field evidence suggests that significantly large vertical upward displacement could occur in the buckled section and, in the worst cases, it might protrude above the ground surface (Palmer et al. 2003). For example, Aynbinder and Kamershtein (1982) showed that a ~70 m section of a buried pipeline displaces vertically up to a maximum distance of ~4.2 m above the ground surface. Sufficient restraint from the soil above the pipeline could prevent excessive displacement and upheaval buckling. As burial is one of the main sources of pipeline installation cost, proper estimation of soil resistance is necessary to select the burial depth—typically expressed as the embedment ratio ($\widetilde{H} = H/D$), where D is the diameter and H is the depth of the center of the pipe. Pipelines embedded at $1 \leq \widetilde{H} \leq 4$ in dense sand are the focus of the present study, although it is understood that in some special scenarios $\widetilde{H}$ could be outside this range, for example, for surface laid offshore pipelines in deep water (Dutta et al. 2015) or the pipelines in ice gouging areas (Pike and Kenny 2016).

During installation of offshore pipelines in sand, ploughs deposit backfill soil in a loose to medium dense state (Cathie et al. 2005); however, it could be subsequently densified due to environmental loading. For example, Clukey et al. (2005) showed that the sandy backfill of a test pipe section densified from relative density (D_r) less than ~57% to ~85–90% in 5 months, which has been attributed to wave action at the test site in the Gulf of Mexico. The uplift resistance offered by soil (F_v) depends on upward displacement (v) and generally comprises three components: (i) the submerged weight of soil being lifted (W_s); (ii) the vertical component of shearing resistance offered by the soil (S_v); and (iii) suction under the pipe (F_{suc}). The component F_{suc} could be neglected for a drained loading condition at low uplift velocities (Bransby and Ireland

2009; Wang et al. 2010). The force–displacement behaviour is generally expressed in normalized form using $N_v=F_v/\gamma HD$ and $\tilde{v}=v/D$, where γ is the unit weight of the soil. Physical experiments show that N_v increases with $\tilde{H}$ and D_r (Trautmann 1983; Bransby et al. 2002; Chin et al. 2006; Cheuk et al. 2008). A close examination of physical model test results in dense sand at $\tilde{H}\leq 4$ shows that N_v increases quickly with $\tilde{v}$ and reaches the peak (N_{vp}) at $\tilde{v}$~0.01–0.05. A quick reduction of N_v occurs after the peak followed by gradual reduction of N_v at large $\tilde{v}$. The ALA guideline for design (ALA 2005) does not explicitly consider the post-peak reduction of N_v and the maximum $N_v=\phi'\tilde{H}/44$ is recommended, where ϕ' is a representative angle of internal friction (in degree). However, DNV (2007) recognized the post-peak reduction of N_v and recommended a N_v–$\tilde{v}$ relation using four linear line segments in which N_v reduces linearly from the peak to a residual value with $\tilde{v}$ and then remains constant.

The load–displacement curves obtained from model tests evolve from complex deformation mechanisms and the stress–strain behaviour of soil above the pipe. To understand these mechanisms, the particle image velocimetry (PIV) technique (White et al. 2003) has been used in recent model tests (Cheuk et al. 2008; White et al. 2008; Thusyanthan et al. 2010; Wang et al. 2010). When the peak uplift resistance mobilizes in medium to dense sand, two inclined symmetric slip planes form in the backfill soil, starting from the pipe springline of the pipe (White et al. 2008). Although the slip planes slightly curve outwards, their inclination with the vertical (θ) is approximately equal to the peak dilation angle (ψ_p) (Fig. 4.1). The vertical inclination of slip planes decrease with $\tilde{v}$, and they become almost vertical at large $\tilde{v}$. A model test conducted by Huang et al. (2015) shows that θ gradually increases in the pre-peak, reaches ~ψ_p at the peak N_v and then decreases in the post-peak zone.

PIV data can provide very useful information on soil deformation patterns; however, the progressive formation of shear bands in dense sand due to strain-softening can be better explained

by using numerical modeling techniques where other correlated parameters (e.g. evolution in strength parameters) can be more readily and directly monitored. More specifically, the post-peak reduction of N_v, as recommended in DNV (2007), could be examined/revised, implementing an appropriate soil constitutive model that can simulate strain-softening in dense sand, change in θ and cover depth with $\tilde{v}$. The pre-peak hardening, post-peak softening, relative density and confining pressure (p') dependent ϕ' and ψ are the common features of the stress–strain behaviour of dense sand. In addition, the mode of shearing (triaxial, TX or plane strain, PS) significantly influences ϕ' and ψ. All of these features of the stress–strain behaviour of dense sand have not been considered in the available guidelines or FE analyses. A large number of FE analyses has been conducted using the Mohr–Coulomb (MC) model with constant ϕ' and ψ and therefore cannot model post-peak reduction of N_v, except for the reduction due to change in cover depth (Yimsiri et al. 2004; Farhadi and Wong 2014). Yimsiri et al. (2004) also used an advanced soil model (Nor-Sand); however, they could not simulate the significant reduction of N_v, as observed in model tests. Chakraborty and Kumar (2014) used the MC model for the lower bound FE limit analysis. Jung et al. (2013) incorporated linear reduction of ϕ' and ψ after the peak with plastic shear strain; however, they did not consider the pre-peak hardening. Jung et al. (2013) also showed the importance of using PS strength parameters for pipe–soil interaction.

In addition to physical and numerical modeling, limit equilibrium and plasticity solutions have also been proposed to calculate the peak uplift resistance, F_{vp} (White et al. 2008; Merifield et al. 2001). As the soil obeys normality condition (i.e. $\theta=\psi=\phi'$), the plasticity solutions give a more non-conservative uplift resistance than the limit equilibrium solutions with $\theta=\psi_p$ ($<\phi'$) (White et al. 2008).

The objective of the present study is to conduct FE analysis to examine uplift behaviour of shallowly embedded pipelines in dense sand ($\tilde{H}\leq 4$). An advanced soil constitutive model is

adopted in FE analysis to simulate not only the peak but also the post-peak uplift resistance. The FE model is validated against a physical model test and numerical results. A set of empirical equations is proposed to develop the uplift resistance versus displacement curve, including the post-peak degradation at large displacement.

4.3 Modeling of Soil

The Mohr-Coulomb (MC) and modified Mohr-Coulomb (MMC) models are used for modeling the soil. In the MMC model, ϕ' and ψ vary with relative density (D_r), mean effective stress (p') and accumulated plastic shear strain (γ^p). The details of the MMC model, including the calibration against laboratory test data, are available in Chapter 3. The mathematical equations are listed in Table 4.1.

The novel aspects of the MMC model, compared to the models of similar type used in pipe–soil interaction analysis (e.g. Jung et al. 2013; Robert and Thusyanthan 2014, Pike 2016), is that the nonlinear variation of ϕ' and ψ with γ^p, including pre-peak hardening and post-peak softening zones, are defined with smooth transitions at the peak and critical state. This nonlinear variation of ϕ' and ψ with γ^p has a considerable influence on the force–displacement response of the pipeline.

4.4 Finite Element Modeling

Two-dimensional FE analyses in plane strain condition are performed using Abaqus/Explicit FE software (Dassault Systèmes 2010). Figure 4.2(a) shows the typical FE mesh at the start of uplifting. Taking advantage of symmetry, only half of the domain is modeled. A dense mesh is used near the pipe (Zone-A), where considerable soil deformation is expected. To avoid mesh distortion issues at large displacements, an adaptive remeshing option is adopted in Zone-A, which creates a new smooth mesh at a regular interval to maintain a good aspect ratio of the elements. In

Abaqus/Explicit, the remeshing is performed using the arbitrary Lagrangian-Eulerian method and without changing the number of elements, nodes and connectivity. The bottom of the FE domain is restrained from horizontal and vertical movement, while all the vertical faces are restrained from any lateral movement.

Four-node bilinear plane strain quadrilateral elements (CPE4R in Abaqus) are used for modeling the soil. The pipe is modeled as a rigid body. The bottom and left boundaries are placed at a sufficiently large distance from the pipe to avoid boundary effects on uplift behaviour.

The pipe–soil interface is modeled by defining the interface friction coefficient (μ) as $\mu=\tan(\phi_\mu)$, where ϕ_μ is the pipe–soil interface friction angle. ϕ_μ depends on pipe surface roughness and ϕ' of the soil around the pipe. With loading, the soil elements around the pipe experience high shear strains that causes a reduction of ϕ'. Therefore, assuming a looser soil condition, $\mu=0.32$ is used. Note that μ has a little influence on the uplift resistance. For example, $\mu=0.2–0.5$ gives less than 1% variation in the peak force. The numerical analysis is conducted in two steps. In the first step, geostatic stress is applied under the $K_0=0.5$ condition. The value of K_0 does not significantly affect uplift resistance (Jung et al. 2013). In the second step, the pipe is displaced in the upward direction by specifying a displacement boundary condition at the reference point (center of the pipe).

The MMC model is implemented in Abaqus by developing a user subroutine VUSDFLD written in FORTRAN. The stress and strain components are called in the subroutine in each time increment. The mean effective stress (p') is calculated from the three principal stresses. The strain components are transferred to the principal strain components and stored as state variables. The plastic strain increment ($\Delta\gamma^p$) in each time increment is calculated as $\Delta\gamma^{\mathrm{p}} = (\Delta\varepsilon_1^{\mathrm{p}} - \Delta\varepsilon_3^{\mathrm{p}})$, where $\Delta\varepsilon_1^{\mathrm{p}}$and $\Delta\varepsilon_3^{\mathrm{p}}$ are the major and minor principal plastic strain components, respectively. The value of γ^{p} is calculated as the sum of $\Delta\gamma^{\mathrm{p}}$ over the period of analysis. In the subroutine, γ^{p} and $p'$are defined as two field variables. The mobilized ϕ' and ψ are defined in the input file as a function of

γ^p and p'in tabular form, using the equations in Table 4.1. Figure 4.1(b) shows the typical variation of ϕ' and ψ with plastic shear strain. During the analysis, the program accesses the subroutine and updates the values of ϕ' and ψ with field variables. A flowchart of the VUSDFLD subroutine for updating the field variables is shown in Appendix G. Note that, although I_D is not updated in each time increment, the volumetric change in soil elements due to shearing and its effects on ϕ' and ψ are captured in the MMC model.

4.5 Model Verification

FE simulation is first performed for a physical model test conducted by Cheuk et al. (2008) at the University of Cambridge and is called the CD (coarse dense sand) test. A 100-mm diameter model pipe section embedded at $\widetilde{H}$=3 in dry Leighton Buzzard silica sand was pulled up slowly at 10 mm/h to capture soil deformation using two digital cameras. However, in FE modeling, the pipe is pulled at ~10 mm/s by maintaining a quasi-static simulation condition. The soil parameters used in this simulation are listed in Table 4.2. Direct shear tests show that Leighton Buzzard silica sands has ϕ_c' of 32° (Cheuk et al. 2008). As ϕ_c' in PS condition could be ~2–4° higher than in direct shear conditions (Lings and Dietz 2004), $\phi_c' = 35°$ is used, which is ~3° higher than DS test results reported by Cheuk et al. (2008). Randolph et al. (2004) showed that Q=10±1 for a variety of quartz and siliceous sands. Analyzing a large number of laboratory tests on different sands, Bolton (1986) suggested A_ψ=5 and k_ψ=0.8 for the plane strain condition. For the variation of ϕ' and ψ with plastic shear strain, Roy et al. (2016) calibrated the MMC model against laboratory test results on Cornell filter sand and obtained the values of C_1, C_2 and m. Cheuk et al. (2008) did not provide any stress–strain curve of Leighton Buzzard silica sand used in physical modeling; therefore, the values of C_1, C_2 and m of this sand are assumed to be the same as Cornell filter sand. The geotechnical

parameters used in FE analyses are listed in Table 4.2. Moreover, Q=10 and R=1 is used (Bolton 1986).

4.5.1 Force–displacement behaviour

Figure 4.3 shows the FE simulated force–displacement curves for $\widetilde{H}$=3, on which the points of interest for further explanation are labeled A–E for the MMC and A′–E′ for the MC model. For the MMC model, N_v increases quickly, reaches the peak at $\tilde{v}$~0.03 and then quickly decreases to point C, primarily due to the strain-softening behaviour of soil. After a slight increase between points C and D, N_v decreases again at a slower rate than in the segment AC. In the present study, the segment AC of the N_v–$\tilde{v}$ curve is termed the "softening segment" and the segment after point C is called the "large deformation segment." The values of N_v at the peak and after softening (i.e. points A and C) are defined as N_{vp} (=$F_{vp}/\gamma HD$) and N_{vs} (=$F_{vs}/\gamma HD$), respectively, where F_{vp} and F_{vs} are peak and after softening uplift resistances, respectively. The dimensionless uplift displacement, $\tilde{v}$, required to mobilize N_{vp} and N_{vs}, are defined as $\tilde{v}_p$ and $\tilde{v}_s$, respectively.

The mobilization of N_v shown in Fig. 4.3 could be explained from progressive development of shear bands, the zones of localized plastic shear strain, $\gamma^p = \int_0^t \sqrt{\frac{3}{2}(\dot{\epsilon}_{ij}^p \dot{\epsilon}_{ij}^p dt)}$, where $\dot{\epsilon}_{ij}^p$ is the plastic deviatoric strain rate tensor (Figs. 4.4(a)–4.4(e)). At N_{vp}, plastic shear strain mainly develops locally in an inclined shear band originating from the springline of the pipe; however, the shear band does not reach the ground surface for formation of a complete slip mechanism (Fig. 4.4(a)). The inclination of the shear band with the vertical (θ) is described by drawing a line from the pipe surface through the highly concentrated γ^p zone. White et al. (2008) suggested that $\theta \sim \psi_p$. As ψ_p varies with p' (Eqs. (4.1–4.3)), they calculated a single representative value of the peak dilation angle (ψ_p^R) using the in-situ p'at the springline of the pipe ($(1+2K_0)\gamma H/3$. For the geotechnical

parameters in Table 4.2, ψ_p^R=25°, which is approximately the same as θ obtained from the present FE analysis (Fig. 4.4(a)). The complete slip mechanism develops at $\tilde{v}>\tilde{v}_p$ when a considerable post-peak degradation of N_v occurs (Fig. 4.4(b)). Similar types of curved failure planes shown in Figs. 4.4(b)–4.4(e) were observed in physical tests (e.g. Stone and Newson 2006; Cheuk et al. 2008; Huang et al. 2015). The formation of complete slip planes after $\tilde{v}_p$ can be attributed from noticeable vertical displacement of the ground surface after N_{vp} in physical tests (Dickin 1994; Bransby et al. 2002; Huang et al. 2015). Note that, adaptive remeshing could not maintain a high quality mesh at a very large pipe displacement. Therefore, the force–displacement curves only up to $\tilde{v}$=1.0 are presented.

It is worth noting that, although it is a different type of loading, because of progressive development of shear bands, the attainment of peak load before the formation of a complete failure mechanism was also found in physical tests and numerical modeling for footing in dense sand (Tatsuoka et al. 1991; Aiban and Znidarčić 1995; Loukidis and Salgado 2011). Note, however, that in the simplified limit equilibrium method (LEM), a complete slip mechanism is assumed to calculate the peak load irrespective of burial depth; for example, White et al. (2008) used the LEM to fit test data for $\tilde{H}$<8.0.

The slight increases in N_v in the segment CD in Fig. 4.3 can be explained using γ^p plots in Figs. 4.4(a)–4.4(d). In the segment ABC of the N_v–$\tilde{v}$ curve, the shear resistance (τ_f) gradually reduces along the inclined shear band that was formed during initial upward displacement (e.g. Figs. 4.4(a)–4.4(c)). However, the location of the shear band shifts considerably to the right at $\tilde{v}$≈0.18–0.4. As the new shear bands form through the soil where τ_f has not been reduced by softening, N_v increases slightly in the segment CD. After point D, the location of the shear band does not change significantly with $\tilde{v}$ (θ remains ~8°). Therefore, the gradual decreases of N_v with $\tilde{v}$ after point D is due to strain-softening in the shear band and the reduction of soil cover depth.

Figure 4.3 also shows that an FE simulated N_v–$\tilde{v}$ curve with the MMC model compares well with the model test results of Cheuk et al. (2008). A slight increase in N_v after a quick post-peak reduction is also observed in model tests at intermediate depth of embedment, as the one shown in Fig. 4.3 and also in other studies (Bransby et al. 2002; Stone and Newson 2006; Chin et al. 2006; Cheuk et al. 2008; Saboya et al. 2012; Eiksund et al. 2013; Huang et al. 2015). However, it does not happen at shallow burial depths. A similar trend is also observed in model tests for the bearing capacity of footing in sand, which has been attributed to progressive formation of slip planes (Aiban and Znidarčić 1995).

The inclination of the shear band gradually reduces with $\tilde{v}$, and at $\tilde{v}$=0.32, $\theta \approx 8°$ (Fig. 4.4(c)). However, θ does not reduce further at $\tilde{v}$>0.32 (Figs. 4.4(c)–4.4(e)). As discussed later, in the limit analysis θ=0 is assumed at large $\tilde{v}$; however, the present FE analysis shows that the shear band does not become completely vertical even at large $\tilde{v}$ (e.g. $\tilde{v}$=0.5). Because of change in mobilized ϕ' and ψ with loading, the failure mechanism changes from an inclined slip plane (Fig. 4.4(b)) to a flow around mechanism (Fig. 4.4(e)). See also the velocity vectors in the inset of Fig. 4.3. Based on PIV results, similar failure mechanisms have been reported from physical experiments (Bransby et al. 2002; Cheuk et al. 2008).

4.5.2 Limitations of Mohr-Coulomb model

To show the advantages of the MMC model, FE simulation is also performed with the MC model. Based on Cheuk et al. (2005, 2008) laboratory test results, ϕ'=52° and ψ=25° are used for the MC model. Although it is not explicitly mentioned in the design guidelines, equivalent values for these two parameters should be carefully selected, as they vary with γ^p. In general, the equivalent values of ϕ' and ψ should be smaller than the peak and higher than the critical state values. A number of previous studies simulated pipe–soil interaction using constant equivalent

values for the MC model (e.g. Yimsiri et al. 2004). Note that an equivalent ϕ' has also been recommended for other geotechnical problems in dense sand, for example, the bearing capacity of shallow foundations (Loukidis and Salgado 2011) and the lateral capacity of pile foundations (API 1987).

Figure 4.3 shows that the MC model calculates slightly higher N_{vp} than the MMC model. This difference will be reduced if lower equivalent values of ϕ' and ψ are considered. However, the key observation is that N_v decreases almost linearly with $\tilde{v}$ after the peak for the MC model, which is very different from the simulation with the MMC model and physical model test results. In order to explain this force–displacement behaviour, γ^p at five $\tilde{v}$ is plotted in Figs. 4.4(f)–4.4(j). The inclination of the shear band (θ) remains almost constant (~25°) during the whole process of upward displacement of the pipe. The linear post-peak reduction of N_v with the MC model is due to the reduction of cover depth with $\tilde{v}$.

In summary, the post-peak reduction of N_v with the MMC model for this $\widetilde{H} = 3$ occurs due to the combined effects of three factors: (i) decreases in size of the failure wedge, (ii) reduction of shear resistance with γ^p, and (iii) reduction of cover depth. The MC model cannot capture the effects of the former two. However, the proposed MMC model can simulate the effects of all three factors. Moreover, the simulations with the MMC model are similar to physical model test results.

DNV (2007) suggested the following equations to develop the force–displacement curve for dense sand for $2.5 \le \widetilde{H} \le 8.5$: $N_{vp} = 1 + f\widetilde{H}$; $N_{vs} = 1 + \alpha_f f\widetilde{H}$; $\tilde{v}_p = (0.5\% \text{ to } 0.8\%)\widetilde{H}$ and $\tilde{v}_s = 3\tilde{v}_p$. The pre-peak behaviour is defined by a bi-linear relation, where the slope changes at (αN_{vp}, $\beta\tilde{v}_p$). Based on DNV (2007) recommendations for dense sand, f=0.6, α_f=0.75,$\tilde{v}_p = 0.008\widetilde{H}$, α=0.75, β=0.2; the force–displacement curve is plotted in Fig. 4.3. Although only one test is simulated, DNV (2007) gives considerably lower N_{vp}, higher N_{vs} and lower $\tilde{v}_s$ than the physical model test and present FE results with the MMC model.

The maximum N_v based on ALA (2005) ($=\phi'\tilde{H}/44$) is shown by two horizontal arrows on the right vertical axis for two ϕ' (Fig. 4.3). Note that ALA (2005) requires a constant equivalent ϕ', and does not consider any post-peak reduction of resistance.

4.6 Mesh Sensitivity

FE results with the MMC model are expected to be mesh sensitive because of strain localization in the shear bands due to strain-softening behaviour of dense sand. The thickness of shear band (t_s) can be approximately estimated from laboratory tests, physical experiments and theoretical investigations (Alshibli and Sture 1999). The ratio between t_s and the mean particle size (d_{50}) varies between 3 and 25—the lower values mostly corresponds to coarse-grained sand (Loukidis and Salgado 2008; Guo 2012). The t_s/d_{50} ratio also decreases with confining pressure and initial density (Pradhan 1997).

As the soil is modeled as continuum in FE analysis, the movement of each soil particle is not simulated. Instead, the width of shear band can be controlled by varying element size, which is generally described by the width or characteristics length of finite element (t_{FE}). Very small t_{FE} gives an unrealistically thin shear band for sand, while large t_{FE} cannot capture strain localization properly. To calculate shaft resistance of a pile in dense sand, Loukidis and Salgado (2008) used $t_{FE}=t_s$ in the zone of strain localization near the pile. On the other hand, the deformed mesh under the footing in dense sand shows $t_s=(2–3)t_{FE}$ (Tejchman and Herle 1999; Tejchman and Górski 2008), which are consistent with model tests results (Tatsuoka et al. 1991). This implies that t_s/t_{FE} depends on loading conditions.

As will be shown later that during uplift of a buried pipeline—which can be viewed as reverse loading of a footing—strain localization extends more than one element. Therefore, $t_{FE}<t_s$ should be used to capture strain localization properly. The model test considered in Fig. 4.3 were

conducted using coarse sand having d_{50}~2.24 mm. Assuming t_s/d_{50}~10, t_s~22.4 mm is calculated, which is also consistent with experimental observation in laboratory—for example, Alshibli and Sture (1999) show t_s~17 mm for coarse sand. In the present study, except for mesh sensitive analysis, the characteristics length (t_{FE}) of the elements in the zone of interest (dense mesh Zone-A in Fig. 4.2(a)) is ~10 mm except for few rows of elements near the pipe where t_{FE}<10 mm.

Several authors proposed element scaling rule to reduce the effects of FE mesh on simulated results (Pietruszczak and Mróz 1981; Moore and Rowe 1990; Andresen and Jostad 2004; Anastasopoulos et al. 2007). Following Anastasopoulos et al. (2007) and assuming the reference FE mesh, t_{FE_ref}=10 mm, analyses are performed for t_{FE}=5 mm and 15 mm, where γ_c^p in Eq. (4.4) is scaled by a factor $f_{scale} = (t_{FE\_ref}/t_{FE})^m$, where m is a constant. Anastasopoulos et al. (2007) suggested m=1 (i.e. f_{scale} is inversely proportional to element size) for fault rupture propagation. However, a number of FE simulations of pipe uplift for varying geotechnical properties, element size, and pipe diameter, show that m~0.7 gives a better f_{scale} than m=1 for mesh independent N_v–$\tilde{v}$ curves. The following are the potential reasons behind non-proportional f_{scale}: (i) nonlinear distribution of γ^p in the shear band (in normal direction) and (ii) number of elements involved in shear band depends on mesh size.

Figure 4.5 shows a sample mesh sensitivity analysis results. If scaling rule is not used (f_{scale}=1), the post-peak reduction of N_v occurs slowly for large mesh, although the mesh size effect on N_v is negligible at very large $\tilde{v}$ because at this stage the shear strength is simply governed by the critical state parameters. The scaling rule brings the N_v–$\tilde{v}$ curves closer for the three mesh sizes. Very similar trend is found for D=200, 300 and 500 mm; although the results are not presented in this paper. Unlike lateral loading (Chapter 6), mesh size effect is not very significant for uplift, unless a very coarse mesh is used. Based on the present FE analyses, t_{FE}=(0.2–0.5)t_s is suggested

to use, where t_s is a function of d_{50} as discuss above. Analysis with this range of small t_{FE} is practically possible using the currently available computing facility. For example, the simulation with the MMC model in Fig. 4.3 takes 4.5 hours with a 3.4 GHz Intel Core i7 processor and 8 GB RAM.

4.7 Effect of Burial Depth

Figure 4.6 shows the load–displacement curves for $\widetilde{H}$ =1–4. FE modeling for $\widetilde{H}$ >4 has been presented in Chapter 5. Although the simulation is performed for every $\widetilde{H}$=0.5 interval, only four curves are shown in Fig. 4.6 for clarity. Two key features of the N_v–$\tilde{v}$ curves are: (i) although N_{vp} (open circles) increase with $\widetilde{H}$, $\tilde{v}_p$~0.03 for the cases analyzed; and (ii) $\tilde{v}_s$ increases with $\widetilde{H}$.

A number of studies and design guidelines discussed $\tilde{v}_p$ and N_{vp}, and therefore, a very brief discussion of these two values is provided. In general, $\tilde{v}_p$ decreases with D_r and increases with $\widetilde{H}$ (Trautmann 1983; Dickin 1994; ALA 2005; DNV 2007). Cheuk et al. (2008) found $\tilde{v}_p$~0.03 or 0.01H from physical model tests on dense sands. For the range of soil properties and burial depths considered in the present FE analysis, $\tilde{v}_p$ does not vary significantly with $\widetilde{H}$ between 1 and 4. However, FE simulations show a significant increase in $\tilde{v}_p$ with $\widetilde{H}$ for deep burial conditions (Chapter 5). Figure 4.7 shows that N_{vp} for the MMC model increases almost linearly with $\widetilde{H}$. Moreover, N_{vp} obtained from the present FE analysis is comparable to available physical model tests and FE results.

The mobilized N_v after a quick post-peak reduction (i.e. N_{vs}), shown by the squares in Fig. 4.6, increases with $\widetilde{H}$. However, unlike $\tilde{v}_p$, the displacement at N_{vs} (i.e. $\tilde{v}_s$) increases with $\widetilde{H}$. The DNV guidelines (DNV 2007) recognized the importance of post-peak softening in upheaval buckling and recommended $\tilde{v}_s$=3$\tilde{v}_p$.

4.8 Proposed Simplified Equations for Uplift Force–Displacement Curve

The solid lines in Fig. 4.6 show the proposed N_v–$\tilde{v}$ relation for a simplified analysis, which is comprised of a bilinear curve up to N_{vs} followed by a slightly nonlinear curve at large displacements. Note that DNV (2007) recommended that N_v remains constant after N_{vs} (cf. Fig. 4.3). The parameters required to define the proposed N_v–$\tilde{v}$ relation are F_{vp}, v_p, F_{vs} and v_s.

4.8.1 Peak resistance

Depending on slip plane formation, *inclined* and *vertical* slip plane models (Fig. 4.1) are commonly used to calculate uplift resistance (Schaminee et al. 1990; White et al. 2008). In the former one, the slip plane forms at an angle θ to the vertical, while θ = 0 in the latter one. Experimental studies show that the vertical slip plane model is primarily applicable to loose sand at medium $\widetilde{H}$ (White et al. 2001; Wang et al. 2010). For medium to dense sand, two symmetrical inclined slip planes form from the springline of the pipe at $\theta \sim \psi_p^R$ (White et al. 2008; Huang et al. 2015).

Following the limit equilibrium method (LEM), the peak uplift resistance (F_{vp}) can be calculated from an inclined slip plane model as the sum of the weight of the lifted soil wedge (W_s) and the vertical component of shearing resistance along the two inclined planes (S_v):

$$F_{vp} = \gamma D^2 \left[\left\{\widetilde{H} - \left(\frac{\pi}{8}\right) + \widetilde{H}^2 \tan\theta\right\} + F_A \widetilde{H}^2\right] \tag{4.11}$$

where

$$F_A = \left(\tan\phi_p' - \tan\theta\right)\left[\frac{1+K_0}{2} - \frac{(1-K_0)\cos 2\theta}{2}\right] \tag{4.12}$$

Equations (4.11 & 4.12) are derived assuming that, the inclined slip surfaces reach the ground when F_{vp} mobilizes, causing the global failure of a soil block. The first part of the right hand side of Eq. (4.11) represents the contribution of W_s while the second part is for S_v.

The lifting of the pipe reduces the cover depth and inclined length of slip planes, although it does not have significant effects on F_{vp} because $\tilde{v}_p$ is very small. However, lifting has a significant effect on F_{vs}, as discussed in the following sections. In order to be consistent in the proposed equations for the peak and post-peak resistances (Eqs. (4.13) & (4.14)), the lifting effect is also incorporated in the following revised equation for the peak resistance. In other words, the uplift resistance is calculated based on current position of the pipe $\left(\tilde{H}-\tilde{v}_p\right)$ instead of initial embedment ratio $\left(\tilde{H}\right)$.

$$F_{vp}=R\gamma D^2\left[\left\{\left(\tilde{H}-\tilde{v}_p\right)-\frac{\pi}{8}+\left(\tilde{H}-\tilde{v}_p\right)^2\tan\theta\right\}+F_A\left(\tilde{H}-\tilde{v}_p\right)^2\right] \quad (4.13)$$

The reduction factor R is discussed in the following sections.

4.8.2 Effects of shear band formation on peak resistance

Figure 4.8 shows the mobilized ϕ' and formation of slip planes for four embedment ratios. While $\theta\sim\psi_p^R=25°$ is used to define the soil wedge in the LEM, the slip plane in FE simulations is located on the right side of this line, although it curves outwards near the ground surface. Therefore, the weight of the lifted wedge in FE simulation is less than in LEM, especially for large $\tilde{H}$ (e.g. $\tilde{H}$=4). Moreover, although $\phi'=\phi_p'$ is used in the LEM, this is valid only for a small segment of the slip plane (e.g. near the point A in Fig. 4.8(a)). Below this point, $\phi'<\phi_p'$ because the large plastic shear strain (γ^p) causes post-peak softening. Above this point, γ^p is not sufficiently large (i.e. $\gamma^p<\gamma_p^p$) to

mobilize ϕ'_p (pre-peak), therefore $\phi' < \phi'_p$ also in this segment of the slip plane. The ratio between the pre- and post-peak segments of the slip plane increases with embedment ratio.

An overestimation of W_s and ϕ' gives a higher F_{vp} in the LEM (F_{vp_LEM}) than FE simulation (F_{vp_FE}). In order to investigate this effect, FE simulations are performed for varying embedment ratio ($\tilde{H}$=1–4), diameter (D=100–500 mm) and relative density of dense sand (D_r=80–90%). It is found that change in D_r for this range has minimal influence on pipeline response because ϕ'_p and ψ_p remain the same, as I_R=4.0 at a low mean stress and high relative density (Bolton 1986) (Eqs. (4.1)–(4.3)), although γ_p^p slightly decreases with an increase in D_r. Note that the MMC model should not be used for loose to medium dense sand as it cannot capture the volumetric compression due to shear.

Figure 4.8(b) shows that the reduction factor R ($=F_{vp\_FE}/F_{vp\_LEM}$) decreases with an increase in embedment ratio, which is because of an overestimation of W_s and ϕ' in LEM as discussed above. Moreover, R is almost independent of pipe diameter (Fig. 4.8 (b)). The overestimation of uplift resistance in LEM is significant at large embedment ratios, for example, the LEM calculates ~25% higher peak resistance than FE calculated value.

4.8.3 Uplift resistance after initial softening

Similar to Eq. (4.13), a simplified equation is proposed for the uplift force after initial softening, F_{vs} (Eq. (4.14)). At this large displacement ($\tilde{v}_s$), the failure planes reach the ground surface (Fig. 4.4(c)) and therefore R=1 is used. As significant strain-softening occurs, ϕ' along the slip planes reduces almost to ϕ'_c. The ground surface heave is significant at this stage ($\tilde{v}=\tilde{v}_s$) (Fig. 4.4(c)). Figure 4.4 shows that, although θ decreases with $\tilde{v}$, surface heave occurs over a large horizontal distance. The dilatant behaviour causes more heave than the cavity below the pipe, which is similar

to as observed in physical modeling (Cheuk et al. 2008). The additional weight due to surface heave is calculated assuming a trapezoidal soil wedge having slope angle α ($\leq\phi'_c$) and height 0.9*v*, as shown in the inset of Fig. 4.10. The base width is obtained by drawing two slip planes at $\theta = \psi_p^R$. Similar type of trapezoidal heave was observed in physical experiments on loose sand; however, it becomes triangular shape when the pipe moves near the ground surface (Schupp et al. 2006; Wang et al. 2012).

As the slip planes do not become completely vertical at large $\tilde{v}$ (Figs. 4.4(c)–4.4(e)), θ=8° is used to calculate F_{vs} using Eq. (4.14).

$$F_{vs} = \gamma D^2 \left[\left\{\left(\tilde{H} - \tilde{v}_s\right) - \frac{\pi}{8} + \left(\tilde{H} - \tilde{v}_s\right)^2 \tan\theta\right\} + \left\{F_A\left(\tilde{H} - \tilde{v}_s\right)^2\right\} + 0.9\tilde{v}_s\left\{1 + \left(\tilde{H} - \tilde{v}_s\right)\tan\psi_p^R\right\}\right] \quad (4.14)$$

4.8.4 Displacement at peak resistance and initial softening

Although it is not noticeable in Fig. 4.6, a very small increase in $\tilde{v}_p$ with $\tilde{H}$ is found, which can be approximately represented as $\tilde{v}_p = 0.002\tilde{H} + 0.025$. However, a considerable increase in $\tilde{v}_s$ with $\tilde{H}$ is found, which can be expressed as $\tilde{v}_s = 0.0035\tilde{H} + 0.1$. However, one should not extrapolate these empirical equations outside this range of $\tilde{H}$ (=1–4) simulated in this study because the failure mechanisms could be very different. For example, the pipeline will be partially embedded if $\tilde{H} < 0.5$. On the other hand, flow around mechanisms govern the response for large $\tilde{H}$.

FE results show that the ratio $\tilde{v}_s/\tilde{v}_p$ is greater than 3—as recommended in DNV (2007)—especially at high $\tilde{H}$. One potential reason is that, at high $\tilde{H}$, the formation of the inclined shear

band continues even after the peak until it reaches the ground surface that requires some additional upward displacement of the pipe (Figs. 4.4(a) & 4.4(b)).

4.9 Comparison of Simplified Equations and FE Results

Figure 4.6 shows that the proposed equations can model the force–displacement behaviour obtained from FE simulations. In this figure, the solid lines are drawn by calculating F_{vp} and F_{vs} using Eqs. (4.13) and (4.14), respectively, and then dividing the values by γHD. The value of R in Eq. (4.13) is obtained from Fig. 4.8(b).

Figure 4.9(a) shows that, Equation 4.13 without any reduction factor (i.e. R=1) calculates higher peak resistance than FE results. When R (=0.8–0.95) is adopted, as in Fig. 4.8(b), the calculated peak resistance using Eq. (4.13) compares well with FE results, which is also comparable to ALA (2005) but higher than DNV (2007) (Fig. 4.7). When the effects of surface heave are considered, the calculated resistance after initial softening using Eq. (4.14) also agrees well with FE results (Fig. 4.9(a)).

The contributions of W_s and S_v on N_{vp} and N_{vs} are evaluated using Eqs. (4.13) and (4.14), and are shown in Fig. 4.9(b). Note that the sum of the first and third part in the curly brackets in Eq. (4.14) is considered as W_s effect on N_{vs}. The vertical resistance offered by W_s is higher than that of S_v. Comparing the contribution of W_s on N_{vp} (where $\theta \approx \psi_p^R = 25°$) and N_{vs} (where $\theta \approx 8°$), it can be concluded that θ has a significant effect on uplift resistance. Similarly, the contribution of S_v on N_v increases significantly with θ, which depends on soil property and more specifically on dilation angle. Therefore, an appropriate soil constitutive model, like the one used in the present study, is required for modeling uplift resistance.

As discussed in the mesh sensitivity section, t_{FE} should be small enough to capture the shear band properly; however, t_{FE} does not have a significant effect on N_v. One of the potential reasons

for this is that a high weight component remains constant (unless the location of the failure planes changes), although strain-softening occurs quickly in the analysis with fine mesh, which reduces the relatively small shear component compared to the weight (Fig. 4.9(b)). Therefore, the sum of these two components (i.e. N_v) does not change significantly with t_{FE} (≤10 mm).

The performance of the proposed simplified equations is explained further plotting F_v against $(\tilde{v} - \tilde{H})$ as in Fig. 4.10. The calculated values using Eqs. (4.13) and (4.14), respectively, are comparable to F_v at the peak and after initial softening in FE analysis (circles and squares). In order to show the importance of the reduction factor R in Eq. (4.13), F_{vp} for R=1 is also plotted in Fig. 4.10. The difference between the calculated peak values of F_v using FE and the analytical solution (Eq. (4.13)) increases with $\tilde{H}$ because of overestimation of W_s and mobilized friction angle as discussed above. The calculated N_{vs} using Eq. (4.14) without surface heave is ~10% smaller than N_{vs} obtained from FE analysis. The contribution of heave increases with pipe displacement for the range of $\tilde{v}$ simulated in this study. Note that downward movement of sand particles and infilling beneath the pipe invert could reduce heave, especially when the pipe moves closer to the ground surface and a large cavity forms below the pipe, as observed in physical experiments (Schupp et al. 2006; Cheuk et al. 2008). This process could not be simulated using the present numerical technique. If it could be simulated, the post-peak segment of the force–displacement curve would move towards the line without heave, and the resistance will be zero when the invert of pipe moves to the ground surface.

Wang and Haigh (2012) showed that the post-peak segments of the uplift curves for loose sand for varying burial depths tend to follow a *backbone curve* similar to Fig. 4.10. There is only one post-peak segment in loose sand. However, an N_v–$\tilde{v}$ curve for dense sand has two post-peak segments—a quick reduction of N_v just after the peak, followed by the gradual reduction after $\tilde{v}_s$. Figure 4.10 shows that, for dense sand, the post-peak segments even after F_{vs}, do not lie on a

unique line. However, the proposed simplified equations can be used to develop the N–$\tilde{v}$ relation, even at large displacement.

4.10 Conclusions

The uplift behaviour of buried pipeline in dense sand is investigated from finite element modeling. The stress–strain behaviour of soil is modeled using a modified Mohr-Coulomb (MMC) model which considers the variation of angles of internal friction (ϕ') and dilation (ψ) with plastic shear strain, density and confining pressure as observed in laboratory tests on dense sand. Comparison with a model test result shows that force–displacement, soil deformation and failure mechanisms could be explained from the variation of ϕ' and ψ with loading. Simplified equations are proposed to establish the force–displacement curves for practical application. The following conclusions can be drawn from this study.

i. Slip planes do not reach the ground surface when the peak resistance is mobilized for higher burial depths.
ii. The proposed MMC model can simulate the rapid reduction of resistance after the peak followed by gradual reduction at large displacement as observed in model tests. However, the Mohr-Coulomb model shows a linear reduction of resistance due to change in cover depth.
iii. For deep embedment (H/D=3–4), soil failure initiates with slip plane mechanisms and then the flow around mechanisms observe at large displacement.
iv. The angle of inclination of the slip planes with vertical (θ) is approximately equal to the peak dilation angle when the peak resistance mobilizes. However, it decreases with upward displacement due to decreases in dilation angle. The angle θ significantly influences the weight of soil wedge and thereby uplift resistance.

v. Uplift resistance at large displacement does not remain constant but decreases with upward displacement.

vi. Displacement requires to complete initial softening increases significantly with *H*/*D* ratio as compared to the peak displacement.

Finally, one of the limitations of the present study is that infilling at the pipe invert at large displacement could not be simulated in this study. Moreover, FE simulations for varying pipe diameter, large burial depth and comprehensive parametric study for soil parameters are not presented here because of space limitation, which are available in Chapter 5.

Acknowledgements

The works presented in this paper have been supported by the Research and Development Corporation of Newfoundland and Labrador, Chevron Canada Limited and the Natural Sciences and Engineering Research Council of Canada (NSERC).

References

Aiban, S. A., and Znidarčić, D. (1995). "Centrifuge modeling of bearing capacity of shallow foundations on sands." *J. of Geotech. Eng.*, 121(10), 704–712.

Alshibli, K., and Sture, S. (1999). "Sand shear band thickness measurements by digital imaging techniques." *J. Comput. Civ. Eng.*, 13(2), 103–109.

American Lifelines Alliance (ALA). (2005). "Guidelines for the Design of Buried Steel Pipe." <https://www.americanlifelinesalliance.com/pdf/Update061305.pdf > (Mar. 13, 2017).

American Petroleum Institute (API). (1987). "Recommended practice for planning, designing and constructing fixed offshore platforms." *API Recommended practice*, 2A (RP 2A), 17th Ed.

Anastasopoulos, I., Gazetas, G., Bransby, M.F., Davies, A., and El Nahas, M.C.R. (2007). "Fault rupture propagation through sand: finite-element analysis and validation through centrifuge experiments." *J. of Geotech. and Geoenv. Eng.*, 133(8), 943–958.

Andresen, L. and Jostad, H.P. (2004). "Analyses of progressive failure in long natural slopes." *Proc., 9th Symp. on Num. Models in Geomech. - NUMOG IX*, Ottawa, 603–608.

Aynbinder, A.B., and Kamershtein, A.G. (1982). "Raschet magistral'nykh truboprovodov na prochnost' i ustoichivost' [Calculation of trunk pipelines for strength and stability]." Nedra, Moscow (In Russian).

Bolton, M. D. (1986). "The strength and dilatancy of sands." *Géotechnique*, 36(1), 65−78.

Bransby, M. F., and Ireland, J. (2009). "Rate effects during pipeline upheaval buckling in sand." *Proc., ICE – Geotech. Eng.*, 162(5), 247–258.

Bransby, M.F., Newson, T. A. and Davies, M. C. R. (2002). "Physical modelling of the upheaval resistance of buried offshore pipelines." *Proc., International conference on physical modelling in geotechnics*, Kitakyushu, Japan.

Cathie D.N., Jaeck C., Ballard J-C and Wintgens J-F. (2005). "Pipeline geotechnics – state-of-the-art." *Proc., Int. Symposium on Frontiers in Offshore Geotechnics*, Taylor & Francis, 95–114.

Chakraborty, D. and Kumar, J. (2014). "Vertical Uplift Resistance of Pipes Buried in Sand." *J. of Pipe. Sys. Eng. and Prac.*, 5(1).

Cheuk, C. Y., White, D. J. and Bolton, M. D. (2005). "Deformation mechanisms during the uplift of buried pipelines in sand." *Proc., 16th International Conference on Soil Mechanics and Geotechnical Engineering*, Osaka, 1685–1688.

Cheuk, C. Y., White, D. J., and Bolton, M. D. (2008). "Uplift mechanisms of pipes buried in sand." *J. Geotech. Geoenv. Eng.*, 134(2), 154–163.

Chin, E. L., Craig, W. H., and Cruickshank, M. (2006). "Uplift resistance of pipelines buried in cohesionless soil." *Proc., 6th Int. Conf. on Physical Modelling in Geotechnics*, Ng, Zhang, and Wang, eds., Vol. 1, Taylor & Francis Group, London, 723–728.

Clukey, E.C., Haustermans, L. and Dyvik, R. (2005). "Model tests to simulate riser–soil interaction effects in touchdown point region." *Proc., International Symposium on Frontiers in Offshore Geotechnics (ISFOG 2005)*, Perth, Australia, 651–658.

Dassault Systèmes. (2010). *ABAQUS* [computer program]. Dassault Systèmes, Inc., Providence, R.I.

Det Norske Veritas (DNV). (2007). "Global buckling of submarine pipelines—Structural design due to high temperature/high pressure." *DNV-RP-F110*, Det Norske Veritas, Baerum, Norway.

Dickin, E.A. (1994). "Uplift resistance of buried pipelines in sand." *Soils and Found.*, 34(2), 41–48.

Dutta, S., Hawlader, B. & Phillips, R. (2015). "Finite element modeling of partially embedded pipelines in clay seabed using Coupled Eulerian–Lagrangian method." *Can. Geotech. J.*, 52(1), 58–72.

Eiksund, G., Langø, H., Øiseth, E. (2013). "Full-scale test of uplift resistance of trenched pipes." *Int. J. of Offshore and Polar Eng.*, 23(4), 298–306.

Farhadi, B., and Wong, C. K. (2014). "Numerical modeling of pipe-soil interaction under transverse direction." *Proc., 10th International Pipeline Conference (IPC 2014)*, Calgary, Alberta, Canada.

Guo, P. (2012). "Critical length of force chains and shear band thickness in dense granular materials." *Acta Geotech.*, 7, 41–55.

Huang, B., Liu, J., Ling, D. and Zhou, Y. (2015). "Application of particle image velocimetry (PIV) in the study of uplift mechanisms of pipe buried in medium dense sand." *J Civil Struct. Health Monit*., 5(5), 599–614.

Jung, J.K., O'Rourke, T.D., and Olson, N.A. (2013). "Uplift soil–pipe interaction in granular soil." *Can. Geotech. J*., 50(7), 744–753.

Lings, M. L., and Dietz, M. S. (2004). "An improved direct shear apparatus for sand." *Géotechnique*, 54(4), 245−256.

Loukidis D and Salgado R. (2011). "Effect of relative density and stress level on the bearing capacity of footings on sand." *Géotechnique*, 61(2), 107–19.

Loukidis, D. and Salgado, R. (2008). "Analysis of the shaft resistance of non-displacement piles in sand." *Géotechnique*, 58(4), 283–296.

Merifield, R. S., Sloan, S. W., Abbo, A. J. and Yu, H. S. (2001). "The ultimate pullout capacity of anchors in frictional soils." *Proc., 10th Int. Conf. on Computer Methods and Advances in Geomechanics*, Tucson, AZ, 1187–1192.

Moore, I. D. and Rowe, R. K. (1990). "Scaling rule for localized plasticity in strain-softening continua." *Proc., 1st Int. Conf. on Computer Aided Assessment of Localized Damage*, Portsmouth, 2, 99–112.

Palmer, A.C., White, D.J., Baumgard, A.J., Bolton, M.D., Barefoot, A.J., Finch, M., Powell, T., Faranski, A.S., and Baldry, J.A.S. (2003). "Uplift resistance of buried submarine pipelines: comparison between centrifuge modelling and full-scale tests." *Géotechnique*, 53(10), 877–883.

Pietruszczak, St. and Mróz, Z. (1981). "Finite element analysis of deformation of strain-softening materials." *Int. J. for Num. Methods in Eng*., 17, 327–334.

Pike, K., and Kenny, S. (2016). "Offshore pipelines and ice gouge geohazards: Comparative performance assessment of decoupled structural and coupled continuum models." *Can. Geotech. J.*, 53(11), 1866–1881.

Pike, K. (2016). "Physical and numerical modelling of pipe/soil interaction events for large deformation geohazards." PhD thesis, Memorial University of Newfoundland, St. John's, Canada.

Pradhan, T. B.S. (1997). "Characteristics of shear band in plane strain compression tests of sand." *Proc., IS-NAGOYA'97*, Deformation and progressive failure in geomechanics, Pergamon, 241–246.

Randolph, M.F., Jamiolkowski, M.B. and Zdravkovic, L. (2004). "Load carrying capacity of foundations." *Proc., Skempton Memorial Conf.,* London, 1, 207–240.

Robert, D. J., and Thusyanthan, N. I. (2014). "Numerical and experimental study of uplift mobilization of buried pipelines in sands", *J. Pipe. Systems Eng. and Prac*., 6(1).

Roy, K., Hawlader, B.C., Kenny, S. and Moore, I. (2016). "Finite element modeling of lateral pipeline−soil interactions in dense sand." *Can. Geotech. J.*, 53(3), 490–504.

Saboya, F.A. Jr., Santiago, P. A.C., Martins, R.R., Tibana, S., Ramires, R.S. and Araruna, J. T. Jr. (2012). "Centrifuge test to evaluate the geotechnical performance of anchored buried pipelines in sand." *J. of Pipe. Sys. Eng. and Prac*., 3(3).

Schaminée, P., Zorn, N., and Schotman, G. (1990). "Soil response for pipeline upheaval buckling analyses: Full-scale laboratory tests and modelling." *Proc., Offshore Technol. Conf.*, Houston, 563–572.

Schupp, J., Byrne, B. W., Eacott, N., Martin, C. M., Oliphant, J., Maconochie, A., and Cathie, D. (2006). "Pipeline unburial behaviour in loose sand." *Proc., 25th Int. Conf. on Offshore Mechanics and Arctic Engineering*, Hamburg, Germany, OMAE2006-92541.

Stone, K. J. L., and Newson, T. A. (2006). "Uplift resistance of buried pipelines: An investigation of scale effects in model tests." Proc., *6th Int. Conf. on Physical Modelling in Geotechnics, Ng, Zhang, and Wang, eds.*, Vol. 1, Taylor & Francis Group, London, 741–746.

Tatsuoka, F., Okahara, M., Tanaka, T., Tani, K., Morimoto, T., and Siddiquee, M. S. A. (1991). "Progressive failure and particle size effect in bearing capacity of a footing on sand." *Geotech. Spec. Publ.*, 27(2), 788–802.

Tejchman, J. and Górski, J. (2008). "Size effects in problems of footings on sand within micro-polar hypoplasticity." *Archives of Hydro-Engineering and Environmental Mechanics*, 55(3–3), 95–124.

Tejchman, J. and Herle, I. (1999). "A "class A" prediction of the bearing capacity of plane strain footings on granular material." *Soils and Foundations*, 39(5), 47–60.

Thusyanthan, N. I., Mesmar, S., Wang, J. and Haigh, S. K. (2010). "Uplift resistance of buried pipelines and DNV-RP-F110." *Proc., Offshore Pipeline and Technology Conference*, Amsterdam, 24–25.

Trautmann, C. (1983). "Behavior of pipe in dry sand under lateral and uplift loading." PhD thesis, Cornell University, Ithaca, NY.

Wang, J., Ahmed, R., Haigh, S. K., Thusyanthan, N. I., and Mesmar, S. (2010). "Uplift resistance of buried pipelines at low cover–diameter ratios." *Proc., Offshore Technol. Conf.*, OTC-2010-20912, Houston.

Wang, J., Haigh, S. K., Forrest, G. and Thusyanthan, N. I. (2012). "Mobilization distance for upheaval buckling of shallowly buried pipelines." *J. Pipe. Syst. Eng. Prac.*, 3(4), 106–114.

White, D. J., Barefoot, A. J. & Bolton, M. D. (2001). "Centrifuge modelling of upheaval buckling in sand." *Int. J. Phys. Modelling Geomech.*, 2, 19–28.

White, D. J., Take, W. A., and Bolton, M. D. (2003). "Soil deformation measurement using particle image velocimetry (PIV) and photogrammetry." *Geotechnique*, 53(7), 619–631.

White, D.J., Cheuk, C.Y, and Bolton, M.D. (2008). "The Uplift resistance of pipes and plate anchors buried in sand." *Géotechnique*, 58(10), 771–779.

Yimsiri, S., Soga, K., Yoshizaki, K., Dasari, G., and O'Rourke, T. (2004). "Lateral and upward soil−pipeline interactions in sand for deep embedment conditions." *J. of Geotech. and Geoenv. Eng.*, 130(8), 830−842.

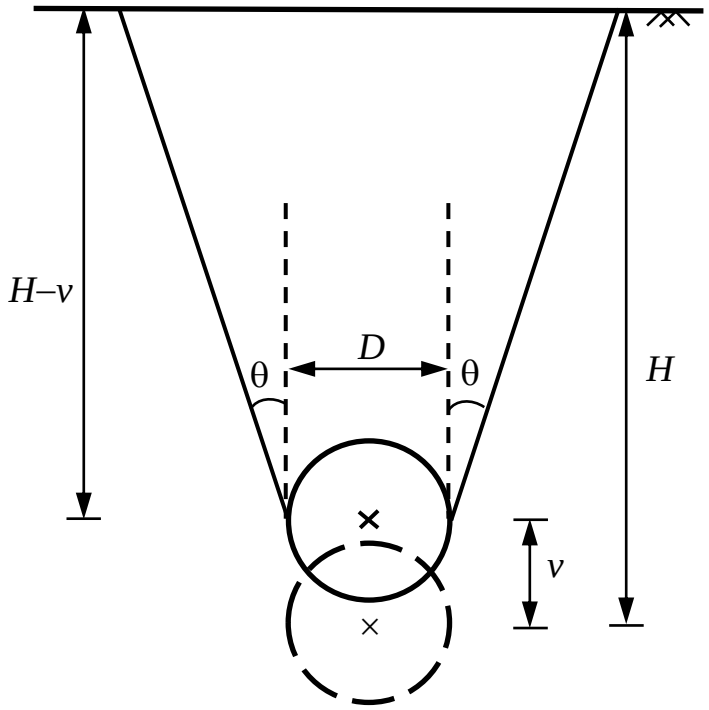

Figure 4.1: Geometry and conceptual failure mechanisms

(a)

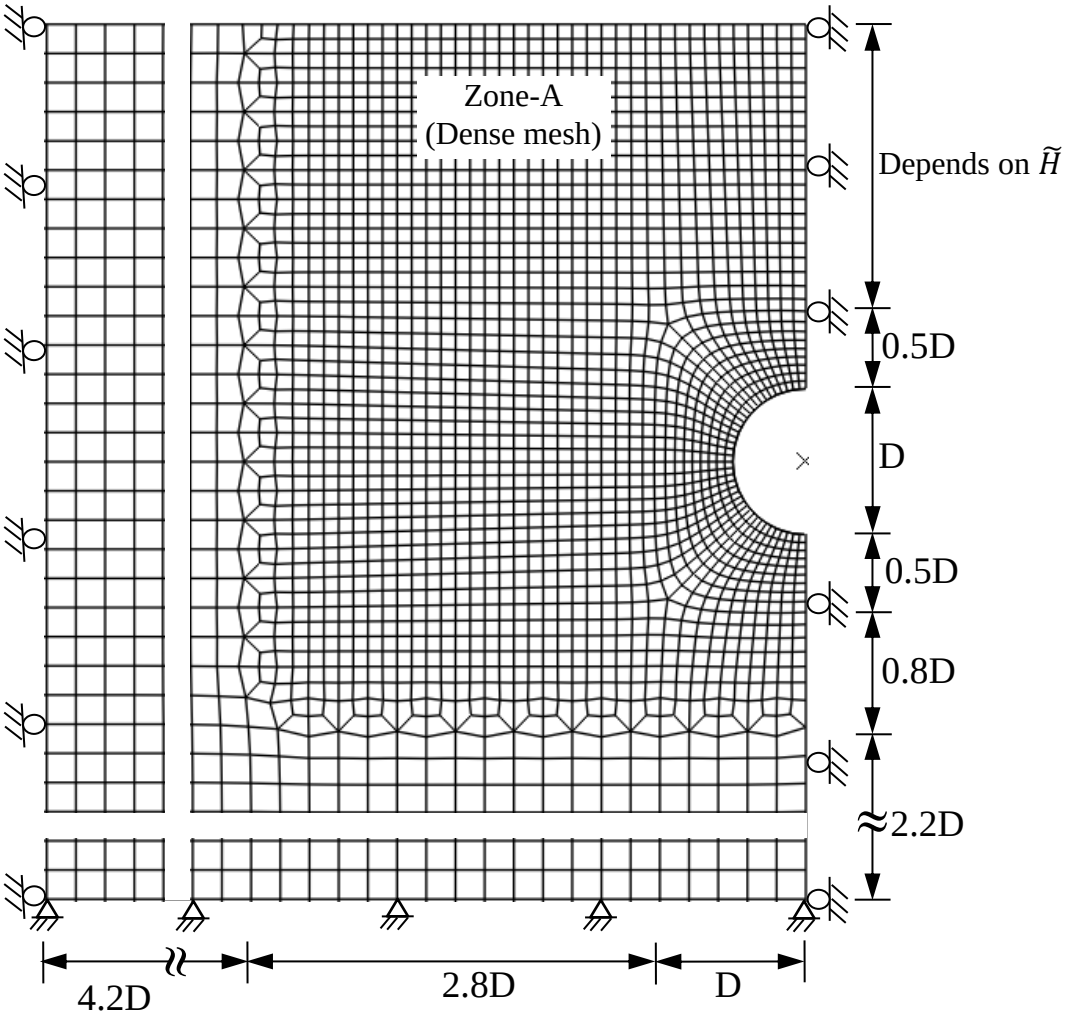

Figure 4.2: Finite element modelling: (a) typical finite element mesh for *D*=100 mm

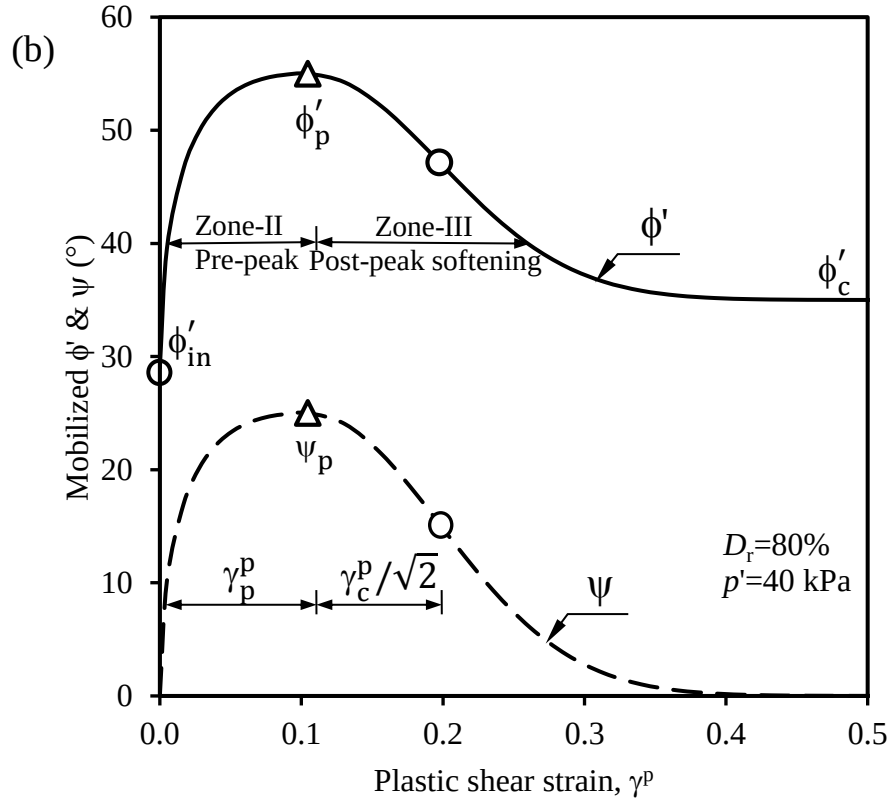

Figure 4.2: Finite element modelling: (b) typical variation of mobilized friction and dilation angle

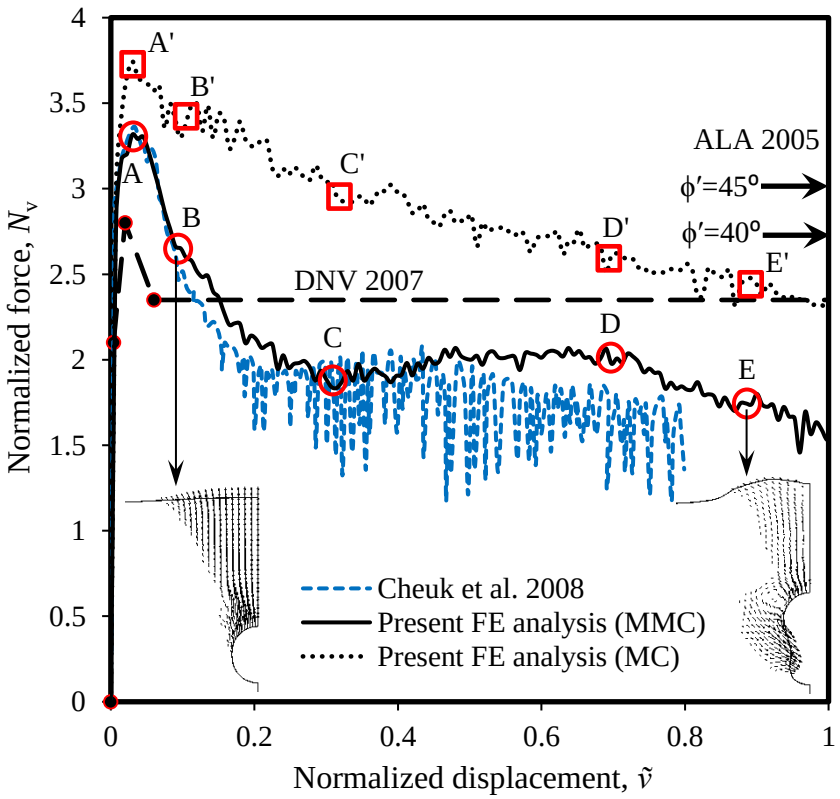

Figure 4.3: Comparison of FE simulation and model test result

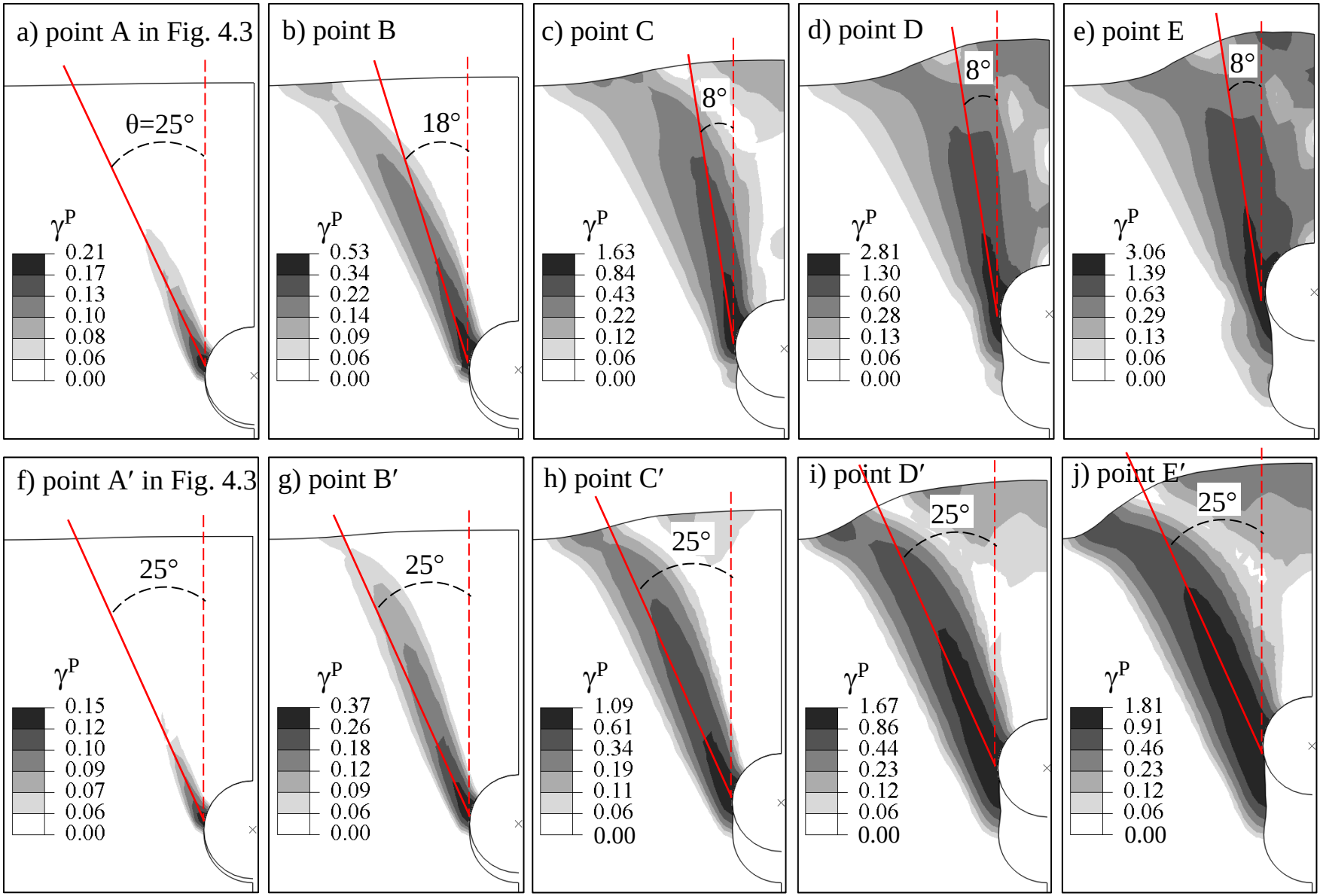

Figure 4.4: Shear band formation: a–e for modified Mohr-Coulomb model and f–j for Mohr-Coulomb model

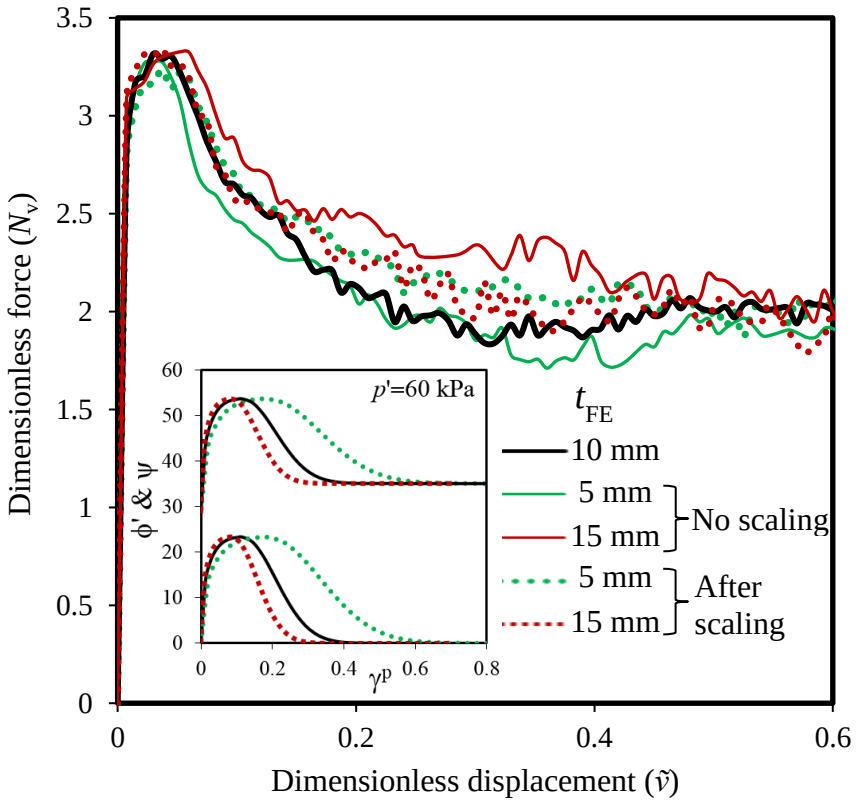

Figure 4.5: Mesh sensitivity analysis with the MMC model

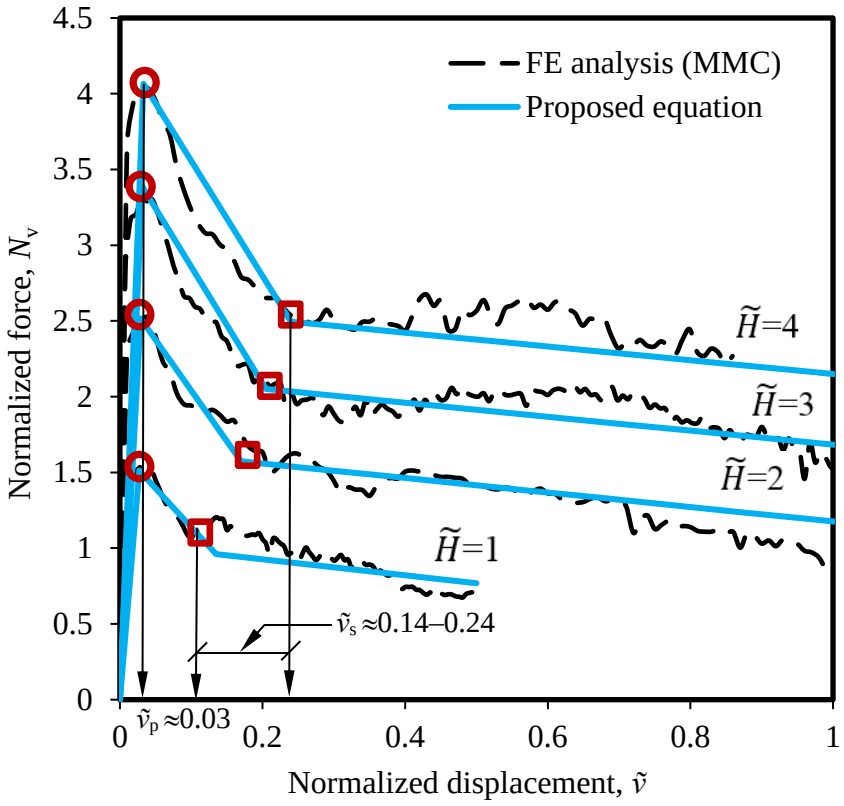

Figure 4.6: Comparison of simplified equations and FE results for different $\tilde{H}$

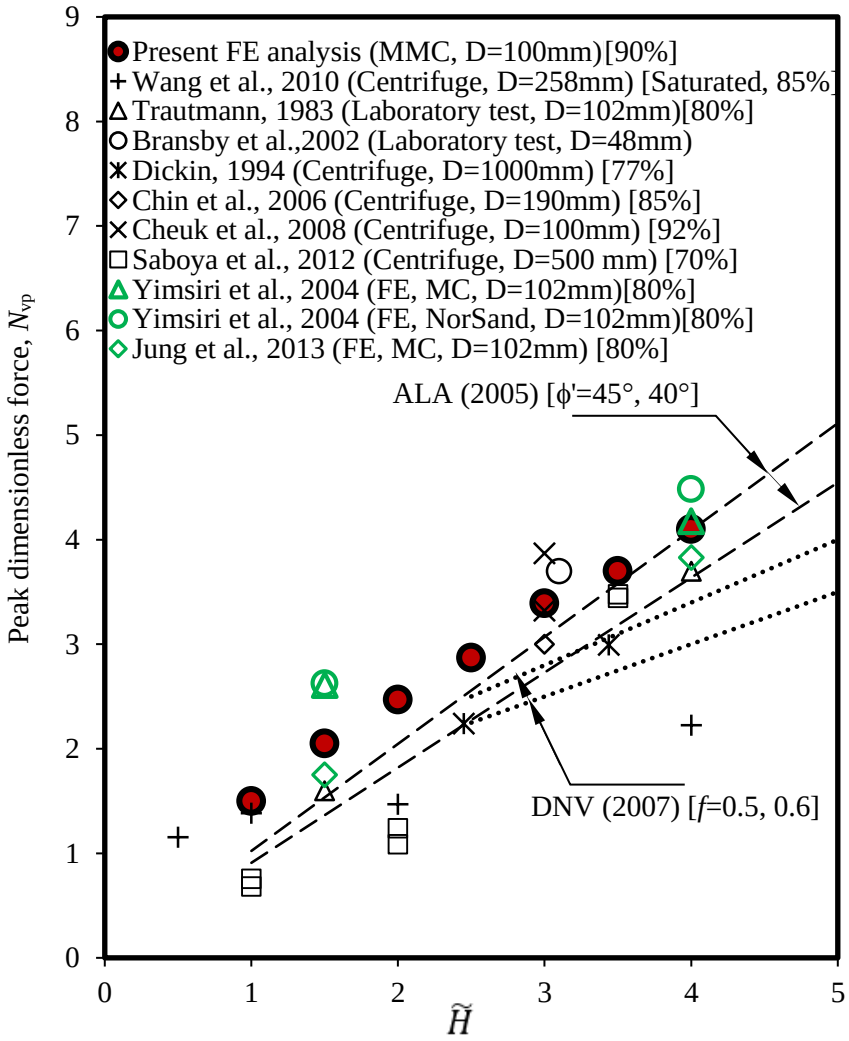

Figure 4.7: Comparison of peak uplift force from numerical analysis and physical model tests

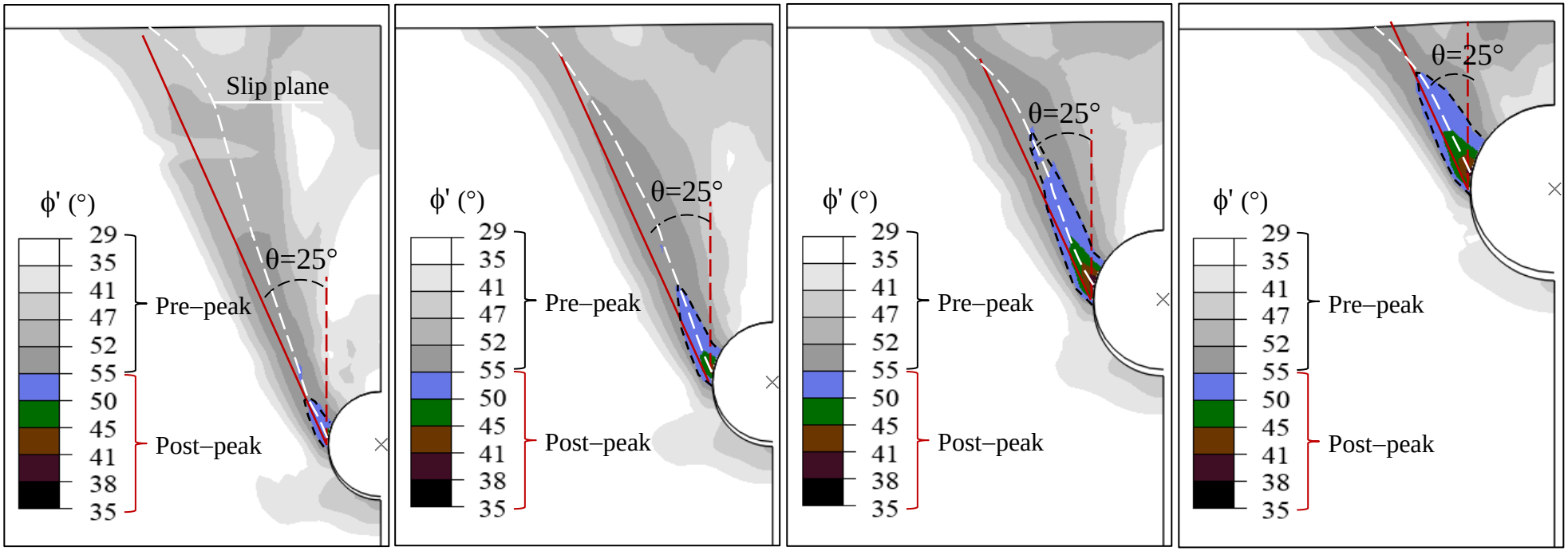

Figure 4.8: Effect of burial depth on R (a) Formation of slip planes for different $\widetilde{H}$

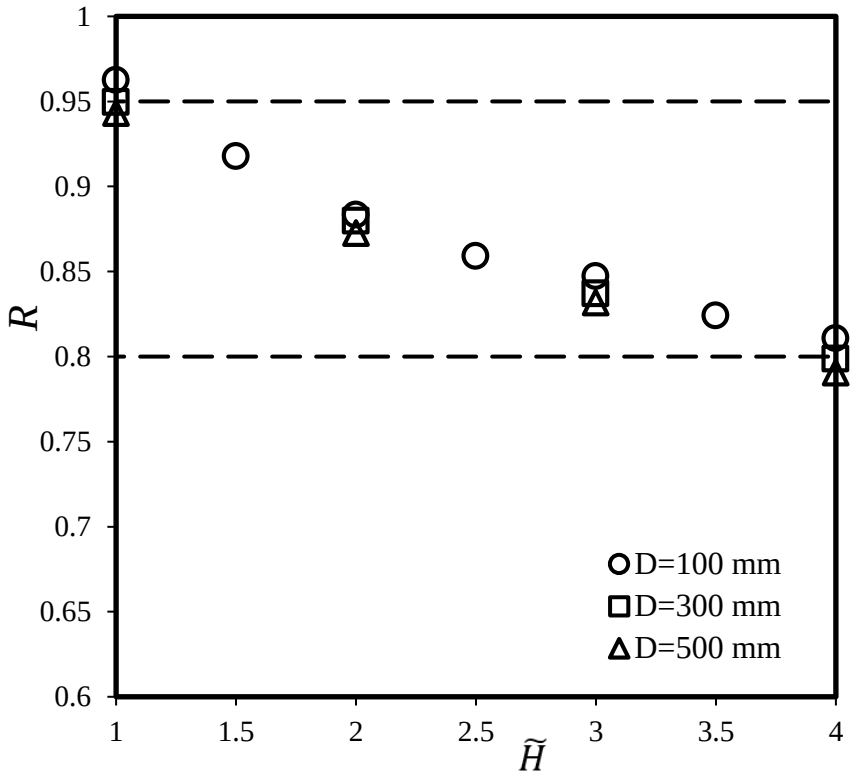

Figure 4.8: Effect of burial depth on R (b) R vs $\widetilde{H}$ plot

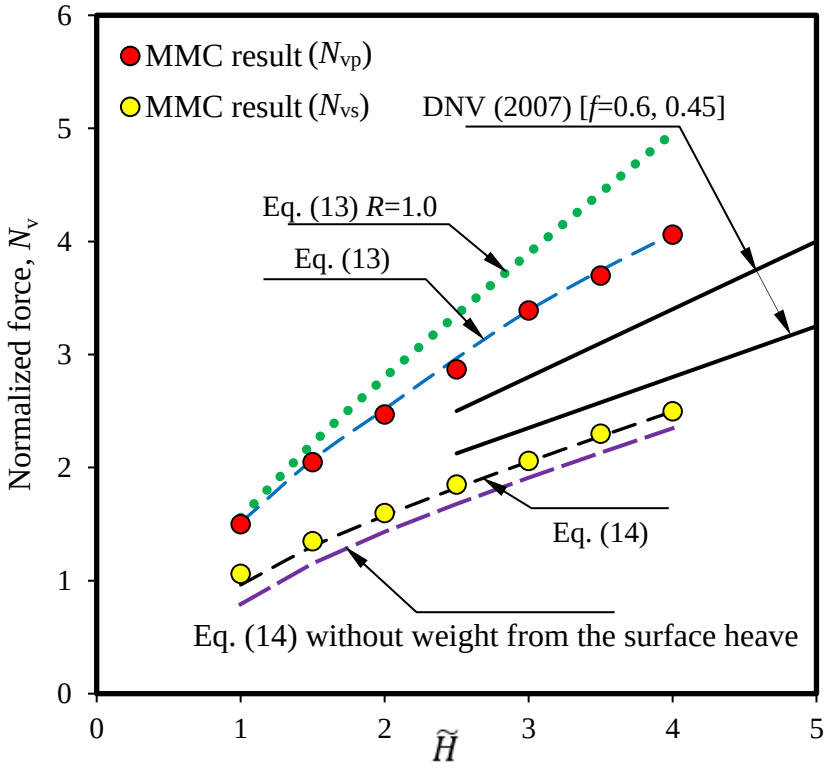

Figure 4.9: Comparison between simplified model and FE analysis (a) peak and post-peak resistances

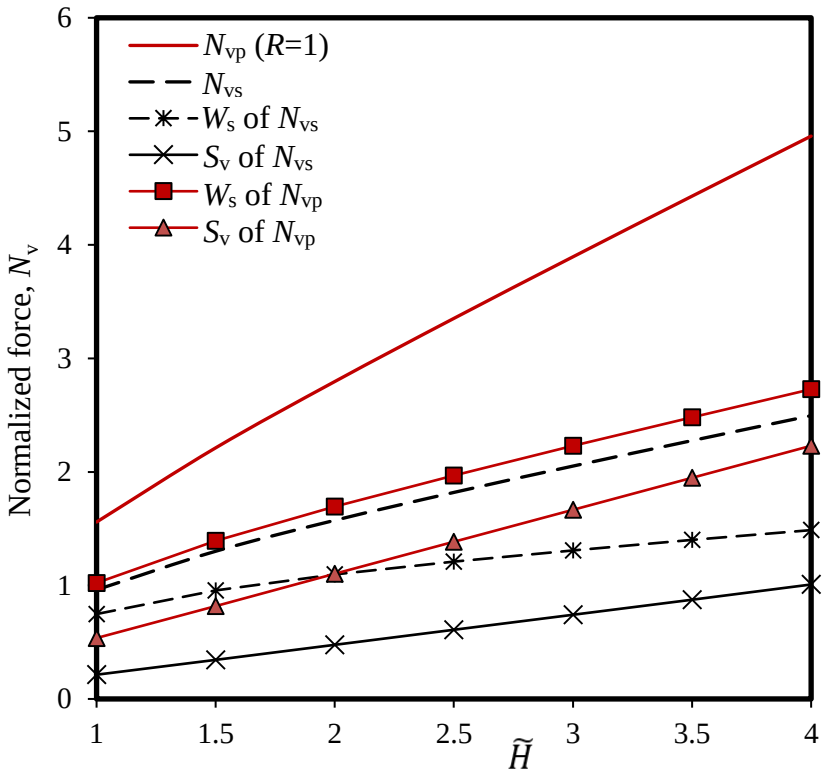

Figure 4.9: Comparison between simplified model and FE analysis (b) Contribution of weight and shear components on peak and post-peak resistances

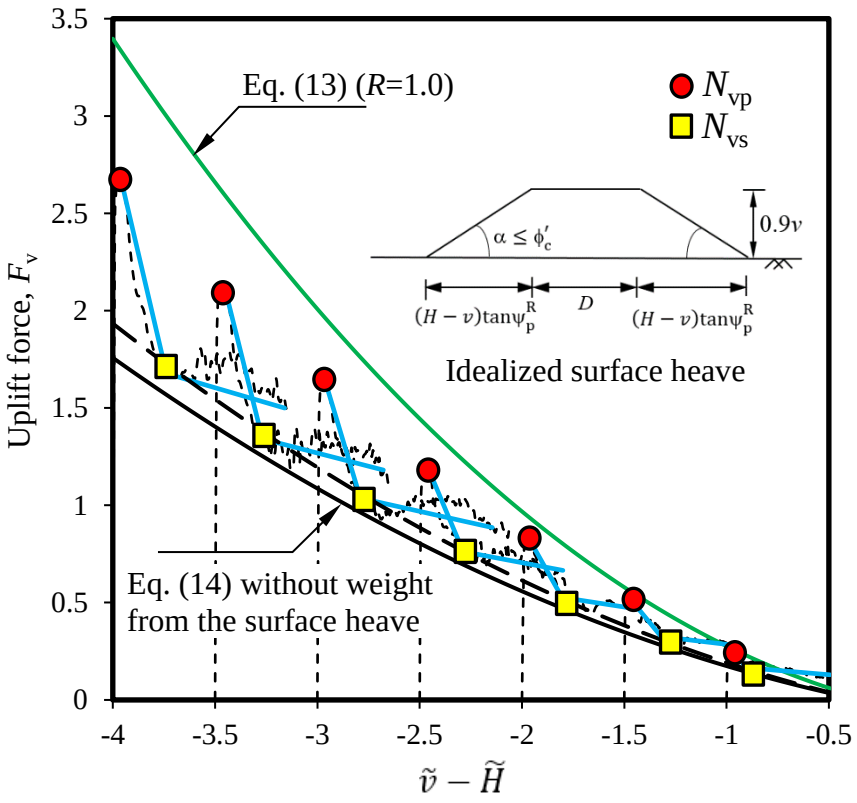

Figure 4.10: Comparison between force–displacement curves from FE analysis and simplified equations

Table 4.1: Equations for Modified Mohr–Coulomb Model (MMC) (summarized from Chapter 3)

Description	Eq. #	Constitutive Equations
Relative density index	(4.1)	$I_R = I_D(Q - \ln p') - R$ where $I_D = D_r(\%)/100$ & $0 \le I_R \le 4$
Peak friction angle	(4.2)	$\phi'_p - \phi'_c = A_\psi I_R$
Peak dilation angle	(4.3)	$\psi_p = \frac{\phi'_p - \phi'_c}{k_\psi}$
Strain-softening parameter	(4.4)	$\gamma_c^p = C_1 - C_2 I_D$
Plastic shear strain at ϕ'_p and ψ_p	(4.5)	$\gamma_p^p = \gamma_c^p \left(\frac{p'}{p'_a}\right)^m$
Mobilized friction angle in Zone-II	(4.6)	$\phi' = \phi'_{in} + \sin^{-1}\left[\left(\frac{2\sqrt{\gamma^p \gamma_p^p}}{\gamma^p + \gamma_p^p}\right)\sin(\phi'_p - \phi'_{in})\right]$
Mobilized dilation angle in Zone-II	(4.7)	$\psi = \sin^{-1}\left[\left(\frac{2\sqrt{\gamma^p \gamma_p^p}}{\gamma^p + \gamma_p^p}\right)\sin(\psi_p)\right]$
Mobilized friction angle in Zone-III	(4.8)	$\phi' = \phi'_c + (\phi'_p - \phi'_c)\exp\left[-\left(\frac{\gamma^p - \gamma_p^p}{\gamma_c^p}\right)^2\right]$
Mobilized dilation angle in Zone-III	(4.9)	$\psi = \psi_p \exp\left[-\left(\frac{\gamma^p - \gamma_p^p}{\gamma_c^p}\right)^2\right]$
Young's modulus	(4.10)	$E = K p'_a \left(\frac{p'}{p'_a}\right)^n$

Table 4.2: Geometry and soil parameters used in the FE analyses

Parameter	Values
External diameter of pipe, D (mm)	100 (300, 500)
K	150
n	0.5
ν_{soil}	0.2
A_ψ	5
k_ψ	0.8
ϕ'_{in} (°)	29
C_1	0.22
C_2	0.11
m	0.25
Critical state friction angle, ϕ'_c (°)	35
Relative density, D_r (%)	90
Unit weight, γ (kN/m^3)	16.87
Interface friction coefficient, μ	0.32
Embedment ratio, $\widetilde{H}$	3 (1, 1.5, 2.0, 2.5, 3.5, 4.0)

Note: Numbers in parenthesis in right column show the values used in the parametric study

CHAPTER 5

Uplift Failure Mechanisms of Pipes Buried in Dense Sand

Co–Authorship: This chapter has been submitted to a journal as a technical paper for review as: Roy, K., Hawlader, B.C., Kenny, S. and Moore, I. (2017), 'Uplift Failure Mechanism of Pipes Buried in Dense Sand.' Most of the research presented in this chapter has been conducted by the first author. He has prepared the draft manuscript. The other authors mainly supervised the research and reviewed the manuscript.

5.1 Abstract

Finite element (FE) modeling of uplift resistance from dense backfill sand is presented in this paper. The pre-peak hardening, post-peak softening, density and confining pressure dependent soil behaviour are implemented in FE analysis to simulate progressive development of shear bands. The location of the shear bands is identified from soil failure mechanisms for a range of burial depths. For shallow-buried pipelines, the inclination of the slip planes to the vertical is approximately equal to the maximum dilation angle when the peak uplift resistance is mobilized and then decreases with upward movement resulting in post-peak reduction of uplift resistance. For deeper conditions, in addition to two inclined slip planes, logarithmic spiral type shear bands form above the pipe. Based on mobilized shear strength parameters and inclination of slip planes, a method to calculate the peak and post-peak uplift resistances, using an equivalent angle of internal friction, is presented.

5.2 Introduction

Buried pipelines in offshore environments generally operate at high pressure and temperature to assure hydrocarbon flow. Temperature increase causes axial expansion, and if it is restrained by axial resistance offered by soil or end fixity, the axial force might be relieved by upheaval or lateral buckling. The vertical movement of the buckled section of the pipeline continues until a stable equilibrium position is reached and, in the worst case scenario, a section of the pipe might be protruded above the seabed/ground surface (Aynbinder & Kamershtein 1982; Guijt 1990; Craig et al. 1990; Finch, 1999; Palmer and Williams 2003; Palmer et al. 2003). During upheaval buckling, a section of pipeline might be displaced significantly through the soil. For example, Nielsen et al. (1990) reported that a 219-mm diameter (D) pipeline in the North Sea displaced from the initial configuration to a maximum vertical distance of ~ 0.5–1.0 m with a wavelength of 50–70 m at 26 locations during the first 7 months after being brought into service. In one section, the pipe displaced vertically ~1.5 m (i.e. 6.8D) through the soil and then protruded a maximum vertical distance of 1.1 m above the seabed. The burial depth of the pipeline during installation was ~6.3D–9.2D.

Burial is one of the main sources of pipeline installation cost. Therefore, proper understanding of soil failure mechanisms during pipe uplift is necessary for estimation of uplift resistance and selection of required burial depth—typically expressed as the H/D ratio ($\widetilde{H}$), where H is the depth of the center of the pipe. Offshore pipelines are generally embedded at $\widetilde{H} \leq 4$; however, in many special scenarios $\widetilde{H}$ could be higher than 4. For example, the burial depth of a 254-mm oil pipeline constructed by Chevron in the south pass block 38 of the Gulf of Mexico changed from $\widetilde{H}$~4 in 1980 to $\widetilde{H}$~24 in 1998 due to sediment deposition (Liu and O'Rourke 2010). Similarly, in the regions where ice gouging is expected, a large $\widetilde{H}$ is maintained to protect the

pipeline from ice gouging effects (Palmer 1990; Hequette et al. 1995; Kenny et al. 2007; Been et al. 2008; Barrette et al. 2015).

During installation of offshore pipelines in sand, ploughs normally deposit backfill soil in a loose to medium dense state (Cathie et al. 2005); however, it could be subsequently densified due to environmental loading. For example, Clukey et al. (2005) showed that the sandy backfill of a test pipe section densified from relative density (D_r) less than ~57% to ~85–90% in 5 months, which has been attributed to wave action at the test site in the Gulf of Mexico.

For drained loading conditions, the uplift resistance (F_v) is the sum of submerged weight of the lifted soil wedge (W_s) and the vertical component of shearing resistance along the slip plane (S_v). F_v also depends on vertical displacement of the pipe (v). The force–displacement behaviour is generally expressed in normalized form using $N_v=F_v/\gamma HD$ and $\tilde{v}=v/D$, where γ is the unit weight of the soil. Most of the physical model tests for uplift resistance were conducted for $\tilde{H} \leq 4$; however, a limited number of tests at deep burial conditions are also available (Trautmann 1983; Dickin 1994). Experimental results show that N_v increases with $\tilde{H}$ and D_r (Trautmann 1983; Bransby et al. 2002; Chin et al. 2006; Cheuk et al. 2008). The model tests on dense sand show that N_v increases quickly with $\tilde{v}$, reaches the peak (N_{vp}) and then decreases with further increase in $\tilde{v}$ (Trautmann 1983; White et al. 2001; Cheuk et al. 2008).

The load–displacement curves obtained from model tests evolve from complex deformation mechanisms and the stress–strain behaviour of soil above the pipe. To understand these mechanisms, the particle image velocimetry (PIV) technique (White et al. 2003) has been used in recent experiments (Cheuk et al. 2005; White et al. 2008; Thusyanthan et al. 2010; Wang et al. 2010). PIV data can provide very useful information on soil deformation patterns; however, the progressive formation of shear bands in dense sand due to strain-softening can be better explained by using numerical modeling techniques where other correlated parameters (e.g. evolution in

strength parameters) can be more readily and directly monitored. White et al. (2008) showed that when the peak uplift resistance mobilizes in medium to dense sand, two inclined symmetric slip planes form in the soil, originating from the pipe waist. Although the slip planes are slightly curved outward, their inclination with the vertical (θ) is approximately equal to the peak dilation angle (ψ_p). Huang et al. (2015) showed that θ is less than ψ_p at a small $\tilde{v}$, which gradually increases with $\tilde{v}$ to the maximum value of (θ~ψ_p) when the peak resistance is mobilized. The vertical inclination of the slip plane then decreases with further increase in $\tilde{v}$, and θ~0 at large $\tilde{v}$, at least for shallow burial conditions (Huang et al. 2015).

Both components of uplift resistance (W_s and S_v) directly depend on the inclination of the slip plane (θ). In addition, for dense sand, the shear resistance of the soil elements along the slip plane depends on plastic shear strain. If the value of θ and shear resistance are known, the uplift resistance can be calculated using the limit equilibrium method (White et al. 2008). To obtain these values, the soil failure mechanisms and progressive development of slip planes need to be examined. The modeling of progressive failure using an appropriate soil constitutive model could also explain the post-peak reduction of uplift resistance as observed in physical model tests and recognized by DNV (2007) in the development of design guidelines.

The main objective of the present study is to conduct FE modeling of uplift behaviour of pipe in dense sand for a wide range of burial depths ($\tilde{H}$=2–10) and diameters (D=100–500 mm). The pipe is moved a sufficiently large distance to obtain θ from the failure patterns at various levels of displacement. A soil model that considers strain-softening behaviour of dense sand is implemented in FE analysis to evaluate the variation of shear strength parameters along the failure planes. A simplified method is proposed to estimate the uplift resistance from θ and mobilized shear strength using the limit equilibrium method.

5.3 Problem Statement and FE Modeling

A section of pipe is placed at the desired burial depth ($\widetilde{H}$) in dense sand and then pulled up vertically. Two-dimensional FE analyses in plane strain condition are performed using Abaqus/Explicit FE software (Dassault Systèmes 2010). Figure 5.1(a) shows the typical FE mesh at the start of pipe uplifting. A dense mesh is used near the pipe (Zone-A), where considerable soil deformation is expected. To avoid mesh distortion issues at large displacements, an adaptive meshing option is adopted in Zone-A, using the arbitrary Lagrangian-Eulerian (ALE) method, which creates new smooth mesh with improved aspect ratios at given intervals. The bottom of the FE domain is restrained from any horizontal and vertical movement, while all the vertical faces are restrained from lateral movement.

Four-node bilinear plane strain quadrilateral elements (CPE4R in Abaqus) are used for modeling the soil, while the pipe is modeled as a rigid body. The bottom and left boundaries are placed at a sufficiently large distance from the pipe to avoid boundary effects on uplift behaviour.

The pipe–soil interface is modeled by defining the interface friction coefficient (μ) as $\mu=\tan(\phi_\mu)$, where ϕ_μ is the pipe–soil interface friction angle. ϕ_μ depends on interface characteristics and relative movement between the pipe and soil and typically lies between 50 and 100% of the peak friction angle (Yimsiri et al. 2004). In the present study, $\phi_\mu=17.5°$ is used.

The numerical analysis is conducted in two steps. In the first step, geostatic stress is applied under the K_0=0.5 condition. A parametric study shows that K_0 does not significantly affect the uplift resistance (Jung et al. 2013). In the second step, the pipe is displaced up by specifying a displacement boundary condition at the reference point (center of the pipe).

5.4 Modeling of soil

Two soil models are used in this study: (i) Mohr-Coulomb (MC) and (ii) a modified Mohr-Coulomb (MMC) model. In the MC model, the angle of internal friction (ϕ') and dilation angle (ψ) are given as input, and remain constant during FE analysis. However, in the MMC model, the mobilized ϕ' and ψ are updated during the progress of FE analysis, as a function of accumulated plastic shear strain (γ^p) and mean effective stress (p'). Note that modified forms of the MC model have also been used in previous studies (Bransby et al. 2001; Yimsiri et al. 2004; Guo and Stolle 2005; Jung et al. 2013; Robert and Thusyanthan 2014). The details of the MMC model used in the present study is presented in Chapter 3. The key features of the MMC model are presented below, while the mathematical equations are listed in Table 5.1 (Eqs. 5.1–5.10).

i) Laboratory tests on dense sand show that ϕ' and ψ vary with D_r, γ^p, p' and mode of shearing (triaxial (TX) or plane strain (PS)). However, constant representative values of ϕ' and ψ are commonly used in the MC model. The peak friction angle (ϕ'_p) increases with D_r but decreases with p' (Bolton 1986; Tatsuoka et al. 1986; Houlsby 1991; Schanz and Vermeer 1996; Hsu and Liao 1998; Lings and Dietz 2004), which are modeled using Eqs. (5.1–5.3) as in the work of Bolton (1986), where ϕ'_c is the critical state friction angle and A_ψ, k_ψ are two constants. Bolton (1986) suggested A_ψ=5.0 and 3.0 for plane strain and triaxial conditions, respectively. Chakraborty and Salgado (2010) recommended A_ψ=3.8 for both TX and PS conditions from their analysis of test results on Toyoura sand. In the present study, A_ψ=5 with $\phi'_p - \phi'_c \leq 20°$ for PS configuration is used (Bolton 1986).

ii) The mobilization of ϕ' and ψ with γ^p is modeled using Eqs. (5.6–5.9). Figure 5.1(b) shows the typical variation of ϕ' and ψ with plastic shear strain. As shown, ϕ' and ψ are gradually

increased from the initial value ($\phi'_{in}, 0$) to the peak (ϕ'_p, ψ_p) at γ^p_p. In the post-peak region, ϕ' and ψ are reduced exponentially, as shown in Eqs. (5.7) and (5.8), from the peak to the critical state ($\phi' = \phi'_c, \psi = 0$) at large γ^p. As the analysis is performed for the PS condition, ϕ'_c =35° is used, which is typically 3°–5° higher than that of the TX configuration (Bishop 1961; Conforth 1964; Pradhan et al. 1988; Yoshimine 2005). Equations (5.4) and (5.5) show that γ^p required to mobilize ϕ'_p and ψ_p decreases with I_D and increases with p'.

iii) The Young's modulus (E) is calculated using Eq. (5.10) (Janbu 1963; Hardin and Black 1966), where p' is the initial confining pressure at the pipe waist, p'_a is the atmospheric pressure (=100 kPa), K is a material constant, and n is an exponent. Equation (5.10) has also been used in previous studies for FE modeling of pipe–soil interaction (Taleb and Moore 1999; Yimsiri et al. 2004; Guo and Stolle 2005; Daiyan et al. 2011; Jung et al. 2013). The Poisson's ratio of 0.2 is used for the soil, which has been considered as the representative value for dense sand (Jefferies and Been 2006).

5.5 Implementation of MMC in Abaqus

The MMC model is implemented in Abaqus by developing a user subroutine VUSDFLD, where the stress and strain components are called in the subroutine in each time increment. The mean effective stress (p') is calculated from the principal stresses. The strain components are transferred to the principal strain components and stored as state variables. The plastic strain increment ($\Delta\gamma^p$) in each time increment is calculated as $\Delta\gamma^p = (\Delta\varepsilon_1^p - \Delta\varepsilon_3^p)$, where $\Delta\varepsilon_1^p$and $\Delta\varepsilon_3^p$ are the major and minor principal plastic strain components, respectively. The value of γ^p is calculated as the sum of $\Delta\gamma^p$ over the period of analysis. In the subroutine, γ^p and $p'$are defined as

two field variables. The mobilized ϕ' and ψ are defined in the input file as a function of γ^p and p'in a tabular form, using the equations in Table 5.1. During the analysis, the program accesses the subroutine and updates the values of ϕ' and ψ with field variables. Note that $\Delta\gamma^p$ and the change in p' in each time increment are very small, which ensure a gradual variation of ϕ' and ψ in FE analysis. Moreover, a stress reversal will cause only elastic strain until it reaches the failure envelope defined by the mobilized ϕ'.

5.6 Model test simulation

FE simulations of two physical model tests are presented in this section. The first test was conducted at the University of Cambridge at a shallow burial depth ($\widetilde{H}$=3) and called the CD test (Cheuk et al. 2008). The second one was conducted at Cornell University (Test–40) at a deep burial condition ($\widetilde{H}$=8) (Trautmann 1983). A 100-mm diameter model pipe section was buried at the desired depth and then extracted at a constant upward velocity. Cheuk et al. (2008) conducted the test on dry dense Leighton Buzzard silica sand (γ=16.87 kN/m^3, D_r=92%), while Trautmann (1983) used the Cornell filter sand (γ=17.7 kN/m^3, D_r=80%). Direct shear tests show that both Cornell filter and Leighton Buzzard silica sands have ϕ'_c of 31°–32° (Trautmann 1983; Cheuk et al. 2008). As ϕ'_c in the plane strain condition is higher than that of in direct shear tests, ϕ'_c=35° is used in this study. Randolph et al. (2004) showed that Q=10±1 for a variety of quartz and siliceous sands. Analyzing a large number of laboratory tests on different sands, Bolton (1986) suggested A_ψ=5 and k_ψ=0.8 for the plane strain condition. For the variation of ϕ' and ψ with plastic shear strain, Roy et al. (2016) calibrated the MMC model against laboratory test results on Cornell filter sand and obtained the values of C_1, C_2 and m. Cheuk et al. (2008) did not provide any stress–strain curve of Leighton Buzzard silica sand used in physical modeling; therefore, the values of C_1, C_2

and *m* of this sand are assumed to be the same as Cornell filter sand. The geotechnical parameters used in FE analyses are listed in Table. 5.2.

5.6.1 Force-displacement behaviour

Figure 5.2 shows the comparison between force–displacement curves obtained from physical model tests and FE simulations. For $\widetilde{H}$=3 with the MMC model, N_v increases quickly with $\tilde{v}$, reaches the peak at $\tilde{v}$~0.03 (point C) and then decreases rapidly to the point F (~60% of N_v at the peak), which is primarily due to the strain-softening behaviour of soil. After a slight increase after point F, N_v decreases again but at a slower rate than in the segment CF.

For the deep burial condition ($\widetilde{H}$=8), N_v increases with $\tilde{v}$, reaches the peak at $\tilde{v}$~0.12 (point H) and then decreases to point I (~72% of N_v at the peak). However, N_v decreases slowly in the segment HI as compared to that in the segment CF for $\widetilde{H}$=3. A slower rate of reduction of N_v for large $\widetilde{H}$ was also found in the physical model tests (Trautmann 1983; Dickin 1994; Chin et al. 2006). After point I, similar to $\widetilde{H}$=3, N_v decreases at a slower rate than in the segment HI.

5.6.2 Limitations of Mohr-Coulomb model

To show the advantages of the MMC model, FE simulations are also performed with the MC model. Based on Trautmann's (1983) laboratory test results, ϕ'=44° and ψ=16° are used for the MC model. Although it is not explicitly mentioned in the design guidelines, these two parameters represent the equivalent values of ϕ' and ψ, which should be carefully selected as they vary with γ^p. In general, the equivalent values of ϕ' and ψ should be smaller than the peak and higher than the critical state values. Note that an equivalent ϕ' has also been recommended for other geotechnical problems in dense sand, for example, the bearing capacity of shallow foundations

(Loukidis and Salgado 2011) and the lateral capacity of pile foundations (API 1987). A number of previous studies simulated pipe–soil or anchor–soil interactions using constant equivalent values for ϕ' and ψ in the MC model (e.g. Yimsiri et al. 2004; Bhattacharya and Kumar 2016).

Figure 5.2 shows that N_{vp} obtained from FE simulation with the MC model is similar to those with the MMC model and from physical model tests. Note, however, that N_{vp} increases with ϕ' and ψ, and therefore appropriate equivalent values for ϕ' and ψ are required to be selected. The key observation in the FE simulations with the MC and MMC models is that N_v decreases almost linearly with $\tilde{v}$ after the peak for the MC model, which is very different from the FE simulations with the MMC model (Fig. 5.2). The rate of decrease of N_v with $\tilde{v}$ after the peak is slow with the MC model compared to the MMC model and physical model test results.

Simulations are also performed with the MC model using the peak ($\phi'=\phi'_p=55°$, $\psi_p=25°$) and critical state ($\phi'=\phi'_c=35°$, $\psi_p=0°$) shear strength parameters. For the peak shear strength parameters, N_{vp} is ~3.8 and the uplift resistance decreases almost linearly with pipe displacement to $N_v=2.4$ at $\tilde{v}=0.8$. In this simulation, the uplift resistance is higher than that calculated with the MMC model (Fig. 5.2). For the critical state parameters, N_{vp} ~ 2.7 and N_v ~1.34 at $\tilde{v}=0.8$, which are lower than the uplift resistance calculated using the MMC model (Fig. 5.2). This implies that, using the peak or critical state shear strength parameters, the force–displacement behaviour for a wide range of pipe displacement cannot be simulated.

The difference between N_v with the MC and MMC models, shown in Fig. 5.2, can be explained further with the progressive development of shear bands, the zones of localized plastic shear strain, $\gamma^p = \int_0^t \sqrt{\frac{3}{2}(\dot{\epsilon}_{ij}^p \dot{\epsilon}_{ij}^p dt)}$, where $\dot{\epsilon}_{ij}^p$ is the plastic deviatoric strain rate tensor and t is the total time in FE analysis (Figs. 5.3(a)–5.3(c)). In the present study, the shear band represents the

narrow zone where sufficiently large γ^p generates to cause strain-softening. At N_{vp}, plastic shear strain mainly develops locally in an inclined shear band originating from the pipe waist; however, the shear band does not reach the ground surface for formation of a complete slip mechanism (Fig. 5.3(a)). The vertical inclination of the shear band (θ) is described by drawing a line from the pipe surface through the highly concentrated γ^p zone (Fig. 5.3(a)). White et al. (2008) suggested that $\theta \sim \psi_p$. As ψ_p varies with p' (Eqs. (5.1–5.3)), they calculated a single representative value of the peak dilation angle (ψ_p^R) using the in-situ p' at the pipe waist ($(1+2K_0)\gamma H/3$. For the geotechnical parameters in Table 5.2, $\psi_p^R=25°$, which is approximately equal to θ obtained from the present FE analysis (Fig. 5.3(a)). The complete slip mechanism develops by formation of a curved outward shear band at $\tilde{v}>\tilde{v}_p$ when a considerable post-peak degradation of N_v occurs (Fig. 5.3(b)). Similar types of curved failure plane, shown in Fig. 5.3(b), were observed in model tests (Stone and Newson 2006; Cheuk et al. 2008; Huang et al. 2015). The formation of complete slip planes after $\tilde{v}_p$ can be attributed to noticeable vertical displacement of the ground surface after N_{vp} in model tests (Dickin 1994; Bransby et al. 2002; Huang et al. 2015). In the segment CF of N_v–$\tilde{v}$ curve (Fig. 5.2), the shear resistance along the inclined shear band that forms during initial upward displacement gradually decreases due to increase in γ^p along these planes (e.g. Figs. 5.3(a)–5.3(b)). The inclination of the shear band gradually reduces with $\tilde{v}$, and at $\tilde{v}=0.32$, $\theta \sim 8°$ (Fig. 5.3(c)). After point F, the location of the shear band does not change significantly with $\tilde{v}$ (θ remains ~8°). The gradual decrease of N_v with $\tilde{v}$ after point F is due to strain-softening in the shear band and reduction of soil cover depth. However, for the MC model, the vertical inclination of the shear band (θ) remains almost constant (~25°) during the whole process of upward displacement of the pipe,

which has been discussed in Chapter 4. The linear post-peak reduction of N_v with the MC model is primarily due to the reduction of cover depth with $\tilde{v}$.

The progressive formation of shear bands with the MMC model can be further explained by mobilization of ϕ' and ψ, as shown in Figs. 5.3(d–i). The maximum values of ϕ' and ψ are mobilized at γ_p^p (Eqs. (5.6) – (5.9) in Table 5.1). In these figures, the sheared zones outside the two dashed lines represent the pre-peak ($\gamma^p < \gamma_p^p$), while the zone inside these two lines represents the post-peak conditions ($\gamma^p > \gamma_p^p$); however, in both conditions $\phi' < \phi_p'$ and $\psi < \psi_p$. Figures 5.3(d) and 5.3(g) show the mobilized ϕ' and ψ when the peak vertical resistance N_{vp} develops at $\tilde{v}_p$~0.03. The maximum ϕ' and ψ mobilize in the soil elements near the dashed lines, where $\gamma^p=\gamma_p^p$. The high shear strain zone ($\gamma^p > \gamma_p^p$) is bounded by these two dashed lines. For a large plastic shear strain, $\phi'=\phi_c'$ and $\psi=0$ (i.e. critical state). At a moderate uplift displacement (e.g. $\tilde{v}$=0.15), γ^p along the entire curved failure plane is sufficiently large ($\gamma^p > \gamma_p^p$), which corresponds to the strain-softening segments of ϕ'–γ^p and ψ–γ^p curves, as shown in Fig. 5.1(b). Mainly because of this strain-softening behaviour of soil, the reduction of N_v occurs after the peak with the MMC model (e.g segment CF in Fig. 5.2). As strain-softening is not considered, the MC model cannot simulate the quick reduction of N_v after the peak (Fig. 5.2). At a large uplift displacement, sufficiently large γ^p generates in the shear band that reduces ϕ' and ψ to ϕ_c' and 0, respectively, as shown in the 3rd column of Fig. 5.3. A soil wedge above the pipe moves up, resulting in considerable ground heave. Even at this level of large displacement, the slip plane does not become completely vertical (θ~8°), as observed in model tests in loose sand. Not shown in this figure, θ remains constant (~ψ) if the MC model is used, even at large $\tilde{v}$, and therefore cannot simulate the post-peak degradation of N_v due to a change in size of the uplifted soil wedge.

Unlike the MC model, ψ is not constant in the MMC model but increases from 0 to ψ_p and then decreases from ψ_p to 0 with γ^P in the pre-peak hardening and post-peak softening zones, respectively (see Fig. 1(b)). The size of the failed soil wedge above the pipe varies with $\tilde{v}$ because θ is a function of ψ (Ilamparuthi and Muthukrishnaiah 1999; White et al. 2008; Huang et al. 2015; Giampa et al. 2016). Figure 5.4 shows the velocity vectors of soil elements for the pre-peak Fig. 5.4(a–c) and post-peak Fig. 5.4(d–g) conditions with the MMC model for $\widetilde{H}$=3. The line f_1 in Fig. 5.4(a) is drawn along the edge of the velocity vectors that approximately represents the location of the slip plane. At this displacement, the soil elements above the pipe move almost vertically and are then inclined outwards near the ground surface (Fig. 5.4(a)), where the stress is very low. This implies that at this very small pipe displacement, $\psi=\psi_{in}\sim 0$ and therefore $\theta\sim 0$ and f_1 is almost vertical. Figure 5.4(b) shows that, at $\tilde{v}$=0.02, the soil deformation region expands horizontally, and the left boundary of the soil wedge shifts from f_1 to f_2, because of the increase in mobilized ψ with γ^P. This type of trumpet–like deformation of soil elements was observed in the physical model tests during the pre-peak stage (Huang et al. 2015). At the peak N_v ($\tilde{v}$=0.03), the left boundary of the soil wedge shifts further to f_3 (Fig. 5.4(c)). The slip plane f_3 is almost a straight line, having $\theta\sim\psi_p^R$, although it is slightly curved outward near the ground surface, as observed in physical model tests (Cheuk et al. 2008; Huang et al. 2015). The slip plane f_3 is generally used to calculate the N_{vp}, based on the limit equilibrium method (White et al. 2008).

Once the peak is reached, the soil deformation region no longer expands with γ^p, rather, it starts to contract—the left boundary of the soil wedge shifts from f_3 to f_4 (Fig. 5.4(d)). At a displacement greater than $\tilde{v}_p$, a complete slip mechanism develops with a noticeable ground heave (Fig. 5.4(d)). With further increase of $\tilde{v}$, the size of the failure wedge reduces and the slip plane moves gradually from f_3 to f_6, as shown in Figs. 5.4(d–f), which is because of the reduction of ψ

with γ^p in the strain-softening zone. A similar type of shifting of the slip planes with upward displacement of the pipe was also observed in the centrifuge tests (Huang et al. 2015). At $\tilde{v}$=0.8, the soil surrounding the pipe starts to fall to fill the cavity that forms beneath it due to upward displacement (Fig. 5.4(g)), which is commonly known as the "flow around" mechanism. Cheuk et al. (2008) also observed flow around mechanism in the model test ($\tilde{H}$=3) at $\tilde{v}$=0.1–0.5. As stated earlier, constant values of ϕ' and ψ are used in the MC model and therefore it cannot simulate the shifting of the slip plane with upward displacement of the pipe.

In summary, the post-peak reduction of N_v with the MMC model for this burial depth ($\tilde{H}$=3) occurs due to the combined effects of three factors: (i) decrease in size of the failure wedge (i.e. reduction of θ), (ii) reduction of shear resistance along the slip planes with γ^p, and (iii) reduction of cover depth. The MC model cannot capture the effects of the former two. The peak force could be matched using representative values of ϕ' and ψ in the MC model. However, the proposed MMC model shows not only the better simulation of the force–displacement response but also explains the possible mechanisms involved in it through a close examination of mobilized ϕ' and ψ and velocity vectors.

The ALA guidelines for pipeline design (ALA 2005) do not explicitly consider the post-peak reduction of N_v and the maximum $N_v=\phi'\tilde{H}/44$ is recommended, where ϕ' is a representative angle of internal friction (in degree). However, DNV (2007) recognized the post-peak reduction of N_v and recommended an N_v–$\tilde{v}$ relation using four linear line segments, in which N_v reduces linearly from the peak to a residual value with $\tilde{v}$ and then remains constant. A detailed comparison of FE simulations using the MMC model with the design guidelines (ALA 2005; DNV 2007) has been presented in Chapter 4.

5.7 Effect of Burial Depth and Diameter

Figure 5.5 shows the load–displacement curves for $\widetilde{H}$ =2–4 for three pipe diameters (D=100, 300 and 500 mm). A detailed FE modeling for $\widetilde{H}$≤4 for D=100 mm, including the mesh sensitivity issue, has been presented in Chapter 4. The key observation is that there is no significant effect of pipe diameter on N_{vp} (Fig. 5.5). A similar observation on uplift resistance was reported by Jung et al. (2016). For the same mesh size (t_{FE}=10 mm), FE analyses for D=300 and 500 mm stop at $\tilde{v}$=0.15–0.3 due to significant mesh distortion around the pipe springline, as the soil tends to move towards the cavity formed beneath the pipe (Fig. 5.5). However, the analysis could be continued up to $\tilde{v}$=0.8 for 100 mm diameter pipe (Fig. 5.2). For a given $\tilde{v}$, the uplift displacement (v) increases with diameter of the pipe (v=$\tilde{v}D$). Therefore, the complete failure mechanisms end at smaller $\tilde{v}$ for larger diameter pipe. A similar observation has been reported by Stone and Newson (2006) from uplift tests in dense sand for three model pipes of diameter 15, 30 and 60 mm. Narrow and clear shear bands were observed in model tests with a smaller mean particle size (d_{50}) (i.e. high D/d_{50}) compared to the tests in coarse sand (low D/d_{50}) (Stone and Newson 2006; Cheuk et al. 2008). Note that Tatsuoka et al. (1997) also showed that the shear bands are clear for high B/d_{50} ratios for footing on dense sand, where B is the width of the footing. Therefore, in order to simulate clear shear bands and a sufficiently large post-peak segment of the N_v–$\tilde{v}$ curve, the following analyses are performed for D=300 mm.

Figure 5.6 shows the force–displacement curves with the MMC model for $\widetilde{H}$ =2–10, in which the points of interest for further explanation are labeled A_1–A_5 at $\tilde{v}_p$, B_1–B_5 at the approximate location where the slope of the N_v–$\tilde{v}$ curve changes (~3.5$\tilde{v}_p$–4.5$\tilde{v}_p$) and C_1–C_5 at large $\tilde{v}$. Three key features of the N_v–$\tilde{v}$ curves are: (i) N_{vp} (open circles) increase with $\widetilde{H}$, (ii) $\tilde{v}_p$ increases

with $\widetilde{H}$, although the increase is not significant for $\widetilde{H}\leq 4$; and (iii) the slope of the curve after N_{vp} (i.e. between the circle and square) decreases with $\widetilde{H}$.

In general, $\tilde{v}_p$ decreases with an increase in D_r and increases with $\widetilde{H}$ (Trautmann 1983; Dickin 1994; ALA 2005; DNV 2007). For the range of soil properties and burial depths considered in the present FE analysis, $\tilde{v}_p$ does not vary significantly with $\widetilde{H}$ between 2 and 4. However, $\tilde{v}_p$ increases with $\widetilde{H}$ for $\widetilde{H}>4$ (Fig. 5.6). At $\tilde{v}_p$, p' is higher for larger $\widetilde{H}$, resulting in higher γ_p^P required to mobilize ϕ_p' and ψ_p. Therefore, $\tilde{v}_p$ increases with $\widetilde{H}$. The present FE analyses can successfully simulate this trend (Fig. 5.6).

Figure 5.7 shows that FE analyses with the MMC model give higher N_{vp} than DNV (2007), and the difference is significant at large burial depths. However, FE results are comparable to ALA (2005) if $\phi'=40°$ is used, although FE calculated N_{vp} slightly higher than ALA (2005) at low $\widetilde{H}$. However, one must be very careful in selecting the value of ϕ', because it varies with γ^p and p', as discussed in previous sections. For example, ALA (2005) with $\phi'=45°$ gives significantly higher N_{vp} than FE calculated values at large $\widetilde{H}$. A detailed discussion on selection of equivalent ϕ' is presented in the "Equivalent friction angle" section.

5.8 Failure Mechanisms

Early studies indicated soil failure mechanisms in uplift tests based on displacement of the failed soil block and ground heave (Trautmann 1983; Schaminee et al. 1990). However, with recent advancements in imaging techniques, such as particle image velocimetry (PIV) (White et al. 2003), the failure mechanism is further studied (Cheuk et al. 2008; White et al. 2008; Thusyanthan et al. 2010; Wang et al. 2010).

Figures 5.8(a–o) show the progressive formation of shear bands for $\widetilde{H}$=2–10 (D=300 mm) at three stages of $\tilde{v}$: (i) at $\tilde{v}_p$ (Figs. 5.8(a–e)), (ii) at intermediate $\tilde{v}$ (~3.5$\tilde{v}_p$ to 4.5$\tilde{v}_p$) (Figs. 5.8(f–j)) and (iii) at large $\tilde{v}$ (Figs. 5.8(k–o)).

At $\tilde{v}_p$, large strain concentration mainly occurs locally in an inclined shear band, f_1, originating from the soil element near the pipe waist; however, the shear band does not reach the ground surface for the formation of a complete slip mechanism (Fig. 5.8(a–e)). At moderate to deep burial conditions ($\widetilde{H}$=6–10), instead of one shear band (f_1 in Fig. 5.8(a)), γ^p localizes in several small shear bands (Figs. 5.8(c–e)). However, as $\tilde{v}$ increases, the shear band f_1 that propagates to the ground surface at $\theta=\psi_p^R=25°$ becomes prominent (2nd and 3rd columns of Fig. 5.8). For $\widetilde{H}$=2, in addition to f_1, another inclined shear band, f_2, forms (Fig. 5.8(f)). As shown in Chapter 4, for D=100 mm, instead of formation of the shear band f_2, the location of f_1 gradually shifts to the right resulting in a diffused plastic shear zone, which could be attributed to the D/d_{50} effect. For $\widetilde{H}$=4, f_1 does not propagate to the ground surface; instead, γ^P localizes in another shear band (f_2) which subsequently reaches the ground surface (Fig. 5.8(g)). For moderate to deep burial conditions ($\widetilde{H}$=6–10) at intermediate displacements, the shear band f_2 creates a triangular compression wedge above the pipe, which is similar to the triangular wedge under a shallow foundation subjected to a vertical load (Fig. 5.8(h–j)).

At large displacement, the formation of shear bands varies with $\widetilde{H}$, as shown in Figs. 5.8 (k–o). For $\widetilde{H}$=2 at $\tilde{v}$~0.22, another shear band, f_3, forms in the almost vertical direction (θ~8°), in addition to the previous shear bands, f_1 and f_2 (Fig. 5.8(k)). As three distinct shear bands form, the soil block bounded by f_3 mainly displaces during further upward movement of the pipe. The soil block bounded by the shear bands f_2 and f_3 will also move upward because of upward shear force in f_3 and the slight push from the bottom of this block. The upward velocity of soil elements in this

block is, therefore, lower than the velocity of soil elements bounded by the shear band, f_3. Similarly, slower movements of the soil elements are found in the soil block bounded by f_1 and f_2. The difference in the rate of movement of the soil blocks bounded by f_1, f_2 and f_3 causes the differential vertical displacement of the ground surface—higher in the center and then gradually decreasing on the left (Fig. 5.8(k)). At a large displacement, the soil around the pipe moves to the cavity below the pipe (see Fig. 5.4(g)) that reduces the cover depth and thereby the uplift resistance, which becomes zero if the invert of the pipe reaches the ground surface. The effect of reduction of cover depth on uplift resistance is significant for shallow burial cases, as discussed in Chapter 4.

For $\widetilde{H}$=4 at $\tilde{v}$~0.32, in addition to f_1, f_2 and f_3, a triangular compression zone bounded by f_4 along with a logarithmic spiral type shear band (f_5) forms (Fig. 5.8(l)). Unlike Figs. 5.8(k) and 5.8(l), for $\widetilde{H}$=6, f_3 does not form from the pipe waist; rather, it forms from a point on f_1 where a logarithmic spiral shear band f_4 ends (Fig. 5.8(m)). For $\widetilde{H}$=8 and 10, in addition to f_1, only a triangular compression zone forms above the pipe along with a fully developed logarithmic spiral shear band (f_3) for $\widetilde{H}$=8 (Fig. 5.8(n)) and a number of diffused logarithmic spiral type shear bands where strain is not sufficiently localized to form clear shear bands for the $\widetilde{H}$=10 case (Fig. 5.8(o)). Large plastic shear strain develops in the soil around the pipe at this stage, which indicates that at this large $\tilde{v}$, ϕ' and ψ in this zone reduce to ϕ'_c and 0, respectively. Therefore, the flow around mechanism is observed at this stage; i.e., soil around the pipe tends to flow towards the cavity beneath it (Figs. 5.8(k–o)).

In summary, depending upon burial depth and vertical displacement, the uplift of a pipe in dense sand could cause trumpet-like and/or flow around failure mechanisms. The flow around mechanisms occur for both deep (e.g. $\widetilde{H}$=10) and shallow burial conditions (e.g. $\widetilde{H}$=2), with large

upward displacement. For shallow-buried pipelines, θ decreases with $\tilde{v}$ due to the decrease in ψ. The MMC model can successfully capture the shear band propagation and explain the failure mechanisms, as observed in physical model tests. However, the process of infilling at large $\tilde{v}$, when a sufficiently large cavity forms beneath the pipe, needs further investigation and is left for future studies.

5.9 Equivalent Friction Angle

The upper bound (UB) solution and limit equilibrium method (LEM) are the two simplified approaches used to calculate uplift resistance (Vermeer and Sutjiadi 1985; White et al. 2008). In the UB solution, N_v is the weight of the lifted soil wedge having $\theta=\phi'_e$, where ϕ'_e is the equivalent friction angle. However, in the limit equilibrium method (LEM), N_v is the sum of the weight of the lifted soil wedge and the vertical component of shearing resistance along the two inclined planes having $\theta=\psi$ ($<\phi'_e$).

$$N_v = \frac{F_{vp}}{\gamma HD} = \left\{1 - \left(\frac{\pi}{8\tilde{H}}\right) + \tilde{H}\tan\theta\right\} + F_A\tilde{H} \tag{5.11}$$

where

$$F_A = \left(\tan\phi'_e - \tan\theta\right)\left[\frac{1+K_0}{2} - \frac{(1-K_0)\cos 2\theta}{2}\right] \tag{5.12}$$

The two critical soil parameters in Eqs. (5.11) and (5.12) are ϕ'_e and θ. White et al. (2008) suggested the use of $\phi'_e = \phi'_p = \phi'_c + 0.8\psi_p$ (Bolton 1986) and $\theta=\psi_p$ to calculate the peak resistance, N_{vp}. As in the work of White et al. (2008), assuming p' in Eq. (5.1) as the in-situ p'at

the pipe waist ((1+2K_0)γH/3, where $K_0 = 1 - \sin\phi'_c$), the representative values for ϕ'_p (=55°) and ψ_p (=25°) are calculated for the soil parameters in Table 5.2. Inserting these values into Eqs. (5.11) and (5.12), N_{vp} is calculated for different $\tilde{H}$, which gives significantly higher uplift resistance than the FE results, especially at large $\tilde{H}$ (Fig. 5.9). This difference is because the mobilized ϕ' along the entire slip plane is not ϕ'_p; rather, it is less than ϕ'_p (either in pre- or post-peak condition as shown in Fig. 5.3(d)). Note that one can get the same value of N_v using the UB and LEM methods by changing ϕ'_e, θ or both. Then, the question is which of these parameters should be changed. The present FE analysis shows that θ~ψ_p when the peak resistance develops (Figs. 5.3 and 5.8). As the weight of the lifted wedge is known, a value of ϕ'_e less than ϕ'_p should be used to match the calculated N_v using Eq. (5.11) with FE results. Figure 5.9 shows that ϕ'_e=45° together with θ=ψ_p=25° gives N_v similar to the peak value obtained from FE analysis. In other words, the N_{vp} can be calculated with the LEM, using θ=ψ_p, but $\phi'_e < \phi'_p$. This also explains the reason behind the over-prediction by LEM as compared to test data in the work of White et al. (2008).

DNV (2007) recommended a linear reduction of N_v from the peak at $\tilde{v}_p$ to a residual value at $3\tilde{v}_p$. The values of N_v at $3\tilde{v}_p$ are obtained from FE results, as shown by the vertical arrows in Fig. 5.6. Up to this level of $\tilde{v}$, strain accumulation mainly continues along the initially formed slip plane at θ=ψ_p, although ϕ' and ψ along the shear band significantly decrease due to an increase in γ^p (Figs. 5.3 and 5.8). Calculated N_v values using Eq. (5.11) with ϕ'_e=35° and θ=ψ_p=25° are shown in Fig. 5.9, which are similar to FE simulated values at $3\tilde{v}_p$. Figure 5.6 also shows that the decrease of N_v continues even after $3\tilde{v}_p$, which is consistent with model test results, as discussed in previous sections (see also Fig. 5.2); however, DNV (2007) recommended constant N_v after $3\tilde{v}_p$.

5.10 Conclusions

Thermal expansion of buried hot oil pipelines may cause upheaval buckling, if the uplift resistance is not sufficient to prevent upward displacement. The limit equilibrium method could be used to calculate uplift resistance; however, the location of the inclined slip planes and mobilized shear strength parameters along these planes need to be known. Physical modeling with PIV shows that the slip planes do not remain at the same location but shift with upward displacement of the pipe, depending upon burial depth and soil properties. In the present study, FE analysis is conducted to examine progressive formation of slip planes and mobilization of frictional resistance along these planes for dense backfill sand. The following conclusions can be drawn from this study:

i) For the range of burial depths considered ($\widetilde{H}$=2–10), the inclination of slip planes (θ) is approximately equal to the maximum dilation angle (ψ_p), when the peak resistance is mobilized.

ii) For shallow buried pipelines, new shear bands having $\theta < \psi_p$ form with large displacement ($\tilde{v} > \tilde{v}_p$). The decrease in ϕ' along the slip plane together with reduction of θ reduces the uplift resistance (N_v) after the peak. The quick reduction of N_v immediately after the peak is due to the effect of the former one, while the gradual reduction of N_v at large displacements is mainly due to the effect of the latter one.

iii) For deeper pipelines, except for the initially formed inclined shear band having $\theta \sim \psi_p$, no additional shear band, as in the shallow buried cases, forms at large displacements. However, a number of logarithmic spiral type shear planes form above the pipe at large $\tilde{v}$. The formation of these shear planes and the reduction of ϕ' along the inclined shear band are the causes of gradual reduction of uplift resistance in these cases.

iv) An equivalent friction angle (ϕ'_e), where $\phi'_p > \phi'_e > \phi'_c$, together with $\theta=\psi_p$ can be used to calculate the peak uplift resistance using the limit equilibrium method.

v) Unlike DNV (2007) guidelines, the decrease of N_v continues even after $3\tilde{v}_p$. For the cases analyzed, FE calculated N_v at $3\tilde{v}_p$ is comparable to the values obtained from the limit equilibrium method using $\phi'_e = \phi'_c$ and $\theta=\psi_p$.

Finally, the present study has also some limitations. Infilling of sand in the cavity beneath the pipe, especially at large displacements, could not be simulated properly. In the FE analysis, the pipe is displaced upward monotonically to a large distance. Although large displacements of pipelines has been observed in the field, as discussed in the introduction, such a displacement could occur due to progressive movement, when the pipeline cannot return to the original configuration during shutdown because of infilling. The effects of temperature cycling and progressive displacement of the pipe are not simulated in this study. Another limitation of this study is related to selection of soil parameters for the MMC model. Additional laboratory tests in plane strain condition are required for a better estimation of model parameters, to define the variation of mobilized friction and dilation angles.

Acknowledgements

The work presented in this paper has been supported by the Research and Development Corporation of Newfoundland and Labrador, Chevron Canada Limited and the Natural Sciences and Engineering Research Council of Canada (NSERC).

Notation

The following abbreviations and symbols are used in this paper:

TX = triaxial;

PS = plane strain;

PIV = particle image velocimetry;

LEM = limit equilibrium method;

MC = Mohr-Coulomb model;

MMC = Modified Mohr-Coulomb model;

UB = upper bound solution;

A_ψ = slope of $(\phi'_p - \phi'_c)$ vs. I_R curve (Eq. (5.2));

m, C_1, C_2 = soil parameters (Eqs. (5.4) and (5.5));

D_r = relative density;

D = diameter of pipe;

E = Young's modulus;

F_A = vertical component of the shear force along the slip plane;

F_v = uplift force;

H = distance from ground surface to the center of pipe;

$\widetilde{H}$ = embedment ratio (=H/D);

I_R = relative density index;

K = material constant;

K_0 = earth pressure coefficient at rest;

N_v = normalized uplift force;

N_{vp} = peak uplift dimensionless force;

Q, R = material constants (Bolton 1986);

S_v = vertical component of the shearing resistance along the slip plane;

W_s = submerged weight of the lifted soil wedge;

d_{50} = mean particle size;

f = shear band;

k_ψ = slope of $(\phi'_p - \phi'_c)$ vs. ψ_p curve (Eq. (5.3));

n = an exponent (Eq. (5.10));

p' = mean effective stress;

p'_a = atmospheric pressure (=100 kPa);

t_{FE} = FE mesh size;

v = vertical displacement of pipe;

$\tilde{v}$ = normalized upward displacement of pipe (=v/D);

$\tilde{v}_p$ = normalized upward displacement of pipe required to mobilize N_{vp};

μ = friction coefficient between pipe and soil;

ν = Poisson's ratio;

θ = angle of vertical inclination of the slip plane;

$\Delta\varepsilon_1^p$ = major principal plastic strain increment;

$\Delta\varepsilon_3^p$ = minor principal plastic strain increment;

$\dot{\epsilon}_{ij}^p$ = plastic deviatoric strain rate;

ϕ' = mobilized angle of internal friction;

ϕ'_{in} = ϕ' at the start of plastic deformation;

ϕ'_p = peak friction angle;

ϕ'_c = critical state friction angle;

ϕ'_e = equivalent friction angle;

ϕ_μ = pipe-soil interface friction angle;

ψ = mobilized dilation angle;

ψ_p = peak dilation angle;

ψ_p^R = representative value of the peak dilation angle;

ψ_{in} = ψ at the start of plastic deformation (=0);

γ = unit weight of soil;

γ^p = engineering plastic shear strain;

γ_p^p = γ^p required to mobilize ϕ'_p;

γ_c^p = strain softening parameter; and

$\Delta\gamma^p$ = plastic strain increment.

References

American Lifelines Alliance (ALA). (2005). "Guidelines for the design of buried steel pipe." <https://www.americanlifelinesalliance.com/pdf/Update061305.pdf > (Mar. 13, 2017).

American Petroleum Institute (API). (1987). "Recommended practice for planning, designing and constructing fixed offshore platforms." API Recommended practice, 2A (RP 2A), 17th Ed.

Aynbinder, A.B., and Kamershtein, A.G. (1982). "Raschet magistral'nykh truboprovodov na prochnost' i ustoichivost' [Calculation of trunk pipe for strength and stability]." Moscow (In Russian).

Barrette, P., Denise, S., and Hossein, B. (2015). "Protecting offshore pipelines against drifting ice: a discussion on standards and guidelines." *Proc., 34th Int. Conference on Ocean, Offshore and Arctic Engineering (OMAE 2015)*, St. John's, Canada.

Been, K., Sancio, R.B., Ahrabian, A., van Kesteren, W., Croasdale, K., and Palmer, A.C. (2008). "Subscour displacement in clays from physical model tests." *Proc., 7th Int. Pipe. Conf.*, Calgary.

Bhattacharya, P., and Kumar, J. (2016). "Uplift capacity of anchors in layered sand using finite-element limit analysis: Formulation and results." *Int. J. Geomech.*, 10.1061/(ASCE)GM.1943-5622.0000560, 04015078.

Bishop, A. W. (1961). "Discussion on soil properties and their measurement." Proc., *5th Int. Conf. on Soil mechanics and Foundation engineering*, vol. III.

Bolton, M. D. (1986). "The strength and dilatancy of sands." *Géotechnique*, 36(1), 65−78.

Bransby, M. F., Newson, T. A., Brunning, P., and Davies, M. C. R. (2001). "Numerical and centrifuge modeling of the upheaval resistance of buried pipelines." *Proc., 20th Int. Conf. on Offshore Mechanics and Arctic Engineering*, Rio de Janeiro, Brazil.

Bransby, M.F., Newson, T. A. and Davies, M. C. R. (2002). "Physical modelling of the upheaval resistance of buried offshore pipelines." *Proc., International conference on physical modelling in geotechnics*, Kitakyushu, Japan.

Cathie D.N., Jaeck C., Ballard J-C and Wintgens J-F. (2005). "Pipeline geotechnics – state-of-the-art." *Proc., Int. Symposium on Frontiers in Offshore Geotechnics*, Taylor & Francis, 95–114.

Chakraborty, T., and Salgado, R. (2010). "Dilatancy and shear strength of sand at low confining pressures." *J. of Geotech. and Geoenv. Eng.*, 136(3).

Cheuk, C. Y., White, D. J. and Bolton, M. D. (2005). "Deformation mechanisms during the uplift of buried pipelines in sand." *Proc., 16th Int. Conf. on Soil Mech. and Geo. Eng*., Osaka, 1685–1688.

Cheuk, C. Y., White, D. J., and Bolton, M. D. (2008). "Uplift mechanisms of pipes buried in sand." *J. Geotech. Geoenv. Eng*., 134(2), 154–163.

Chin, E. L., Craig, W. H., and Cruickshank, M. (2006). "Uplift resistance of pipelines buried in cohesionless soil." *Proc., 6th Int. Conf. on Physical Modelling in Geotechnics*, Ng, Zhang, and Wang, eds., Vol. 1, Taylor & Francis Group, London, 723–728.

Clukey, E.C., Haustermans, L. and Dyvik, R. (2005). "Model tests to simulate riser–soil interaction effects in touchdown point region." *Proc., International Symposium on Frontiers in Offshore Geotechnics (ISFOG 2005)*, Perth, Australia, 651−658.

Conforth, D.H. (1964). "Some experiments on the influence of strain conditions on the strength of sand." *Géotechnique*, 14, 143−167.

Craig, I.G., Nash, N.W. and Oldfield, G.A. (1990). "Upheaval buckling: A practical solution using hot water flushing technique." *Proc., Off. Tech. Conf.*, Houston, Texas, 539–550.

Daiyan, N., Kenny, S., Phillips, R., and Popescu, R. (2011). "Investigating pipeline–soil interaction under axial–lateral relative movements in sand." *Can. Geotech. J.*, 48(11), 1683−1695.

Dassault Systèmes. (2010). ABAQUS [computer prog.]. Dassault Systèmes, Inc., Providence, R.I.

Det Norske Veritas (DNV). (2007). "Global buckling of submarine pipelines—Structural design due to high temperature/high pressure." DNV-RP-F110, Det Norske Veritas, Baerum, Norway.

Dickin, E.A. (1994). "Uplift resistance of buried pipelines in sand." *Soils and Found*., 34(2), 41-48.

Finch, M. (1999). "Upheaval buckling and flotation of rigid pipelines: The influence of recent geotechnical research on the current state of the art." *Proc., Off. Tech. Conf*., Houston, Texas.

Giampa, J., Bradshaw, A., and Schneider, J. (2016). "Influence of dilation angle on drained shallow circular anchor uplift capacity." *Int. J. Geomech.*, 10.1061/(ASCE)GM.1943-5622.0000725, 04016056.

Guijt, J. (1990). "Upheaval buckling of offshore pipelines: Overview and introduction." *Proc., Off. Tech. Conf.*, Houston, Texas.

Guo, P., and Stolle, D. (2005). "Lateral pipe-soil interaction in sand with reference to scale effect." *J. of Geotech. and Geoen. Eng.*, 131(3).

Hardin, B .O., and Black, W. L. (1966). "Sand stiffness under various triaxial stress." *J. of the Soil Mech. and Found. Div.*, ASCE, 92(SM2), 27−42.

Héquette, A., Desrosiers, M. and Barnes, P.W. (1995). "Sea ice scouring on the inner shelf of the southeastern Canadian Beaufort Sea." *Marine Geology*, 128 (3–4), 201–219.

Houlsby, G.T. (1991). "How the dilatancy of soils affects their behaviour." *Proc., 10th European Conference on Soil Mechanics and Foundation Engineering*, Florence, 4, 1189−1202.

Hsu, S.T., and Liao, H.J. (1998). "Uplift behaviour of cylindrical anchors in sand." *Can. Geotech. J.*, 35(1), 70–80.

Huang, B., Liu, J., Ling, D. and Zhou, Y. (2015). "Application of particle image velocimetry (PIV) in the study of uplift mechanisms of pipe buried in medium dense sand." *J Civil Struct. Health Monit.*, 5(5), 599–614.

Ilamparuthi, K. and Muthukrishnaiah, K. (1999). "Anchors in sand bed: Delineation of rupture surface." *Ocean Eng.*, 26, 1249–1273.

Janbu, N. (1963). "Soil compressibility as determined by oedometer and triaxial tests." *Proc., European Conf. on Soil Mech. and Found. Eng.*, Wiesbaden, Germany, Vol. 1, 19−25.

Jefferies, M., and Been, K. (2006). *Soil liquefaction: a critical state approach*. Second edition, Taylor & Francis, New York.

Jung, J.K., O'Rourke, T.D., and Olson, N.A. (2013). "Uplift soil–pipe interaction in granular soil." *Can. Geotech. J.*, 50(7), 744–753.

Jung, J.K., O'Rourke, T.D., and Argyrou, C. (2016). "Multi-directional force–displacement response of underground pipe in sand." *Can. Geotech. J.*, 53(11), 1763–1781.

Kenny, S., Palmer, A.C., and Been, K. (2007). "Design challenges for offshore pipelines in arctic environments." *Proc., IBC Oil and Gas in Arctic and Cold Waters*.

Lings, M. L., and Dietz, M. S. (2004). "An improved direct shear apparatus for sand." *Géotechnique*, 54(4), 245−256.

Liu, J.X., and O'Rourke, M. (2010). "Response of offshore pipelines to landslides." *Proc., Off. Tech. Conf.*, Houston, Texas.

Loukidis, D. and Salgado, R. (2011). "Effect of relative density and stress level on the bearing capacity of footings on sand." *Géotechnique*, 61(2), 107–19.

Nielsen, N.J.R, Lyngberg, B. and Pedersen, P.T. (1990). "Upheaval buckling failures of insulated pipelines: A case story." *Proc., Off. Tech. Conf.*, Houston, Texas, 581–592.

Palmer, A. (1990). "Design of marine pipelines in seabed vulnerable to ice scour." *Workshop on Ice Scouring and the Design of offshore pipelines*, Calgary, Canada, 167–178.

Palmer, A.C., White, D.J., Baumgard, A.J., Bolton, M.D., Barefoot, A.J., Finch, M., Powell, T., Faranski, A.S., and Baldry, J.A.S. (2003). "Uplift resistance of buried submarine pipelines: comparison between centrifuge modelling and full-scale tests." *Géotechnique*, 53(10), 877–883.

Palmer, A.C. and Williams, P. J. (2003). "Frost heave and pipeline upheaval buckling." *Can. Geotech. J.*, 40, 1033–1038.

Pradhan, T.B.S., Tatsuoka, F., and Horii, N. (1988). "Strength and deformation characteristics of sand in torsional simple shear." *Soils and Foundations*, 28(3), 131−148.

Randolph, M.F., Jamiolkowski, M.B. and Zdravkovic, L. (2004). "Load carrying capacity of foundations." *Proc., Skempton Memorial Conf.*, London, 1, 207–240.

Robert, D. J., and Thusyanthan, N. I. (2014). "Numerical and experimental study of uplift mobilization of buried pipelines in sands", *J. Pipe. Systems Eng. and Prac.*, 6(1).

Roy, K., Hawlader, B.C., Kenny, S. and Moore, I. (2016). "Finite element modeling of lateral pipeline−soil interactions in dense sand." *Can. Geotech. J.*, 53(3), 490–504.

Saboya, F.A. Jr., Santiago, P. A.C., Martins, R.R., Tibana, S., Ramires, R.S. and Araruna, J. T. Jr. (2012). "Centrifuge test to evaluate the geotechnical performance of anchored buried pipelines in sand." *J. of Pipe. Sys. Eng. and Prac.*, 3(3).

Schaminée, P., Zorn, N., and Schotman, G. (1990). "Soil response for pipeline upheaval buckling analyses: Full-scale laboratory tests and modelling." *Proc., Off. Technol. Conf.*, Houston, 563-572.

Schanz, T., and Vermeer, P. A. (1996). "Angles of friction and dilatancy of sand." *Géotechnique*, 46(1), 145–151.

Stone, K. J. L., and Newson, T. A. (2006). "Uplift resistance of buried pipelines: An investigation of scale effects in model tests." *Proc., 6th Int. Conf. on Physical Modelling in Geotechnics*, Ng, Zhang, and Wang, eds., Vol. 1, Taylor & Francis Group, London, 741–746.

Taleb, B. and Moore, I.D. (1999). "Metal culvert response to earth loading – Performance of two−dimensional analysis." *Transportation Research*, Record No. 1656, Underground and Other Structural Design Issues, National Research Council, Washington, 25−36.

Tatsuoka, F., Sonoda, S., Hara, K., Fukushima, S., and Pradhan, T.B.S. (1986). "Failure and deformation of sand in torsional shear." *Soils and Foundations*, 26 (4), 79–97.

Tatsuoka, F., Goto, S., Tanaka, T., Tani, K., and Kimura, Y. (1997). "Particle size effects on bearing capacity of footing on granular material." *Proc., Deformation and Progressive Failure in Geomechanics* (eds.: A. Asaoka, T. Adachi and F. Oka), Pergamon, 133–138.

Thusyanthan, N. I., Mesmar, S., Wang, J. and Haigh, S. K. (2010). "Uplift resistance of buried pipelines and DNV-RP-F110." *Proc., Off. Pipeline and Tech. Conf.,* Amsterdam, 24–25.

Trautmann, C. (1983). "Behavior of pipe in dry sand under lateral and uplift loading." PhD thesis, Cornell University, Ithaca, NY.

Vermeer, P. A. and Sutjiadi, W. (1985). "The uplift resistance of shallow embedded anchors." *Proc., 11th Int. Conf. Soil Mech. Found. Eng.,* San Francisco, 1635–1638.

Wang, J., Ahmed, R., Haigh, S. K., Thusyanthan, N. I., and Mesmar, S. (2010). "Uplift resistance of buried pipelines at low cover−diameter ratios." *Proc., Off. Technol. Conf.,* OTC-2010-20912.

White, D. J., Barefoot, A. J. & Bolton, M. D. (2001). "Centrifuge modelling of upheaval buckling in sand." *Int. J. Phys. Modelling Geomech.,* 2, 19–28.

White, D. J., Take, W. A., and Bolton, M. D. (2003). "Soil deformation measurement using particle image velocimetry (PIV) and photogrammetry." *Géotechnique*, 53(7), 619–631.

White, D.J., Cheuk, C.Y, and Bolton, M.D. (2008). "The Uplift resistance of pipes and plate anchors buried in sand." *Géotechnique*, 58(10), 771–779.

Yimsiri, S., Soga, K., Yoshizaki, K., Dasari, G., and O'Rourke, T. (2004). “Lateral and upward soil–pipeline interactions in sand for deep embedment conditions.” *J. of Geotech. and Geoenv. Eng.*, 130(8), 830−842.

Yoshimine, M. (2005). “Archives–soil mechanics laboratory.” Tokyo Metropolitan University, <http://geot.civil.ues.tmu.ac.jp/archives/> (April 4, 2015).

(a)

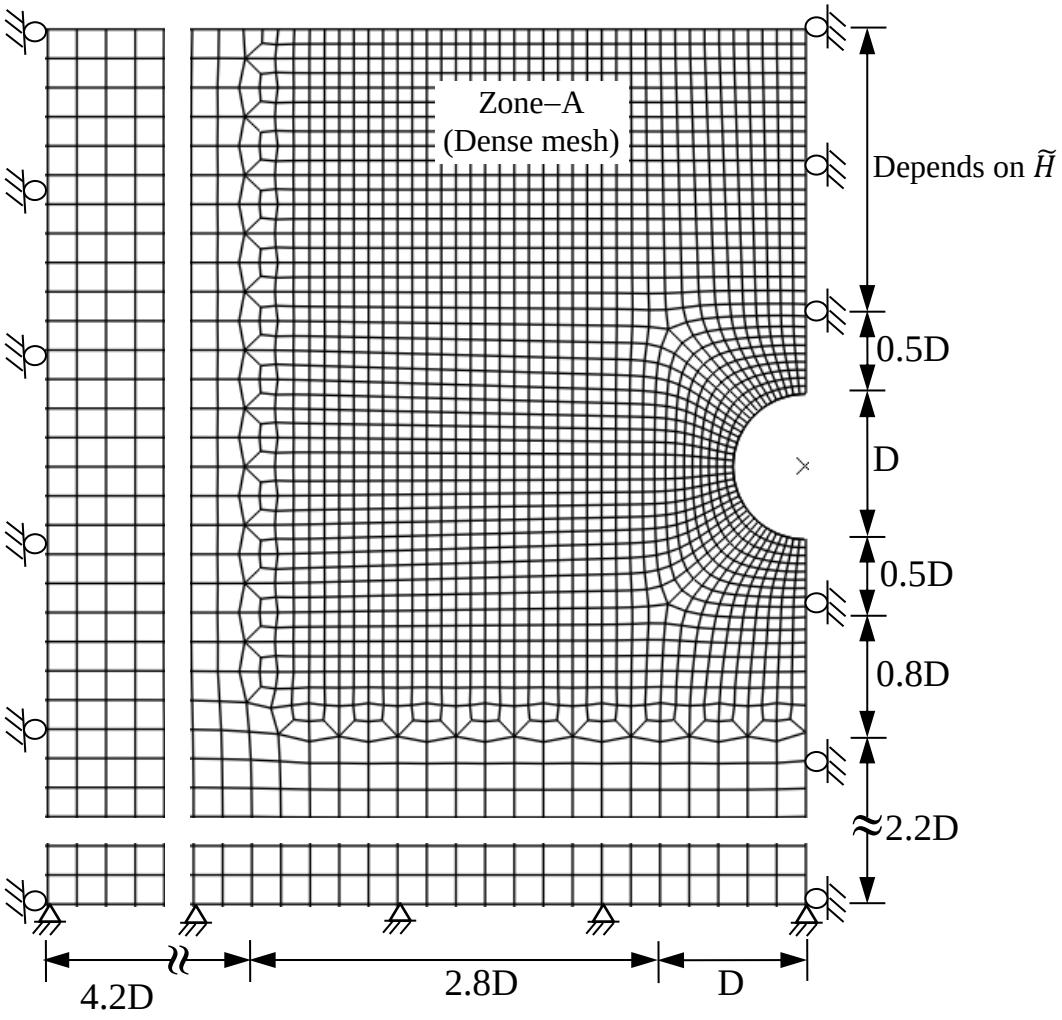

Figure 5.1: Finite element modeling: (a) typical finite element mesh for *D*=100 mm

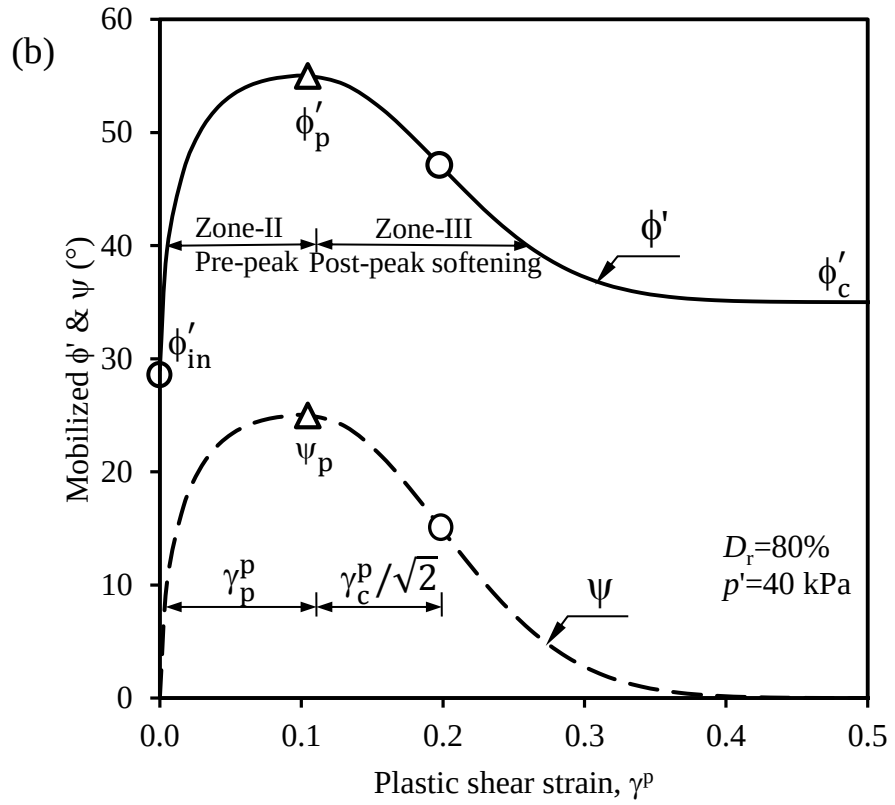

Figure 5.1: Finite element modelling: (b) typical variation of mobilized friction and dilation angle

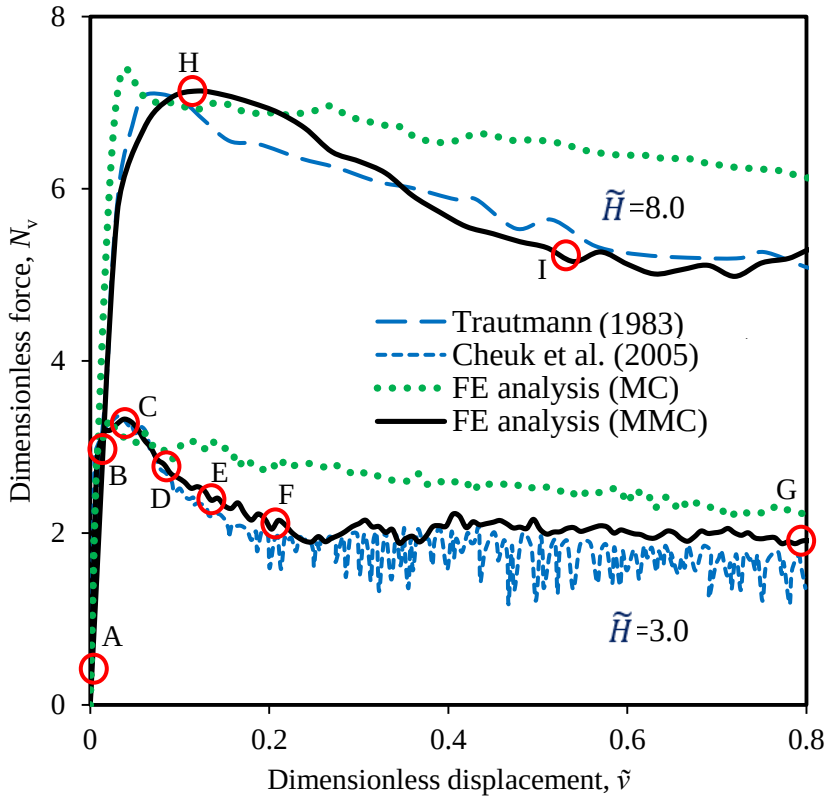

Figure 5.2: Comparison of FE simulation and model test results

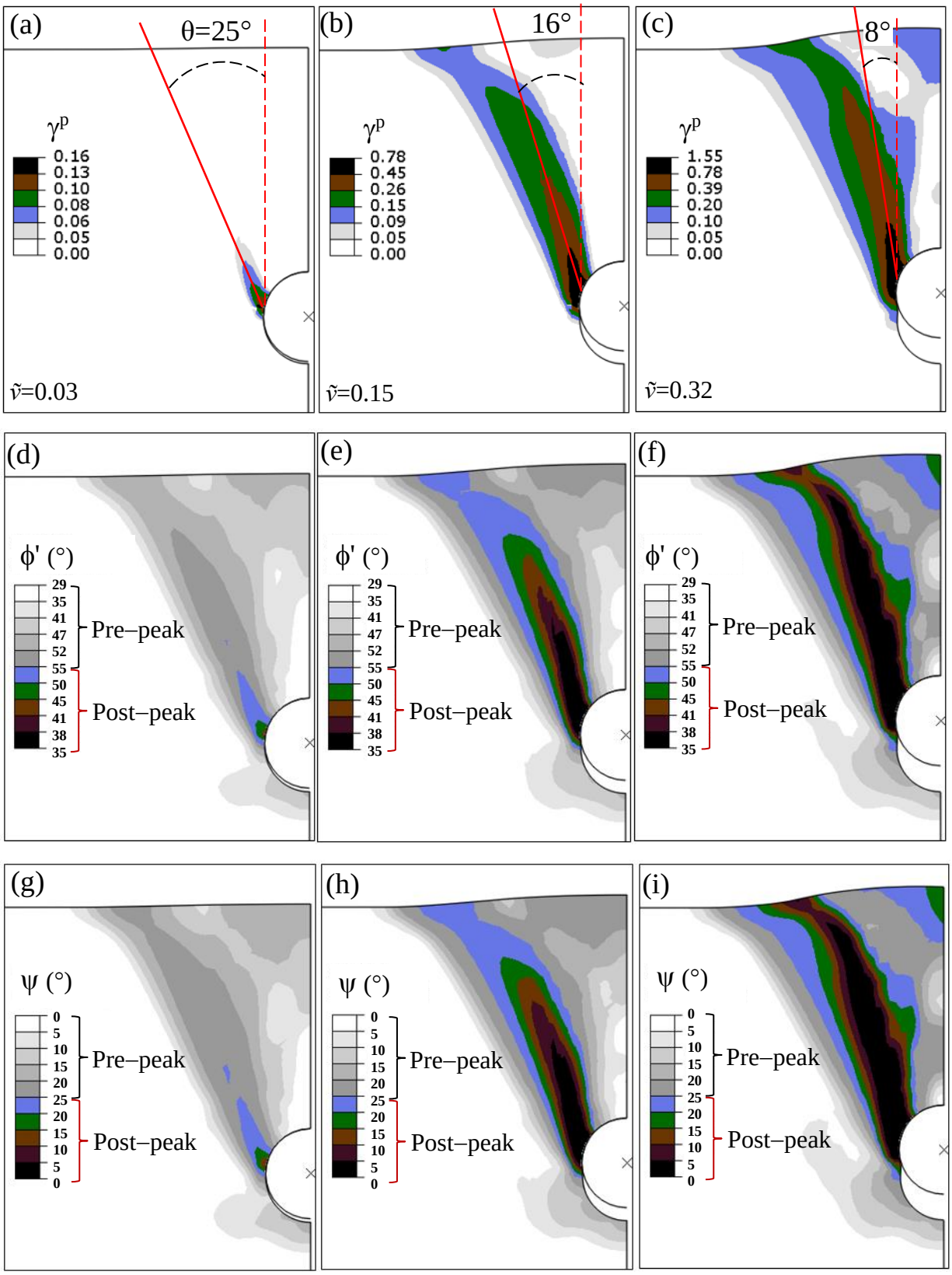

Figure 5.3: FE simulation with the MMC model: a–e for shear band formation, d–f for mobilized ϕ' and g–i for mobilized ψ

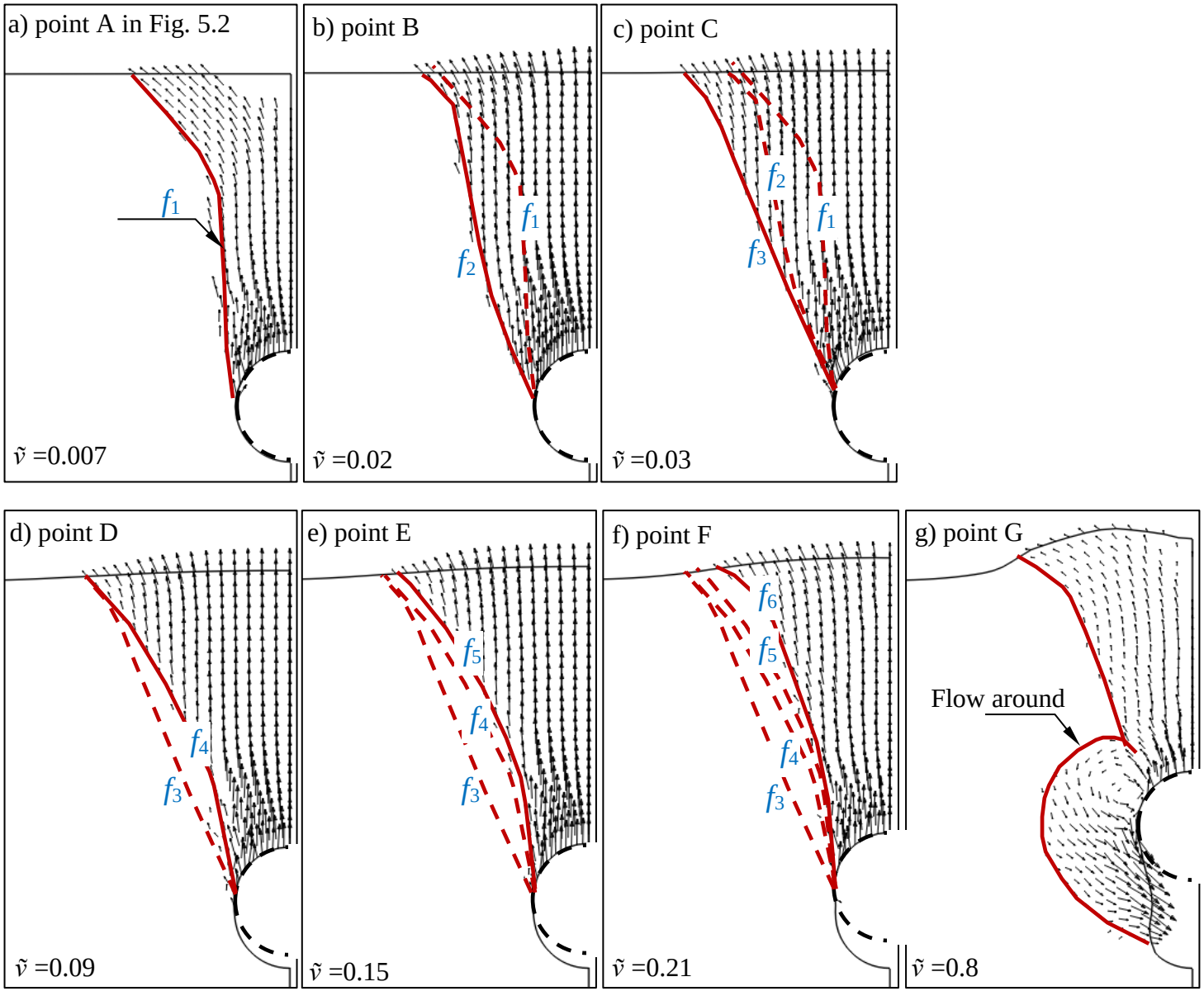

Figure 5.4: Velocity vector for FE analysis with the MMC model: a–c for pre–peak and d–g for post–peak condition

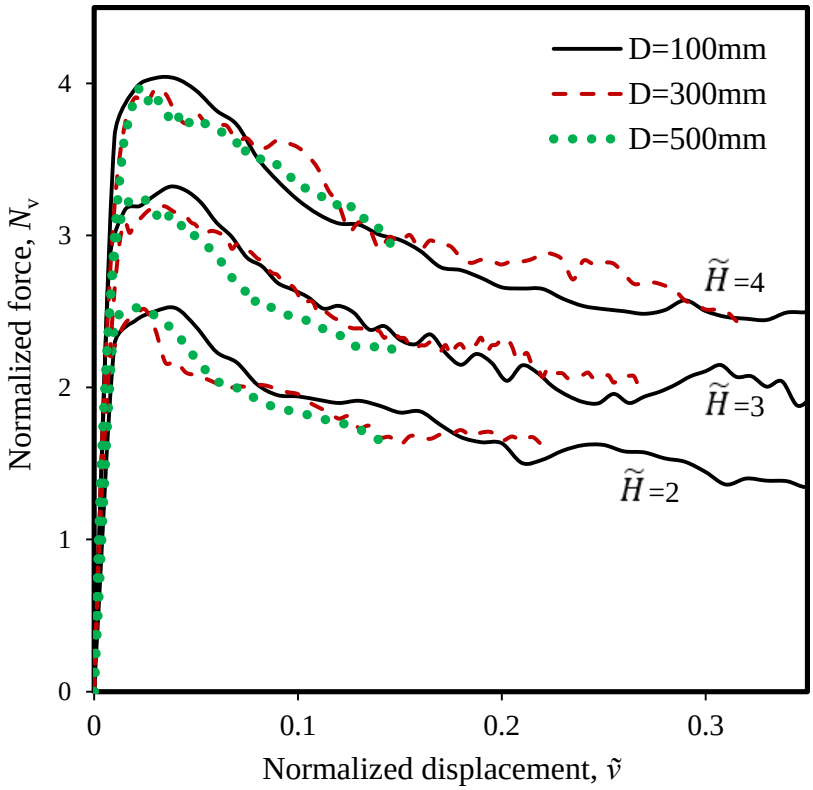

Figure 5.5: Effect of diameter on dimensionless uplift force N_v

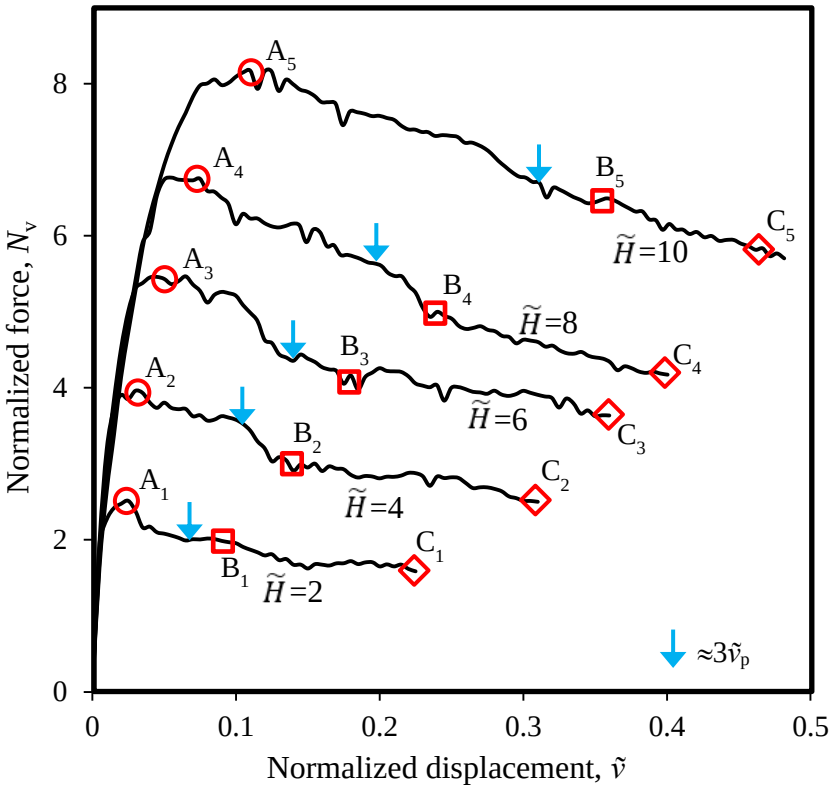

Figure 5.6: Uplift force–displacement curves for different $\widetilde{H}$ (D=300mm)

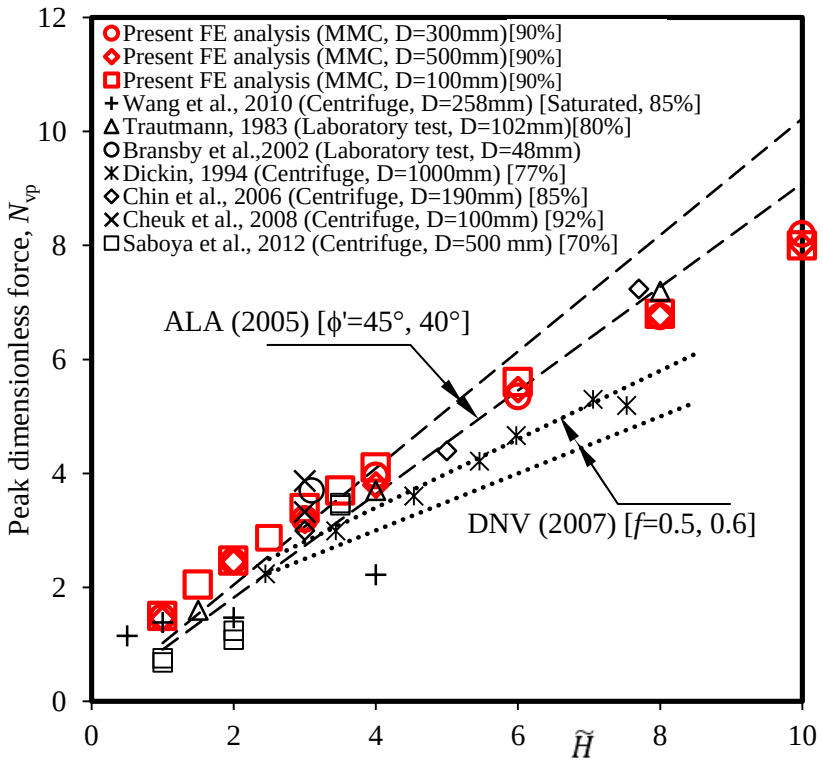

Figure 5.7. Comparison of peak uplift resistance from FE analysis and physical model tests

	At peak condition ($\tilde{v}_p$)	At intermediate $\tilde{v}$	At moderately large $\tilde{v}$
$\tilde{H}$=2	a) point A_1 in Fig. 5.6 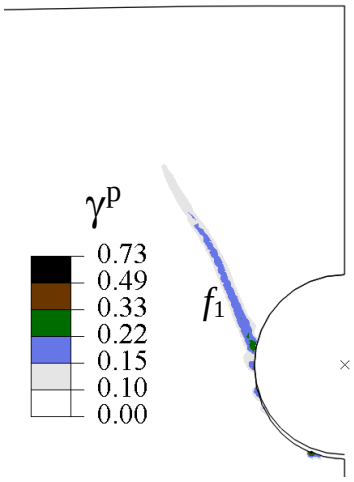	f) point B_1 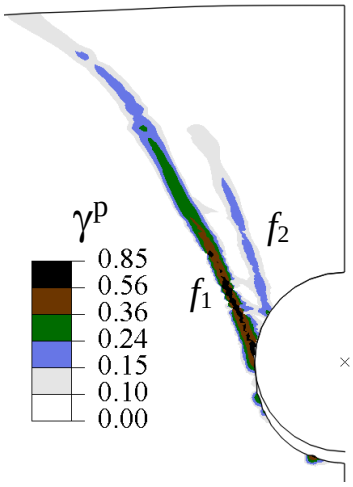	k) point C_1 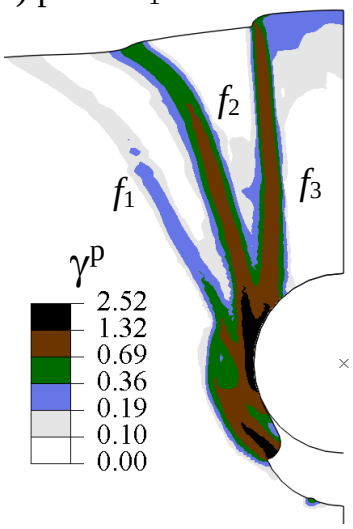
$\tilde{H}$=4	b) point A_2 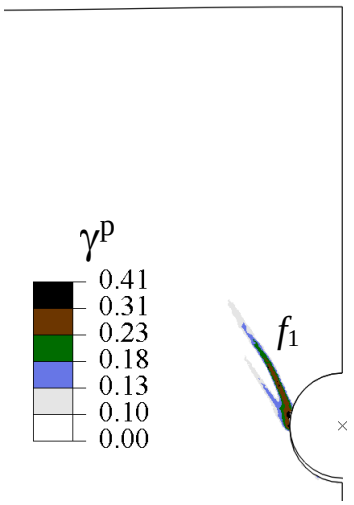	g) point B_2 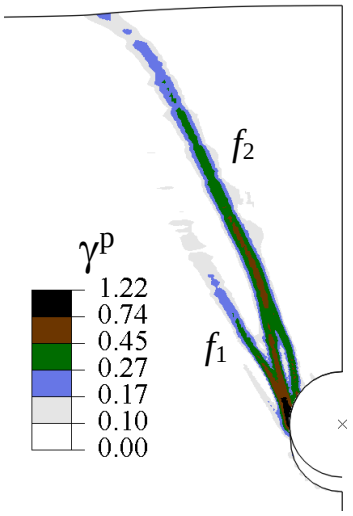	l) point C_2 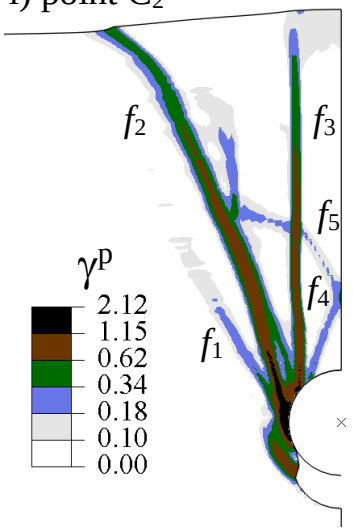

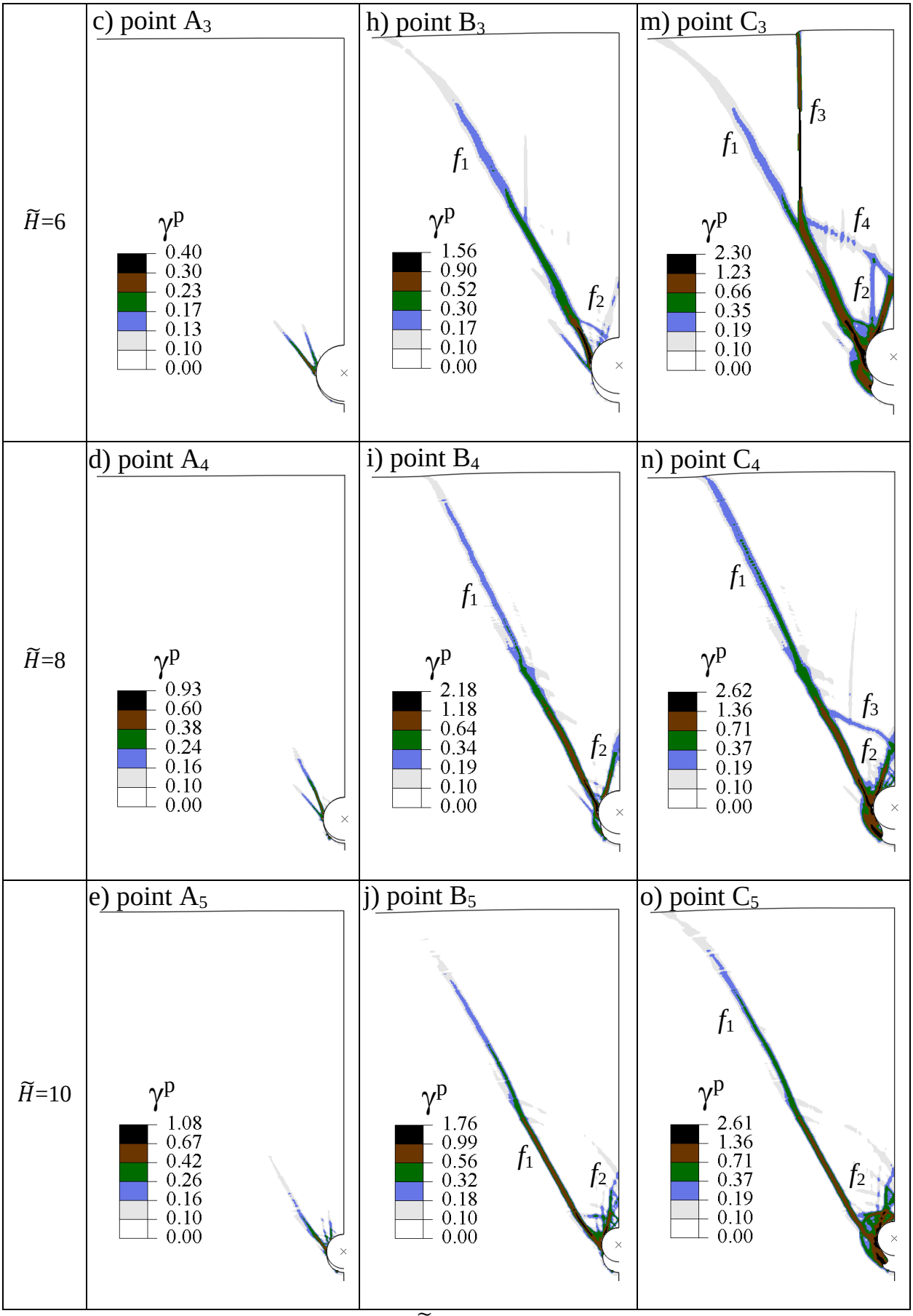

Figure 5.8. Plastic shear strain for different $\widetilde{H}$ (D=300mm)

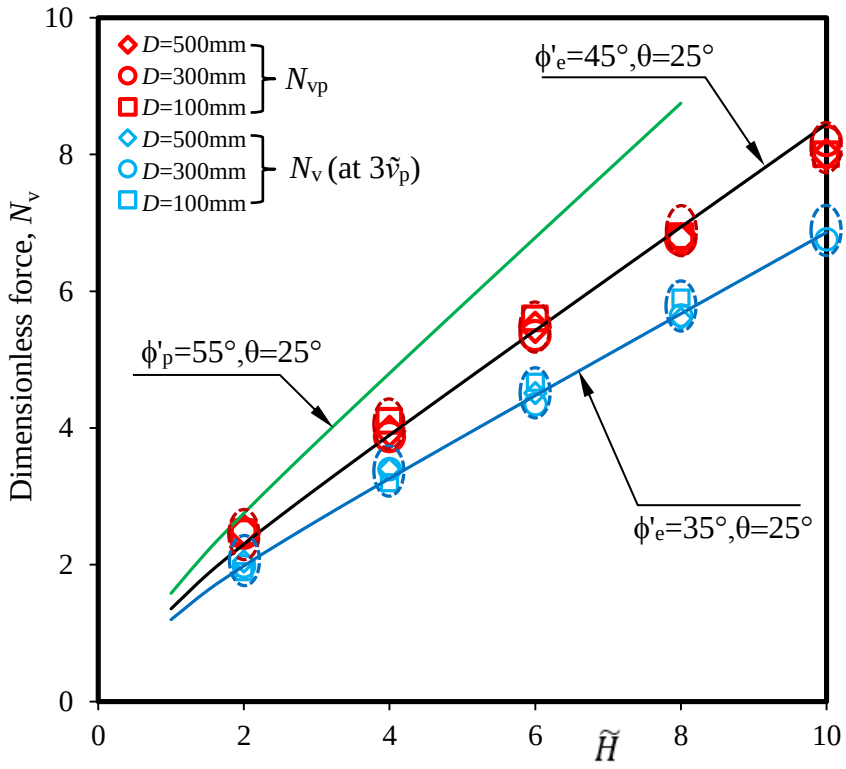

Figure 5.9: Simplified equations for N_{vp} and N_{vs} at different $\tilde{v}$

Table 5.1: Equations for Modified Mohr–Coulomb Model (MMC) (summarized from Chapter 3)

Description	Eq. #	Constitutive Equations
Relative density index	(5.1)	$I_R = I_D(Q - \ln p') - R$ where $I_D = D_r(\%)/100$ & $0 \le I_R \le 4$
Peak friction angle	(5.2)	$\phi'_p - \phi'_c = A_\psi I_R$
Peak dilation angle	(5.3)	$\psi_p = \frac{\phi'_p - \phi'_c}{k_\psi}$
Strain-softening parameter	(5.4)	$\gamma_c^p = C_1 - C_2 I_D$
Plastic shear strain at ϕ'_p and ψ_p	(5.5)	$\gamma_p^p = \gamma_c^p \left(\frac{p'}{p'_a}\right)^m$
Mobilized friction angle in Zone-II	(5.6)	$\phi' = \phi'_{in} + \sin^{-1}\left[\left(\frac{2\sqrt{\gamma^p \gamma_p^p}}{\gamma^p + \gamma_p^p}\right)\sin(\phi'_p - \phi'_{in})\right]$
Mobilized dilation angle in Zone-II	(5.7)	$\psi = \sin^{-1}\left[\left(\frac{2\sqrt{\gamma^p \gamma_p^p}}{\gamma^p + \gamma_p^p}\right)\sin(\psi_p)\right]$
Mobilized friction angle in Zone-III	(5.8)	$\phi' = \phi'_c + \left(\phi'_p - \phi'_c\right)\exp\left[-\left(\frac{\gamma^p - \gamma_p^p}{\gamma_c^p}\right)^2\right]$
Mobilized dilation angle in Zone-III	(5.9)	$\psi = \psi_p \exp\left[-\left(\frac{\gamma^p - \gamma_p^p}{\gamma_c^p}\right)^2\right]$
Young's modulus	(5.10)	$E = K p'_a \left(\frac{p'}{p'_a}\right)^n$

Table 5.2: Geometry and soil parameters used in the FE analyses

Parameter	Values
External diameter of pipe, D (mm)	100 (300, 500)
K	150
n	0.5
ν_{soil}	0.2
A_ψ	5
k_ψ	0.8
ϕ'_{in} (°)	29
C_1	0.22
C_2	0.11
m	0.25
Critical state friction angle, ϕ'_c (°)	35
Relative density, D_r (%)	80, 90
Unit weight, γ (kN/m^3)	16.87, 17.7
Interface friction coefficient, μ	0.32
Embedment ratio, $\widetilde{H}$	3 & 8 (2, 4, 6, 8, 10)

Note: Numbers in parenthesis in right column show the values used in the parametric study

CHAPTER 6

Lateral Resistance of Pipes and Strip Anchors Buried in Dense Sand

Co-Authorship: This chapter has been submitted to a journal as a technical paper for review as: Roy, K., Hawlader, B.C., Kenny, S. and Moore, I. (2017), 'Lateral Resistance of Pipes and Strip Anchors Buried in Dense Sand.' Most of the research in this chapter has been conducted by the first author. He also prepared the draft manuscript. The other authors mainly supervised the research and reviewed the manuscript

6.1 Abstract

The response of buried pipes and vertical strip anchors in dense sand under lateral loading is compared based on finite element (FE) modeling. Incorporating strain-softening behaviour of dense sand, the progressive development of shear bands and the mobilization of friction and dilation angles along the shear bands are examined, which could explain the variation of peak and post-peak resistances for anchors and pipes. The normalized peak resistance increases with embedment ratio and becomes almost constant at large burial depths. When the height of an anchor is equal to the diameter of the pipe, the anchor gives approximately 10% higher peak resistance than that of the pipe. The transition from the shallow to deep failure mechanisms occurs at a larger embedment ratio for anchors than pipes. A simplified method is proposed to estimate the lateral resistance at the peak and also after softening at large displacement.

6.2 Introduction

Buried pipelines are one of the most efficient modes of transportation of hydrocarbons, both in onshore and offshore environments. Pipelines might be subjected to lateral loading due to relative movement between soil and pipe. To develop the force–displacement relationships, in addition to the research on buried pipelines, studies on strip anchors (simply referred to as "anchor" in this paper) have been utilized, assuming that a geometrically similar pipe and anchor essentially behave in a similar fashion (Dickin 1994; Ng 1994). However, comparing the behaviour of buried pipes and anchors, some contradictory results have been obtained. Based on centrifuge tests, Dickin (1994) showed no significant difference between uplift behaviour of pipes and anchors. Reanalyzing 61 tests on model pipes and 54 on anchors, White et al. (2008) showed that the same limit equilibrium (LE) method overpredicts the maximum uplift resistance (mean value) of pipes by 11%, while it underpredicts the anchor resistance by 14%. The authors suggested that this significant discrepancy might be due to the existence of a systematic difference between pipe and anchor behaviour. Very limited research comparing lateral resistance of pipes and anchors is available. In a limited number of centrifuge tests, Dickin (1988) showed no significant difference between the force–displacement curves for pipes and anchors up to the peak resistance; however, the anchors give higher resistance than pipes after the peak.

Pipelines and anchors buried in dense sand are the focus of the present study. Anchors can be installed directly in dense sand (Das and Shukla 2013). In many situations, the sand around the pipeline might densify, even after installation. For instance, Clukey et al. (2005) showed that the sandy backfill densified from relative density (D_r) less than ~57% to ~85–90% in 5 months, which has been attributed to wave action at the test site in the Gulf of Mexico.

The behaviour of buried pipes and anchors can be compared through physical modeling and numerical analysis. Physical modeling is generally expensive, especially the full-scale tests at large burial depths, in addition to having some inherent difficulties, including the examination of the progressive formation of thin shear bands in dense sand. Through a joint research project between Memorial University of Newfoundland and Queen's University, Canada, the authors and their co-workers used the particle image velocimetry (PIV) technique (White et al. 2003) in full-scale tests for lateral pipe–soil interaction in both loose and dense sand (Burnett 2015). While PIV results provide deformation of the soil particles and location of the shear bands, tests on a wide range of burial depths could not be conducted. In addition, a number of centrifuge tests were also conducted using the geotechnical centrifuge at C-CORE (Daiyan et al. 2011; Debnath 2016).

Force–displacement behaviour is generally expressed in normalized form using $N_h=F_h/(\gamma HD)$ and $\tilde{u}=u/D$, where D is the diameter of the pipe (replace D with height of the anchor (B) for anchor–soil interaction), γ is the unit weight of the soil, F_h is the lateral force, H is the depths of the center of the pipe/anchor and u is the lateral displacement. The burial depth is also expressed in normalized form using the "embedment ratio, $\widetilde{H}=H/D$."

A considerable number of physical experiments were conducted on lateral pipe–soil interaction (Trautmann 1983; Hsu 1993; Daiyan et al. 2011; Burnett 2015; Monroy et al. 2015). Guo and Stolle (2005) compiled data from 11 experimental tests on dense sand and showed that the maximum dimensionless force (N_{hp}) increases with $\widetilde{H}$ and decreases with an increase in pipe diameter. Note, however, that a very limited number of tests for large diameters at large $\widetilde{H}$ are available. Most of the tests for $\widetilde{H}>7$ were conducted using small diameter pipe (D=25–50 mm), except for the Trautmann (1983) tests with a 102-mm diameter pipe. Physical experiments on dense sand also show a reduction of resistance after the peak (Trautmann 1983).

When the N_h–$\tilde{u}$ relation is used to calculate force on the pipe due to ground movement (e.g. landslide), the use of the maximum dimensionless force (N_{hp}) is conservative because it gives a higher force on the pipe. The existing design guidelines recommend simplified methods to calculate N_{hp} based on angle of internal friction of the soil, ϕ' (ALA 2005). However, as discussed in the following sections, N_{hp} depends on mobilized shear resistance of soil along the slip planes that form due to relative displacement between the pipe and surrounding soil.

Similar to pipeline research, a large number of experimental studies have been conducted on lateral anchor–soil interaction, with a main focus on the maximum capacity, N_{hp} (Neely et al. 1973; Das et al. 1977; Akinmusuru 1978; Dickin and Leung 1983; Hoshiya and Mandal 1984; Choudhary and Das 2017). Most of the theoretical studies on anchors are based on the rigid plastic behaviour of soil (Chattopadhyay and Pise 1986; Murray and Geddes 1987). Using the Mohr-Coulomb model for sand, FE (Rowe and Davis 1982; Dickin and King 1993) and FE limit analyses (Murray and Geddes 1989; Merifield and Sloan 2006; Kumar and Sahoo 2012; Bhattacharya and Kumar, 2013) have been conducted to calculate the maximum resistance. Similar to pipes, physical experiments show a post-peak degradation of lateral resistance for anchors in dense sand (Neely et al 1973; Dickin and Leung 1983). Therefore, the use of resistance after post-peak reduction might be safe in dense sand because the anchor might undergo considerably large displacement. Sutherland (1988) recognized that FE analyses with an elastoplastic model give unsatisfactory results for dense sand. Therefore, some studies suggested that the modeling of progressive development of shear bands would better simulate the response of anchors in dense sand (Tagaya et al. 1983; Abdel Rahman et al. 1992; Sakai and Tanaka 2007).

The lateral resistance evolves from a complex deformation mechanism and the stress–strain behaviour of soil around the pipe/anchor. More specifically, the progressive development of shear

bands in dense sand due to strain-softening and mobilization of shear resistance along these planes governs the lateral resistance. The stress–strain behaviour of dense sand involves the pre-peak hardening, post-peak softening, relative density and confining pressure (p') dependent ϕ' and ψ. Therefore, single representative values of ϕ' and/or ψ for the Mohr-Coulomb model in FE simulation or in simplified limit equilibrium analysis should be carefully selected. For anchors, Dickin and Leung (1983) showed that the peak friction angle gives considerably higher resistance compared to the experimental results. Similarly, for pipelines in dense sand, O'Rourke and Liu (2012) showed that ALA (2005) or PRCI (2004) guidelines that adopted Hansen's (1961) study on piles give N_{hp} more than twice of Trautmann and O'Rourke's (1983) recommendations based on physical modeling.

The aim of the present study is to conduct FE analyses to identify potential reasons behind the similarities and differences between the response of pipes and anchors in dense sand subjected to lateral loading. The progressive formation of shear bands with lateral displacement is simulated implementing a modified form of the Mohr-Coulomb model for dense sand. The mobilization of ϕ' and ψ along the shear band is examined to explain soil failure mechanisms and mobilized resistances at the peak and post-peak degradation stages. Finally, a set of simplified equations is proposed for practical applications.

6.3 Problem Statement and FE Modeling

An anchor or a section of pipe is placed at the desired embedment ratio ($\widetilde{H}$) in dense sand and then pulled laterally. Two-dimensional FE analyses on plane strain condition are performed using Abaqus/Explicit FE software (Dassault Systèmes 2010). Figure 6.1 shows the typical FE mesh at the start of lateral loading. To avoid mesh distortion issues at large displacements, an adaptive meshing option is adopted using the arbitrary Lagrangian-Eulerian (ALE) method, which

creates new smooth mesh with improved aspect ratios at given intervals. The bottom of the FE domain is restrained from any horizontal and vertical movement, while all the vertical faces are restrained from lateral movement.

Four-node bilinear plane strain quadrilateral elements (CPE4R in Abaqus) are used for modeling the soil while the pipe/anchor is modeled as a rigid body. The thickness of the anchor is 200 mm. Analyses are also performed for other thicknesses (100–300 mm); however, no significant effects on lateral resistance are found. The bottom and left boundaries are placed at a sufficiently large distance from the pipe/anchor to avoid boundary effects on lateral resistance.

The interface between pipe/anchor and soil is modeled using the interface friction coefficient (μ) as $\mu=\tan(\phi_\mu)$, where ϕ_μ is the interface friction angle. ϕ_μ depends on interface characteristics and relative movement between the pipe/anchor and soil and typically lies between 50 and 100% of the peak friction angle (Yimsiri et al. 2004). In the present study, $\phi_\mu=17.5°$ is used.

The numerical analysis is conducted in two steps. In the geostatic step, all the soil elements are brought to the in-situ stress condition. In the second step, the pipe/anchor is displaced laterally by specifying a displacement boundary condition at the reference point (center of the pipe/anchor).

6.4 Modeling of soil

Two soil models are used in this study: (i) Mohr-Coulomb (MC) and (ii) a modified Mohr-Coulomb (MMC) model. In the MC model, the angles of internal friction (ϕ') and dilation (ψ) are given as input, which remain constant during FE analysis. However, in the MMC model, the mobilized ϕ' and ψ are updated during the progress of FE analysis, as a function of accumulated plastic shear strain (γ^p) and mean effective stress (p'). Note that modified forms of the MC model have also been used in previous studies (Guo and Stolle 2005; Jung et al. 2013; Robert and

Thusyanthan 2014). The details of the MMC model used in the present study have been presented by the authors elsewhere (Roy et al. 2016). The key features of the MMC model are presented below, while the mathematical equations are listed in Table 6.1 (Eqs. (6.1)–(6.10)).

i) Laboratory tests on dense sand show that ϕ' and ψ vary with D_r, γ^p, p' and mode of shearing (triaxial (TX) or plane strain (PS)). However, constant representative values of ϕ' and ψ are commonly used in the MC model. The peak friction angle (ϕ'_p) increases with D_r but decreases with p' (Bolton 1986; Houlsby 1991), which are modeled using Eqs. (6.1) to (6.3) as in the work of Bolton (1986), where ϕ'_c is the critical state friction angle and A_ψ and k_ψ are two constants. Bolton (1986) suggested A_ψ=5.0 and 3.0 for plane strain and triaxial conditions, respectively. Chakraborty and Salgado (2010) recommended A_ψ=3.8 for both TX and PS conditions from their analysis of test results on Toyoura sand. In the present study, A_ψ=5 with $\phi'_p - \phi'_c \leq 20°$ for PS configuration is used (Bolton 1986).

ii) The mobilization of ϕ' and ψ with γ^p is modeled using Eqs. (6.6) to (6.9), which show that ϕ' and ψ gradually increase from the initial value (ϕ'_{in}, 0) to the peak (ϕ'_p, ψ_p) at γ^p_p (see the pre-peak zone of the example plot in the inset of Table 6.1). In the post-peak region, ϕ' and ψ are reduced exponentially, as in Eqs. (6.7) and (6.8), from the peak to the critical state ($\phi' = \phi'_c, \psi = 0$) at large γ^p. As the analysis is performed for the PS condition, ϕ'_c =35° is used, which is typically 3°–5° higher than that of the TX configuration (Bishop 1961; Cornforth 1964; Pradhan et al. 1988; Yoshimine 2005).

iii) The Young's modulus (E) is calculated using Eq. (6.10) (Janbu 1963; Hardin and Black 1966), where p' is the initial confining pressure at the pipe waist, p'_a is the atmospheric pressure (=100 kPa), K is a material constant, and n is an exponent. Equation (6.10) has also been used in

the previous studies for FE modeling of pipeline–soil interaction (Yimsiri et al. 2004; Guo and Stolle 2005; Daiyan et al. 2011; Jung et al. 2013). The Poisson's ratio of 0.2 is used for the soil, which is considered as the representative value for dense sand (Jefferies and Been 2006).

The implementation of the MMC model in Abaqus using a user defined subroutine has been discussed elsewhere (Roy et al. 2016, 2017).

6.5 Model tests simulations

In order to show the performance of the present FE modeling, simulations are first performed for two 1g model tests with 100-mm diameter pipes and two centrifuge tests with 1,000-mm high strip anchors (in prototype scale), conducted by Trautmann (1983) and Dickin and Leung (1983), respectively. These tests were conducted in dense sand having D_r~80%. FE simulations are performed for $\widetilde{H}$=1.5 and 5.5 for pipes and $\widetilde{H}$=1.5 and 4.5 for anchors, to explain the effects of the embedment ratio. The soil parameters used in FE simulations are listed in Table 6.2. Further details on lateral pipe–soil interaction and performance of the MMC model can be found in Roy et al. (2016).

6.5.1 Force–displacement behaviour of anchor under lateral loading

Figure 6.2 (a) shows the normalized force–displacement curves for anchors. The FE simulation with the MMC model for $\widetilde{H}$=1.5 shows that N_h increases with $\tilde{u}$, reaches the peak (N_{hp}) at $\tilde{u}$~0.05 (point A) and then quickly decreases to point B, which is primarily due to the strain-softening behaviour of dense sand. After that, N_h remains almost constant. In the present study, the rapid reduction of the lateral resistance segment of the N_h–$\tilde{u}$ curve (e.g. segment AB for $\widetilde{H}$=1.5) is called the "softening segment," while the segment after softening (e.g. segment after point B) is

the "large-deformation segment." Although some cases show a slight decrease in resistance in the large deformation segment, the resistance at the end of softening segment (e.g. at point B) is considered to be the "residual resistance (N_{hr})."

For comparison, centrifuge test results from Dickin and Leung (1983) are also plotted in Fig. 6.2(a). The following are the key observations: (i) N_{hp} and N_{hr} obtained from FE analysis with the MMC model is comparable to those obtained from the centrifuge tests; (ii) both centrifuge and FE simulations with the MMC model have softening and large-deformation segments in the N_h–$\tilde{u}$ curve, (iii) $\tilde{u}$ required to mobilize a N_h (e.g. N_{hp} and N_{hr}) is significantly higher in centrifuge tests than in FE simulations. Regarding this discrepancy, it is to be noted here that, conducting 1g and centrifuge tests for uplift resistance in dense sand, Palmer et al. (2003) showed that while the peak resistances obtained from these tests are comparable, the normalized mobilization distance in the centrifuge is significantly higher than that required in 1g tests. They also inferred that the centrifuge scaling law may not be fully applicable to strain localization and shear band formation in dense sand, although the magnitude of resistance could be successfully modeled. The present FE analysis for lateral anchor–soil interaction also shows a similar trend, which implies that the mobilization distance in FE analysis might be comparable to 1g tests. Note that a similar trend of post-peak reduction of N_h in dense sand was also reported in other studies (Neely et al. 1973; Hoshiya and Mondal 1984).

A very similar trend is found for $\widetilde{H}$=4.5 when the centrifuge test results are compared with FE simulation using the MMC model. However, in this case, N_{hr} and the large-deformation segment of the N_h–$\tilde{u}$ curve could not be identified from centrifuge test results as the test was stopped at $\tilde{u}$=0.4, before the completion of softening. FE calculated N_{hp} and N_{hr} for $\widetilde{H}$=4.5 are higher than those values for $\widetilde{H}$=1.5.

6.5.2 Force–displacement behaviour of pipe under lateral loading

Figure 6.2(b) shows that the force–displacement curves obtained from FE analysis with the MMC model are very similar to the model test results of Trautmann (1983). For a high $\widetilde{H}$ (=5.5), there is a post-peak reduction of N_h; however, for a low $\widetilde{H}$ (=1.5), no significant post-peak reduction of N_h is found. Unlike Fig. 6.2(a), no significant discrepancy in the normalized mobilization distance between the model test and FE simulation results is found, because in this case the tests were conducted at 1g while the tests presented in Fig. 6.2(a) were conducted at 40g.

The model tests conducted by Audibert and Nyman (1978) using a 25-mm diameter pipe buried in dense Carver sand also show similar response: no significant post-peak degradation of N_h for shallow-buried ($\widetilde{H}$=1.5 and 3.5), but a considerable post-peak degradation for deeper pipelines ($\widetilde{H}$=6.5 and 12.5).

6.5.3 Limitations of the Mohr-Coulomb model

To show the advantages of the MMC model, three FE simulations with the MC model are performed for $\widetilde{H}$=1.5 using three sets of ϕ' and ψ values (ϕ'=50°,ψ=19°; ϕ'=44°,ψ=16° and ϕ'=35°,ψ=0°). Here, for a given ϕ', the value of ψ is calculated using Eq. (6.2) in Table 6.1. As expected, for the MC model, N_h increases with $\tilde{u}$, reaches the peak (N_{hp}) and then remains constant (Fig. 6.2(a)). Figure 6.2(a) also shows that the MC model for ϕ'=44° and ψ=16° gives N_{hp} comparable to the peak of the centrifuge test results. For ϕ'=50° and ψ=19°, N_{hp} is significantly higher, and for ϕ'=35° and ψ=0°, N_{hp} is significantly lower than the centrifuge test results. Although it is not explicitly mentioned in the design guidelines, equivalent (representative) values for these two parameters should be carefully selected, as they vary with γ^p (Roy et al. 2016). In general, the equivalent values of ϕ′ and ψ should be smaller than the peak and higher than the critical state

values. For example, Dickin and Leung (1983) mentioned that if the peak friction angle obtained from laboratory tests is used, the theoretical models (Neely et al. 1973; Ovesen and Stromann 1972) significantly overestimate the resistance as compared to model test results. Therefore, although ϕ'_p>50° was obtained from laboratory tests, they used an equivalent friction angle of 39.4°–43.5° to calculate N_{hp}. Another key observation from Fig. 6.2(a) is that the simulations with the MC model do not show any post-peak degradation of N_h, as observed in centrifuge tests.

The difference between the N_h–$\tilde{u}$ curves with the MC and MMC model can be further explained from the progressive development of shear bands, the zones of localized plastic shear strain, $\gamma^p = \int_0^t \sqrt{\frac{3}{2}\left(\dot{\epsilon}_{ij}^p \dot{\epsilon}_{ij}^p dt\right)}$, where $\dot{\epsilon}_{ij}^p$ is the plastic deviatoric strain rate tensor (Figs. 6.3(a–d)). These figures show the variations of γ^p at points C, D, E and F in Fig. 6.2(a). Three distinct shear bands (f_1–f_3) form in all the cases. However, the approximate angle of the shear band f_1 to the vertical increases with ϕ' and ψ, as shown by drawing lines through the shear bands (Fig. 6.3(e)), which in turn increases the size of the passive failure wedge and thereby lateral resistance. An opposite trend, a decrease in size of the active failure wedge (on the left side of the anchor) with an increase in ϕ' and ψ—is found; however, the active zone does not have a significant effect on lateral resistance.

6.6 Mesh sensitivity

As the MMC model considers the strain-softening behaviour of dense sand, FE simulations with this model are expected to be mesh sensitive. More specifically, the formation of shear bands and mobilization of ϕ' and ψ need to be modeled properly. For sand, the ratio between the thickness of the shear band (t_s) and the mean particle size (d_{50}) varies between 3 and 25; the lower values

mostly correspond to coarse-grained sands (Loukidis and Salgado 2008; Guo 2012). As the soil is modeled as a continuum in the FE analysis, the width of the shear band can be controlled by varying element size, which is generally described by the width or characteristic length of the finite element (t_{FE}). Very small t_{FE} gives an unrealistically thin shear band, while large t_{FE} cannot capture strain localization properly. The ratio of t_s/t_{FE} also depends on loading conditions. For example, Loukidis and Salgado (2008) used $t_{FE}=t_s$ in the zone of strain localization near the pile to calculate the shaft resistance in dense sand. However, the deformed mesh under the footing in dense sand shows $t_s\sim(2–3)t_{FE}$ (Tejchman and Herle 1999; Tejchman and Górski 2008), which is consistent with model tests results (Tatsuoka et al. 1991). As will be shown later, during lateral movement of the pipe, strain localization extends to more than one element. Therefore, $t_{FE}<t_s$ should be used to capture the strain localization properly. Assuming $d_{50}\sim0.5$ mm and $t_s/d_{50}\sim25$ for fine sand, $t_s\sim12.5$ mm is calculated, which is also consistent with experimentally observed shear band width. For example, Sakai et al. (1998) showed $t_s\sim9$ mm for fine Soma sand and Uesugi et al. (1988) found $t_s\sim8$ mm for Seto sand.

Several authors proposed element scaling rules to reduce the effects of FE mesh on simulated results (Pietruszczak and Mróz 1981; Moore and Rowe 1990; Andresen and Jostad 2004; Anastasopoulos et al. 2007). using the work of Anastasopoulos et al. (2007) and assuming the reference FE mesh $t_{FE\_ref}=10$ mm, analyses are performed for $t_{FE}=30$ mm and 50 mm, where γ_c^p in Eq. (6.4) is scaled by a factor of $f_{scale}=(t_{FE\_ref}/t_{FE})^m$, where m is a constant. Anastasopoulos et al. (2007) suggested $m=1$ (i.e. f_{scale} is inversely proportional to element size) for fault rupture propagation. However, a number of FE simulations of lateral loading of pipes for varying geotechnical properties, element size, and pipe diameter show that $m\sim0.7$ gives a better f_{scale} than $m=1$ for mesh independent N_h–$\tilde{u}$ curves. As an example, for $D_R=80\%$, $\gamma_c^p=0.132$ for both 50-mm

and 10-mm mesh, when the scaling rule is not used. However, γ_c^p=0.132*(10/50)$^{0.7}$=0.043 for 50-mm and γ_c^p=0.132 for 10-mm mesh when the scaling rule is used.

Figure 6.4 shows the sample mesh sensitivity analysis results for a 500-mm diameter pipe. If the scaling rule is not used, the peak resistance and the rate of post-peak degradation are considerably higher for coarse mesh (e.g. t_{FE}=50 mm) than for fine mesh (t_{FE}=10 mm). However, the mesh size effect on N_h is negligible at very large $\tilde{u}$, because at this stage the shear strength along the shear bands is simply governed by the critical state parameters. Figure 6.4 also shows that the scaling rule brings the N_h–$\tilde{u}$ curves closer for the three mesh sizes. A very similar trend is found for other diameters, although the results are not presented in this paper. In the present study, except for mesh sensitive analysis, the characteristic length (t_{FE}) of the elements is ~10 mm, except for a few rows of elements near the pipe where t_{FE}<10 mm.

6.7 Peak anchor resistance

Figure 6.5 shows that the peak resistance obtained from FE analyses with the MMC model is higher for a 500-mm anchor than that of a1000-mm anchor. The rate of increase of N_{hp} with $\widetilde{H}$ reduces at large embedment ratios, and approximately after $\widetilde{H}$=7–8, N_{hp} remains almost constant. Physical model test results available in the literature are also included in this figure for comparison. A significant difference between N_{hp} for different anchor heights is also evident in these physical model tests; for example, compare the diamonds and triangles in Fig. 6.5 that represent N_{hp} for 50-mm and 1,000-mm anchors, respectively. Similarly, the peak resistances in small-scale 1g tests for B~50 mm (Neely et al. 1973; Das et al. 1977; Rowe and Davis 1982) are higher than those for large anchor heights of B=500–1,000 mm (Dickin and Leung 1983). In other words, there is a “size

effect" on N_{hp}, and that can be simulated with the MMC model. Further discussion on this issue is provided later in the "Proposed simplified equations" section.

6.8 Comparison of response between pipes and strip anchors

A total of eight FE analyses with the MMC model are conducted for four embedment ratios ($\widetilde{H}$=2–8) and B=D=500 mm, to identify the similarities and differences between lateral anchor– and pipe–soil interaction.

6.8.1 Force–displacement Behaviour

Figure 6.6 shows the N_h–$\tilde{u}$ curves for both pipe and anchor, on which the points of interest for further explanation are labeled (circles, squares and diamonds are for the peak, residual and large displacements, respectively). Similar to physical model test results for anchors and pipes (Dickin and Leung 1983; Hoshiya and Mandal 1984; Trautmann 1983; Paulin et al. 1998), N_h increases with $\tilde{u}$, reaches the peak value and then decreases to a residual value. For deeper conditions (e.g. $\widetilde{H}$=6 & 8), the decrease in N_h continues even at large $\tilde{u}$; however, for simplicity, the N_h after the square symbols is assumed to be constant (residual) for further discussion. Figure 6.6 also shows that, for a given $\widetilde{H}$ and B (=D), an anchor offers higher resistance than pipe. Note that, in a limited number of centrifuge tests, Dickin (1988) found higher residual resistance for an anchor than a similar-sized (B=D) pipe, although the peak resistances were similar. In other words, there is a "shape effect" on lateral resistance (i.e. higher resistance in the anchor), and that can be simulated using the MMC model. In addition, $\tilde{u}$ required to mobilize the resistance is higher in the anchor than for the pipe (e.g. $\tilde{u}$ at A′ is greater than $\tilde{u}$ at A, Fig. 6.6).

Figure 6.6 also shows the lateral resistance of a pipe for $\widetilde{H}$=30 (blue broken line). As shown, no significant increase in peak resistance occurs for an increase in $\widetilde{H}$ from 8 to 30. Moreover, the post-peak degradation of resistance for $\widetilde{H}$=30 is not significant.

6.8.2 Failure Mechanisms

The trend of lateral resistance shown in the previous sections can be further explained from the progressive development of shear bands (Figs. 6.7(a)–(x)). For small embedment ratios ($\widetilde{H}$=2–4), the lateral displacement of the pipe or anchor results in formation of active and passive soil wedges, which is known as "wedge" type failure (Figs. 6.7 (a–l)). For a pipe at $\widetilde{H}$=2, γ^p accumulates mainly in three shear bands, and the length of the shear bands increases with lateral displacement of the pipe (Figs. 6.7(a–c)). At the peak, γ^p generates in the shear bands mainly near the pipe, while γ^p is very small when it is far from the pipe. This implies that, in the segments of the shear band far from the pipe, γ^p is not sufficient to mobilize the peak friction and dilation angles. Figure 6.7(b) shows that significant γ^p generates in the shear band which reduces ϕ' and ψ of the soil elements in the shear bands. At large displacements, the accumulation of γ^p in the shear bands continues together with a significant movement of the wedges resulting in ground heave above the passive wedge and settlement above the active wedge. A very similar pattern of failure planes and ground movement has been reported from physical model tests (Paulin et al. 1998; O'Rourke et al. 2008; Burnett 2015; Monroy et al. 2015).

Similar to the pipe case, three shear bands develop progressively for an anchor (Figs. 6.7(d–f)). At the peak, γ^p in the shear band is higher for the anchor than for the pipe (Figs. 6.7(a) and 6.7(d)). Moreover, a larger passive wedge forms for the anchor than for the pipe (compare Fig. 6.7(b) and 6.7(e)). The distance between the center of the anchor and the point where f_1 reaches

the ground surface (l_a) is ~4.5B, while for the pipe, this distance (l_p) is ~4D. Because of this larger size of the passive wedge ($l_a > l_p$), the anchor offers higher resistance than pipe, as shown in Fig. 6.6. A similar response is found for $\widetilde{H}$=4 (Figs. 6.7(g–l)); however, l_a/l_p~1.3 (as compared to l_a/l_p~1.1 for $\widetilde{H}$=2), which is the primary reason for a significant difference between the resistances for pipe and anchor for $\widetilde{H}$=4 (Fig. 6.6). Dickin and Leung (1985) observed the formation of similar failure planes in their centrifuge tests for $\widetilde{H}$=2.5 and 4.5.

For a moderate embedment ratio ($\widetilde{H}$=6 & 8), at the peak, plastic deformation occurs mainly around the pipe (Fig. 6.7(m)). However, for the anchor, two horizontal shear bands in the front and a curved shear band at the back form at this stage (Fig. 6.7(p)). Three distinct shear bands, similar to the small embedment ratio cases, form at relatively large $\tilde{u}$ (Figs. 6.7(n) & 6.7(q)). At large $\tilde{u}$, a number of shear bands also form around the pipe and anchor, which also influence the force-displacement behaviour. Not shown in Fig. 6.7, at large burial depths ($\widetilde{H}$=15), only local flow around mechanisms are observed both for anchor and pipe.

In summary, the force–displacement curves obtained from the model tests or numerical analysis evolve from complex soil failure mechanisms during lateral loading. Because of the considerable difference in soil failure mechanisms, anchors offer higher resistance than pipes.

6.9 Proposed Simplified Equations

A set of simplified equations is proposed in this section to calculate the peak (N_{hp}) and residual (N_{hr}) resistances for pipes and anchors. These equations are developed based on the following trend observed in model tests and the present FE simulations: (i) both N_{hp} and N_{hr} increase with $\widetilde{H}$; however, N_{hp} remains constant after a critical embedment ratio ($\widetilde{H}_c$); (ii) the difference between N_{hp} and N_{hr} is not significant at large $\widetilde{H}$; (iii) for a given $\widetilde{H}$, the smaller the pipe

diameter or anchor height, the higher the N_{hp} and N_{hr}; (iv) for a given B=D, anchor resistance is higher than pipe resistance.

In order to capture these phenomena, the following equations are proposed:

$$N_{hp} = N_{hp0}\widetilde{H}^{m_p} f_D f_s \qquad \text{for } \widetilde{H} \le \widetilde{H}_c \tag{6.11}$$

$$N_{hp} = N_{hp0}\widetilde{H}_c^{m_p} f_D f_s \qquad \text{for } \widetilde{H} > \widetilde{H}_c \tag{6.12}$$

$$N_{hr} = N_{hr0}\widetilde{H}^{m_r} f_D f_s \qquad \text{with } N_{hs} \le N_{hp} \tag{6.13}$$

where N_{hp0} and N_{hr0} are the values of N_{hp} and N_{hr}, respectively, for a reference diameter of the pipe (D_0) and embedment ratio ($\widetilde{H}_0$); f_D is a size factor (e.g. the effects of D/D_0 for pipes and B/B_0 for anchors); f_s is a shape factor (i.e. pipe or anchor); and m_p and m_r are two constants.

In the present study, D_0=500 mm and $\widetilde{H}_0$=1 are used. Guo and Stolle (2005) used their FE calculated resistance for a 330-mm diameter pipe buried at $\widetilde{H}$=2.85 as the reference value to estimate the peak resistance for other pipe diameters and embedment ratios. To provide a simplified equation for the reference resistance, the following equation proposed by O'Rourke and Liu (2012) for shallow-buried pipeline is used in the present study.

$$N_{hp0} = \frac{\left(\widetilde{H} + 0.5\right)^2 \tan\left(45° + \frac{\phi'_e}{2}\right)(\sin\beta + \mu\cos\beta)}{2\widetilde{H}(\cos\beta - \mu\sin\beta)} \tag{6.14}$$

where ϕ'_e is the equivalent friction angle, μ=$\tan\phi'_e$, and $\beta = 45° - \phi'_e/2$ is the inclination of an assumed linear slip plane to the horizontal datum that generates from the bottom of the pipe to form the passive wedge (i.e. an approximate linear line through the shear band f_1 in Fig. 6.3(d)).

When the peak resistance is mobilized, the plastic shear strain along the entire shear band is not the same—in some segments $\gamma^p < \gamma^p_p$ (i.e. pre-peak hardening state) while in some segments $\gamma^p > \gamma^p_p$ (i.e. post-peak softening state). Therefore, if one wants to use only one approximate value of ϕ' for the entire length of the shear band, (i.e. ϕ'_e in Eq. (6.14)), it should be less than ϕ'_p.

Therefore, ϕ'_e=44° is used in Eq. (6.14) to calculate N_{hp0}. Note that a similar approach of using ϕ'_e to calculate the bearing capacity of footing on dense sand, where shear bands form progressively, has been presented by Loukidis and Salgado (2011). Similarly, a representative value of ϕ' ($<\phi'_p$) has also been used to calculate the anchor resistance (Dickin and Leung 1983; Dickin 1994).

To calculate N_{hr0}, $\mu=\tan\phi'_c$ is used, because, at this stage, significant plastic shear strains generate along the entire length of the failure plane that reduce ϕ' to the critical state value (e.g. Fig. 6.7(b)). It is also found that β does not change significantly with lateral displacement (e.g. see Figs. 6.7(a–c)). Therefore, β is calculated using ϕ'_e=44°.

Similar to the work of Guo and Stolle (2005), the size factor is calculated using $f_D = 0.91(1 + D_0/(10D))$. The present FE results also show that $\widetilde{H}_c$ is higher for smaller size pipes or anchors, which is incorporated using $\widetilde{H}_c = f_{Hc}\widetilde{H}_{c0}$, where $f_{Hc} = 0.6(1 + D_0/(1.5D))$.

For the geometry and soil properties used in the present study, the peak resistance remains constant after $\widetilde{H}$~7.5 for a 500-mm diameter pipe. Therefore, $\widetilde{H}_{c0} = 7.5$ is used for the reference condition. It is also found that the calculated resistances using Eqs. (6.11) to (6.13) fit well with the FE results for m_p=0.37 and m_r=0.5. Note that, Guo and Stolle (2005) found m_p=0.35 as the representative value from their FE analysis. FE analyses also show that, for a given B=D, the anchor resistance is ~10% higher than pipe resistance (i.e. f_s=1.0 for pipes and f_s=1.1 for anchors).

Figure 6.8(a) shows that N_{hp} and N_{hr} obtained from Eqs. (6.11) to (6.13) match well with FE calculated values. The considerable difference between N_{hp} for different pipe dimeters is similar to that in the work of Guo and Stolle (2005). For a large embedment ratio (e.g. $\widetilde{H}$>10 for D=500 mm), N_{hp}=N_{hr}. Physical model tests on dense sand also show no significant reduction of post-peak reduction of resistance at large $\widetilde{H}$ (Hsu 1993).

Figure 6.8(b) shows that, when f_s=1.1 is used for the anchor, Eqs. (6.11) to (6.13) calculate N_{hp} and N_{hr} similar to FE results. A significant difference in N_{hp} between small and large sized

anchors at large $\widetilde{H}$ was also found in physical model tests, as shown in Fig. 6.5 (compare the triangles and diamonds). In order to show the importance of the shape factor f_s, N_{hp} for the reference pipe (D_0=500 mm) is also shown in this figure, which is below the FE calculated values for a 500-mm high anchor.

In summary, while Guo and Stolle (2005) found a gradual increase in N_{hp} for pipe with the embedment ratio, the present study shows that both N_{hp} and N_{hr} increase with $\widetilde{H}$ for pipes and anchors, and reach a constant maximum value after a large $\widetilde{H}$. For practical purposes, without conducting FE analysis, the reference resistance could be calculated using the O'Rourke and Liu (2012) analytical solution with an equivalent friction angle. The present FE analysis and the simplified equations provide a method to estimate the peak and residual resistances.

6.10 Conclusions

Under lateral loading, the behaviour of buried pipelines and vertical strip anchors are generally assumed to be similar. In the present study, the similarities and differences between the behaviour of pipes and vertical strip anchors in dense sand subjected to lateral loading are examined through a comprehensive FE analysis. A modified Mohr-Coulomb (MMC) model for dense sand that captures the variation of friction and dilation angles with plastic shear strain, confining pressure and relative density are implemented in the FE analysis. The plastic shear strain localization (shear band) is successfully simulated, which can explain the soil failure mechanisms and the variation in lateral resistance for pipes and anchors for a wide range of embedment ratios. The proposed MMC model can simulate the peak resistance and also the post-peak degradation, as observed in physical model tests, which cannot be done using the Mohr-Coulomb model. The following conclusions can be drawn from the present study:

- The peak and residual resistances (N_{hp} and N_{hr}) increase with the embedment ratio ($\widetilde{H}$) both for pipes and anchors. However, after a critical $\widetilde{H}$, N_{hp} remains almost constant. The anchor resistance is ~10% higher than that of a similar-sized pipe.
- The critical embedment ratio ($\widetilde{H}_c$) is higher for smaller diameter pipe.
- The difference between N_{hp} and N_{hr} is significant at small to moderate $\widetilde{H}$; however, the difference is not significant at large $\widetilde{H}$.
- Both N_{hp} and N_{hr} are higher for smaller diameter pipes and a smaller height of anchors.
- At a small $\widetilde{H}$, the soil failure mechanisms involve dislocation of active and passive wedges bounded by three distinct shear bands. At an intermediate $\widetilde{H}$, the active and passive wedges form at large displacements of the anchor/pipe. However, at a large $\widetilde{H}$, flow around mechanisms govern the behaviour.
- The transition from shallow to deep failure mechanisms occurs at a lower $\widetilde{H}$ in pipes than in anchors.
- The mobilized ϕ' along the entire length of the shear band at the peak or post-peak degradation stages is not constant, because it depends on plastic shear strain. Even when N_{hp} is mobilized, $\phi' = \phi'_p$ only in a small segment of the shear band. Therefore, an equivalent friction angle, ϕ'_e ($< \phi'_p$) is required to match the peak resistance in test results. At a very large displacement, ϕ' in the shear bands ~ϕ'_c because of significant strain accumulation in these zones.
- The proposed simplified equations can be used to estimate the peak and residual resistances of pipes and anchors for a wide range of embedment ratios.

One practical implication of the present numerical study is that the parametric study can complement existing experimental data because it covers a wide range of pipe diameters and burial

depths, including the cases of large diameter pipes and large embedment ratios, which represent the conditions of very costly full-scale tests.

Acknowledgements

The work presented in this paper was supported by the Research and Development Corporation of Newfoundland and Labrador, Chevron Canada Limited and the Natural Sciences and Engineering Research Council of Canada (NSERC).

References

Abdel Rahman, M.A., Othman, M.A., and Edil, T.B. (1992). "Effect of plate flexibility on behaviour of shallow anchors." *Soil Found. Jpn. Soc. Soil. Mech. Found. Eng.*, 32(3), 137–143.

Akinmusuru, J. O. (1978). "Horizontally loaded vertical anchor plates in sand." *J. Geotech. Eng. Div.*, 104(2), 283–286.

American Lifelines Alliance (ALA). (2005). "Guidelines for the design of buried steel pipe." <https://www.americanlifelinesalliance.com/pdf/Update061305.pdf > (Mar. 13, 2017).

Anastasopoulos, I., Gazetas, G., Bransby, M.F., Davies, A., and El Nahas, M.C.R. (2007). "Fault rupture propagation through sand: finite-element analysis and validation through centrifuge experiments." *J. of Geotech. and Geoenv. Eng.*, 133(8), 943–958.

Andresen, L. and Jostad, H.P. (2004). "Analyses of progressive failure in long natural slopes." Proc., *9th Symp. on Num. Models in Geomech. NUMOG IX*, Ottawa, 603–608.

Audibert, J.M.E., and Nyman, K.J. (1978). "Soil restraint against horizontal motion of pipes." Intl. *J. of Rock Mech. and Mining Sci. and Geomech.*, 15(2), A29.

Bhattacharya, P. and Kumar, J. (2013). “Seismic pullout capacity of vertical anchors in sand.” *Geomech Geoeng Int J*, 8(3), 191–201.

Bishop, A. W. (1961). “Discussion on soil properties and their measurement.” *Proc., 5th Int. Conf. on Soil mech. and Found.n eng.*, 3.

Bolton, M. D. (1986). “The strength and dilatancy of sands.” *Géotechnique*, 36(1), 65−78.

Burnett, A. (2015). “Investigation of full scale horizontal pipe-soil interaction and large strain behaviour of sand.” M.A.Sc. thesis, Queen's University, Canada.

Chakraborty, T., and Salgado, R. (2010). “Dilatancy and shear strength of sand at low confining pressures.” *J. of Geotech. and Geoenv. Eng*., 136(3).

Chattopadhyay, B.C., and Pise, P.J. (1986). “Uplift capacity of pile in sand.” *J. of Geotech. Eng*., ASCE, 112(9), 888–904.

Choudhary, A.K. and Dash, S.K. (2017). “Load-carrying mechanism of vertical plate anchors in sand.” *Int. J. Geomech*., 17(5).

Clukey, E.C., Haustermans, L. and Dyvik, R. (2005). “Model tests to simulate riser–soil interaction effects in touchdown point region.” *Proc., Intl. Symp. on Fron. in Offshore Geotech. (ISFOG 2005)*, Perth, Australia, 651–658.

Conforth, D.H. (1964). “Some experiments on the influence of strain conditions on the strength of sand.” *Géotechnique*, 14, 143−167.

Daiyan, N., Kenny, S., Phillips, R., and Popescu, R. (2011). “Investigating pipeline–soil interaction under axial–lateral relative movements in sand.” *Can. Geotech. J*., 48(11), 1683−1695.

Dassault Systèmes. (2010). ABAQUS [computer prog.]. Dassault Systèmes, Inc., Providence, R.I.

Das, B. M., Seeley, G. R., and Das, S. C. (1977). "Ultimate resistance of deep vertical anchor in sand." *Soils Found*., 17(2), 52–56.

Das, B.M. and Shukla, S.K. (2013). *Earth Anchors*. 2nd edition, J. Ross Publishing Inc, USA.

Debnath, P. (2016). "Centrifuge modeling of oblique pipe–soil interaction in dense and loose sand." M.Eng. thesis, Memorial University of Newfoundland, Canada.

Det Norske Veritas (DNV). (2007). "Global buckling of submarine pipelines—Structural design due to high temperature/high pressure." *DNV-RP-F110*, Baerum, Norway.

Dickin, E.A. (1988). "Stress-displacement of buried plates and pipes." *Proc., International Conference on Geotechnical Centrifuge Modelling*, Centrifuge 88, Paris, France.

Dickin, E.A. (1994). "Uplift resistance of buried pipelines in sand." *Soils and Found*., 34(2), 41-48.

Dickin, E. A., and Leung, C. F. (1983). "Centrifuge model tests on vertical anchor plates." *J. Geotech. Eng*., 12(1503), 1503–1525.

Dickin, E. A., and Leung, C. F. (1985). "Evaluation of design methods for vertical anchor plates." *J. Geotech. Eng*., 4(500), 500–520.

Dickin, E.A. and King, G.J.W. (1993). "Finite element modelling of vertical anchor walls in sand." *Develop. in Civil & Cons. Eng. Comp*., Civil-Comp Press, Edinburgh, UK.

Guo, P. (2012). "Critical length of force chains and shear band thickness in dense granular materials." *Acta Geotech*., 7, 41–55.

Guo, P., and Stolle, D. (2005). "Lateral pipe-soil interaction in sand with reference to scale effect." *J. of Geotech. and Geoenv. Eng*., 131(3).

Hansen, J.B. and Christensen, N.H. (1961). "The ultimate resistance of rigid piles against transversal forces." *Geoteknisk Institut*, Copenhagen.

Hardin, B .O., and Black, W. L. (1966). “Sand stiffness under various triaxial stress.” *J. of the Soil Mech. and Found. Div.*, ASCE, 92(SM2), 27−42.

Houlsby, G.T. (1991). “How the dilatancy of soils affects their behaviour.” *Proc., 10th European Conf. on Soil Mech. and Found. Eng.*, Florence, 4, 1189–1202.

Hoshiya, M. and Mandal, J. N. (1984). “Some studies of anchor plates in sand.” *Soils Found.*, 24(1), 9–16.

Hsu, T. (1993). "Rate effect on lateral soil restraint of pipelines." *Soils and Found.*, 33(4), 159–169.

Janbu, N. (1963). “Soil compressibility as determined by oedometer and triaxial tests.” *Proc., Euro. Conf. on Soil Mech. and Found. Eng.*, Wiesbaden, Germany, (1), 19−25.

Jefferies, M., and Been, K. (2006). *Soil liquefaction: a critical state approach*. 2nd edition, Taylor & Francis, New York.

Jung, J.K., O’Rourke, T.D., and Olson, N.A. (2013). “Lateral soil-pipe interaction in dry and partially saturated sand.” *J. of Geotech. and Geoenv. Eng.*, 139(12), 2028–2036.

Kumar, J., and Sahoo, J. P. (2012). “An upper bound solution for pullout capacity of vertical anchors in sand using finite elements and limit analysis.” *Int. J. Geomech.*, 12(3), 333–337.

Loukidis, D. and Salgado, R. (2008). “Analysis of the shaft resistance of non-displacement piles in sand.” *Géotechnique*, 58(4), 283–296.

Loukidis, D. and Salgado, R. (2011). “Effect of relative density and stress level on the bearing capacity of footings on sand.” *Géotechnique*, 61(2), 107–19.

Merifield, R. S. and Sloan, S. W. (2006). “The ultimate pullout capacity of anchors in frictional soils.” *Can. Geotech. J.*, 43(8), 852–868.

Monroy, M., Wijewickreme, D., Nyman, D.J. and Honegger, D.G. (2015). "Soil restraint on steel buried pipelines under reverse fault displacement." *Proc., 6th Intl. Conf. on Earthquake Geotech. Eng.*, Christchurch, New Zealand.

Moore, I.D. and Rowe, R.K. (1990). "Scaling rule for localized plasticity in strain-softening continua." *Proc., 1st Int. Conf. on Comp. Aided Assess. Loca. Damage*, Portsmouth, 2, 99–112.

Murray, E.J., and Geddes, J.D. (1989). "Resistance of passive inclined anchors in cohesionless medium." *Géotechnique*, 39(3), 417–431.

Neely, W. J., Stewart, J. G., and Graham, J. (1973). "Failure loads of vertical anchor plates in sand." *J. Soil Mech. Found. Div.*, 99(9), 669–685.

Ng, P.C.F (1994). "Behaviour of buried pipelines subjected to external loading." PhD thesis, University of Sheffield, UK.

O'Rourke, M.J., and Liu, X. (2012). "Seismic design of buried and offshore pipelines." *MCEER Monograph*, MCEER-12-MN04.

O'Rourke, T. D., et al. (2008). "Geotechnics of pipeline system response to earthquakes." *Proc., 4th Decennial Geotech. Earthquake Eng. and Soil Dyn. Conf. (GEESD IV)*, ASCE, Sacramento, Calif.

Ovesen, N.K. and Stromann, H. (1972). "Design methods for vertical anchor slabs in sand." *Proc., Specialty Conf. on Perfor. of Earth and Earth-Supported Struc.*, ASCE, 2(1), 1481–1500.

Palmer, A.C., White, D.J., Baumgard, A.J., Bolton, M.D., Barefoot, A.J., Finch, M., Powell, T., Faranski, A.S., and Baldry, J.A.S. (2003). "Uplift resistance of buried submarine pipelines: comparison between centrifuge modelling and full-scale tests." *Géotechnique*, 53(10), 877–883.

Paulin, M.J., Phillips, R., Clark, J.I., Trigg, A. and Konuk, I. (1998). "Full-scale investigation into pipeline/soil interaction." *Proc., Intl. Pipe. Conf. (IPC)*, 779–787.

Pietruszczak, St. and Mróz, Z. (1981). "Finite element analysis of deformation of strain-softening materials." *Int. J. for Num. Methods in Eng*., 17, 327–334.

Pipeline Research Council International (PRCI). (2004). "Guidelines for the Seismic Design and Assessment of Natural Gas and Liquid Hydrocarbon Pipelines, Pipeline Design, Construction and Operations." Edited by Honegger, D. G., and Nyman D. J., October 2004.

Pradhan, T.B.S., Tatsuoka, F., and Horii, N. (1988). "Strength and deformation characteristics of sand in torsional simple shear." *Soils and Found*., 28(3), 131−148.

Robert, D. J., and Thusyanthan, N. I. (2014). "Numerical and experimental study of uplift mobilization of buried pipelines in sands." *J. Pipe. Sys. Eng. and Prac*., 6(1).

Rowe, R.K. and Davis, E.H. (1982). "Behaviour of anchor plates in sand." *Géotechnique*, 32(1), 25–41.

Roy, K., Hawlader, B.C., Kenny, S. and Moore, I. (2017). "Upward Pipe–Soil interaction for shallowly buried pipelines in dense sand." [Under review].

Roy, K., Hawlader, B.C., Kenny, S. and Moore, I. (2016). "Finite element modeling of lateral pipeline−soil interactions in dense sand." *Can. Geotech. J*., 53(3), 490–504.

Sakai, T., and Tanaka, T. (2007). "Experimental and numerical study of uplift behavior of shallow circular anchor in two-layered sand." *J. Geotech. Geoenviron. Eng*., 133(4), 469–477.

Sakai, T., Erizal, and Tanaka, T. (1998). "Particle size effect of anchor problem with granular materials." *Proc., 4th Euro. Conf. on Num. Methods in Geotech. Eng*., Udine, 181–200.

Sutherland, H.B. (1988). "Uplift resistance of soils." *Géotechnique*, 38(4), 493–516.

Tagaya, K., Tanaka, A., and Aboshi, H. (1983). "Application of finite element method to pullout resistance of buried anchor." *Soils and Foundations,* 23(3), 91–104.

Tatsuoka, F., Okahara, M., Tanaka, T., Tani, K., Morimoto, T., and Siddiquee, M. S. A. (1991). "Progressive failure and particle size effect in bearing capacity of a footing on sand*." Geotech. Spec. Publ*., 27(2), 788–802.

Tejchman, J. and Górski, J. (2008). "Size effects in problems of footings on sand within micro-polar hypoplasticity." *Archives of Hydro-Eng. and Environ. Mech*., 55(3–3), 95–124.

Tejchman, J. and Herle, I. (1999). "A "class A" prediction of the bearing capacity of plane strain footings on granular material." *Soils and Found*., 39(5), 47–60.

Trautmann, C. (1983). "Behavior of pipe in dry sand under lateral and uplift loading." PhD thesis, Cornell University, Ithaca, NY.

Trautmann, C.H. and O'Rourke, T.D. (1983). "Load-Displacement Characteristics of a Buried Pipe Affected by Permanent Earthquake Ground Movements." *Earthquake Behavior and Safety of Oil and Gas Storage Facilities, Buried Pipe. and Equip.*, PVP-77, ASME, New York, June.

Uesugi, M., Kishida, H., and Tsubakihara, Y. (1988). "Behavior of sand particles in sand-steel friction." *Soils Found*., 28(1), 107–118.

White, D. J., Take, W. A., and Bolton, M. D. (2003). "Soil deformation measurement using particle image velocimetry (PIV) and photogrammetry." *Géotechnique*, 53(7), 619–631.

White, D.J., Cheuk, C.Y, and Bolton, M.D. (2008). "The Uplift resistance of pipes and plate anchors buried in sand." *Géotechnique*, 58(10), 771–779.

Yimsiri, S., Soga, K., Yoshizaki, K., Dasari, G., and O'Rourke, T. (2004). "Lateral and upward soil–pipeline interactions in sand for deep embedment conditions." *J. of Geotech. and Geoenv. Eng*., 130(8), 830−842.

Yoshimine, M. (2005). “Archives–soil mechanics laboratory.” Tokyo Metropolitan University, <http://geot.civil.ues.tmu.ac.jp/archives/> (April 4, 2015).

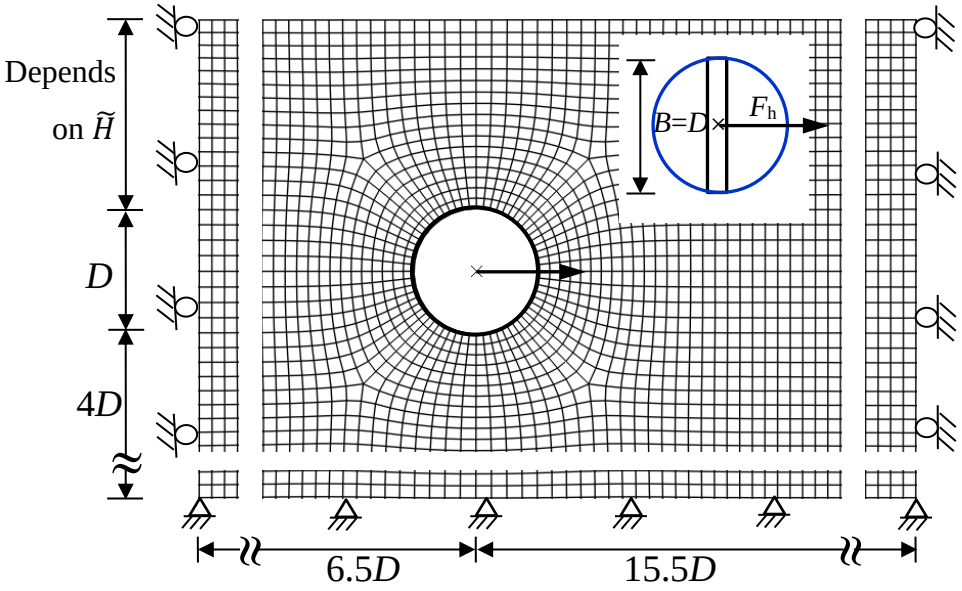

Figure 6.1: Typical finite element mesh for D=500 mm

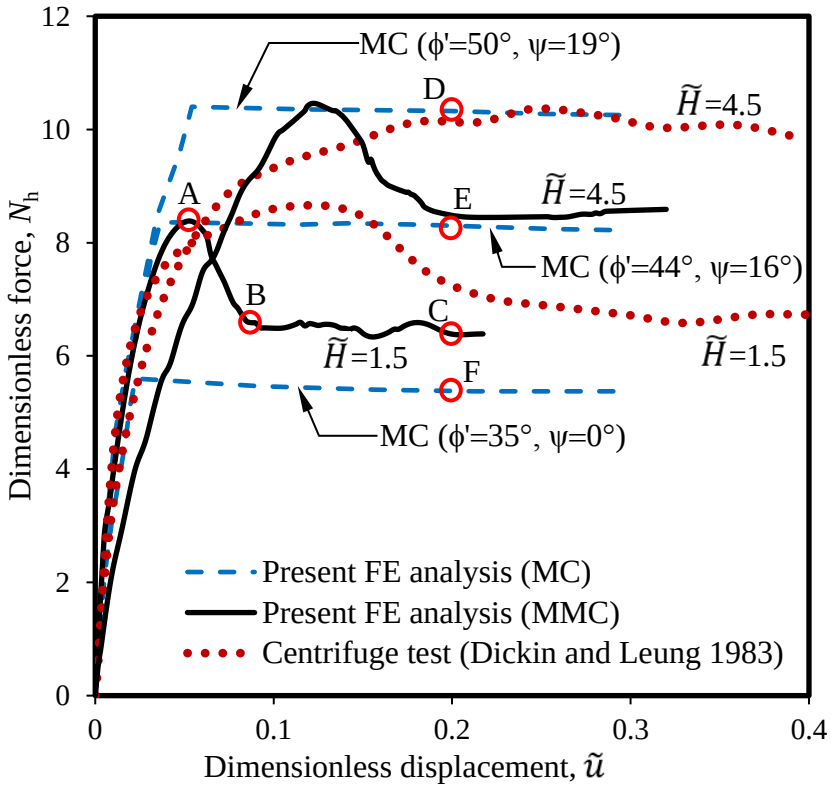

Figure 6.2: Comparison of present FE analyses with physical model test results (a) anchor

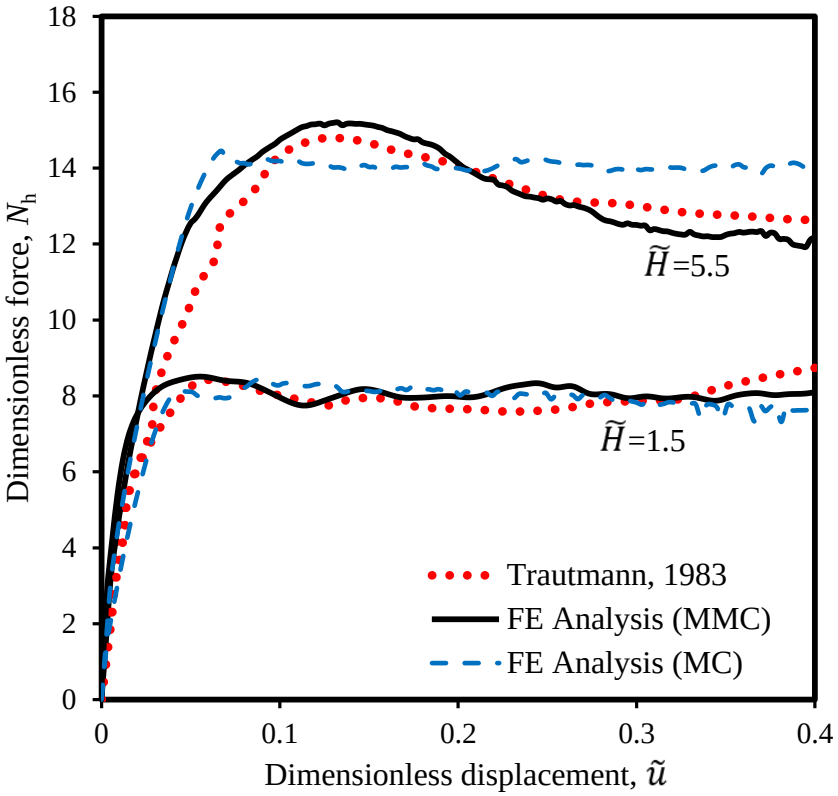

Figure 6.2: Comparison of present FE analyses with physical model test results (b) pipe (after Roy et al. 2016)

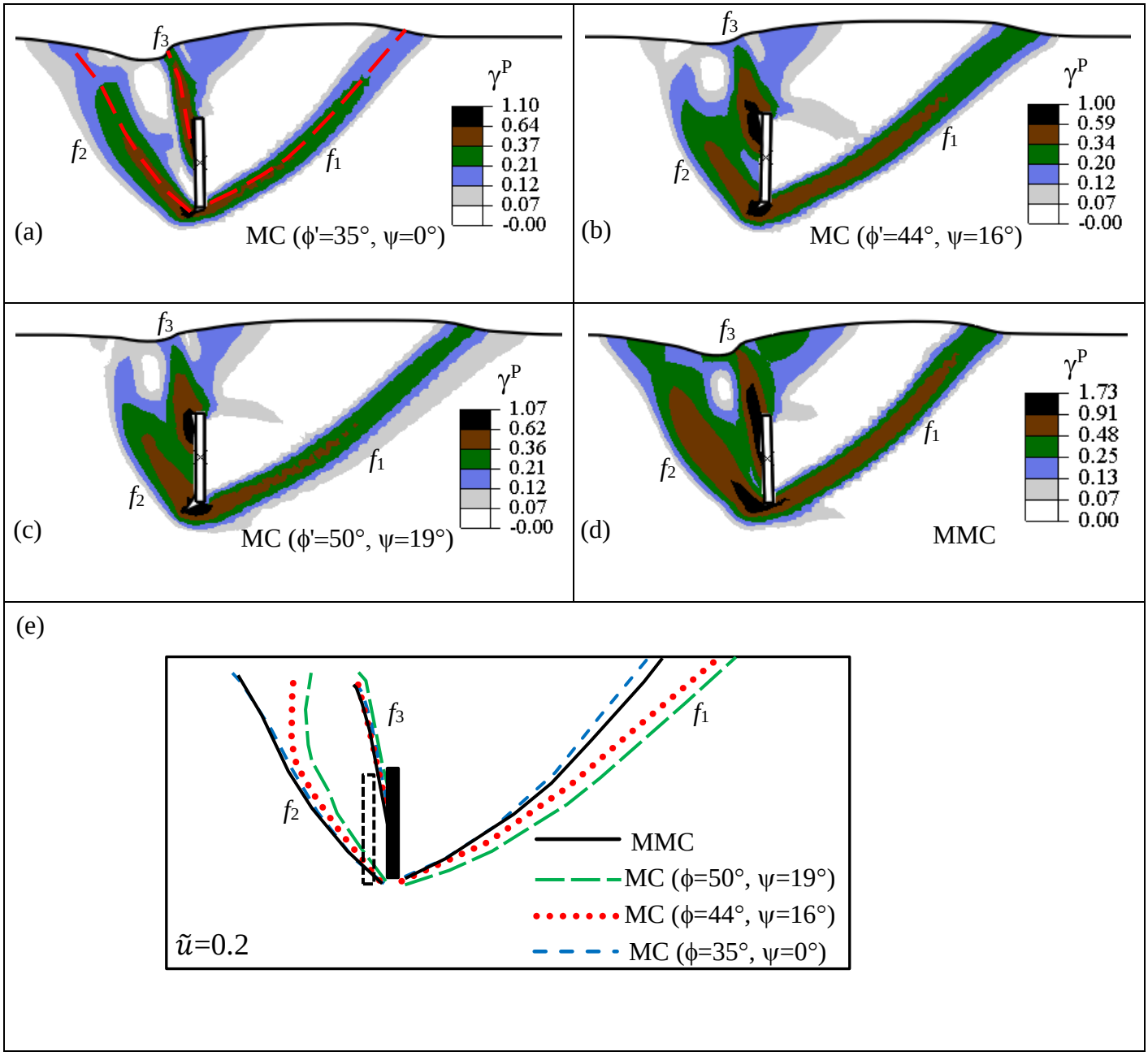

Figure 6.3: Shear band formation for 1000-mm high strip anchor with MC and MMC models

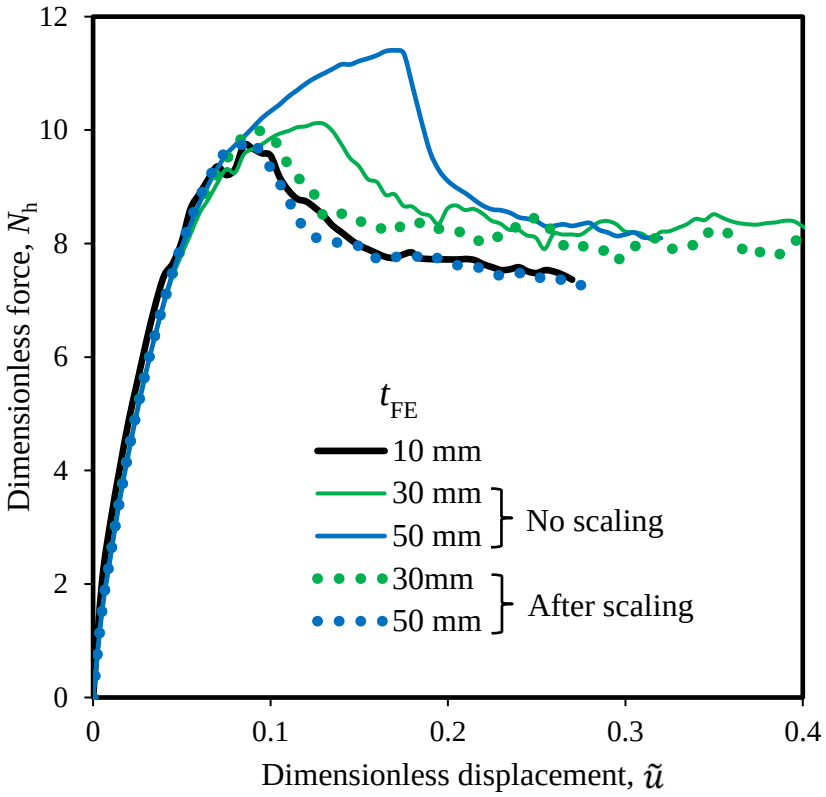

Figure 6.4: Mesh sensitivity analysis for 500-mm diameter pipe with MMC model

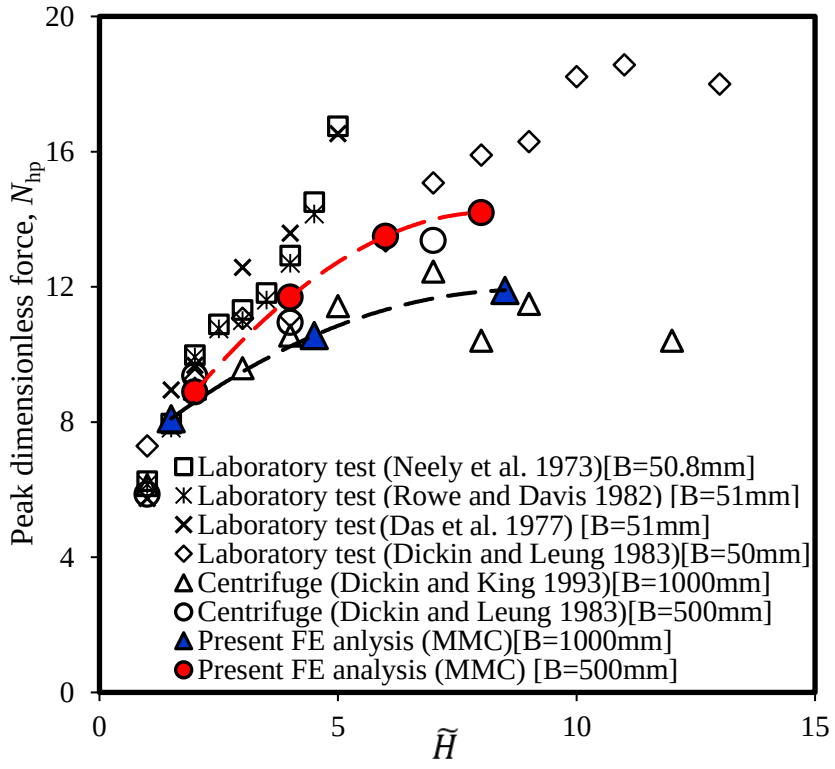

Figure 6.5: Peak lateral resistance of anchors with burial depth

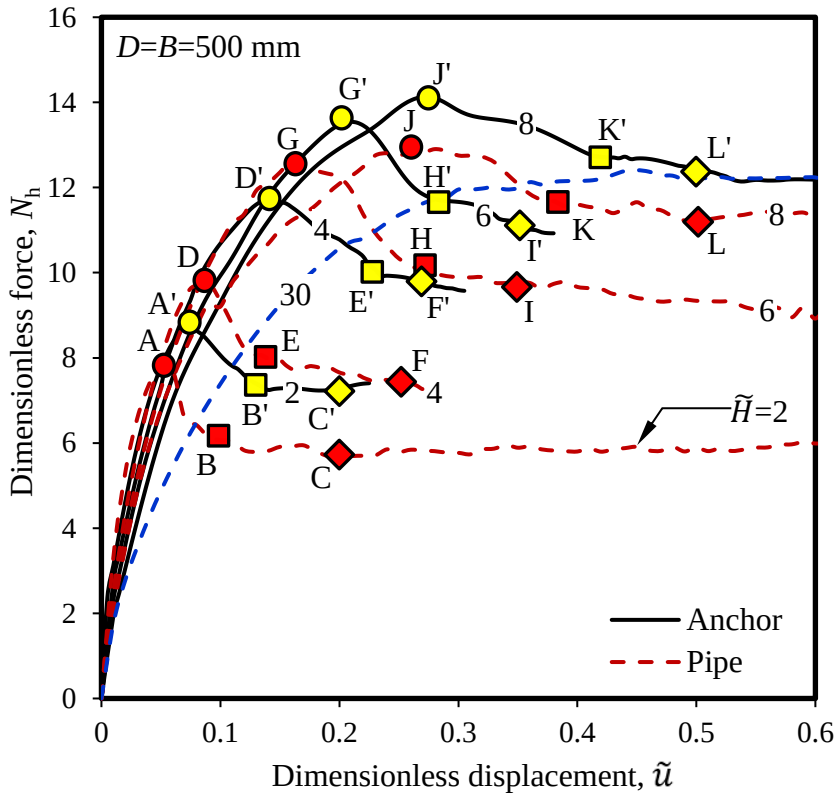

Figure 6.6: Comparison of N_h–$\tilde{u}$ curves for pipes and strip anchors (B=D=500 mm)

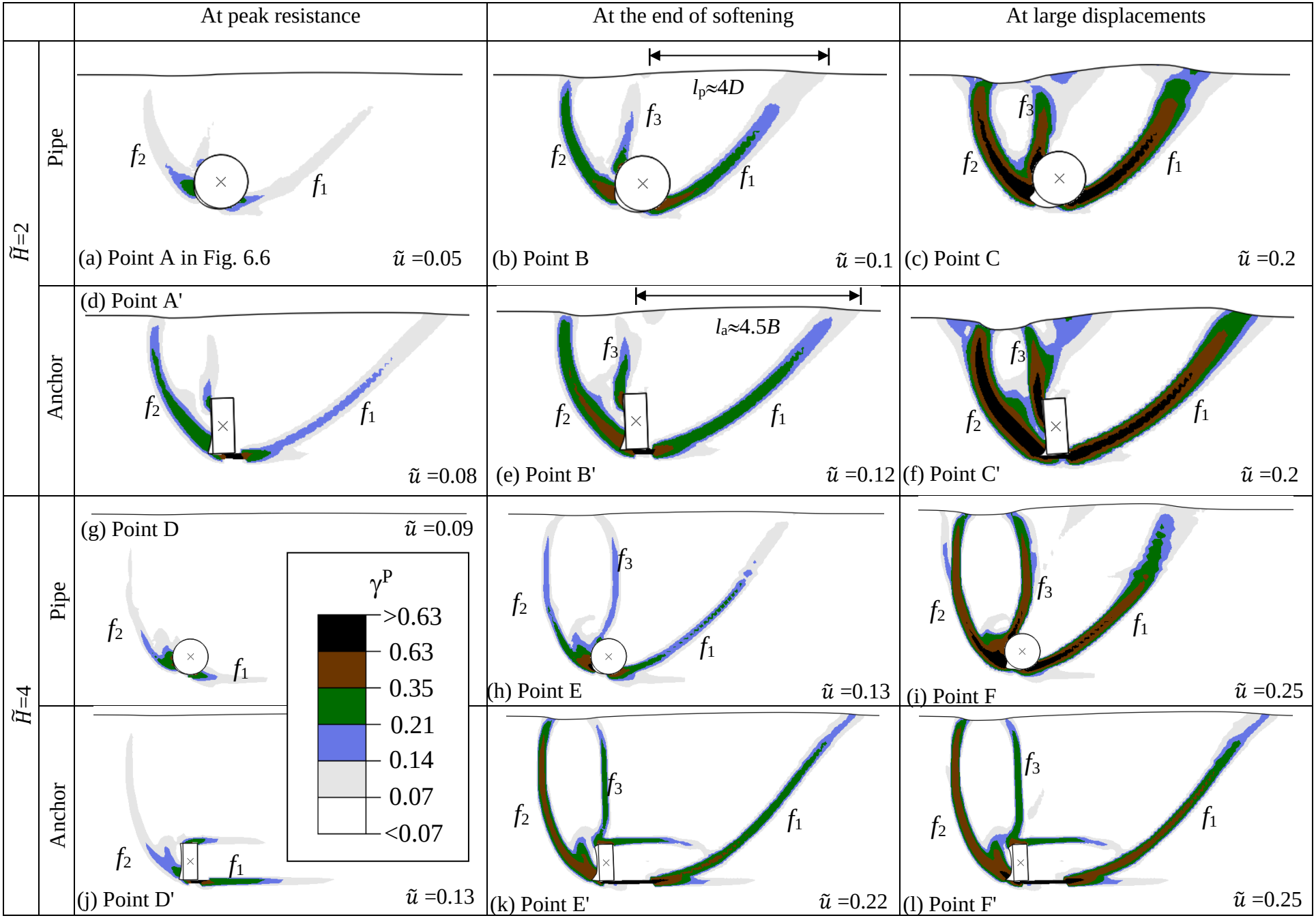
At peak resistance
At the end of softening
At large displacements
$\tilde{H}$=2
Pipe
Anchor
$\tilde{H}$=4
l_p≈4D
l_a≈4.5B
f_1
f_2
f_3
(a) Point A in Fig. 6.6 $\tilde{u}$ =0.05
(b) Point B $\tilde{u}$ =0.1
(c) Point C $\tilde{u}$ =0.2
(d) Point A' $\tilde{u}$ =0.08
(e) Point B' $\tilde{u}$ =0.12
(f) Point C' $\tilde{u}$ =0.2
(g) Point D $\tilde{u}$ =0.09
(h) Point E $\tilde{u}$ =0.13
(i) Point F $\tilde{u}$ =0.25
(j) Point D' $\tilde{u}$ =0.13
(k) Point E' $\tilde{u}$ =0.22
(l) Point F' $\tilde{u}$ =0.25
γ^P
>0.63
0.63
0.35
0.21
0.14
0.07
<0.07

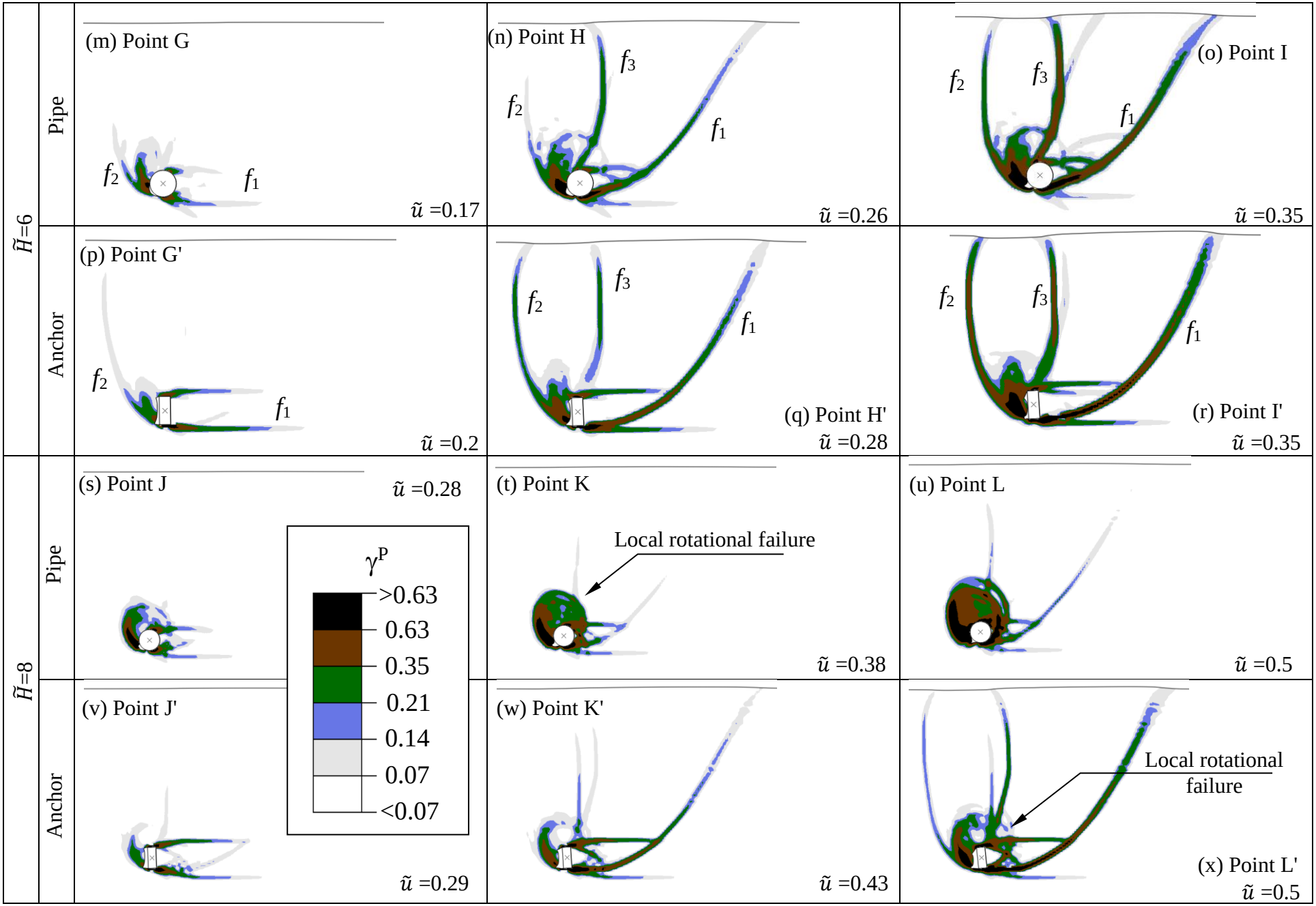

Figure 6.7: Failure mechanism for 500-mm diameter pipe and 500-mm high anchor

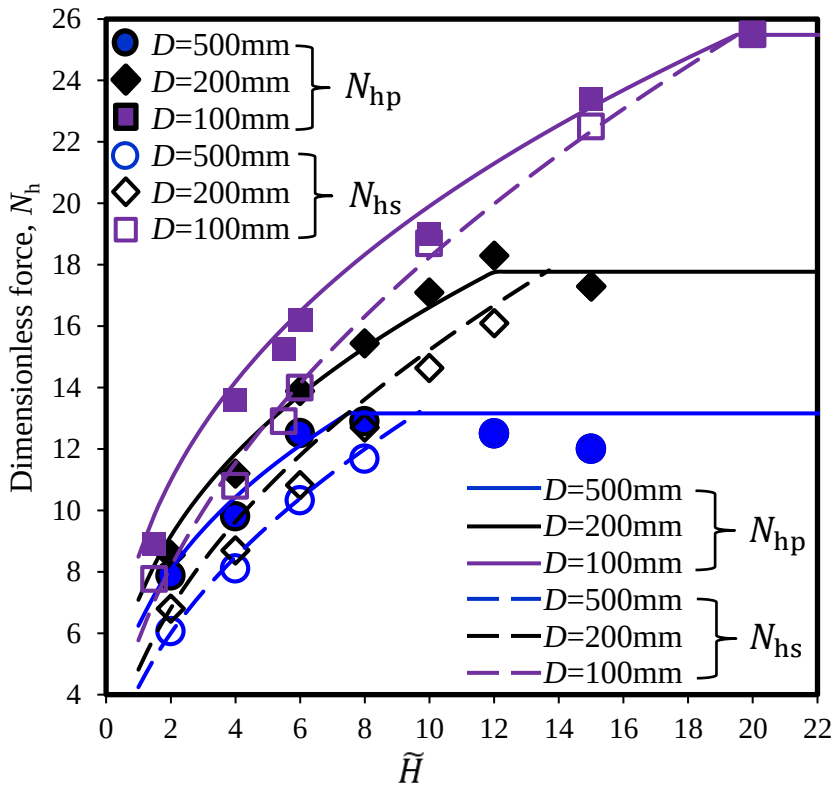

Figure 6.8: Comparison of simplified equations and finite element results (a) for pipe

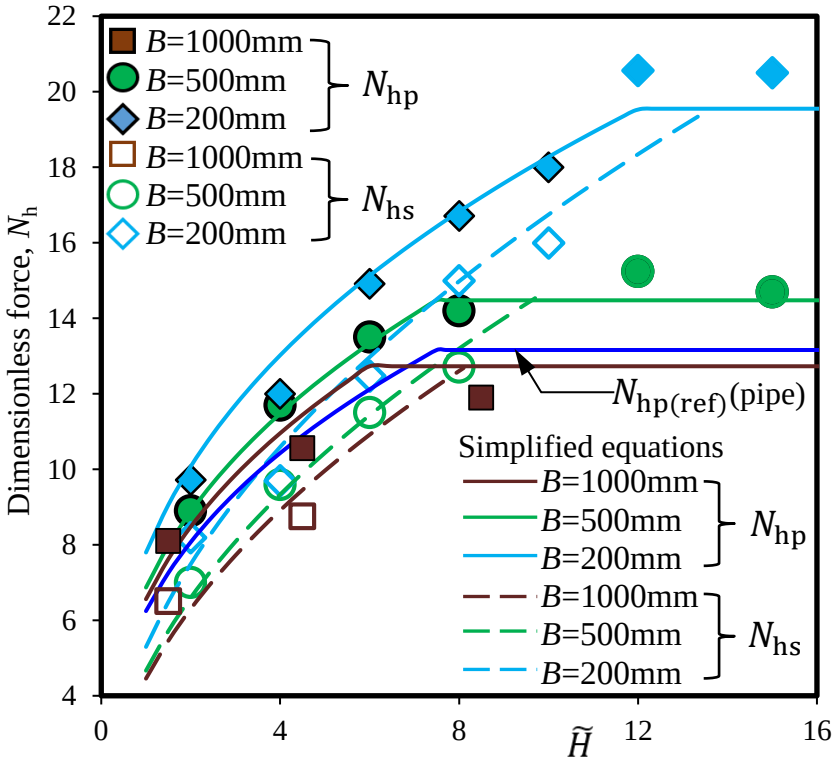

Figure 6.8: Comparison of simplified equations and finite element results (b) for anchor

Table 6.1: Equations for Modified Mohr–Coulomb Model (MMC) (summarized from Roy et al. 2016)

Description	Eq. #	Constitutive Equation	Soil Parameters
Relative density index	(6.1)	$I_R = I_D(Q - \ln p') - R$	$I_D = D_r(\%)/100$, Q=10, R=1
Peak friction angle	(6.2)	$\phi'_p - \phi'_c = A_\psi I_R$	ϕ'_c, A_ψ
Peak dilation angle	(6.3)	$\psi_p = \frac{\phi'_p - \phi'_c}{k_\psi}$	k_ψ
Strain softening parameter	(6.4)	$\gamma_c^p = C_1 - C_2 I_D$	C_1, C_2
Plastic shear strain at ϕ'_p	(6.5)	$\gamma_p^p = \gamma_c^p \left(\frac{p'}{p'_a}\right)^m$	p'_a, m
Mobilized friction angle at Zone–II	(6.6)	$\phi' = \phi'_{in} + \sin^{-1}\left[\left(\frac{2\sqrt{\gamma^p \gamma_p^p}}{\gamma^p + \gamma_p^p}\right)\sin(\phi'_p - \phi'_{in})\right]$	
Mobilized dilation Angle at Zone–II	(6.7)	$\psi = \sin^{-1}\left[\left(\frac{2\sqrt{\gamma^p \gamma_p^p}}{\gamma^p + \gamma_p^p}\right)\sin(\psi_p)\right]$	
Mobilized friction angle at Zone–III	(6.8)	$\phi' = \phi'_c + (\phi'_p - \phi'_c)\ \exp\left[-\left(\frac{\gamma^p - \gamma_p^p}{\gamma_c^p}\right)^2\right]$	
Mobilized dilation angle at Zone–III	(6.9)	$\psi = \psi_p \exp\left[-\left(\frac{\gamma^p - \gamma_p^p}{\gamma_c^p}\right)^2\right]$	
Young's modulus	(6.10)	$E = K p'_a \left(\frac{p'}{p'_a}\right)^n$	K, n

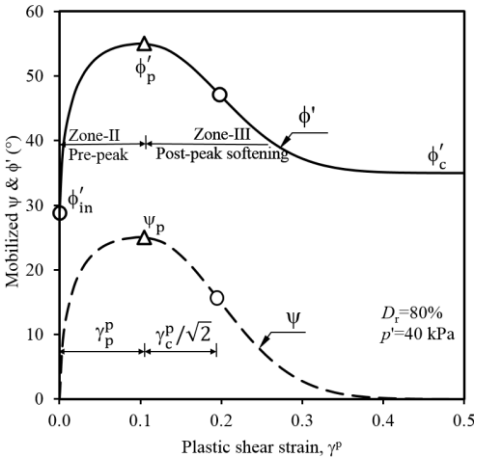

ϕ'_{in}=Initial friction angle, γ^p=Accumulated engineering plastic shear strain

Table 6.2: Geometry and soil parameters used in the FE analyses

Parameter	Model test (Parametric Study)
External diameter of pipe, D (mm)	100 (200, 500)
Height of the strip anchor, B (mm)	1000 (200, 500)
Thickness of the strip anchor, t (mm)	200 (100)
K	150
n	0.5
p_a (kN/m^2)	100
ν_{soil}	0.2
A_ψ	5
k_ψ	0.8
ϕ'_{in}	29°
C_1	0.22
C_2	0.11
m	0.25
Critical state friction angle, ϕ'_c	35°
Relative density, D_r (%)	80
Unit weight, γ (kN/m^3)	16, 17.7
Interface friction coefficient, μ	0.32
Embedment ratio, $\widetilde{H}$	1.5, 4.5, 5.5 (2, 4, 6, 8, 10, 12, 15)

Note: Numbers in parenthesis in right column show the values used in the parametric study

CHAPTER 7

Conclusions and Recommendations for Future Research

7.1 Conclusions

The performance of buried pipelines under lateral or upward loading is an important engineering consideration for the safe and economical design of pipelines for oil and gas transportation. The complex nature of pipe–soil interaction is governed by the nonlinear behaviour of soil around the pipeline, which is a function of a wide range of variables, such as soil density, mean stress and failure mechanisms, including the accumulation of plastic shear strain in the form of shear bands, during loading. Based on finite element (FE) analysis using Abaqus/Explicit FE software, the lateral and upward pipe–soil interactions are studied in this thesis.

Recognizing the limitations of the built-in Mohr-Coulomb model for sand, which is typically used in FE modeling of pipe–soil interaction, a robust yet simple modified Mohr-Coulomb (MMC) model is proposed, that considers the variation of angles of internal friction and dilation with plastic shear strain, loading condition, density and confining pressure, as observed in laboratory tests on dense sand. The MMC model is implemented in Abaqus/Explicit using a user-defined subroutine.

In the development of design guidelines for pipelines, theoretical and experimental studies on anchor behaviour are also used, assuming that a geometrically similar pipe and anchor behave in a similar fashion. The similarities and differences between the responses of these two types of structures are also examined in the present study to explore the use of the theories and model test results on anchors for the evaluation of pipeline behaviour.

The following general conclusions are drawn through the course of this thesis. The problem specific conclusions are presented at the end of each chapter (Chapters 3–6) and in the appendices (Appendices A–F).

The modelling of buried pipelines subjected to lateral movement is presented in Chapter 3. The details of the MMC model, including its calibration against laboratory test data, is also presented in this chapter. The inclusion of pre-peak hardening and post-peak softening behaviour of dense sand in the MMC model can capture the initiation and propagation of shear bands and thereby soil failure mechanisms. The force–displacement curves obtained from FE analysis using the MMC model are consistent with physical test results (Fig. 3.8). The peak lateral resistance can be calculated using the built-in MC model; however, constant values of representative friction and dilation angles (ϕ' and ψ) are required. On the other hand, pressure and plastic shear strain dependent friction and dilation angles in the MMC model give better simulation of lateral resistance for a wide range of pipe displacements, including peak and residual lateral resistances.

A large number of physical model tests on dense sand, as compiled in Tables 2.1 and 2.5 and discussed in Chapter 6, show size effects (also called “scale effects” by some researchers), which can be described as: for a given condition, the larger the pipe diameter, the smaller the normalized lateral resistance. The size effects have also been reported in previous studies (e.g. Guo and Stolle 2005). The size effects can cause considerable confusion in the interpretation of physical test results. The size effects resulting from two potential sources can be reduced using the present MMC model, compared to the MC model. Firstly, the size effect due to stress dependency is reduced because, in the MMC model, the values of mobilized ϕ' and ψ decrease with mean effective stress. For a given embedment ratio, a larger diameter pipe is placed at a larger burial depth; therefore, the higher mean effective stress in the soil elements around the pipe gives lower

ϕ' and ψ, and thereby, lower lateral resistance. Secondly, the size effects due to progressive formation of the failure plane can also be reduced using the MMC model. For a larger diameter pipe, a complete failure plane does not form when the peak resistance is mobilized. Moreover, in some segments of the failure planes, the accumulated plastic shear strain is higher or lower than the strain required to mobilize ϕ'_p and ψ_p. This implies that when progressive failure is simulated, the average ϕ' and ψ along the entire failure plane is less than ϕ'_p and ψ_p, respectively. Therefore, the MMC model gives a lower soil resistance than the MC model using constant values of ϕ'_p and ψ_p. The size effects due to these two factors cannot be explained with constant ϕ' and ψ, as typically used in numerical analyses with the MC model. Moreover, the size effects have not been explicitly considered in the design guidelines (ALA 2005; DNV 2007).

Chapter 4 presents FE modeling of the uplift behaviour of buried pipelines in dense sand for shallow burial conditions. Physical model tests show that the uplift resistance does not remain constant but decreases with upward displacement after the peak. Even the peak uplift resistance (N_{vp}) is overestimated by the upper bound solution because the assumption of $\psi=\phi'$ results in overestimation of the dilation angle and thereby the size of the lifted soil block. The proposed MMC model can overcome these limitations. When the peak resistance mobilizes, the vertical inclination of the slip planes (θ) is approximately equal to the peak dilation angle (ψ_p), which is less than ϕ'. Moreover, θ decreases with upward displacement due to a decrease in the dilation angle. One of the key contributions of the present study is that the FE analysis with the MMC model can capture the post-peak reduction of uplift resistance due to the following three key factors: (i) decrease in shear resistance along the failure plane due to reduction of ϕ' with accumulated plastic shear strain (ii) decrease in size of the failure wedge due to decrease in ψ and

(iii) reduction of cover depth. The first two factors result in rapid reduction of uplift resistance immediately after the peak, as observed in model tests. The last factor is responsible for gradual reduction of uplift resistance during large displacements. The effects of the first two factors on uplift resistance cannot be simulated using the MC model, where constant ϕ' and ψ are used. Also, based on a comprehensive parametric study, a set of simplified equations is proposed to obtain uplift force–displacement curves for practical applications, which provides the uplift resistance not only at the peak but also at large displacements.

Progressive formation of shear bands and the mobilized values of friction and dilation angles along the shear band significantly influence the shape of the force–displacement curve. The progressive formation of shear bands for upward pipe–soil interaction is examined in Chapter 5 to investigate soil failure mechanisms for a wide range of burial depths and pipe diameters. For shallow buried pipelines, in addition to the inclined shear bands that develop at an angle equal to ψ_p during mobilization of the peak resistance, new shear bands form during large displacements having vertical inclinations of less than ψ_p. However, for deeper pipelines, in addition to the inclined slip planes, a number of logarithmic spiral type shear bands form above the pipe during large upward displacements. It is shown that the peak uplift resistance for intermediate embedment ratios might be underestimated or overestimated by the available simplified methods such as the vertical slip surface model or inclined slip surface model based on upper bound solution ($\theta=\phi'_p$) or the limit equilibrium method based on $\theta=\psi_p$. Progressive formation of shear bands plays a major role on mobilized uplift resistance. Based on a comprehensive parametric study over a wide range of pipe diameters and burial depths, a simplified method is proposed to calculate the peak and also the post-peak uplift resistances, using an equivalent angle of internal friction.

Assuming that buried pipes and vertical strip anchors essentially behave in a similar fashion, studies on anchors have also been utilized in the past to develop the force–displacement relationships for buried pipelines. Chapter 6 investigates the similarities and differences between the response of buried pipes and anchors subjected to lateral loading. The present numerical study shows that an anchor offers ~10% higher resistance than that of a similar-sized pipe. For both pipe and anchor, the normalized peak resistance increases with burial depth and becomes almost constant at large burial depths. The difference between the peak and residual resistances for similar-sized pipes and anchors is significant at small to moderate embedment ratios (Fig. 6.8). The transition from shallow to deep failure mechanisms occurs at a lower burial depth for pipes than anchors. Similar to buried pipes, as discussed in previous sections, anchors show size effects—the normalized peak and residual lateral resistances are higher for a smaller height of anchor. The transition from shallow to deep failure mechanisms occurs at a lower embedment ratio for a larger diameter pipe than a smaller diameter pipe (Fig. 6.8(a)). Again, a set of simplified equations is proposed in Chapter 6 for estimation of the peak and residual lateral resistances for a practical range of pipe diameters and burial depths. The critical embedment ratio after which the lateral resistance does not increase with the embedment ratio is also identified.

An important implication of the proposed MMC model for pipe–soil interaction analysis is that the peak lateral or uplift resistance cannot be calculated simply using the peak friction angle (ϕ'_p) and peak dilation angle (ψ_p). For example, as shown in Fig. 4.3, the use of constant ϕ'_p and ψ_p in the MC model calculates ~16% higher peak uplift resistance (N_{vp}) than the calculated N_{vp} with mobilized ϕ' and ψ in the MMC model and N_{vp} obtained from physical model tests. On the other hand, ALA (2005) recommended simplified equations for estimation of the peak lateral and uplift resistances for a range of representative ϕ' between 0 and 45°. In other words, for estimation of

the peak resistance using the design guidelines or the MC model in FE analysis, a representative value of ϕ' ($< \phi'_p$) is required, which adds some additional uncertainties. However, if the MMC model is used, the mobilization of ϕ' and ψ can be defined using ϕ'_p and ϕ'_c obtained from laboratory test results, as shown in Table 4.1.

Another practical implication of the present numerical study with the MMC model is that the parametric study can complement existing experimental data, as it covers a wide range of pipeline diameters and anchor heights. Reduced-scale physical experiments at 1g using smaller diameter pipes than typically used in the field (to be cost-effective) might have significant size effects due to low effective stresses in the soil elements around the pipeline. Expected stresses in the soil elements can be maintained in centrifuge modelling by increasing gravitational acceleration; however, this significantly over-predicts the displacement required to mobilize the soil resistance (Dickin and Leung 1983; Palmer et al. 2003), which implies that the strain localization in the shear bands in dense sand is not properly modelled in centrifuge tests. In the present study, the numerical modeling is first validated against full-scale tests and then parametric studies are performed for a wide range of pipe diameters and burial depths, including the cases of large diameter pipes and large embedment ratios, which represent the conditions of very costly full-scale tests.

In terms of practical applications of the present study, the proposed simple and easy-to-use expressions can be used for estimation of lateral and uplift resistances at the peak and residual conditions. In addition, the proposed equations for backbone curve can be used to estimate the uplift resistances during large upward displacements of the pipe. As shown in the present study, not only the equivalent friction angle, as commonly used in design guidelines, but also its variation with plastic shear strain and mean effective stress and the mobilization of the dilation angle play a significant role in lateral and uplift resistances. The peak lateral resistance can be used in a bilinear

force–displacement relation for horizontal springs for a conservative structural design, when the spring is used to define the force on the pipeline. The uplift resistance is a key design parameter for upheaval buckling of buried pipelines. The use of the peak uplift resistance, without post-peak degradation, to define the force–displacement behaviour of the vertical soil spring might give a non-conservative structural design. Modelling the buckling behaviour due to temperature increase, as occurs in hot oil pipelines during operation, the author and his co-workers showed that, when the post-peak degradation of uplift resistance is considered, the critical buckling temperature decreases considerably in some cases (for details, please see Arman et al. 2017). The DNV (2007) design guidelines considered the post-peak reduction of uplift resistance. The present study suggests simplified methods for estimation of the peak and residual resistances.

7.2 Recommendations for Future Research

The following are some areas which could be studied further.

(i) The present study considers dense sand only; however, the modelling technique developed in the present study is also applicable to pipes buried in medium dense or loose sand, provided that the appropriate stress–strain behaviour of loose or medium dense sand is incorporated. In those cases, shearing might cause volumetric contraction ($\psi<0$), which need to be considered in the modification of the Mohr–Coulomb model.

(ii) The present study focuses on numerical simulation of pure lateral and upward pipe–soil interactions. However, combined effects (e.g. lateral–vertical loading) could be studied using a similar modelling technique and the proposed MMC model.

(iii) As pipe–soil interaction is a three-dimensional problem, combined modelling of structural and geotechnical responses could be conducted using a full three-dimensional model.

However, the three-dimensional continuum FE modeling of a long pipe may not be practical because of the significant increase in computational cost.

(iv) A very limited number of physical model tests for large diameter pipes with large embedment ratios is available in the literature. Additional tests for these conditions could be very useful for further validation of the present numerical simulations and simplified approaches. However, large-scale experiments are generally expensive.

(v) The soil elements around shallow buried pipelines have low effective stresses, especially during uplift. Laboratory test apparatus, with a high level of accuracy to measure stresses and deformations at low effective stress levels, might provide improved stress–strain behaviour of soil.

(vi) The simulations are performed only for plane strain condition. If the pipe displaces in a different direction, such as oblique loading, an appropriate failure surface on the deviatoric plane needs to be considered.

(vii) Some of the soil parameters of the modified Mohr–Coulomb model are obtained from the calibration of the model against triaxial compression test results. However, the displacement of a pipe or anchor might cause stresses in soil elements different from triaxial condition. Further studies, including laboratory tests under various loading condition, are required for a better estimation of these soil parameters.

REFERENCES

ALA (2005). “Guidelines for the design of buried steel pipe.” American Lifelines Alliance, <https://www.americanlifelinesalliance.com/pdf/Update061305.pdf > (Mar. 13, 2017).

Akinmusuru, J. O. (1978). “Horizontally loaded vertical anchor plates in sand.” *J. Geotech. Eng. Div*., 104(2), 283–286.

Almahakeri, M., Fam, A., and Moore, I.D. (2012). “The flexural behaviour of buried steel and composite pipes pulled relative to dense sand: experimental and numerical investigation.” *Proc., 9th Int. Conf. on Pipelines*, IPC2012, September 24−28, Calgary, Canada. IPC 2012-90158, 9.

Arman, R.A., Roy, K., Hawlader, B.C. and Dhar, A. (2017), “Finite element analysis of upheaval buckling of submarine pipelines with initial imperfection’, *Proc., 70th Can. Geotech. Eng. Conf.*, GeoOttawa 2017, Ottawa, Ontario, Canada, October 1–4.

ASCE (1984). “Guidelines for the seismic design of oil and gas pipeline systems.” American Society of Civil Engineers, Committee on gas and liquid fuel life lines, Technical Council on Life line Earthquake Engineering, ASCE, New York.

Atkinson, J. H. (2000). “Non-linear soil stiffness in routine design.” *Géotechnique*, 50(5), 487–508.

Audibert, J.M.E., and Nyman, K.J. (1975). "Coefficients of subgrade reaction for the design of buried piping", *Proc., ASCE Specialty Conf. on Struc. Design of Nuc. Plant Fac.*, December 8–December 10, 109−141.

Audibert, J.M.E., and Nyman, K.J. (1977). "Soil restraint against horizontal motion of pipes", *J. of the Geotech. Eng. Div. ASCE,* 103(NGT10), 1119−1142.

Badv, K. and Daryani, K. E. (2010). "An investigation into the upward and lateral soil-pipeline interaction in sand using finite difference method." *Ira. J. of Sci. and Tech.*, Transaction B: Engineering, 34(B4), 433–445.

Barefoot A. J. (1998). "Modelling the uplift resistance of buried pipes in a drum centrifuge." MPhil thesis, Cambridge University Engineering Department.

Barrette, P., Denise, S., and Hossein, B. (2015). "Protecting offshore pipelines against drifting ice: a discussion on standards and guidelines." *Proc., 34th Int. Conf. on Ocean, Off. and Arc. Eng.* (OMAE 2015), St. John's, Canada.

Been, K., Sancio, R.B., Ahrabian, A., van Kesteren, W., Croasdale, K., and Palmer, A.C. (2008). "Subscour displacement in clays from physical model tests." *Proc., 7th Int. Pipe. Conf.*, Calgary.

Bolton, M. D. (1986). "The strength and dilatancy of sands." *Géotechnique*, 36(1), 65−78.

Bhattacharya, P. and Kumar, J. (2013). "Seismic pullout capacity of vertical anchors in sand." *Geomech. Geoeng. Int. J.*, 8(3), 191–201.

Bransby, M. F., Newson, T. A., Brunning, P., and Davies, M. C. R. (2001). "Numerical and centrifuge modeling of the upheaval resistance of buried pipelines." *Proc., 20th Int. Conf. on Off. Mech. and Arc. Eng.*, Rio de Janeiro, Brazil.

Bransby, M.F., Newson, T. A. and Davies, M. C. R. (2002). "Physical modelling of the upheaval resistance of buried offshore pipelines." *Proc., Int. Conf. on Phy. Mod.. in Geotech.*, Kitakyushu, Japan.

Bransby, M. F., and Ireland, J. (2009). "Rate effects during pipeline upheaval buckling in sand." *Proc., ICE – Geotech. Eng.*, 162(5), 247–258.

Burnett, A. (2015). "Investigation of full scale horizontal pipe-soil interaction and large strain behaviour of sand." M.A.Sc. thesis, Queen's University, Canada.

Chakraborty, D., and Kumar, J. (2014). "Vertical uplift resistance of pipes buried in sand." *J. Pipe. Syst. Eng. Pract*., 10.1061/(ASCE)PS.1949 -1204.0000149, 04013009.

Cheong, T.P., Soga, K. and Robert, D.J. (2011). "3D FE analyses of buried pipeline with elbows subjected to lateral loading." *J. Geotech. & Geoenviron. Eng.*, 137(10), 939–948.

Cheuk, C. Y., White, D. J. and Bolton, M. D. (2005). "Deformation mechanisms during the uplift of buried pipelines in sand." *Proc., 16th Int. Conf. on Soil Mech. and Geo. Eng*., Osaka, 1685–1688.

Cheuk, C. Y., White, D. J., and Bolton, M. D. (2008). "Uplift mechanisms of pipes buried in sand." *J. Geotech. & Geoenv. Eng*., 134(2), 154–163.

Chin, E. L., Craig, W. H., and Cruickshank, M. (2006). "Uplift resistance of pipelines buried in cohesionless soil." *Proc., 6th Int. Conf. on Phy. Model. in Geotech.*, Ng, Zhang, and Wang, eds., Vol. 1, Taylor & Francis Group, London, 723–728.

Choobbasti A.J, Firouzian S, Vahdatirad M.J, Barari A. and Razaei D. (2009). "Modelling of the uplift response of buried pipelines." *Ejge*, 14, 1–15.

Chattopadhyay, B.C., and Pise, P.J. (1986). "Uplift capacity of pile in sand." *J. of Geotech. Eng.*, ASCE, 112(9), 888–904.

Choudhary, A.K. and Dash, S.K. (2017). "Load-carrying mechanism of vertical plate anchors in sand." *Int. J. Geomech*., 17(5).

Clukey, E.C., Haustermans, L. and Dyvik, R. (2005). "Model tests to simulate riser–soil interaction effects in touchdown point region." *Proc., Int. Sym. on Fron. in Off. Geotech.* (ISFOG 2005), Perth, Australia, 651–658.

Das, B. M., Seeley, G. R., and Das, S. C. (1977). "Ultimate resistance of deep vertical anchor in sand." *Soils Found.*, 17(2), 52–56.

Dassault Systèmes. (2010). ABAQUS [computer prog.]. Dassault Systèmes, Inc., Providence, R.I.

Daiyan, N., Kenny, S., Phillips, R., and Popescu, R. (2011). "Investigating pipeline–soil interaction under axial–lateral relative movements in sand." *Can. Geotech. J.*, 48(11), 1683−1695.

Dickin, E.A. (1988). "Stress-displacement of buried plates and pipes." *Proc., Int. Conf. on Geotech. Cent. Mod.*, Centrifuge 88, Paris, France.

Dickin, E.A. (1994). "Uplift resistance of buried pipelines in sand." *Soils and Found.*, 34(2), 41−48.

Dickin, E. A., and Leung, C. F. (1983). "Centrifuge model tests on vertical anchor plates." *J. Geotech. Eng.*, 12(1503), 1503–1525.

Dickin, E. A., and Leung, C. F. (1985). "Evaluation of design methods for vertical anchor plates." *J. Geotech. Eng.*, 4(500), 500–520.

Dickin, E.A. and King, G.J.W. (1993). "Finite element modelling of vertical anchor walls in sand." *Develop. in Civil & Cons. Eng. Comp.*, Civil-Comp Press, Edinburgh, UK.

di Prisco, C. and Galli, A. (2006). "Soil-pipe interaction under monotonic and cyclic loads: experimental and numerical modelling", *Proc., 1st Euro Med. Sym. in Adv. on Geomat. and Struc.* (AGS '06), 755–760.

DNV (2007). "Global buckling of submarine pipelines—Structural design due to high temperature/high pressure." DNV-RP-F110, Det Norske Veritas, Baerum, Norway.

EGIG (2005). Gas Pipeline Incidents, European Gas Pipeline Incident Data Group, Groningen, the Netherlands. 6th EGIG Report 1970-2004, No. EGIG 05-R-0002.

Farhadi, B. and Wong, R. C. K. (2014). "Numerical modeling of pipe-soil interaction under transverse direction." *Proc., Int. Pipe. Conf.*, Calgary, Canada. IPC 2014-33364.

Guo, P.J. (2005). "Numerical modelling of pipe–soil interaction under oblique loading." *J. of Geotech. & Geo-environ. Eng.* ASCE, 131, 260–8.

Guo, P., and Stolle, D. (2005). “Lateral pipe-soil interaction in sand with reference to scale effect.” *J. of Geotech. & Geoenviron. Eng.*, ASCE, 131(3), 338−349.

Ha, D., Abdoun, T.H., O’Rourke, M.J., Symans, M.D., O’Rourke, T.D., Palmer, M.C. and Stewart, H.E. (2008). “Buried high-density polyethylene pipelines subjected to normal and strike-slip faulting - A centrifuge investigation.” *Can. Geotech. J.l*, 45(12), 1733–1742.

Hansen, J.B. and Christensen, N.H. (1961). “The ultimate resistance of rigid piles against transversal forces.” *Geoteknisk Institut,* Copenhagen.

Héquette, A., Desrosiers, M. and Barnes, P.W. (1995). “Sea ice scouring on the inner shelf of the southeastern Canadian Beaufort Sea.” *Mar. Geo.*, 128 (3–4), 201–219.

Hoshiya, M. and Mandal, J. N. (1984). “Some studies of anchor plates in sand.” *Soils. & Found*., 24(1), 9–16.

Hsu, T. (1993). "Rate effect on lateral soil restraint of pipelines", *Soils. & Found*., 33 (4), 159−169.

Hsu, S.T., and Liao, H.J. (1998). “Uplift behaviour of cylindrical anchors in sand.” *Can. Geotech. J*., 35(1), 70–80.

Hsu, T.W., Chen, Y.J., and Hung, W.Y. (2006). “Soil restraint to oblique movement of buried pipes in dense sand.” *J. of Trans. Eng.*, 132(2), 175–181.

Huang, B., Liu, J., Lin, P. and Ling, D. (2014). “Uplifting behavior of shallow buried pipe in liquefiable soil by dynamic centrifuge test.” *The Sci. World J.*, Article ID: 838546.

Huang, B., Liu, J., Ling, D. and Zhou, Y. (2015). “Application of particle image velocimetry (PIV) in the study of uplift mechanisms of pipe buried in medium dense sand.” *J Civil Struct. Health Monit*., 5(5), 599–614.

Jung, J., O’Rourke, T., and Olson, N. (2013a). “Lateral soil-pipe interaction in dry and partially saturated sand.” *J. of Geotech. and Geoenv. Eng.*, 139(12), 2028−2036.

Jung, J., O'Rourke, T., and Olson, N. (2013b). "Uplift soil–pipe interaction in granular soil." *Can. Geotech. J.*, 50(7), 744−753.

Jung, J.K., O'Rourke, T.D., and Argyrou, C. (2016). "Multi-directional force-displacement response of underground pipe in sand." *Can. Geotech. J.* Special Issue on Pipeline Geotechnics, 53, 1763–1781.

Karimian H, Wijewickreme D and Honegger D. (2006). "Full-scale laboratory testing to assess methods for reduction of soil loads on buried pipes subject to transverse ground movement." *Proc., 6th Int. Pipe. Conf.*, Calgary, Canada.

Kenny, S., Palmer, A.C., and Been, K. (2007). "Design challenges for offshore pipelines in arctic environments." *Proc., IBC Oil and Gas in Arctic and Cold Waters*.

Kouretzis, G.P., Sheng, D., and Sloan, S.W. (2013). "Sand-pipeline-trench lateral interaction effects for shallow buried pipelines." *Comp. and Geotech.*, 54, 53–59.

Kumar, J., and Sahoo, J. P. (2012). "An upper bound solution for pullout capacity of vertical anchors in sand using finite elements and limit analysis." *Int. J. Geomech.*, 12(3), 333–337.

Lings, M. L., and Dietz, M. S. (2004). "An improved direct shear apparatus for sand." *Geotechnique*, 54(4), 245−256.

Liu, J.X., and O'Rourke, M. (2010). "Response of offshore pipelines to landslides." *Proc., Off. Tech. Conf.*, Houston, Texas.

Loukidis, D. and Salgado, R. (2011). "Effect of relative density and stress level on the bearing capacity of footings on sand." *Géotechnique*, 61(2), 107–19.

Mair, R. J. (1993). "Developments in geotechnical engineering research: Applications to tunnels and deep excavations." Unwin Memorial Lecture 1992, *Proc. Inst. Civ. Engrs. Cil. Eng.*, 3, 27–41.

Merifield, R. S., Sloan, S. W., Abbo, A. J. and Yu, H. S. (2001). "The ultimate pullout capacity of anchors in frictional soils." *Proc., 10th Int. Conf. on Com. Methods and Adv. in Geomech.*, Tucson, AZ, 1187–1192.

Merifield, R. S. and Sloan, S. W. (2006). "The ultimate pullout capacity of anchors in frictional soils." *Can. Geotech. J.*, 43(8), 852–868.

Matyas, E. L. and Davis, J. B. (1983). "Experimental study of earth loads on rigid pipes." *J. of Geotech. Eng.*, 109(2), 202–209.

Mitchell, J.K., and Soga, K. (2005). *Fundamentals of soil behavior*. 3rd Edition. John Wiley & Sons, Hoboken.

Mohri, Y., Fujita, N. and Kawabata, T. (2001). "A simulation on uplift resistance of buried pipe by DEM." *Proc., Adv. in Pipe. Eng. and Const.*, Pipelines 2001, San Diego, 1–12.

Murray, E.J., and Geddes, J.D. (1989). "Resistance of passive inclined anchors in cohesionless medium." *Géotechnique*, 39(3), 417–431.

Neely, W. J., Stewart, J. G., and Graham, J. (1973). "Failure loads of vertical anchor plates in sand." *J. Soil Mech. Found. Div.*, 99(9), 669–685.

Ng, P.C.F (1994). "Behaviour of buried pipelines subjected to external loading." PhD thesis, University of Sheffield, UK.

Nielson, N.J.R, Lyngberg, B. and Pedersen, P.T. (1990). "Upheaval buckling failures of insulated pipelines: A case story." *Proc., Off. Tech. Conf.*, Houston, Texas, 581–592.

O'Rourke, M.J., and Liu, X. (2012). "Seismic design of buried and offshore pipelines." MCEER Monograph, MCEER-12-MN04.

O'Rourke, T. D. and Turner, J. E. (2006). "Earthquake soil-pipeline interaction in partially saturated sand." *Proc., 8th U.S. National Conf. on Earth. Eng.*, April 18–22, San Francisco, CA, Paper No. 1361.

Ovesen, N.K. (1964). "Anchor slabs, calculation methods and model tests", *Geoteknisk Institut (Danish Geotechnical Inst)*, Bulletin, no. 16, 39.

Palmer, A. (1990). "Design of marine pipelines in seabed vulnerable to ice scour." *Workshop on Ice Scouring and the Design of off. Pipe.*, Calgary, Canada, 167–178.

Palmer, A. C., White, D.J., Baumgard, A.J., Bolton, M.D., Barefoot, A.J., Finch, M., Powell, T., Faranski, A. S. and Baldry, A.S. (2003). "Uplift resistance of buried submarine pipelines: comparison between centrifuge modeling and full-scale tests." *Géotechnique*, 53(10), 877–883.

Paulin, M.J., Phillips, R., Clark, J.I., Hurley, S., and Trigg, A. (1997). "Establishment of a full-scale pipeline/soil interaction test facility and results from lateral and axial investigations in sand." *Proc., 16th Int. Conf. of Off. Mech. and Arc. Eng.*, Yokohama, Japan, April 13–17.

Pike, K., Kenny, S., and Hawlader, B. (2014). "Numerical and constitutive model development to aid design against pipeline geohazards." *J. of Pipe. Eng.*, 13(3), 201.

Pike, K. (2016). "Physical and numerical modelling of pipe/soil interaction events for large deformation geohazards." PhD thesis, Memorial University of Newfoundland, St. John's, Canada.

PRCI (2003). "Extended Model for Pipe Soil Interaction." Pipeline Research Council International, Contract No: PR-271-0184.

PRCI (2009). "Guidelines for constructing natural gas and liquid hydrocarbon pipelines through areas prone to landslide and subsidence hazards." Pipeline Research Council International.

Rajah, S. (2014). "Soil parameters for assessing axial and transverse behavior of restrained pipelines - Part 2: Transverse behavior." *Proc., Pipelines 2014: From Underg. to the Fore. of Inno. and Sustain.*, American Society of Civil Engineers (ASCE), Portland, OR, August 3–6, 1849–1863.

Randolph, R.F. (2012). "Offshore geotechnics–the challenges of deepwater soft sediments." *Proc., GeoCongress 2012*, March 25–29, California, USA, 241–371.

Robert, D. and Thusyanthan, N. (2015). "Numerical and Experimental Study of Uplift Mobilization of Buried Pipelines in Sands." *J. Pipe. Syst. Eng. Pract*., 6(1), 04014009.

Rowe, P. W. (1962). "The stress-dilatancy relation for static equilibrium of an assembly of particles in contact." *Proc. of the Royal Society,* A269, 500–527.

Rowe, P. W. (1969). "Progressive failure and strength of a sand mass." *Proc. of 7th Int. Conf. on Soil Mech. & Found. Eng.*, 1, 341–349.

Rowe, R.K. and Davis, E.H. (1982). "Behaviour of anchor plates in sand." *Géotechnique*, 32(1), 25–41.

Roy, K. (2012). "Finite element analyses of soil/pipeline interactions in sand with an advanced constitutive model." M.Eng. thesis, Memorial University of Newfoundland, St. John's, Canada.

Saboya, F., Jr., Santiago, P., Martins, R., Tibana, S., Ramires, R., and Araruna, J., Jr. (2012). "Centrifuge Test to Evaluate the Geotechnical Performance of Anchored Buried Pipelines in Sand." *J. Pipe. Syst. Eng. Pract.*, 3(3), 84–97.

Sakanoue, T. (2008). "Study on soil-pipeline interaction due to large ground deformation." *Proc., 14th World Conf. on Earth. Eng.*, Beijing, China.

Schaminée, P. E. L., Zorn, N. F., and Schotman, G. J. M. (1990). "Soil response for pipeline upheaval buckling analysis: Full-scale laboratory tests and modelling." *Proc., Off. Tech. Conf.*, OTC, Houston, TX.

Scarpelli, G., Sakellariadi, E., and Furlani, G. (1999). "Longitudinal pipeline–soil interaction: results from field full scale and laboratory testing." *Proc., 12th European Conf. on Soil Mech. and Geotech. Eng.,* 511.

Suzuki, K and Yamada, T. (2006). "Double strain-softening and diagonally crossing shear bands of sand in drained triaxial tests." *Int. J. Geomech*, 6 (6), 440–446.

SYNER-G (2010). Systemic Seismic Vulnerability and Risk Analysis for Buildings, Lifeline Networks and Infrastructures Safety Gain, Bureau de Recherches Geologiques et Minieres (BRGM), Project No: 244061.

Thusyanthan, N. I., Mesmar, S., Wang, J. and Haigh, S. K. (2010). "Uplift resistance of buried pipelines and DNV-RP-F110." *Proc., Off. Pipe. and Tech. Conf.,* Amsterdam, 24–25.

Trautmann, C. (1983). "Behavior of pipe in dry sand under lateral and uplift loading." PhD thesis, Cornell University, Ithaca, NY.

Trautmann, C.H. and O'Rourke, T.D. (1985). "Lateral force-displacement response of buried pipe." *J. of Geotech. Eng.*, 111(9), 1077−1092.

Wang, J., Ahmed, R., Haigh, S. K., Thusyanthan, N. I. and Mesmar, S. (2010). "Uplift resistance of buried pipelines at low cover-diameter ratios." *Proc., Off. Tech. Conf.,* Houston.

White, D. J., Take, W. A., and Bolton, M. D. (2003). "Soil deformation measurement using particle image velocimetry (PIV) and photogrammetry." *Géotechnique*, 53(7), 619–631.

White, D. J., Barefoot, A. J. and Bolton, M. D. (2001). "Centrifuge modelling of upheaval buckling in sand." *Int. J. of Physical Model. in Geotech.,* 2(1), 19–28.

White, D.J., Cheuk, C.Y, and Bolton, M.D. (2008). "The Uplift resistance of pipes and plate anchors buried in sand." *Géotechnique*, 58(10), 771–779.

Xie, X., Symans, M., O'Rourke, M. J., Abdoun, T. H., O'Rourke, T. D., Palmer, M. C., and Stewart, H. E. (2013). "Numerical modeling of buried HDPE pipelines subjected to normal faulting: A case study." *Earthq. Spectra,* 29(2), 609–632.

Yimsiri, S., Soga, K., Yoshizaki, K., Dasari, G., and O'Rourke, T. (2004). "Lateral and upward soil–pipeline interactions in sand for deep embedment conditions." *J. of Geotech. & Geoenv. Eng.*, 130(8), 830−842.

Yimsiri, S. and Soga, K. (2006). "DEM analysis of soil–pipeline interaction in sand under lateral and upward movements at deep embedment." *J. of South.t Asian Geotech. Soc.*, 37, 83−94.

Yoshizaki, K. and Sakanoue, T. (2004). "Analytical study on soil-pipeline interaction due to large ground deformation." *Proc., 13th World Conf. on Earthq. Eng.,* B.C., Canada.

APPENDIX A

Influence of Low Confining Pressure on Lateral Pipeline/Soil Interaction in Dense Sand

This paper has been published and presented in 33rd International Conference on Ocean, Offshore and Arctic Engineering (OMAE 2014), San Francisco, California, USA, June 8–13, 2014. Most of the research work presented in this paper was conducted by the first author. He also prepared the draft manuscript. The other authors supervised the research and reviewed the manuscript.

Proceedings of the ASME 2014 33rd International Conference on Ocean, Offshore and Arctic Engineering
OMAE2014
June 8-13, 2014, San Francisco, California, USA

OMAE2014-24601

INFLUENCE OF LOW CONFINING PRESSURE IN MODELING OF LATERAL PIPELINE/SOIL INTERACTION IN DENSE SAND

Kshama Roy
PhD Student
Memorial University of Newfoundland
St. John's, NL, Canada

Bipul Hawlader
Associate Professor
Memorial University of Newfoundland
St. John's, NL, Canada

Shawn Kenny
Associate Professor
Carleton University
Ottawa, ON, Canada

ABSTRACT

Buried pipelines are extensively used for transporting water and hydrocarbons. Geohazards and associated ground movements represent a significant threat to pipeline integrity that may result in pipeline damage and potential failure. Safe, economic and reliable operation of pipeline transportation systems is the primary goal of the pipeline operators and regulatory agencies. The pipes are often buried at a shallow depth and therefore the behaviour of soil at low stress level need to be considered for proper modeling of the response of pipelines. In this study, finite element (FE) modeling of pipeline/soil interaction is presented, where the stress-stain behaviour of soil at low stress level is implemented. At first, triaxial test results are simulated to validate the proposed model and numerical techniques. Pipeline/soil interaction in plane strain condition is then simulated for lateral loading. The Arbitrary Lagrangian-Eulerian (ALE) method available in Abaqus/Explicit is used for FE modeling. One of the main advantages of this method is that it can simulate large deformation behaviour. The variation of non-dimensional lateral force with non-dimensional displacement is examined for different depth of embedment of pipeline and soil conditions. Finally, shear band formation in soil due to lateral movement of the pipe is presented.

INTRODUCTION

Buried pipelines are extensively used for transporting water and hydrocarbons. According to the Canadian Energy Pipeline Association (CEPA), in Canada, more than 830,000 kilometers of buried pipelines deliver natural gas and petroleum products from field development areas to market [6]. The liquid hydrocarbon and natural gas products are usually transported through buried pipelines, which traverse large distances through a variety of soils. Geohazards and the associated ground movement represent a significant threat to pipeline integrity that may result in pipeline damage and potential failure. In certain situations, pipelines can be exposed to potential ground failures such as surface faulting, liquefaction-induced soil movements, and landslide induced permanent ground deformation (PGD). These ground movements might cause excessive stresses in pipelines and pipelines might be damaged.

Theoretical and experimental studies were conducted in the past to determine the forces on pipelines due to relative movement of the soil in specific directions, namely longitudinal, transverse horizontal, or transverse vertical (e.g. [3], [13], [14], [22], [23], [28], [29], [30], [34], [37], [38]). Guo and Stolle [12] compiled data from 11 experimental studies and showed a wide variation in non-dimensional peak force. In order to understand the mechanism further, FE analyses in Lagrangian framework have been also performed in the past (e.g. [9], [12], [17], [39], [40]). Yimsiri et al. [40] conducted a comprehensive FE analysis using Abaqus/Standard FE software with the Mohr-Coulomb and Nor-Sand soil constitutive models. The degradation of soil strength parameters after the peak was not considered in this study. Guo and Stolle [12] showed the scale effects on non-dimensional force and displacement from a comprehensive FE analysis using the Abaqus/Standard FE software. Similarly, Daiyan et al. [9] conducted FE analyses using Abaqus/Standard and compared with centrifuge test results. The non-linear variation of shear strength parameters obtained from triaxial test results have been used in these studies. Using a linear variation of friction angle and dilation angle with plastic strain, the post-

peak softening was also incorporated in the FE analysis for pipeline/soil interaction analyses ([17], [24]). A recent study [17] showed the importance of using plane strain strength parameters for pipeline/soil interaction modeling.

The pipelines are often buried at a shallow depth and therefore the stresses in the soil around the pipe before any movement is generally lower than typical geotechnical problems such as foundations. Therefore, the behaviour of soil masses around the pipeline at low stress level need to be considered properly.

Present study mainly focuses the finite element simulation of buried pipelines in dense sand. Although limited, some experimental studies on dense sand at low stress level are available in the literature (e.g. [1], [11], [19], [25], [32], [33]). Ponce and Bell [25] showed that sand exhibits a strong increase in friction and dilatancy angles when the confining pressure decreases in triaxial tests. However, Fukushima and Tatsuoka [11] found a weaker variation.

Another important experimental observation is that the behaviour of sand in triaxial and simple shear conditions is different. For example, Ahmed [1] conducted tests on crushed silica sand in drained triaxial (TX) and plane strain (PS) loading conditions. The peak friction angle (ϕ'_p) obtained from his test results are shown in Fig. 1. Three key features of these test results need to be mentioned. Firstly, the peak friction angle in plane strain condition ($\phi_p'^{PS}$) is higher than the peak friction angle in triaxial condition ($\phi_p'^{TX}$), and the value of $\phi_p'^{PS} - \phi_p'^{TX}$ is higher at low stress level. Secondly, the both $\phi_p'^{PS}$ and $\phi_p'^{TX}$ increase with increase in relative density. Finally, the peak friction angle decreases with increase in confining pressure.

The main objective of the present study is to analyze lateral pipeline/soil interaction of buried pipes in dense sand. An advanced simulation tool, which is even suitable for large deformation analysis is used for FE analyses. A modified Mohr-Coulomb (MC) model with confining pressure dependent peak friction angle and the dilation angle is used. In addition, the dependency of mobilized friction angle (ϕ') and dilation angle (ψ) with engineering plastic shear strain (γ_p) is used to simulated the strain hardening and softening behaviour of dense sand. The lateral resistance from the present FE analyses is compared with the available numerical and experimental results. Finally, the mechanism of failure of soil is investigated.

FINITE ELEMENT FORMULATION

Two-dimensional pipeline/soil interaction analyses are conducted using the ABAQUS/Explicit FE software. The Arbitrary Lagrangian-Eulerian method available in Abaqus/Explicit is used. The main advantages of using Abaqus/Explicit over Abaqus/Standard is that the pipe can be moved sufficiently large distance avoiding numerical issues due to mesh distortion as encountered in the Abaqus/standard, especially in the zone of shear strain localization. Therefore, the formation of shear band can be better simulated in Abaqus/Explicit.

Figure 2 shows the typical FE model used in this study. For FE modeling of soil, 4-node bilinear plane strain quadrilateral, reduced integration, hourglass control element (CPE4R) is used. The pipe is modeled as a rigid body. Abaqus/cae is used to generate the finite element mesh. The structured mesh, as shown in Fig 2, is generated by zoning the soil domain. Denser mesh is used near the pipe. The total number of elements and shapes can be defined in the structured mesh, which cannot be done in the auto generated default meshing option in Abaqus. In this study, structured mesh is used because it gives better results, less numerical issues and is computationally more efficient than auto generated mesh.

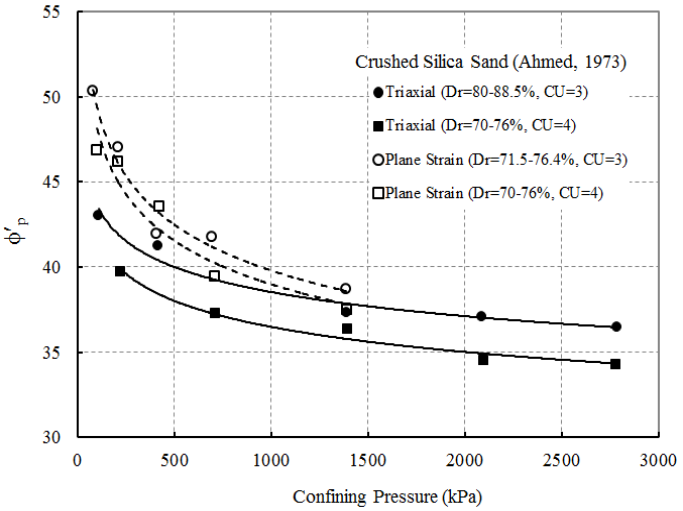

Figure 1. Test results on crushed silica sand (after Ahmed, 1973)

The bottom of the FE domain is restrained from any vertical movement, while all the vertical faces are restrained from any lateral movement using roller supports (Fig. 2). No displacement boundary condition is applied on the top face, and therefore the soil can move freely. The pipe is placed at the desired location. The depth of the pipe is measured in terms of *H*/*D* ratio, where *H* is the depth from the top of the soil to the center of the pipe and *D* is the external diameter of the pipe. The locations of the bottom and right boundaries with respect to the location of the pipe are sufficiently large and therefore boundary effects on predicted lateral resistance, displacement and soil failure mechanisms are not found. This is verified from a number of FE analyses setting these boundaries at larger distances than that shown in Fig. 2.

The interface between pipe and soil is simulated using the contact surface approach available in Abaqus/Explicit. The Coulomb friction model is used for the frictional interface between the outer surface of the pipe and sand. In this method, the friction coefficient (μ) is defined as $\mu=\tan(\phi_\mu)$, where ϕ_μ is the pipeline/soil interface friction angle. The value of ϕ_μ depends on the interface characteristics and relative movement between the pipe and soil. The larger value of ϕ_μ represents the characteristics of rough uncoated pipes with rusty or corroded

surfaces, while the lower values would correspond to pipes with smooth coating. The value of ϕ_μ varies between ϕ'^{TX}_p and $\phi'^{TX}_p/2$ [40]. The value of μ equal to 0.32 is used in this study.

The numerical analysis is conducted in two main steps. The first step is a geostatic stress step that accounts for the effects of soil weight and defines the initial stress state in the soil. The initial stress or the geostatic stress step definition is very important for pipeline/soil interaction analyses. It is to be noted here that if the geostatic condition is not properly modeled with appropriate initial stress condition, the response in subsequent loading might be erroneous and/or additional numerical issues might be encountered, because the behaviour of sand is effective stress dependent. In this study, it has been properly defined and the calculated stresses at the end of geostatic step are same as expected in situ stress.

In the second step, the pipe is moved in the lateral direction specifying a displacement boundary condition at the reference point of the pipe.

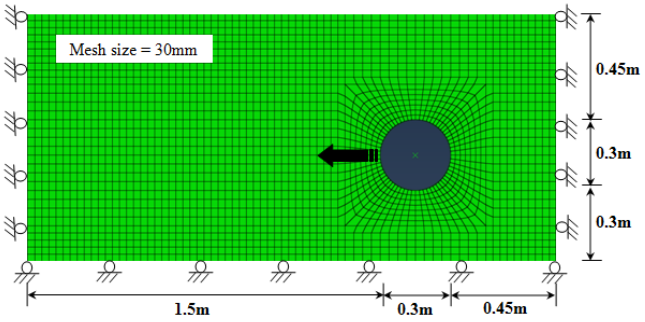

Figure 2. Typical finite element mesh at D=0.3m and H/D=2

MODELING OF SOIL BEHAVIOUR

The Mohr-Coulomb model is one of the simple models that reasonably model the behaviour of sand. This model has been used by many researchers in the past for pipeline/soil interaction analysis. In this study, a modified form of Mohr-Coulomb model is used incorporating the following key features as observed in laboratory tests.

Angle of internal friction in PS conditions

Pipeline/soil interaction in plane strain condition is simulated in this study. The strength of sand is usually characterized by the angle of internal friction. Mayne and Kulhawy [21] compiled a large volume of test data and showed that, in general, the peak friction angle of dense sand in PS is approximately 10% to 20% higher than that of in TX condition. Experimental results on dense sands also show that ϕ'^{PS}_p is more than 5° higher than ϕ'^{TX}_p [31]. Furthermore, experimental evidence shows that ϕ'_p decreases with increase in mean effective stress at failure (p'), and generally follows a linear relation with lnp'. Bolton [5] analyzed the strength and dilatancy of 17 sands in TX and PS tests and proposed the following empirical relations:

$$\phi'^{TX}_p - \phi'^{TX}_c = 3I_R \quad \text{for triaxial} \tag{1}$$

$$\phi'^{PS}_p - \phi'^{PS}_c = 5I_R \quad \text{for plane strain} \tag{2}$$

Where I_R is the relative density index defined as $I_R = I_D(Q - \ln p') - R$ with I_D =relative density (=D_r(%)/100). The subscripts p and c represent the peak and critical state, respectively. Bolton [5] also showed that the values of Q=10 and R=1 fit most of the test data, although it might vary with type of sand and p' [7]. As triaxial tests are widely used for geotechnical characterization, appropriate care need to be taken for estimation of ϕ'_p for pipeline/soil interaction analysis in plane strain condition. It is to be noted here that a similar attempt has been taken to estimate ϕ'^{PS}_p from direct shear test results [20] and showed that ϕ'^{PS}_p is approximately 5 degrees higher than the peak friction angle obtained from direct shear test.

Equation 2 is used to model pipeline/soil interaction in PS condition in the present study, although the authors understand that additional laboratory tests at low p' are required to check the validity of this equation further.

Unlike ϕ'_p, the critical state friction angles may not differ considerably in PS and TX conditions. Experimental evidences shows that ϕ'^{PS}_c is few degrees higher than ϕ'^{TX}_c. Bishop [4] and Conforth [8] conducted drained tests on sands over a range of densities at a wide range of confining pressure and showed that ϕ'^{PS}_c is approximately 4° higher than ϕ'^{TX}_c. Similar results were obtained from laboratory tests on Toyoura sand ([26], [33]), and have shown that $\phi'^{PS}_c \approx 34.5° - 38°$ while $\phi'^{TX}_c \approx 33°$.

The maximum dilation angle (ψ_p), which occurs at the peak shear strength, are related to the peak and critical state friction angles in plane strain condition as [5]:

$$\phi'^{PS}_p = \phi'^{PS}_c + 0.8\psi_p \tag{3}$$

In this study, $\phi'^{TX}_c = 31°$ and $\phi'^{PS}_c = 35°$ are used.

Stress-strain behaviour of dense sand

In the modified Mohr-Coulomb model, the mobilized shear strength parameters (ϕ' and ψ) are varied with accumulated plastic shear strain (γ_p) as shown in Fig. 3. In the pre-yield zone, both ϕ' and ψ increase from (ϕ'_{in} and ψ_{in}) to the peak values at γ^p_p, and therefore strain hardening occurs in this zone. Experimental evidence shows that the plastic shear strain at peak, γ^p_p decreases with increasing relative density and increases with increasing p'. For example, from direct shear tests, Lings and Dietz [20] showed that for a dense sand (D_r=90%) the peak friction angle is mobilized at horizontal displacement of 1.5 mm and 3.5 mm under normal stress of 25 kPa and 251 kPa,

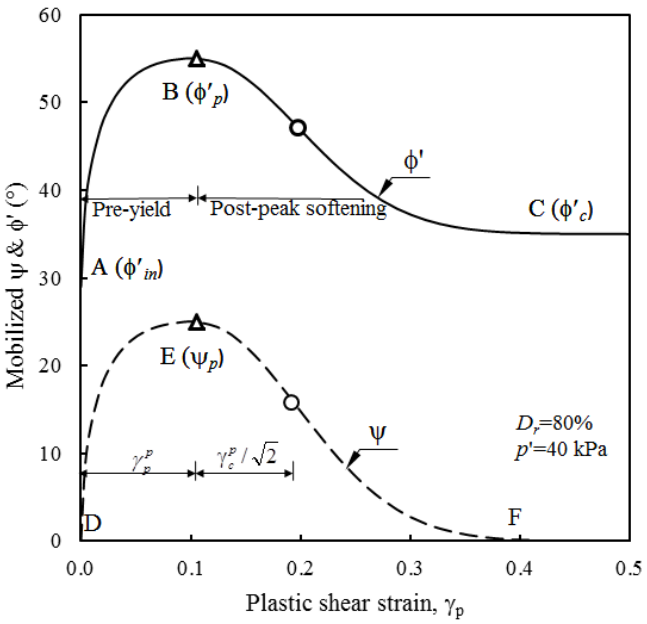

Figure 3. Modeling of stress-strain behaviour of dense sand

respectively. In order to capture the non-uniqueness of γ_p^p, in this study the behaviour is defined as:

$$\gamma_p^p = \gamma_p^c \left(p'/p'_a\right)^{0.252} \tag{4}$$

$$\gamma_c^p = \left(22.1 - 11.2 D_r\right)/100 \tag{5}$$

where γ_c^p = strain softening parameter, which is explained further in the following sections and p'_a= reference pressure = 100 kPa.

The following sine function is then used to model the variation of mobilized ϕ′ and ψ in the pre-yield zone.

$$\phi' = \phi'_{in} + \left[\sin^{-1}\left(\frac{2\sqrt{\gamma^p \gamma_p^p}}{\gamma^p + \gamma_p^p}\right)\sin\left(\phi'_p - \phi'_{in}\right)\right] \tag{6}$$

$$\psi = \sin^{-1}\left[\left(\frac{2\sqrt{\gamma^p \gamma_p^p}}{\gamma^p + \gamma_p^p}\right)\sin\left(\psi_p\right)\right] \tag{7}$$

The value of ψ_p can be calculated using Eq. 3. The lines AB and DE in Fig. 3 show the variation of ϕ′ and ψ, respectively, in the pre-yield zone for D_r=80% and p'=40 kPa.

If the shearing is continued, both ϕ′ and ψ will decrease with plastic strain as shown in Fig. 3. This zone is referred as "post-peak softening zone." The following exponential functions are used to define the curve BC and EF to model the variation of ϕ′ and ψ, respectively.

$$\phi' = \phi'_c + \left(\phi'_p - \phi'_c\right)\exp\left\{-\left(\frac{\gamma^p - \gamma_p^p}{\gamma_c^p}\right)^2\right\} \quad \text{curve BC} \tag{8}$$

$$\psi = \psi_p \exp\left\{-\left(\frac{\gamma^p - \gamma_p^p}{\gamma_c^p}\right)^2\right\} \quad \text{curve EF} \tag{9}$$

The strain softening parameter γ_c^p controls the shape of the post-peak curves. After some algebraic calculation, it can be shown from Eqs. (8) and (9) that the point of inflection of the post-peak softening curve occurs at a shear strain of $\gamma_c^p/\sqrt{2}$ greater than γ_p^p which is shown by the open circle in Fig. 3. It is to be noted here that the modified Mohr-Coulomb model with strain dependent ϕ′ and ψ have been also used in the past for modeling dense sand. Anastaspoulos et al. [2] used a simple straight line to model post-peak degradation. Jung et al. [17] used that concept for pipeline/soil interaction analysis. In those studies, pre-yield behaviour was not considered, rather the stress-strain behaviour before the peak was assumed to be elastic. The soil constitutive model is then implemented in Abaqus using a user subroutine written in FORTRAN.

PERFORMANCE OF SOIL CONSTITUTIVE MODEL

In order to show the performance of the soil constitutive model described in the previous sections and also to validate the present FE implementation, a set of triaxial test results [15] are simulated first. The FE simulation is performed for consolidated isotropically drained triaxial tests on dense sand (D_r=70%) for a wide range of confining pressures of 20-320 kPa. The value of $\phi_c'^{TX} = 31°$ is used. The variation of $\phi_p'^{TX}$ is defined by using Eq. (1). The calculated deviatoric stress and volumetric strain are shown in Fig. 4, which show that the proposed soil constitutive model can successfully simulate the stress-strain behaviour of dense sand for a wide range of confining pressures including the low stress levels, which is the interest of the present study in pipeline/soil interaction modeling. The markers in Fig. 4 indicate data from test results whereas the solid lines represent data from FE analysis. These observations provide confidence in the modeling approach and numerical procedures implemented in Abaqus/Explicit FE analysis.

SIMULATION OF PIPELINE/SOIL INTERACTION

After verification of soil constitutive model performance in triaxial condition, FE simulations are performed for pipelines buried in dense sand (D_r=80%) under lateral loading in plane strain condition. The FE results are first verified with the results of model tests conducted by Trautmann [34]. These test results have been also used by previous researchers to validate numerical modeling performance. For example, Yimsiri et al. [40] reanalyzed the direct shear test results presented by Trautmann [34] for estimation of soil parameters and used $\phi'_c = 31°$ in their FE analyses. As mentioned before that ϕ′ in PS is higher than ϕ′ in triaxial and direct shear test ([20], [26])) a

value of $\phi'_c = 35°$ is used in the present study. The peak friction angle is calculated using Eq. (2) with a maximum value of

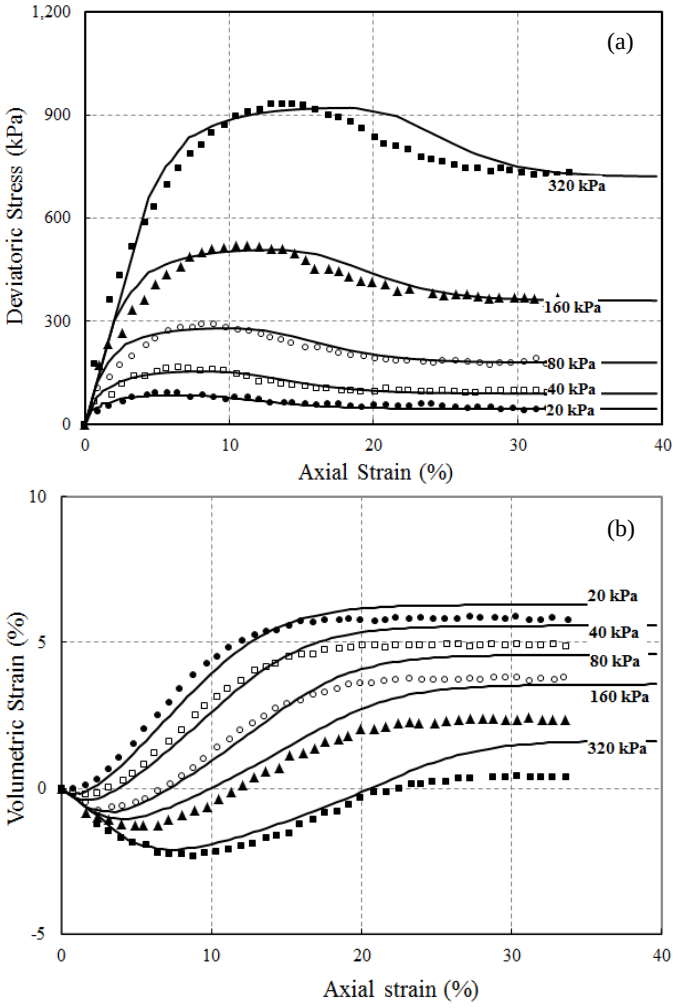

Figure 4. Comparison between FE and laboratory test results of Hsu and Liao (1998) [Markers: Test data, Solid line: FE analysis]

$\phi'^{PS}_p - \phi'^{PS}_c$ equal to 20° as suggested by Bolton [5]. The unit weight of dry sand used for model test was 17.7 kN/m^3 that corresponds to a relative density of 80%. The Poisson's ratio of 0.2 is used, which is considered as the best representative value for dense sand [16]. The modulus of elasticity (E) is varied with initial mean effective stress (σ_m) as $E = E_0\left(\sigma_m / \sigma_{m(ref)}\right)^n$, where E_0 is the value of E at reference pressure ($\sigma_{m(ref)}$) , and n is a material constant. Parameters used in the FE analysis are summarized in Table 1.

RESULTS

Figure 5 shows the variation of dimensionless force with dimensionless lateral displacement for two burial depths (H/D=2 and H/D=6). The FE results compare very well with model test results [34].

Table 1: Soil parameters used in the FE analyses

Parameter	Values	
	Trautmann (1983) model test	Parametric study
External diameter of pipe, D	102 mm	300 mm
Poisson's ratio, ν_{soil}	0.2	0.2
E_0	15000 kN/m^2	15000 kN/m^2
n	0.5	0.5
$\sigma_{m(ref)}$	100 kN/m^2	100 kN/m^2
Poisson's ratio, ν_{soil}	0.2	0.2
Critical state friction angle, ϕ'_c	35°	35°
Unit weight, γ	17.7 kN/m^3	17.7 kN/m^3
Interface friction co-efficient, μ	0.32	0.32
Depth of pipe, H/D	2 & 6	2, 4, 6, & 10

Figure 6 shows the comparison of displacement vector between model test and FE analysis for H/D=6. The top figure shows the displacement vector at a lateral displacement of 30 mm, while the bottom figure shows the displacement vector in Trautmann [34] test #24. The displacement vectors obtained from the FE analyses are very similar to the test results.

Similar comparisons are also performed for other tests conducted by Trautmann [34] for lateral loading and good agreement was observed. However, they are not presented in this paper due to space limitations.

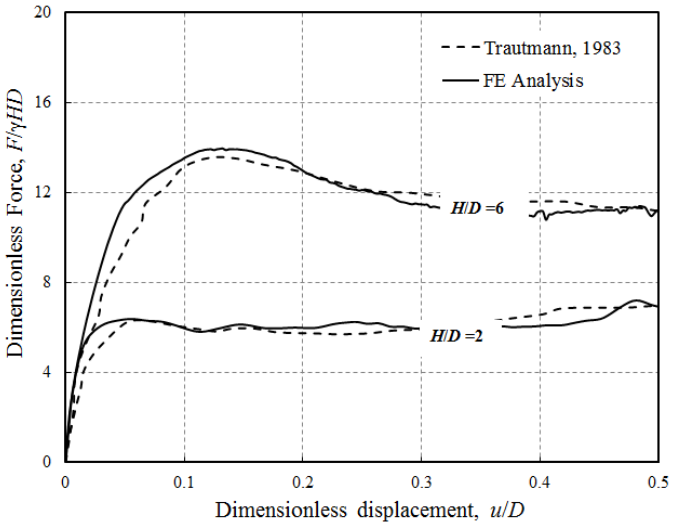

Figure 5. Comparison of FE results with the large scale test results (Trautmann, 1983)

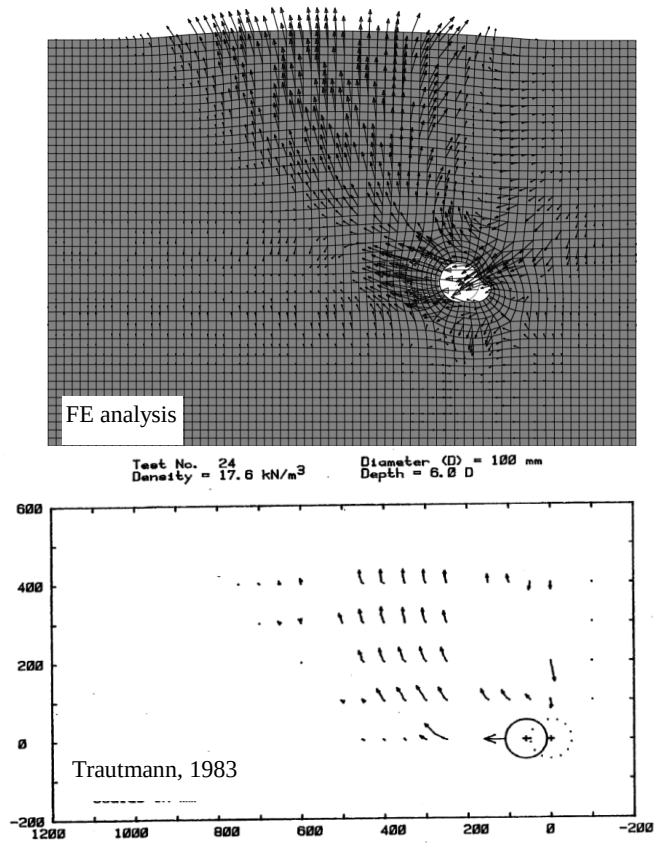

Figure 6. Comparison of displacement vectors between FE results and large scale test results for H/D=6

The effects of pipe diameter on the soil force-displacement response are further examined in this section through FE modeling of a 300 mm diameter pipe. Analyses are performed for four H/D ratios (=2, 4, 6 & 10). The normalized force-displacement curves for these analyses are shown in Fig. 7. For the same H/D ratio (=2 and 6) but different D (=102 mm), the normalized force displacement curves are also shown in this figure.

The peak dimensionless force is one of the main parameters in the current pipeline design practice. The peak dimensionless force obtained from the present FE analyses for D=300 mm are plotted with H/D ratio in Fig. 8. For comparison, the results of physical model tests and some FE analyses available in the literature are also plotted in this figure.

Figures 7 and 8 show that:

(1) The dimensionless force increases with H/D but dependent on diameter of the pipe [Fig. 7].

(2) The peak dimensionless force increases with the increase of H/D [Fig. 8].

(3) For a given pipe diameter D, the displacement required to mobilize the maximum soil resistance (u_p) increases with increase in H/D ratio [Fig. 7].

(4) For H/D=2, the calculated dimensionless peak force for a pipe of larger diameter (D=300 mm) is slightly higher than that of smaller diameter (D=102 mm) pipe. However, the opposite response is found for H/D=6 (Fig. 7).

(5) For H/D=constant i.e. H/D=6, the displacement required to mobilize the peak dimensionless force is higher in larger diameter pipe (Fig. 7). Note that this is dependent upon the value of E.

(6) For a given H/D, the values of peak dimensionless force obtained from FE analyses and physical model tests vary significantly. The cause of this difference might be the constitutive models and FE modeling techniques used in numerical studies and test conditions in physical modeling.

Similar to the peak dimensionless force, the mobilized displacement at the peak (u_p) is equally important in the design. The value of u_p obtained from the force-displacement curve of the present FE analyses are comparable with previous studies. For example, u_p is equal to 93 mm for H/D=10, where D=300 mm. Hansen [14] suggest to use $u_p = 0.04(H+D/2)$, which gives 126 mm. Similarly, according to Trautmann [34] $0.03(H+D/2)$=94.5 mm, PRCI [27] $0.04(H+D/2)$=126.0 mm and Ovensen [22] $0.036h$ = 113.4 mm can be calculated for u_p. Note that in Ovensen [22], h represents the distance from the ground surface to the base of the pipe.

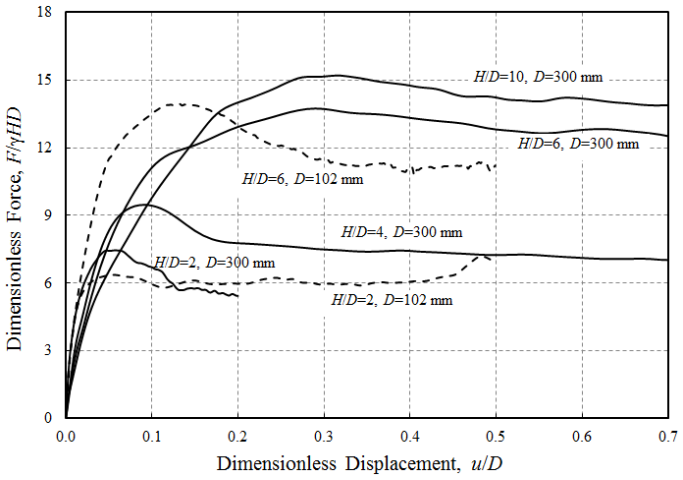

Figure 7. Force-displacement curves for different H/D ratio and diameter

FAILURE PATTERN

In this section, the mechanism of failure of soil under lateral displacement of the pipe is investigated. The soil failure mechanism can be categorized into two simple modes, "wedge" and "plow through." For shallow burial depth, the lateral movement of the pipe in dense sand results in upward and lateral movement of a soil wedge in front of the pipe. On the other hand, in deep burial conditions, the lateral movement of the pipe results in soil flowing around the pipe with negligible deformation at the surface, which is known as plow through failure mode.

In order to explain soil failure mechanism, consider the FE simulation of a pipeline at a moderate depth H/D=6 and D=300 mm. The plastic shear strain developed in the soil at a lateral displacement of 150 mm is shown in Fig. 9. FV1 in the legend

of Fig. 9 represents the plastic shear strain (FV1=γ_{max}=ε_1-ε_3), where ε_1 and ε_3 are the major and minor principal plastic shear

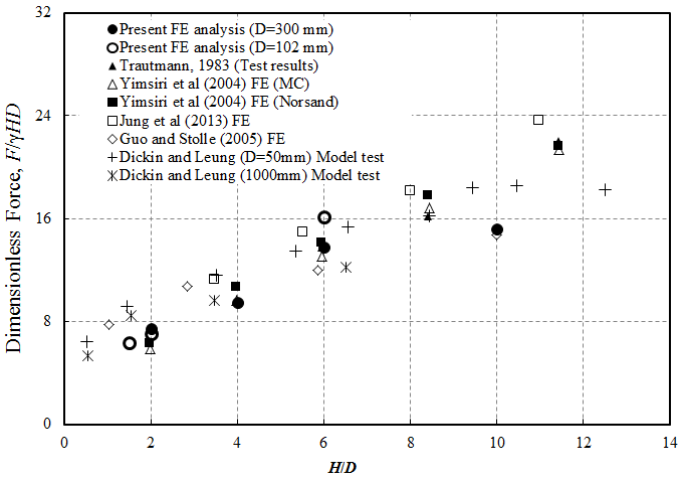

Figure 8. Comparison of peak resistance with previous studies

strain, respectively. The value of FV1 is calculated in each increment using the user subroutine VUSDFLD in the Abaqus/Explicit. As shown in Fig. 9 that significantly higher plastic shear strain developed in some narrow zones at this level of lateral displacement. Proper utilization of adaptive meshing techniques in Abaqus/Explicit enables successful modeling of such large strains without significant numerical issues. The strain localization at this stage forms mainly three shear bands (Fig. 9). The shear strains in the soil between two bands are not significant compared to the shear strain in the band. The modeling of these shear bands is important at large strains.

Figure 9 shows that a small wedge is formed just in front of the pipe (left side). This is very similar to the wedge under a shallow foundation subjected to vertical load. After this wedge, the shear strain localization formed the shear band-1 in the form of a log spiral curve and continued to the ground surface. Behind the pipe (right side) the soil is displaced and filled the gap formed by the movement of the pipe. This created two additional shear bands (2 and 3) as shown in Fig. 9. During lateral loading at this stage, the soil block between the shear bands 1 and 2 moves upward and creates a heave, while the soil block between the shear bands 2 and 3 moves downward that causes settlement at the ground surface.

Turner [36] identified three shear bands associated with the failure mechanism of soil, as shown in Fig. 10. Comparing Figs. 9 and 10 it can be concluded that the present FE model can successfully simulate the strain localization and ground surface displacement pattern for a pipe under lateral load.

Although it is not presented in this paper, the shear bands for other burial depths are also successfully modeled and the details will be presented in a future publication.

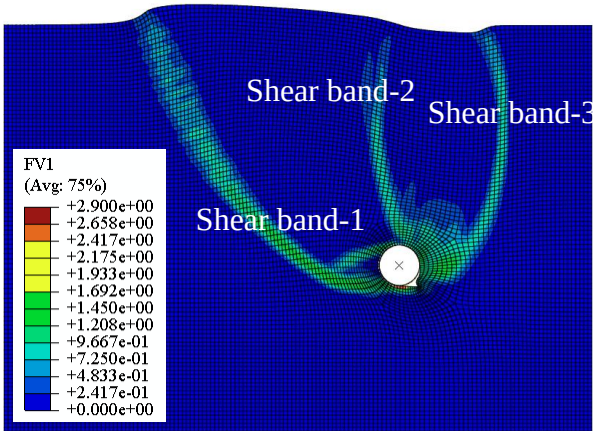

Figure 9. Strain localization in ALE pipeline/soil interaction model (D=300 mm, H/D=6)

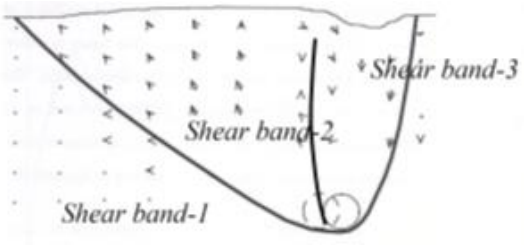

Figure 10. Schematic of shear band formation in soil (after Turner, 2004)

CONCLUSIONS

The pipeline/soil interactions associated with relative movement of the pipeline in the lateral direction is numerically investigated in this study. The FE simulations are performed for two-dimensional plane strain condition. The key features considered in modeling of the behaviour of dense sands are: (i) the decrease of peak friction angle with increase in effective stress at failure, (ii) an improved stress-strain behaviour of dense sand, including the pre-yield hardening and post-peak softening with plastic shear strain; and (iii) plane strain strength parameters, which are different from triaxial or direct shear strength parameters. The FE modeling is performed using Abaqus/Explicit FE software, which can simulate even large strain response utilizing adaptive meshing techniques.

The present FE model can simulate successfully the triaxial test results for a wide range of confining pressures, including the tests under low confining pressures.

For pipelines, the calculated force-displacement curves match well with model test results of Trautmann [34]. With increase in burial depth ratio (H/D), the peak dimensionless force and the displacement required to mobilize this peak force increase, although these values are dependent on the diameter of the pipe for the range analyzed in this study. The results obtained from the present FE analyses are consistent with previous

studies. Finally, the strain localization/shear bands simulated in the present FE analysis are very similar to those observed in model tests.

ACKNOWLEDGMENTS

The work presented in this paper was funded by the Research and Development Corporation (RDC) Newfoundland and Labrador and NSERC Discovery and CRD grants.

REFERENCES

[1] Ahmed, S.M.U. 1973, "A study of the influence of confining pressure on the behaviour of sands*"*, M.Sc. Thesis, McGill University, Montreal, Canada.

[2] Anastasopoulos, I., Gazetas, G., Bransby, M., Davies, M. & El Nahas, A. 2007, "Fault rupture propagation through sand: Finite-element analysis and validation through centrifuge experiments", *Journal of Geotechnical and Geoenvironmental Engineering*, vol. 133, no. 8, pp. 943-958.

[3] Audibert, J.M.E. & Nyman, K.J. 1978, "Soil restraint against horizontal motion of pipes", *International Journal of Rock Mechanics and Mining Sciences and Geomechanics Abstracts*, vol. 15, no. 2, pp. A29-A29.

[4] Bishop, A. W. 1961, "Discussion on soil properties and their measurement", *Proceedings of 5th Int. Conf. on Soil mechanics and Foundation engineering* vol. III.

[5] Bolton, M. D. 1986, "The strength and dilatancy of sands", *Geotechnique*, vol. 36, no. 1, pp. 65-78.

[6] CEPA (The Canadian Energy Pipeline Association 2013, Retrieved from: http://www.cepa.com/.

[7] Chakraborty, T. & Salgado, R. 2010, "Dilatancy and Shear Strength of Sand at Low Confining Pressures", *Journal of Geotechnical and Geoenvironmental Engineering*, vol. 136, no. 3, pp. 527-532.

[8] Conforth, D.H. 1964, "Some experiments on the influence of strain conditions on the strength of sand.", *Geotechnique*, vol. 14, pp. 143-167.

[9] Daiyan, N., Kenny, S., Phillips, R. & Popescu, R. 2011, "Investigating pipeline–soil interaction under axial–lateral relative movements in sand", *Canadian Geotechnical Journal*, vol. 48, no. 11, pp. 1683-1695.

[10] Dickin, E.A. & Leung, C.F. 1983, "Centrifugal Model Tests on Vertical Anchor Plates", *Journal of Geotechnical Engineering*, vol. 109, no. 12, pp. 1503-1525.

[11] Fukushima, S. & Tatsuoka, F. 1984, "Strength and deformation characteristics of saturated sand at extremely low pressures", *Soils and Foundations*, vol. 24, no. 4, pp. 30-48.

[12] Guo, P. & Stolle, D. 2005, "Lateral pipe-soil interaction in sand with reference to scale effect", *Journal of Geotechnical and Geoenvironmental Engineering*, vol. 131, no. 3, pp. 338-349.

[13] Guo, P. 2005, "Numerical modeling of pipe-soil interaction under oblique loading", *Journal of Geotechnical and Geoenvironmental Engineering*, vol. 131, no. 2, pp. 260-268.

[14] Hansen, J. B. 1961, "The ultimate resistance of rigid piles against transversal forces." *Bulletin No. 12*, Danish Geotechnical Institute, Copenhagen, Denmark, 5–9.

[15] Hsu, S.T. & Liao, H.J. 1998, "Uplift behaviour of cylindrical anchors in sand", *Canadian Geotechnical Journal*, vol. 35, no. 1, pp. 70-80.

[16] Jefferies, M. & Been, K. 2006, "*Soil liquefaction: a critical state approach",* Taylor & Francis, New York.

[17] Jung, J., O'Rourke, T. & Olson, N. 2013, "Lateral Soil-Pipe Interaction in Dry and Partially Saturated Sand", *Journal of Geotechnical and Geoenvironmental Engineering*, vol. 139, no. 12, pp. 2028-2036.

[18] Jung, J.K. & Zhang, K. 2011, "Finite Element Analyses of Soil-Pipe Behavior in Dry Sand under Lateral Loading", *Reston, VA: ASCE Proceedings Of The Pipelines 2011 Conference, July 23-27, 2011, Seattle, Washington |d 20110000*, , pp. 312-324.

[19] Lancelot, L., Shahrour, I. & Al Mahmoud, M. 2006, "Failure and dilatancy properties of sand at relatively low stresses", *Journal of Engineering Mechanics-ASCE*, vol. 132, no. 12, pp. 1396-1399.

[20] Lings, M. L., and Dietz, M. S. 2004, "An Improved Direct Shear Apparatus for Sand." *Geotechnique*, Vol. 54, No. 4, pp. 245-256.

[21] Mayne, P. W., Kulhawy, F. H., Kay, J. N. 1991, "Observations on the development of pore-water stresses during piezocone penetration in clays", *Canadian Geotechnical Journal*, vol. 27, no. 4, pp. 418–428

[22] Ovesen, N. K. 1964, "Anchor slabs, calculation methods and model tests." *Bulletin No. 16*, The Danish Geotechnical Institute, Copenhagen, Denmark.

[23] Paulin, M. J. 1998, "An investigation into pipelines subjected to lateral soil loading." PhD thesis, Memorial Univ. of Newfoundland, St. John's, Canada.

[24] Pike, K., Kenny, S. & Hawlader, B. 2013, "Advanced analysis of pipe/soil interaction accounting for strain localization", *Proceeding, GéoMontréal 2013, the 66th Canadian Geotechnical Conference and the 11th Joint CGS/IAH-CNC Groundwater Conference*.

[25] Ponce, V.M. & Bell, J.M. 1971, "Shear Strength of Sand at Extremely Low Pressures", *Journal of the Soil Mechanics and Foundations Division*, vol. 97, no. 4, pp. 625-638.

[26] Pradhan, T.B.S., Tatsuoka, F. & Horii, N. 1988, "Strength and deformation characteristics of sand in torsional simple shear", *SOILS AND FOUNDATIONS*, vol. 28, no. 3, pp. 131-148.

[27] PRCI Report 2003, "Extended Model for Pipe Soil Interaction*"* C-CORE and Doug Honegger, D.G. Honegger Consulting, St. John's, NL, Canada.

[28] Ranjan, G. & Arora, V. B. 1980, "Model studies on anchors under horizontal pull in clay", *Proc 3rd Australia-New Zealand Conference on Geomechanics, Wellington, 12–16 May 1980,* vol. 1, pp. 65–70.

[29] Rizkalla, M., Poorooshasb, F., and Clark, J. I. 1992, "Centrifuge modelling of lateral pipeline/soil interaction." *Proc., 11th Offshore Mechanics and Arctic Engineering Symp*.

[30] Scarpelli, G., Sakellariadi, E., & Furlani, G. 1999, "Longitudinal pipeline-soil interaction: results from field full scale and laboratory testing", *Twelfth European Conference on Soil Mechanics and Geotechnical Engineering* , pp. 511.

[31] Schanz, T. & Vermeer, P. A. 1996, "Angles of friction and dilatancy of sand", *Geotechnique,* vol. 46(1), pp 145–151

[32] Stroud, M.A. 1971, "The Behavior of Sand at Low Stress Levels in the Simple Shear Apparatus", PhD thesis, University of Cambridge.

[33] Tatsuoka, F., Sakamoto, M., Kawamura, T., Fukushima, S. 1986, "Strength and deformation characteristics of sand in plane strain compression at extremely low pressures", *Soils and Foundations,* vol. 26, no. 1, pp. 65–84.

[34] Trautmann, C. 1983, "Behavior of pipe in dry sand under lateral and uplift loading", PhD thesis, Cornell University, Ithaca, NY.

[35] Trautmann, C.H. & O'Rourke, T.D. 1985, "Lateral Force-Displacement Response of Buried Pipe", *Journal of Geotechnical Engineering,* vol. 111, no. 9, pp. 1077-1092.

[36] Turner, J.E. 2004, 'Lateral force-displacement behavior of pipes in partially saturated sand", M.S. Thesis, Cornell University, Ithaca, NY.

[37] Vesic, A.S. 1969, "Breakout Resistance of Objects Embedded in Ocean Bottom", Duke Univ, Durham, NC, USA.

[38] Wijewickreme, D., Karimian, H. & Honegger, D. 2009, "Response of buried steel pipelines subjected to relative axial soil movement", *Canadian Geotechnical Journal,* vol. 46, no. 7, pp. 735-735.

[39] Xie, X. 2008, "Numerical analysis and evaluation of buried pipeline response to earthquake-induced ground fault rupture", PhD thesis, Rensselaer Polytechnic Institute, New York.

[40] Yimsiri, S., Soga, K., Yoshizaki, K., Dasari, G. & O'Rourke, T. 2004, "Lateral and upward soil-pipeline interactions in sand for deep embedment conditions", *Journal of Geotechnical and Geoenvironmental Engineering,* vol. 130, no. 8, pp. 830-842.

APPENDIX B

Finite Element Modeling of Uplift Pipeline/Soil Interaction in Dense Sand

This paper has been published and presented in 6th Canadian Geohazards Conference (Geohazards6), Kingston, Ontario, Canada, 2014. Most of the research work presented in this paper was conducted by the first author. He also prepared the draft manuscript. The other authors supervised the research and reviewed the manuscript.

Finite Element Modeling of Uplift Pipeline-Soil Interaction in Dense Sand

Kshama Roy, Bipul Hawlader
Memorial University of Newfoundland, St. John's, NL, Canada
Shawn Kenny
Carleton University, Ottawa, ON, Canada
Ian Moore
Queen's University, Kingston, ON, Canada

ABSTRACT
Buried pipelines are one of the most efficient and popular methods to transport natural gas and petroleum products. Geohazards and the associated ground movement represent a significant threat to pipeline integrity that may result in pipeline damage and potential failure. Pipelines are often buried at shallow depth and therefore the behaviour of soil at low stress level needs to be considered for proper modeling of the pipeline response when subjected to upward movement. In this study, finite element (FE) modeling of pipeline-soil interaction is presented, where the stress-stain behaviour of soil at low stress level, including post-peak softening, is implemented. At first, triaxial test results are simulated to validate the proposed model and numerical techniques. Pipeline-soil interaction in the plane strain condition is then simulated for uplift loading. The Arbitrary Lagrangian-Eulerian (ALE) method available in Abaqus/Explicit is used for FE modeling. One of the main advantages of this method is that it can simulate large deformation behaviour. The variation of non-dimensional uplift force with non-dimensional displacement is examined for different depths of embedment.

RÉSUMÉ
Canalisations enterrées sont l'une des méthodes les plus efficaces et les plus populaires pour le transport de gaz naturel et de produits pétroliers. Aléas géologiques et les mouvements au sol associée représentent une menace importante pour l'intégrité du pipeline qui peut entraîner des dommages causés au pipeline et l'échec potentiel. Les pipelines sont souvent enterrés à faible profondeur et donc le comportement de sol à faible niveau de stress doit être pris en considération pour une bonne modélisation de la réponse du pipeline lorsqu'il est soumis à un mouvement vers le haut. Dans cette étude, éléments finis (FE) la modélisation de l'interaction pipeline - sol est présentée, où le comportement contrainte - tache de sol à faible niveau de stress, y compris post-pic ramollissement, est mis en œuvre. Dans un premier temps, les résultats des tests triaxiaux sont simulées pour valider le modèle proposé et les techniques numériques. Interaction pipeline - sol à l'état de déformation plane est ensuite simulé pour le soulèvement de chargement. La méthode disponible dans Abaqus/ Explicit arbitraire Lagrange - Eulerian (ALE) est utilisé pour la modélisation FE. L'un des principaux avantages de cette méthode est qu'elle permet de simuler le comportement de déformation importante. La variation de la force de soulèvement non - dimensionnelle avec un déplacement non - dimensionnelle est examinée pour différentes profondeurs de l'encastrement.

1 INTRODUCTION

Energy pipelines are one of the most efficient and popular ways to deliver natural gas and petroleum products from field development areas to market. The liquid hydrocarbon and natural gas products are usually transported through buried pipelines, which traverse large distances through a variety of soils. Geohazards and the associated ground movement represent a significant threat to pipeline integrity that may result in pipeline damage and potential failure. In certain situations, pipelines can be exposed to potential ground failures such as surface faulting, liquefaction-induced soil movements, and landslide induced permanent ground deformation (PGD). These ground movements might cause excessive stresses in pipelines and pipelines might be damaged. Therefore, both pipeline integrity and safety are major concerns for pipeline operators and agencies.

Theoretical and experimental studies were conducted in the past to determine the forces on pipelines or anchor plates for upward movement, namely Trautmann, 1983; Dickin, 1988; Schaminee et al., 1990; Ng and springman, 1994; Hsu and Liao, 1997; Hsu and Liao, 1998; Bransby et al., 2001; White et al., 2001; Palmer et al., 2003; El-Gharbawy, 2006; Chin et al., 2006; Schupp et al., 2006; Byrne et al., 2008; Cheuk et al., 2008; Wang et al., 2009; Chen and Chu, 2010; Chou et al., 2011; Chen et al., 2012; Kumar and Naskar, 2012; Horikawa et al., 2012; Shinkai et al., 2012; Williams et al., 2013, Chakraborty and Kumar, 2013; Jung et al., 2013. Schaminee et al. (1990) identified that for uplift loading, dilatant soil such as dense sand shows a stiff initial response up to the peak resistance which is followed by post-peak softening. Sherif (2006) conducted several model tests for uplift movement of pipe to investigate the response of pipeline buried in loose silty sand. Cheuk et al. (2008) presented a set of model test results for uplift resistance. In these tests a novel image analysis technique based on particle image velocimetry (PIV) and close range photogrammetry were used to track the soil movement. Based on these results, four stages of soil deformation mechanisms are proposed. In order to understand the mechanism further, FE analyses in the

Lagrangian framework have also been performed (e.g. Yimsiri et al., 2004; Daiyan et al., 2011; Xie, 2012; Jung et al., 2013). Yimsiri et al. (2004) conducted a comprehensive FE analysis using Abaqus/Standard FE software with the Mohr-Coulomb and Nor-Sand soil constitutive models. The degradation of soil strength parameters after the peak was not considered in that study.

Pipelines are often buried at shallow depth and therefore the stresses in the soil around the pipe before any movement are generally lower than typical geotechnical problems such as foundations. Therefore, the behaviour of soil masses around the pipeline at low stress level needs to be considered.

The main focus of the present study is to simulate the response of buried pipelines in dense sand. Although limited, some experimental studies on dense sand at low stress level are available in the literature (e.g. Ponce and Bell, 1971; Stroud, 1971; Ahmed, 1973; Fukushima and Tatsuoka, 1984; Tatsuoka et al., 1986; Lancelot, 2006). Ponce and Bell (1971) showed that sand exhibits a strong increase in friction and dilatancy angles when the confining pressure decreases in triaxial tests. However, Fukushima and Tatsuoka (1984) found a weaker variation.

Another important experimental observation is that the behaviour of sand differs in triaxial and simple shear conditions. For example, Ahmed (1973) conducted tests on crushed silica sand in drained triaxial (TX) and plane strain (PS) loading conditions. The peak friction angle (ϕ'_p) obtained from his test results are shown in Fig. 1. Three key features of these test results need to be mentioned. Firstly, the peak friction angle for the plane strain condition ($\phi_p'^{PS}$) is higher that the peak friction angle in the triaxial condition ($\phi_p'^{TX}$), and the value of $\phi_p'^{PS} - \phi_p'^{TX}$ is higher at low stress level. Secondly, both $\phi_p'^{PS}$ and $\phi_p'^{TX}$ increase with increase in relative density. Finally, the peak friction angle decreases with increase in confining pressure.

The main objective of the present study is to analyze pipeline-soil interaction during uplift of buried pipes in dense sand. An advanced simulation tool suitable for large deformation analysis is used for the FE analyses. A modified Mohr-Coulomb (MC) model with confining pressure dependent peak friction angle and dilation angle is used. In addition, the dependency of mobilized friction angle (ϕ') and dilation angle (ψ) on engineering plastic shear strain (γ_p) is used to simulate strain hardening and softening behaviour for dense sand. The uplift resistance from the present FE analyses is compared with available experimental results.

2 MODELING OF SOIL BEHAVIOUR

The Mohr-Coulomb model is one of the simple models that reasonably represent the behaviour of sand. It has been used by many researchers in the past for pipeline-soil interaction analysis. In this study, a modified form of Mohr-Coulomb model is used incorporating the following key features as observed in laboratory tests.

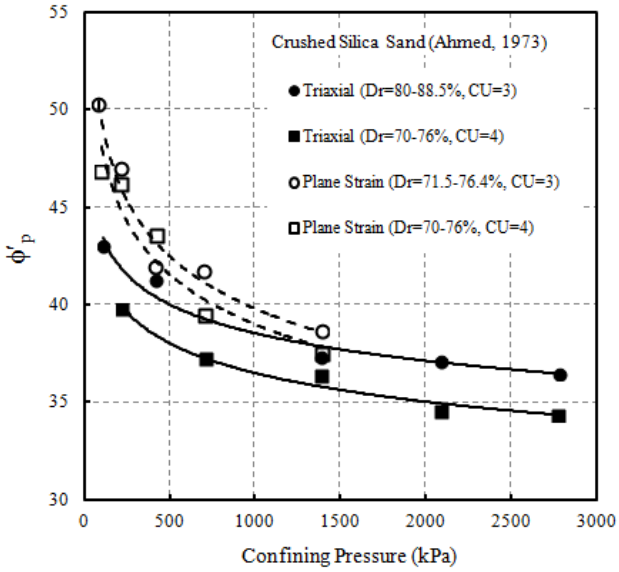

Figure 1. Test results for crushed silica sand (after Ahmed, 1973)

2.1 Angle of internal friction in PS conditions

Pipeline-soil interaction in plane strain condition is simulated in this study. The strength of sand is usually characterized by the angle of internal friction. Kulhawy and Mayne (1990) compiled a large volume of test data and showed that, in general, the peak friction angle of dense sand in PS is approximately 10% to 20% higher than the TX condition. Experimental results on dense sands also show that $\phi_p'^{PS}$ is more than 5° higher than $\phi_p'^{TX}$ (Schanz and Vermeer, 1996). Furthermore, experimental evidence shows that ϕ'_p decreases with increase in mean effective stress at failure (p'), and generally follows a linear relation with lnp'. Bolton (1986) analyzed the strength and dilatancy of 17 sands in TX and PS tests and proposed the following empirical relations:

$$\phi_p'^{TX} - \phi_c'^{TX} = 3I_R \qquad \text{for triaxial} \qquad [1]$$

$$\phi_p'^{PS} - \phi_c'^{PS} = 5I_R \qquad \text{for plane strain} \qquad [2]$$

Where I_R is the relative density index defined as $I_R = I_D(Q - \ln p' - R$ with I_D=relative density (=D_r(%)/100). The subscripts p and c represent the peak and critical state, respectively. Bolton (1986) also showed that the values of Q=10 and R=1 fit most of the test data, although it might vary with type of sand and p' (Chakrabarty and Salgado 2010). As triaxial tests are widely used for geotechnical characterization, appropriate care need to be taken for estimation of ϕ'_p for pipeline-soil interaction analysis in plane strain condition. It is to be noted here that a similar attempt has been taken to estimate $\phi_p'^{PS}$ from direct shear test results (Lings and Dietz, 2004) and showed that $\phi_p'^{PS}$ is approximately 5 degrees higher than the peak friction angle obtained from direct shear test.

Equation 2 is used to model pipeline-soil interaction in PS condition in the present study, although the authors understand that additional laboratory tests at low p' are required to check the validity of this equation further.

Unlike ϕ'_p, the critical state friction angles may not differ considerably in PS and TX conditions. Experimental evidence shows that $\phi_c^{'PS}$ is few degrees higher than $\phi_c^{'TX}$. Bishop (1961) and Conforth (1964) conducted drained tests on sands over a range of densities at a wide range of confining pressure and showed that $\phi_c^{'PS}$ is approximately 4° higher than $\phi_c^{'TX}$. Similar results were obtained from laboratory tests on Toyoura sand (Tatsuoka et al., 1986; Pradhan et al., 1988), and have shown that $\phi_c'^{PS} \approx 34.5° - 38°$ while $\phi_c'^{TX} \approx 33°$.

The maximum dilation angle (ψ_p), which occurs at the peak shear strength, are related to the peak and critical state friction angles in plane strain condition as (Bolton 1986):

$$\phi_p'^{PS} = \phi_c'^{PS} + 0.8\psi_p \qquad [3]$$

In this study, $\phi_c'^{TX} = 31°$ and $\phi_c'^{PS} = 35°$ are used.

2.2 Stress-strain behaviour of dense sand

In the modified Mohr-Coulomb model, the mobilized shear strength parameters (ϕ' and ψ) are varied with accumulated plastic shear strain (γ_p) as shown in Fig. 2. In the pre-yield zone, both ϕ' and ψ increase from (ϕ'_{in} and ψ_{in}) to the peak values at γ_p^p, and therefore strain hardening occurs in this zone.

Experimental evidence shows that the plastic strain at peak, γ_p^p decreases with increasing relative density and increases with increasing p'. For example, from direct shear tests, Lings and Dietz (2004) showed that for a dense sand (D_r=90%) the peak friction angle is mobilized at horizontal displacement of 1.5 mm and 3.5 mm under normal stress of 25 kPa and 251 kPa, respectively. In order to capture the non-uniqueness of γ_p^p, in this study the behaviour is defined as:

$$\gamma_p^p = \gamma_p^c \left(p'/p'_a\right)^{0.252} \qquad [4]$$

$$\gamma_c^p = \left(22.1 - 11.2D_r\right)/100 \qquad [5]$$

where γ_c^p = strain softening parameter, which is explained further in the following sections, and p'_a= reference pressure = 100 kPa.

The following sine function is then used to model the variation of mobilized ϕ' and ψ in the pre-yield zone.

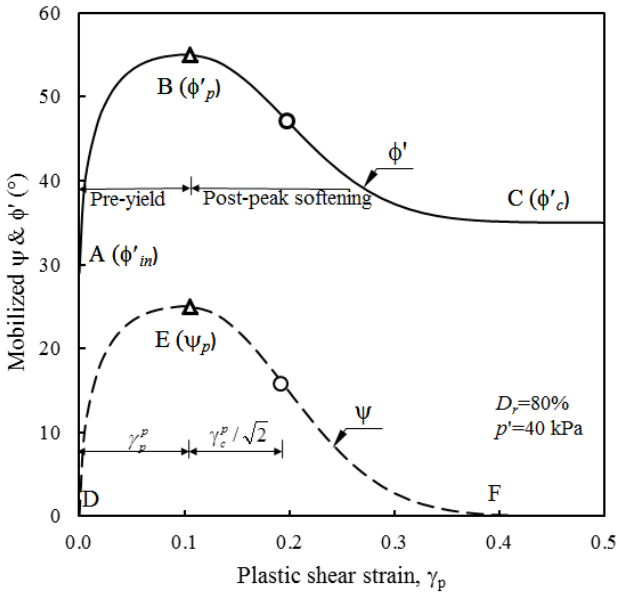

Figure 2. Modeling of stress-strain behaviour of dense sand

$$\phi' = \phi'_{in} + \sin^{-1}\left[\left(\frac{2\sqrt{\gamma^p \gamma_p^p}}{\gamma^p + \gamma_p^p}\right)\sin\left(\phi'_p - \phi'_{in}\right)\right] \qquad [6]$$

$$\psi = \sin^{-1}\left[\left(\frac{2\sqrt{\gamma^p \gamma_p^p}}{\gamma^p + \gamma_p^p}\right)\sin\left(\psi_p\right)\right] \qquad [7]$$

The value of ψ_p can be calculated using Eq. 3. The lines AB and DE in Fig. 3 show the variation of ϕ' and ψ, respectively, in the pre-yield zone for D_r=80% and p'=40 kPa.

If the shearing is continued, both ϕ' and ψ will decrease with plastic strain as shown in Fig. 2. This zone is referred as "post-peak softening zone." The following exponential functions are used to define the curve BC and EF to model the variation of ϕ' and ψ, respectively.

$$\phi' = \phi'_c + \left(\phi'_p - \phi'_c\right)\exp\left[-\left(\frac{\gamma^p - \gamma_p^p}{\gamma_c^p}\right)^2\right] \quad \text{curve BC} \quad [8]$$

$$\psi = \psi_p \exp\left[-\left(\frac{\gamma^p - \gamma_p^p}{\gamma_c^p}\right)^2\right] \quad \text{curve EF} \quad [9]$$

The strain softening parameter γ_c^p controls the shape of the post-peak curves. After some algebraic calculation, it can be shown from Eqs. (8) and (9) that the point of inflection of the post-peak softening curve occurs at a shear strain of $\gamma_c^p/\sqrt{2}$ greater than γ_p^p which is shown by the open circle in Fig. 2. It is to be noted here that the

modified Mohr-Coulomb model with strain dependent ϕ' and ψ have also been used in the past for modeling dense sand. Anastaspoulos et al. (2007) used a simple straight line to model post-peak degradation. Jung et al. (2013) used that concept for pipeline-soil interaction analysis. In those studies, pre-yield behaviour was not considered, rather the stress-strain behaviour before the peak was assumed to be elastic.

The soil constitutive model is then implemented in Abaqus/Explicit using a user subroutine written in FORTRAN.

3 PERFORMANCE OF SOIL CONSTITUTIVE MODEL

In order to show the performance of the soil constitutive model described in the previous sections and also to validate the present FE implementation, a set of triaxial test results (Hsu and Liao, 1998) are simulated first. The FE simulation is performed for consolidated isotropically drained triaxial tests on dense sand (D_r=70%) for a wide range of confining pressures of 20-320 kPa. The value of $\phi_c'^{TX} = 31°$ is used. The variation of $\phi_p'^{TX}$ is defined by using Eq. (1). The calculated deviatoric stress and volumetric strain are shown in Fig. 3, which show that the proposed soil constitutive model can successfully simulate the stress-strain behaviour of dense sand for a wide range of confining pressures including the low stress levels, which is the interest of the present study in pipeline-soil interaction modeling. These observations provide confidence in the modeling approach and numerical procedures implemented in Abaqus/Explicit FE analysis.

4 FINITE ELEMENT FORMULATION

Two-dimensional pipeline-soil interaction analyses are performed using the Arbitrary Lagrangian-Eulerian method available in Abaqus/Explicit 6.10 EF1. The main advantages of using Abaqus/Explicit over Abaqus/Standard is that the pipe can be moved sufficiently large distance avoiding numerical issues due to mesh distortion as encountered in the Abaqus/standard, especially in the zone of shear strain localization in the shear bands. Therefore, the formation of shear band can be better simulated in Abaqus/Explicit.

Figure 4 shows the typical FE model used in this study. Taking the advantage of symmetry, only half of the domain is modeled. The depth of the pipe is measured in terms of *H*/*D* ratio, where *H* is the depth from the top of the soil to the center of the pipe and *D* is the external diameter of the pipe. The centre of the pipe is placed at 2D above the bottom boundary. The thickness of soil above the centre of the pipe varies with *H*/*D* ratio. For example, in the simulation of *H*/*D*=4, the distance from the centre to the ground surface is 400 mm for D=100 mm. The left boundary is placed at 2.5 D from the pipe. The distances from the pipe to the bottom and left boundaries are sufficiently large and therefore boundary effects on predicted uplift resistance, displacement and soil failure mechanisms are not found. This is verified from a number of FE analyses, setting these boundaries at larger distances than that shown in Fig. 4.

For FE modeling of soil, 4-node bilinear plane strain quadrilateral, reduced integration, hourglass control element (CPE4R) is used. The pipe is modeled as a rigid body. Abaqus/cae is used to generate the finite element mesh. The structured mesh, as shown in Fig 4, is generated by zoning the soil domain. Denser mesh is used near the pipe. The total number of elements and shapes can be defined in the structured mesh, which cannot be done in the auto generated default meshing option in Abaqus. In this study, structured mesh is used because it gives better results, less numerical issues and computationally efficient than with auto generated mesh.

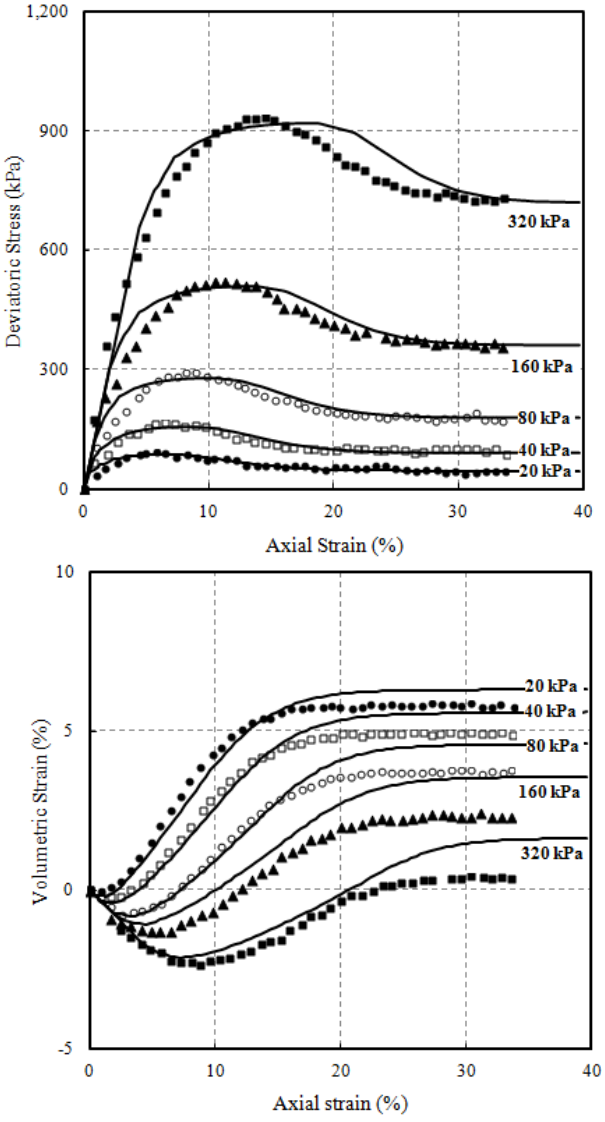

Figure 3. Comparison between FE and laboratory test results of Hsu and Liao (1998)

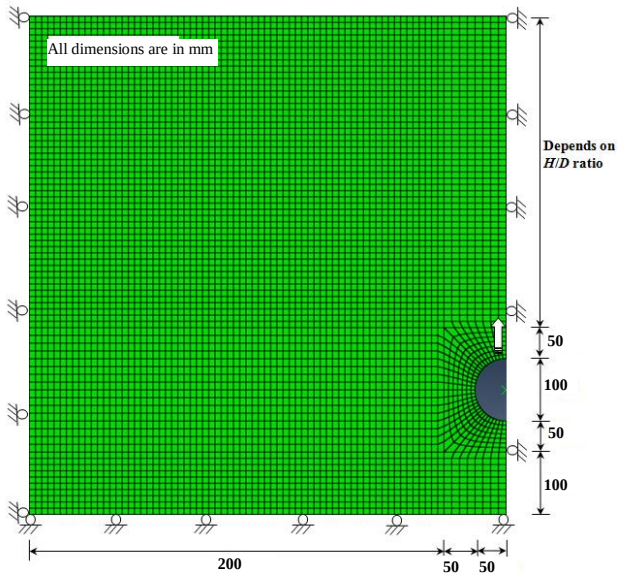

Figure 4. Typical finite element mesh

The bottom of the FE domain is restrained from any vertical movement, while all the vertical faces are restrained from any lateral movement using roller supports (Fig. 4). No displacement boundary condition is applied on the top face, and therefore the soil can move freely.

The interface between pipe and soil is simulated using the contact surface approach available in Abaqus/Explicit. The Coulomb friction model is used for the frictional interface between the outer surface of the pipe and sand. In this method, the friction coefficient (μ) is defined as $\mu=\tan(\phi_\mu)$, where ϕ_μ is the pipeline-soil interface friction angle. The value of ϕ_μ depends on the interface characteristics and relative movement between the pipe and soil. The larger value of ϕ_μ represents the characteristics of rough uncoated pipes with rusty or corroded surfaces, while the lower values would correspond to pipes with smooth coating. The value of ϕ_μ varies between $\phi_p^{'TX}$ and $\phi_p^{'TX}/2$ (Yimsiri et al, 2004). The value of μ equal to 0.32 is used in this study.

The numerical analysis is conducted in two main steps. The first step is a geostatic stress step that accounts for the effects of soil weight and defines the initial stress state in the soil. The initial stress or the geostatic stress step definition is very important for pipeline-soil interaction analyses. It is to be noted here that if the geostatic condition is not properly modeled with appropriate initial stress condition, the response in subsequent loading might be erroneous and/or additional numerical issues might be encountered, because the behavior of sand is effective stress dependent. In this study, it has been properly defined and the calculated stresses at the end of geostatic step are same as expected in situ stress.

In the second step, the pipe is moved in the upward direction specifying a displacement boundary condition at the reference point of the pipe.

5 SIMULATION OF PIPELINE-SOIL INTERACTION

After verification of soil constitutive model performance in triaxial condition, FE simulations are performed for pipelines buried in dense sand (D_r=80%) under uplift loading in plane strain condition. The FE results are first verified with the results of model tests conducted by Trautmann (1983). These test results have also been used by previous researchers to validate numerical modeling performance. For example, Yimsiri et al. (2004) reanalyzed the direct shear test results presented by Trautmann and O'Rourke (1983) for estimation of soil parameters and used $\phi'_c = 31°$ in their FE analyses. As mentioned before that ϕ' in PS is higher than ϕ' in triaxial and direct shear test (Pradhan et al., 1988; Lings and Dietz, 2004) a value of $\phi'_c = 35°$ is used in the present study. The peak friction angle is calculated using Eq. (2) with a maximum value of $\phi'^{PS}_p - \phi'^{PS}_c$ equal to 20° as suggested by Bolton (1986). The unit weight of dry sand used for model test was 17.7 kN/m^3 that corresponds to a relative density of 80%. A Poisson's ratio of 0.2 is used, which is considered as the best representative value for dense sand (Jefferies and Been, 2006). The modulus of elasticity (E) is varied with initial mean effective stress (σ_m) as $E = E_0\left(\sigma_m / \sigma_{m(ref)}\right)^n$, where E_0 is the value of E at reference pressure ($\sigma_{m(ref)}$), and n is a material constant. Parameters used in the FE analysis are summarized in Table 1.

Table 2: Soil Parameters used in the FE analysis

Parameter	Values
External diameter of pipe, D	100 mm
Poisson's ratio, ν_{pipe}	0.3
E_0	15,000 kN/m^2
n	0.5
$\sigma_{m(ref)}$	100 kN/m^2
Poisson's ratio, ν_{soil}	0.2
Critical state friction angle, ϕ'_c	35°
Unit weight, γ	17.7 kN/m^3
Interface friction co-efficient, μ	0.32
Depth of pipe, H/D	1.5, 4 & 8

6 RESULTS

The solid lines in Fig. 5 show the variation of dimensionless force ($F/\gamma HD$) with dimensionless upward displacement (v/D) from the initial position for three burial depths (H/D=1.5, 4 and *8*). As shown, the force on the pipe increases with displacement and reaches to the peak and then decreases in the post-peak zone. In order to show the performance of the present FE model, the force-displacement curves obtained in the full-scale tests (Trautmann, 1983) are also plotted in Fig. 5. The present FE model can successfully simulate the trend of force-displacement curves, although in the FE analyses for lower H/D (=1.5 & 4) the peak resistance is developed at larger displacement and the rate of post-peak softening is

slower than that observed in the full-scale tests. In the present FE analyses, the exact conditions of the tests, including soil properties, may not be properly simulated. Moreover, the soil around the pipe is relatively at very low stress level because these tests were conducted at shallow depths. As mentioned before, the modeling of stress-strain behaviour of soil at such low stress level is difficult. These might be some causes of discrepancy between the force-displacement curves obtained from the full-scale tests and FE analyses.

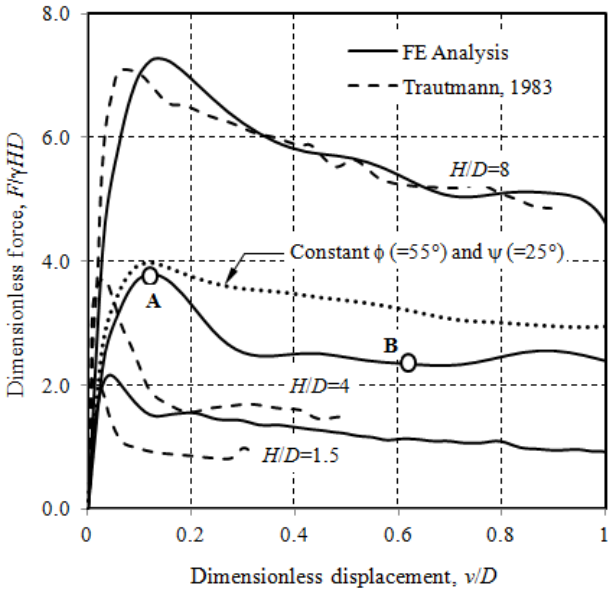

Figure 5. Comparison of FE results with the large scale test results (Trautmann, 1983)

One of the key questions is whether the post-peak softening behavior of soil, as shown in Fig. 2, is important for modeling uplift behavior of pipeline. To show that, FE simulation is performed for constant values of ϕ' (=55°) and ψ (=25°) for *H*/*D*=4. The force-displacement curve is shown in Fig. 5. Note that, these values should be carefully selected that should be representative of average values of ϕ' and ψ although they actually vary with strain. In general, the values of ϕ' and ψ should be lower than the peak and higher than critical state. Number of previous studies simulated the response using such constant values. As shown in Fig. 5 that constant ϕ' and ψ cannot simulate the force-displacement curves properly, especially the post-peak zone. There is a slight decrease in uplift force after the peak because the burial depth is reduced with upward movement of the pipe. However, it is significantly different from the observed softening in the full-scale tests. Therefore, the post-peak stress-strain behaviour of soil needs to be incorporated in the FE analyses for better simulation.

Figure 6 shows the mobilized ϕ' and ψ for *H*/*D*=4 at a very large displacement (*v*/*D*=0.62). The point B in Fig. 5 shows the location. As shown in Fig. 6, ϕ' and ψ mainly vary in a wedge of soil above the pipe where plastic shear strain is developed. Outside this wedge the soil is elastic. The soil elements around the shear band (shown by dashed line) reach to the critical state ($\phi'=\phi'_c$ and $\psi=0$) because of significant plastic shear strain. Therefore, the soil block right side of this band mainly moves upward due to upward movement of the pipe. Not only in the shear band, a zone of soil above the pipe, is also reached to the critical state. Therefore, the soil moves easily into the void under the pipe at this stage.

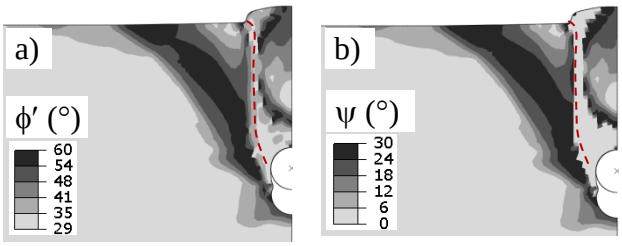

Figure 6. Contour plot of ϕ' and ψ for *H*/*D*=4 and *D*=100mm at v/D=0.62

7 CONCLUSIONS

The pipeline-soil interactions associated with relative movement of the pipeline in the vertical upward direction is numerically investigated in this study. The FE simulations are performed for two-dimensional plane strain condition. The key features considered in modeling of the behaviour of dense sands are: (i) the decrease of peak friction angle with increase in effective stress at failure, (ii) an improved stress-strain behaviour of dense sand, including the pre-yield hardening and post-peak softening with plastic shear strain; and (iii) plane strain strength parameters, which are different from triaxial or direct shear strength parameters. The FE modeling is performed using Abaqus/Explicit FE software, which can simulate even large strain response utilizing adaptive meshing techniques.

The present FE model can simulate successfully the triaxial test results for a wide range of confining pressures, including the tests under low confining pressures.

For pipelines, the calculated force-displacement curves match well with model test results of Trautmann (1983). The peak dimensionless force increases with increase in burial depth ratio (*H*/*D*). The results obtained from the present FE analyses are consistent with previous studies.

ACKNOWLEDGEMENTS

The work presented in this paper was funded by the Research and Development Corporation (RDC), Newfoundland and Labrador and NSERC Discovery and CRD grants.

REFERENCES

Ahmed, S.M.U. 1973, “A study of the influence of confining pressure on the behaviour of sands”, M.Sc. Thesis, McGill University, Montreal, Canada.

Anastasopoulos, I., Gazetas, G., Bransby, M., Davies, M. & El Nahas, A. 2007, "Fault rupture propagation through sand: Finite-element analysis and validation through centrifuge experiments", *Journal of Geotechnical and Geoenvironmental Engineering,* vol. 133, no. 8, pp. 943-958.

Bishop, A. W. 1961, "Discussion on soil properties and their measurement", *Proceedings of 5th Int. Conf. on Soil mechanics and Foundation engineering* vol. III.

Bolton, M. D. 1986, "The strength and dilatancy of sands", *Geotechnique*, vol. 36, no. 1, pp. 65-78.

Bransby, M. F., Newson, T. A., Brunning, P., and Davies, M. C. R. 2001, "Numerical and centrifuge modeling of the upheaval resistance of buried pipelines." *Proc., 20th Int. Conf. on Offshore Mechanics and Arctic Engineering*, Rio de Janeiro, Brazil.

Byrne, B. W., Schupp, J., Martin, C. M., Oliphant, J., Maconochie, A. & Cathie, D. 2008, "Experimental modeling of the unburial behaviour of pipelines." *Proc. Offshore Technol. Conf.*, Houston, TX, paper OTC-2008-19573.

CEPA (The Canadian Energy Pipeline Association 2013, Retrieved from: http://www.cepa.com/.

Chakraborty, T. & Salgado, R. 2010, "Dilatancy and Shear Strength of Sand at Low Confining Pressures", *Journal of Geotechnical and Geoenvironmental Engineering,* vol. 136, no. 3, pp. 527-532.

Chakraborty, D. & Kumar, J. 2014, "Vertical Uplift Resistance of Pipes Buried in Sand", *Journal of Pipeline Systems Engineering and practice,* vol. 5, no. 1, 04013009.

Chen, Y. & Chu, T. 2012, "Evaluation of uplift interpretation criteria for drilled shafts in gravelly soils", *Canadian Geotechnical Journal,* vol. 49, pp. 70-77.

Cheuk, C. Y., White, D. J. & Bolton, M. D. 2008, "Uplift mechanisms of pipes buried in sand." *J. Geotech. Geoenviron. Engg* 134, No. 2, pp. 154–163.

Chin, E. L., Craig, W. H., and Cruickshank, M. 2006, "Uplift resistance of pipelines buried in cohesionless soil." *Proc., 6th Int. Conf. on Physical Modelling in Geotechnics*. Ng, Zhang, and Wang, eds., Vol.1, Taylor & Francis Group, London, pp. 723–728.

Chou, J.C., Kutter, B.L., Travasarou, T., and Chacko, J.M. 2011. "Centrifuge modeling of seismically induced uplift for the BART Transbay Tube." *Journal of Geotechnical and Geoenvironmental Engineering*, **137**(8): 754–765.

Conforth, D.H. 1964, "Some experiments on the influence of strain conditions on the strength of sand.", *Geotechnique,* vol. 14, pp. 143-167.

Daiyan, N., Kenny, S., Phillips, R. & Popescu, R. 2011, "Investigating pipeline–soil interaction under axial–lateral relative movements in sand", *Canadian Geotechnical Journal,* vol. 48, no. 11, pp. 1683-1695.

Dickin, E.A. & Leung, C.F. 1983, "Centrifugal Model Tests on Vertical Anchor Plates", *Journal of Geotechnical Engineering,* vol. 109, no. 12, pp. 1503-1525.

Dickin, E.A. 1994, "Uplift Resistance of Buried Pipelines in Sand", *Soils and Foundation,* vol. 34, no. 2, pp. 41-48.

El-Gharbawy, S. 2006, "Uplift Capacity of Buried Offshore Pipelines." *Proceedings of the Sixteenth International Offshore and Polar Engineering Conference, San Francisco, California, USA, May 28-June 2, 2006.*

Fukushima, S. & Tatsuoka, F. 1984, "Strength and deformation characteristics of saturated sand at extremely low pressures", *Soils and Foundations,* vol. 24, no. 4, pp. 30-48.

Guo, P. & Stolle, D. 2005, "Lateral pipe-soil interaction in sand with reference to scale effect", *Journal of Geotechnical and Geoenvironmental Engineering,* vol. 131, no. 3, pp. 338-349.

Horikawa, H., Tsunasawa, Y., Shinkai, H. and Suzuki, N. 2012, "Upheaval buckling of small diameter pipelines induced by strong ground shaking." *Proc., 9th Int. Pipeline Conf.,* Calgary, Alberta, Canada.

Hsu, S.T. & Liao, H.J. 1998, "Uplift behaviour of cylindrical anchors in sand", *Canadian Geotechnical Journal,* vol. 35, no. 1, pp. 70-80.

Jefferies, M. & Been, K. 2006, "*Soil liquefaction: a critical state approach",* Taylor & Francis, New York.

Jung, J., O'Rourke, T. & Olson, N. 2013, "Uplift soil–pipe interaction in granular soil", *Canadian Geotechnical Journal,* vol. 50, pp. 744-753.

Kumar, J. & Naskar, T. 2012, "Vertical uplift capacity of a group of two coaxial anchors in a general c–ϕ soil", *Canadian Geotechnical Journal,* vol. 49, pp. 367-373.

Lancelot, L., Shahrour, I. & Al Mahmoud, M. 2006, "Failure and dilatancy properties of sand at relatively low stresses", *Journal of Engineering Mechanics-ASCE,* vol. 132, no. 12, pp. 1396-1399.

Lings, M. L., and Dietz, M. S. 2004, "An Improved Direct Shear Apparatus for Sand." *Geotechnique*, Vol. 54, No. 4, pp. 245-256.

Mayne, P. W., Kulhawy, F. H., Kay, J. N. 1991, "Observations on the development of pore-water stresses during piezocone penetration in clays", *Canadian Geotechnical Journal,* vol. 27, no. 4, pp. 418–428

Ng, C. W. W., and Springman, S. M. 1994, "Uplift resistance of buried pipelines in granular materials." *Centrifuge 94*, Leung, Lee, and Tan, eds., pp. 753–758.

Palmer, A. C. 2003. "Uplift resistance of buried submarine pipelines: Comparison between centrifuge modelling and full-scale tests." *Géotechnique*, 53(10), pp. 877–883.

Pike, K., Kenny, S. & Hawlader, B. 2013, "Advanced analysis of pipe/soil interaction accounting for strain localization", *Proceeding, GéoMontréal 2013, the 66th Canadian Geotechnical Conference and the 11th Joint CGS/IAH-CNC Groundwater Conference*.

Ponce, V.M. & Bell, J.M. 1971, "Shear Strength of Sand at Extremely Low Pressures", *Journal of the Soil Mechanics and Foundations Division,* vol. 97, no. 4, pp. 625-638.

Pradhan, T.B.S., Tatsuoka, F. & Horii, N. 1988, "Strength and deformation characteristics of sand in torsional simple shear", *Soils and Foundations,* vol. 28, no. 3, pp. 131-148.

PRCI Report 2003, "Extended Model for Pipe Soil Interaction" C-CORE and Doug Honegger, D.G. Honegger Consulting, St. John's, NL, Canada.

Schaminée, P. E. L., Zorn, N. F., and Schotman, G. J. M. 1990, “Soil response for pipeline upheaval buckling analyses: full-scale laboratory tests and modeling.” *Proc., 22nd Annual Offshore Technology Conf., OTC6486*, 563–572.

Schupp, J., Byrne, B. W., Eacott, N., Martin, C. M., Oliphant, J., Maconochie, A., and Cathie, D. 2006, “Pipeline unburial behaviour in loose sand.” *Proc., 25th Int. Conf. on Offshore Mechanics and Arctic Engineering*, Hamburg, Germany, OMAE2006-92541.

Schanz, T. & Vermeer, P. A. 1996, "Angles of friction and dilatancy of sand”, *Geotechnique*, vol. 46(1), pp 145–151

Shinkai, H., hatsuda, Y. and Suzuki, N. 2012, “Seismic design guidelines to mitigate upheaval buckling of small diameter pipes.” *Proc., 9th Int. Pipeline Conf.,* Calgary, Alberta, Canada.

Stroud, M.A. 1971, “The Behavior of Sand at Low Stress Levels in the Simple Shear Apparatus”, PhD thesis, University of Cambridge.

Tatsuoka, F., Sakamoto, M., Kawamura, T., Fukushima, S. 1986, "Strength and deformation characteristics of sand in plane strain compression at extremely low pressures”, *Soils and Foundations,* vol. 26, no. 1, pp. 65–84.

Trautmann, C. 1983, “Behavior of pipe in dry sand under lateral and uplift loading”, PhD thesis, Cornell University, Ithaca, NY.

Wang, J., Ahmed, R., Haigh, S. K., Thusyanthan, N. I. & Mesmar, S. 2010, “Uplift resistance of buried pipelines at low coverdiameter ratios.” *Proc. Offshore Technol. Conf.*, Houston, TX, paper OTC-2010-20912.

White, D. J., Barefoot, A. J., and Bolton, M. D. 2001, “Centrifuge modeling of upheaval buckling in sand.” *Int. J. Physical Modeling in Geotechnics*, 2(1), pp. 19–28.

Williams, E.S., Byrne, B.W. & Blakeborough, A. 2013, "Pipe uplift in saturated sand: rate and density effects”, *Geotechnique*, vol. 63(11), pp 946–956.

Wijewickreme, D., Karimian, H. & Honegger, D. 2009, "Response of buried steel pipelines subjected to relative axial soil movement", *Canadian Geotechnical Journal,* vol. 46, no. 7, pp. 735-735.

Xie, X. 2008, “Numerical analysis and evaluation of buried pipeline response to earthquake-induced ground fault rupture”, PhD thesis, Rensselaer Polytechnic Institute, New York.

Yimsiri, S., Soga, K., Yoshizaki, K., Dasari, G. & O'Rourke, T. 2004, "Lateral and upward soil-pipeline interactions in sand for deep embedment conditions", Journal of Geotechnical and Geoenvironmental Engineering, vol. 130, no. 8, pp. 830-842.

APPENDIX C

Effects of Post-peak Softening Behavior of Dense Sand on Lateral and Upward Displacement of Buried Pipelines

This paper has been published and presented in 34th International Conference on Ocean, Offshore and Arctic Engineering (OMAE 2015), St. John's, Newfoundland and Labrador, Canada, May 31–June 5, 2015. Most of the research work presented in this paper was conducted by the first author. He also prepared the draft manuscript. The other authors supervised the research and reviewed the manuscript.

Proceedings of the ASME 2015 34th International Conference on Ocean, Offshore and Arctic Engineering
OMAE2015
May 31-June 5, 2015, St. John's, Newfoundland, Canada

OMAE2015-42138

EFFECTS OF POST-PEAK SOFTENING BEHAVIOR OF DENSE SAND ON LATERAL AND UPWARD DISPLACEMENT OF BURIED PIPELINES

Kshama Roy
PhD Candidate
Memorial University of Newfoundland
St. John's, NL, Canada

Bipul Hawlader
Associate Professor
Memorial University of Newfoundland
St. John's, NL, Canada

Shawn Kenny
Associate Professor
Carleton University
Ottawa, ON, Canada

Ian Moore
Professor and Canada Research Chair in Infrastructure Engineering, GeoEngineering Centre at Queen's – RMC, Queen's University,
Kingston, ON, Canada

ABSTRACT

Buried pipelines are extensively used in onshore and offshore for transportation of hydrocarbons. The response of pipeline due to lateral and upward relative displacements is one of the major concerns in pipeline design. Both physical modeling and numerical analyses have been performed in the past to understand pipeline-soil interaction mechanisms. The numerical analyses are generally performed using finite element (FE) modeling techniques. For the pipelines buried in sand, a large number of analyses available in the literature have been performed using the Mohr-Coulomb model assigning constant values of angle of internal friction (ϕ') and dilation (ψ). However, dense sand shows post-peak softening behavior and the behavior of sand also depends on mode of shearing, such as triaxial (TX), direct shear (DS) or direct simple shear (DSS) conditions. In the present study, FE analysis of buried pipelines in dense sand is presented. The first set of analyses are performed using the built-in Mohr-Coulomb model in Abaqus FE software with constant angles of internal friction and dilation, as typically used in previous FE analysis of pipeline-soil interaction. The second set of analyses are performed using a modified Mohr-Coulomb model where pre-peak hardening, post-peak softening, density and confining pressure dependent friction and dilation angles are considered. The FE analyses are performed using the Arbitrary Lagrangian-Eulerian (ALE) approach available in Abaqus/Explicit FE software. The modified Mohr-Coulomb model is implemented in Abaqus FE software using a user defined subroutine. Shear band formation due to strain localization and failure patterns for both lateral and upward pipeline-soil interactions are discussed from the simulations with MC and MMC models. FE results show that the MMC model can simulate the load-displacement behavior and failure pattern better than the simulations with the MC model.

INTRODUCTION

Buried pipelines are safe, efficient and economic means of transporting large quantities of natural resources over large distances. According to Pipeline 101 [26], the USA has a network of more than 185,000 miles (≈298,000 km) of liquid petroleum pipelines, nearly 320,000 miles (≈515,000 km) of gas transmission pipelines, and more than 2 million miles of gas distribution pipelines. According to the Canadian Energy Pipeline Association (CEPA), in Canada, a network of approximately 115,000 km of underground energy transmission pipelines operates every day transporting oil and natural gas [7]. Pipelines carry a large quantity of energy sources and fuels which need to be kept under controlled conditions to ensure very minimum risks to public and the environments. Geohazards and the associated ground movements represent a significant threat to pipeline integrity that may result in pipeline damage and

failure [22]. In certain situations, pipelines might pass through a zone of potential ground failures, such as surface faulting, liquefaction-induced soil movements, and landslide induced permanent ground deformation (PGD). These ground movements might cause excessive stresses in pipeline and it might be damaged.

Experimental and theoretical studies have been conducted in the past to estimate the forces acting on pipelines due to relative movement of the soil in specific directions, namely axial, lateral and upward (e.g. [4], [6], [8], [9], [11], [13], [15], [17], [18], [23], [24], [25], [28], [32], [33], [34], [35], [37], [38], [39], [40], [41]). On the basis of these extensive research works, several pipeline design guidelines have been developed (e.g. [2], [3], [12]).

The pipelines buried is dense sand is the main focus of the present study. The dashed lines in Figs. 1(a) and 1(b) show some experimental results for the lateral and upward loading, respectively [35]. The force-displacement curves are presented in normalized form, which are discussed further in the following sections. As shown, in both lateral (Fig. 1a) and vertical (Fig. 1b) loading, the dimensionless force increases with dimensionless displacement to the peak and then decreases. The post-peak decrease of the normalized force is high in the vertical loading as compared to the lateral loading. In the present study, it is shown that an appropriate soil constitutive model needs to be incorporated to simulate the force-displacement curves including the post-peak degradation segments.

In the existing design guidelines, sand is assumed to have a constant friction angle to quantify the resistance of soil against the movement of pipes. However, pre-peak hardening, post-peak softening, density and confining pressure dependent angles of internal friction and dilation are the common features of the stress-strain behavior of dense sand [16]. The mode of shearing also significantly influences the behavior ([5], [20], [27]). All these features of the stress-strain behavior of dense sand have not been considered in any of the guidelines or in the available FE modeling. For example, API (2007) recommended an empirical equation for estimating the representative value of ϕ' as a function of relative density (D_r) but did not mention about the pre-peak hardening or post-peak softening. Yimsiri [43] used the built-in Mohr-Coulomb model (MC) in Abaqus with constant ϕ' and ψ. They also conducted FE analyses using the Nor-Sand soil constitutive model. Guo and Stolle [14] and Daiyan [10] considered the effects of mean effective stress (p') and plastic shear strain on ϕ' and ψ but did not incorporate the effects of density on plastic shear strain requires to mobilize the peak value. Robert [29] and Jung ([17], [18]) incorporated the post-peak softening using a linear variation ϕ' and ψ with plastic strain, but did not consider the pre-peak hardening. However, Jung ([17], [18]) showed the importance of using plane strain strength parameters for pipeline-soil interaction modeling.

In the present study FE simulation is performed for buried pipelines in dense sand. The behavior of sand in triaxial and simple shear conditions is different. For example, Ahmed [1] conducted tests on crushed silica sand in drained triaxial (TX) and plane strain (PS) loading conditions and found that the peak

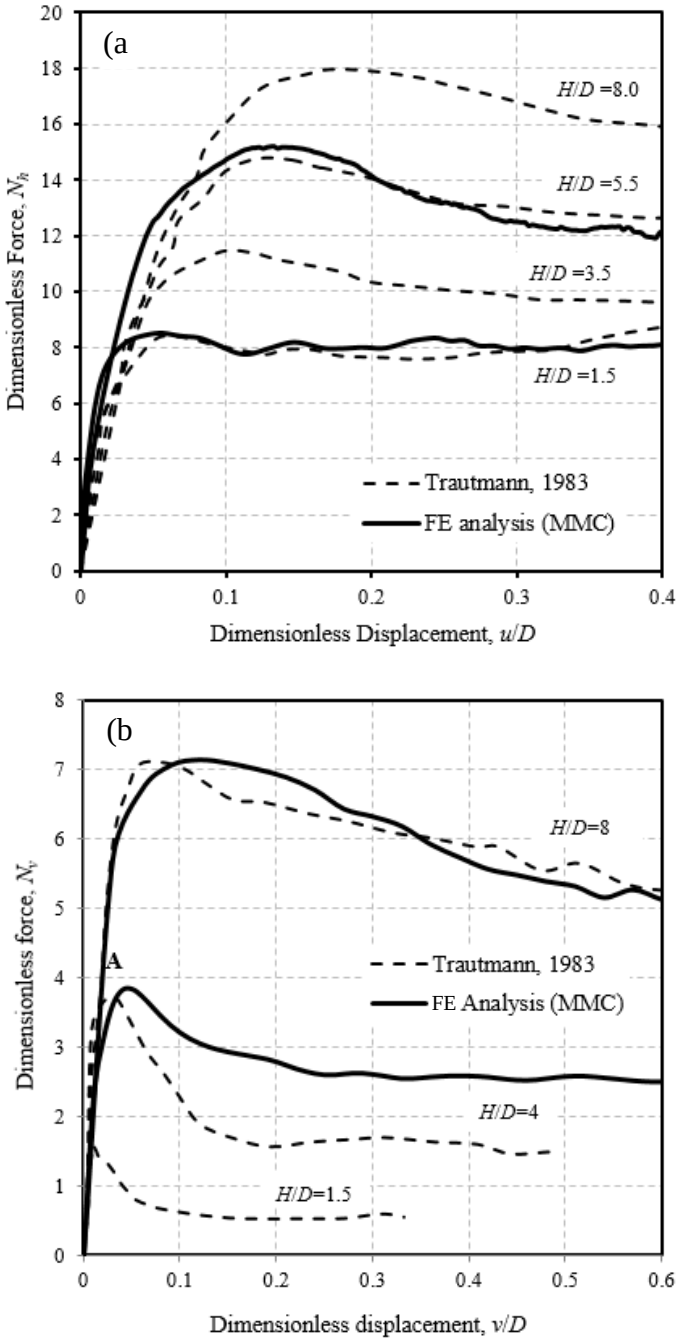

Figure 1. Force-displacement curves for pipe loading tests for D=102mm (a) Lateral (b) Uplift, redrawn from Trautmann [35]

friction angle in plane strain ($\phi_p'^{PS}$) is higher than the peak friction angle in triaxial ($\phi_p'^{TX}$) condition, and the difference between these two (i.e. $\phi_p'^{PS} - \phi_p'^{TX}$) increases with decrease in confining pressure. Moreover, both $\phi_p'^{PS}$ and $\phi_p'^{TX}$ increase with increase in

relative density and the peak friction angle decreases with increase in confining pressure.

FINITE ELEMENT FORMULATION

Two-dimensional pipeline-soil interaction analyses are performed using the Abaqus/Explicit FE software. Figures 2 and 3 show the typical FE models developed for lateral and upward pipeline-soil interaction analyses, respectively. Taking the advantage of symmetry, only half of the domain is modeled for uplift pipeline-soil interaction analyses (Fig. 3). For FE modeling of soil, 4-node bilinear plane strain quadrilateral, reduced integration, hourglass control element (CPE4R) is used. The pipe is modeled as a rigid body.

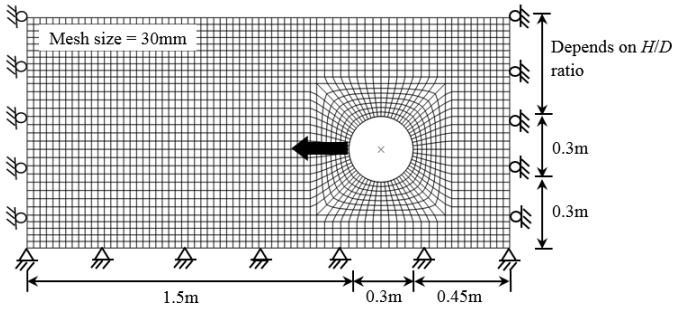

Figure 2. Typical finite element mesh for lateral loading for D=0.3m and H/D=2

The bottom of the FE domain is restrained from any horizontal and vertical movement, while all the vertical faces are restrained from any lateral movement (Figs. 2 and 3). No displacement boundary condition is applied on the top face, and therefore the soil can move freely. The depth of the pipe is measured in terms of H/D ratio, where H is the vertical distance from the top surface of the soil to the center of the pipe and D is the outer diameter of the pipe. As the boundaries are placed at sufficiently large distance, their effects on lateral and uplift resistance, displacement of soil elements and failure mechanisms are not found. This has been verified by a number of FE analyses setting these boundaries at larger distances than that shown in Figs. 2 and 3.

The interface between pipe and soil is simulated using the contact surface approach available in Abaqus/Explicit. The Coulomb friction model is used for the frictional interface between the outer surface of the pipe and sand. In this method, the friction coefficient (μ) is defined as $\mu=\tan(\phi_\mu)$, where ϕ_μ is the pipeline-soil interface friction angle. The value of ϕ_μ depends on the interface characteristics and relative movement between the pipe and soil. The larger value of ϕ_μ represents the characteristics of rough uncoated pipes with rusty or corroded surfaces, while the lower values would correspond to pipes with smooth coating. The value of ϕ_μ varies between $\phi_p'^{TX}$ and $\phi_p'^{TX}/2$ [43]. The value of μ equal to 0.32 is used in this study.

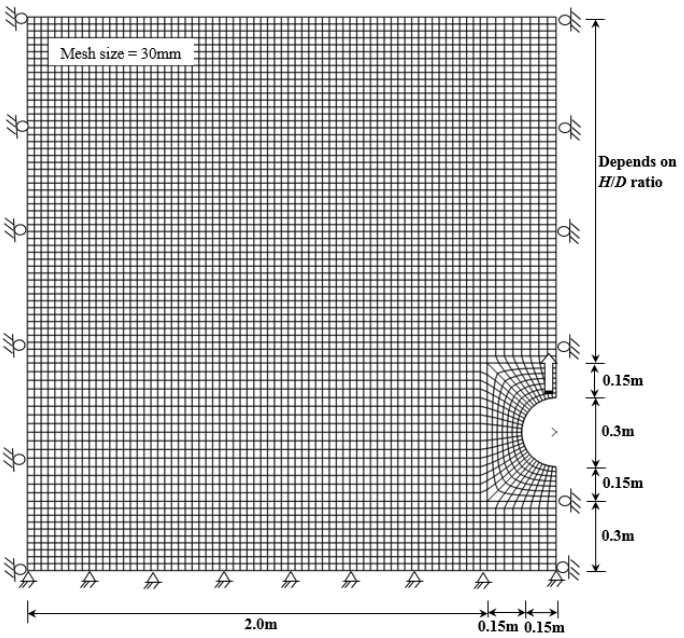

Figure 3. Typical finite element mesh for upward loading for D=0.3m and H/D=6

The numerical analysis is conducted in two main steps. The first step is a geostatic stress step that accounts for the effects of soil weight and defines the initial stress state in the soil. In the second step, the pipe is displaced in the desired direction (lateral or uplift) specifying a displacement boundary condition at the reference point of the pipe.

MODELING OF SOIL BEHAVIOR

One of the key components that significantly influences the success of FE modeling of pipeline-soil interaction is the constitutive behavior of soil ([21], [43]). The Mohr-Coulomb model is one of the simple models that has been used by many researchers in the past for pipeline-soil interaction analysis (e.g. [19], [42], [43]). Two soil strength parameters (ϕ' and ψ) are required to be defined as input parameters for the built-in Mohr-Coulomb model in Abaqus. However, the post-peak softening behavior of dense sand is well-known. In other words, ϕ' and ψ decrease from the peak value with plastic shear strain. In the present study, analyses are performed using two models. In the first one, the built-in Mohr-Coulomb model is used with three sets of ϕ' and ψ values. In the second one, a modified Mohr-Coulomb (MMC) model is used where ϕ' and ψ are varied with plastic shear strain, mean stress and loading condition. A detailed discussion of the MMC model and estimation of model parameters are available in Roy et al. ([30], [31]) and is not repeated here. However, the constitutive equations are summarized in Table 2. The geometry and soil parameters used in the present FE analysis are shown in Table 1.

It is to be noted here that mesh size influences FE simulation results when softening behavior of soil is considered. However, in the present study these issues have not been addressed.

Table 1: Parameters used in FE analyses

Parameters		Values	
		MC	MMC
Outer diameter of pipe, D (mm)		300	
Parameters for Young's modulus	K	150	
	n	0.5	
	p'_a (kN/m^2)	100	
Poisson's ratio, ν_{soil}		0.2	
Parameters for variation of $\phi'$and ψ	A_ψ	-	5
	k_ψ	-	0.8
	ϕ'_{in}	-	29°
	C_1	-	0.22
	C_2	-	0.11
	m	-	0.25
Critical state friction angle, ϕ'_c		-	35°
Relative density, D_r (%)		80	
Unit weight, γ (kN/m^3)		17.7	
Interface friction coefficient, μ		0.32	
Depth of pipe, H/D		Lateral (2, 4, 6, 10) Uplift (2, 4, 6, 8, 10)	
Friction angle for MC model		44°, 39°	-
Dilation angle for MC model		16°, 10°	-

Abaqus does not have any direct option for modeling stress-strain behavior of the proposed MMC model; therefore, it is implemented in a user subroutine VUSDFLD. The stress and strain components are called in the subroutine in each time increment. From the stress components, p' is calculated. The strain components are transferred to the principal strain components and stored as state variables. The plastic strain increment ($\Delta\gamma^p$) in each time increment is calculated as $\Delta\gamma^p = (\Delta\varepsilon_1^p - \Delta\varepsilon_3^p)$, where $\Delta\varepsilon_1^p$ and $\Delta\varepsilon_3^p$ are the major and minor principal plastic strain components, respectively. The value of γ^p is calculated as the sum of $\Delta\gamma^p$ over the period of analysis. In the subroutine, γ^p and p' are defined as two field variables FV1 and FV2, respectively. In the input file, using Eqs. (1-8) (Table 2), the mobilized ϕ' and ψ are defined in tabular form as a function of γ^p and p'. During the analysis, the program accesses to the subroutine and updates the values of ϕ' and ψ with field variables.

RESULTS

In order to show the performance of the MMC model, 4 analyses (2 lateral and 2 vertical uplift) are performed and the results compared with model test results [35]. To be consistent with model tests, D=102 mm is used in this set of analyses. The soil parameters used in the analysis are listed in Table 1. Figures 1(a) and 1(b) show that the force-displacement curves with the MMC model match very well with the model test results. Further details could be found in authors' previous studies ([30], [31).

Figure 4 shows the variation of dimensionless force, N_h ($=F/\gamma HD$) with dimensionless lateral displacement (u/D) for H/D=4 for two soil models. Analysis for the critical state friction angle with MC model (ϕ'=35° and ψ=0°) is also included in the figure for further comparison. The solid line in Fig. 4 represents the result with the MMC model while the dotted lines represent results with the MC model. The force-displacement curve for the MMC model shows a strain softening behavior after the peak while the force-displacement curve for the MC model remains almost horizontal from the peak value. This is due to the fact that in the MC model ϕ' and ψ are constant. As shown in Fig. 1(a), post-peak degradation of normalized force was observed in the model test [35]. The peak N_h with the MMC model is comparable to the peak N_h with MC model when ϕ'=44° and ψ=16° is used. However, N_h at large displacements (e.g. u/D=0.6) with the MMC model is comparable to the N_h with MC model with ϕ'=35° and ψ=0°. Therefore, the question is which values of ϕ' and ψ should be used in numerical modeling because it is known that ϕ' and ψ varies with plastic strain and therefore mobilized values of ϕ' and ψ in the course of pipe movement is not constant. In other words, the representative constant values of ϕ' and ψ for the MC model should be carefully selected. In this particular example (Fig. 4), if someone is interested only in the peak force, ϕ'=44° and ψ=16° could be used. However, the complete force displacement curve could be simulated if the MMC model is used.

Figure 5 shows analyses for uplift loading for H/D=6. For MMC model, N_h increases with vertical displacement, reaches the peak and then decreases in the post- peak zone. For MC model, there is a slight decrease in the uplift force after the peak as the burial depth reduces with upward movement of the pipe. However, it is significantly different from observed softening with the MMC model (solid line). Therefore, the post-peak stress-strain behavior of soil needs to be incorporated in the FE analyses for better simulation.

The peak dimensionless force is one of the main parameters in the current pipeline design practice. The peak dimensionless force obtained from the present FE analyses for D=300 mm are plotted with H/D ratio in Figs. 6 and 7 for lateral and uplift loadings, respectively. The variation of the peak dimensionless force for the MC model with ϕ'=44° and ψ=16° and MMC model is comparable. As expected, lower shear strength parameters (ϕ'=39° and ψ=10°) gives lower lateral and uplift resistances.

Table 2: Equations for Modified Mohr-Coulomb Model (MMC) (summarized from Roy et al. [30], [31])

Description	Eq. #	Constitutive Equation	Soil Parameters
Relative density index	(1)	$I_R = I_D(Q - \ln p') - R$	$I_D = D_r(\%)/100$, Q=10, R=1 (Bolton [5])
Peak friction angle	(2)	$\phi'_p - \phi'_c = A_\psi I_R$	ϕ'_c, A_ψ
Peak dilation angle	(3)	$\psi_p = \dfrac{\phi'_p - \phi'_c}{k_\psi}$	k_ψ
Strain softening parameter	(4)	$\gamma_c^p = C_1 - C_2 I_D$	C_1, C_2
Plastic strain at ϕ'_p	(5)	$\gamma_p^p = \gamma_c^p \left(p'/p'_a\right)^m$	p'_a, m
Mobilized friction angle at Zone-II	(6)	$\phi' = \phi'_{in} + \sin^{-1}\left[\left(\dfrac{2\sqrt{\gamma^p \gamma_p^p}}{\gamma^p + \gamma_p^p}\right)\sin\left(\phi'_p - \phi'_{in}\right)\right]$	
Mobilized dilation angle at Zone-II	(7)	$\psi = \sin^{-1}\left[\left(\dfrac{2\sqrt{\gamma^p \gamma_p^p}}{\gamma^p + \gamma_p^p}\right)\sin\left(\psi_p\right)\right]$	
Mobilized friction angle at Zone-III	(8)	$\phi' = \phi'_c + \left(\phi'_p - \phi'_c\right)\exp\left[-\left(\dfrac{\gamma^p - \gamma_p^p}{\gamma_c^p}\right)^2\right]$	
Mobilized dilation angle at Zone-III	(9)	$\psi = \psi_p \exp\left[-\left(\dfrac{\gamma^p - \gamma_p^p}{\gamma_c^p}\right)^2\right]$	
Young's modulus	(10)	$E = K\, p'_a \left(\dfrac{p'}{p'_a}\right)^n$	K, n

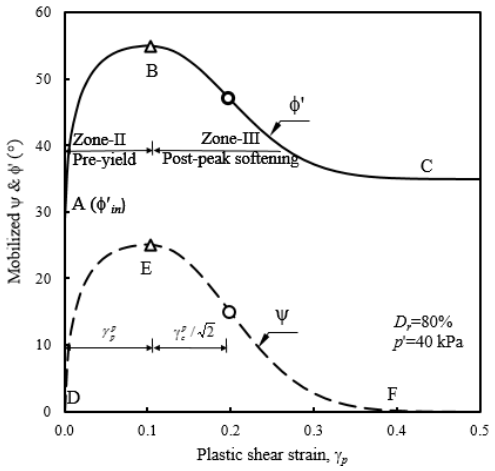

ϕ'_{in} = Initial friction angle, γ^p = Accumulated engineering plastic shear strain

The insets of Fig 4 show the plastic shear strains (field variable FV1 in Abaqus) when the peak resistance is mobilized. The shear band does not reach the ground surface for the MMC model (Inset-I) while it reaches the ground surface for the MC model (Inset-II). Similar behavior is shown for upward loading (insets in Fig. 5). This implies that for the MC model a complete failure plane is developed at a displacement near the peak, and with further displacement the dimensionless force does not change because ϕ' and ψ on this plane are constant. The reduction in dimensionless force (Figs. 4 and 5) is because of upward displacement of the pipe from its original position. On the other hand, in MMC model, plastic strains mainly concentrate near the pipe when the peak dimensionless force is mobilized. With further displacement of the pipe, the size of the plastic zone increases and at a large displacement a complete failure plane develops, which is discussed later.

FAILURE PATTERN

In this section, the mechanisms of failure of soil due to lateral and upward displacements of the pipe are investigated. The mechanisms of shear band formation and propagation with loading for both MC and MMC models are compared. For lateral pipeline-soil interaction, the soil failure mechanisms can be categorized into two simple modes, "wedge" and "plow through" [22]. For shallow burial depths, the lateral movement of the pipe in dense sand results in upward and lateral movement of a soil wedge in front of the pipe. In order to explain the soil failure mechanisms, consider the FE simulation of lateral pipeline-soil interaction at a moderate depth of H/D=4 for D=300 mm. The plastic shear strains developed in soil at a lateral displacement of 120 mm (u/D=0.4) is shown in Fig. 8.

As shown in Fig. 8, significantly large plastic shear strains develop in some narrow zones at this level of lateral displacement. The strain localization at this stage forms mainly

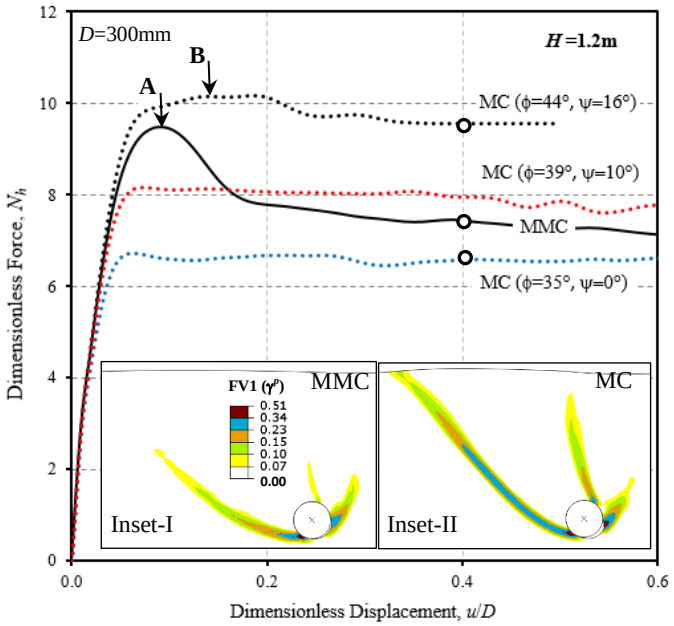

Figure 4. Comparison between MC and MMC for Lateral loading for D=300 mm and H/D=4

three shear bands, f_1, f_2 and f_3 (Fig. 8). The shear strains in the soil between two shear bands are not significant compared to the shear strains in the bands. The shear bands in Fig. 8 are very similar to model tests of Turner [36] in dense sand (Fig. 9).

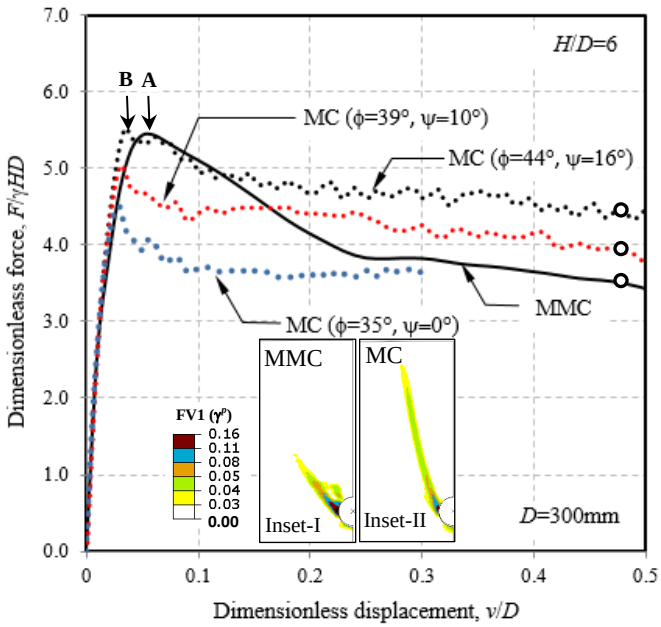

Figure 5. Comparison between MC and MMC for Upward loading for D=300 mm and H/D=6

Shear bands of almost similar pattern are also found in the FE simulations with the MMC model for $H/D \leq 6$ and is not repeated here. At large depths, flow-around mechanisms govern the failure of soil. Further details about this shear band formation can be found in Roy et al. [30].

The difference between the shape of the force-displacement curves for MMC and MC model (Fig. 4) could be explained further using the mobilized shear strength parameters (ϕ' and ψ) along the shear bands and their formation. The solid lines through the highly concentrated γ^p zone (Fig. 8) are drawn for

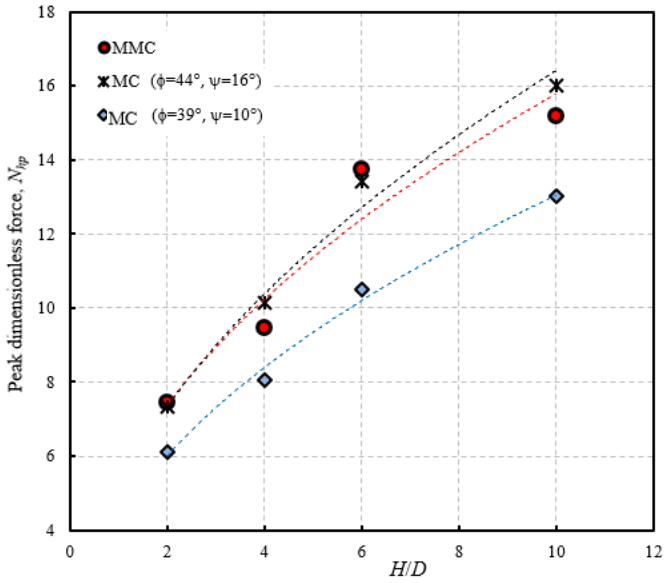

Figure 6. Comparison of peak resistance for Lateral loading

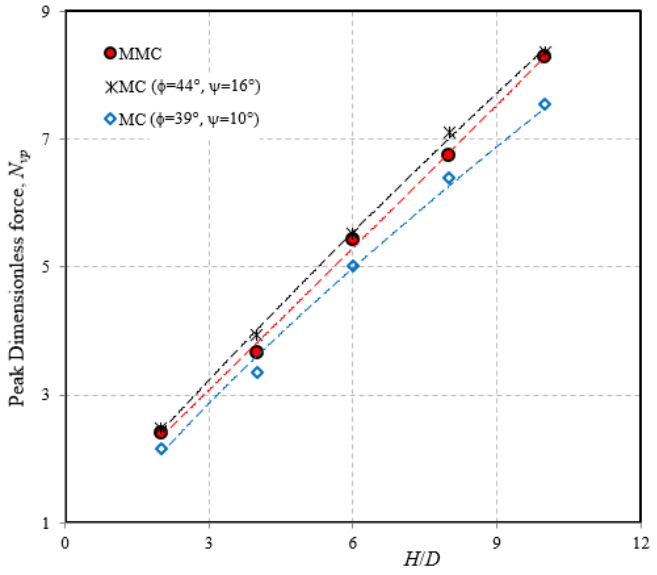

Figure 7. Comparison of peak resistance for Uplift loading

further investigation of the location of the shear bands for various conditions. Similar to Fig. 8, the locations of the shear bands are

obtained for ϕ'=44° and ψ=16° and ϕ'=39° and ψ=10° and plotted in Fig. 10 for u/D=0.4.

Figure 10 shows that the inclination of the shear band with the horizontal plane decreases with increase in shear strength parameters (ϕ' and ψ) in the passive failure zone (left side), while the trend is opposite in the active failure zone (right side). However, in the MMC model, ϕ' and ψ are not constant but varies with plastic shear strain. The strain localization initiates at a high values of ϕ' and ψ near the peak which eventually reduce to the critical state at large displacements. The mobilized dilation angle during the initiation of the shear band influences the shape of the failure wedge and thereby the reaction force. As the post-peak softening of stress-strain behavior is not considered, the MC model cannot simulate the degradation of N_h after the peak as shown in Fig. 4 although it can predict the peak dimensionless force similar to the MMC model.

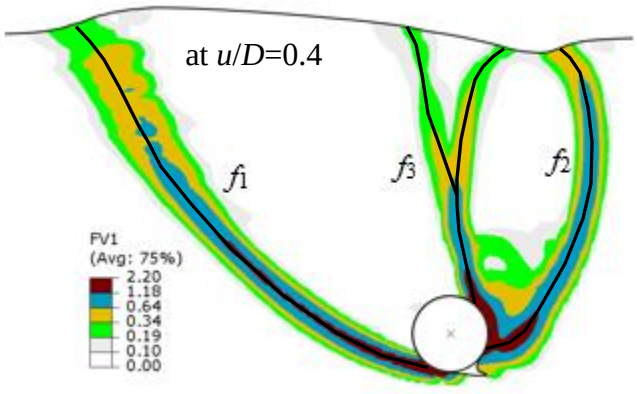

Figure 8. Strain localization for lateral pipeline-soil interaction analysis with MMC (D=300 mm, H/D=4)

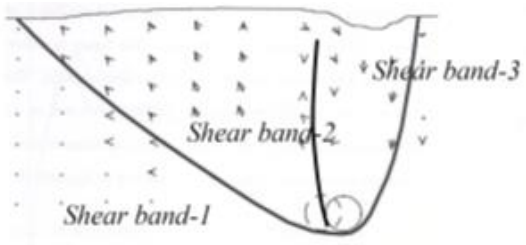

Figure 9. Schematic of shear band formation in soil (after Turner, 2004)

Similar to lateral loading, the strain localization and shear band formation for H/D=6 during upward loading at an upward displacement of 144 mm (i.e. v/D=0.48) is shown in Fig. 11. With increase in upward displacement, the extent of strain localization increases and the shear band, f_1 reaches the ground surface and at a very large displacement (v/D=0.48), another shear band (f_2) is formed, almost in vertical direction as shown in Fig. 11. Further details about the shear band formation in case of upward loading can be found in Roy et al. ([31]).

For MC model, the shear strains around f_1 increases without formation of additional shear band as shown in Fig. 12 with dotted lines.

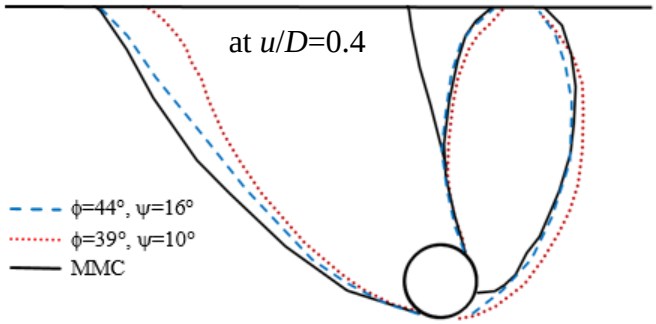

Figure 10. Shear band locations for lateral loading (D=300 mm, H/D=4)

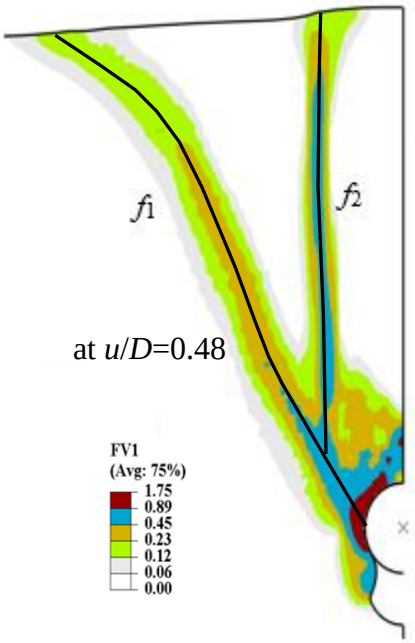

Figure 11. Strain localization for upward pipeline−soil interaction analysis with MMC (D=300 mm, H/D=6)

The shear band for ϕ'=44° and ψ=16° is located in the left of the shear band that formed for ϕ'=39° and ψ=10°, which implies that with increase in shear strength parameters the size of the failure wedge increases and that also contributes to the higher value of N_v as shown in Fig. 5. Although FE analysis with MC model (ϕ'=44° and ψ=16°) can predict the peak dimensionless force similar to the analysis with the MMC model, it is clear from Fig. 12 that shear band formation in both cases are completely different. As post-peak softening has been observed in model tests (Fig. 1), it can be concluded that the MMC model, which considers the post-peak softening behavior of dense sand, can better model the pipeline-soil interaction mechanisms and force-displacement response.

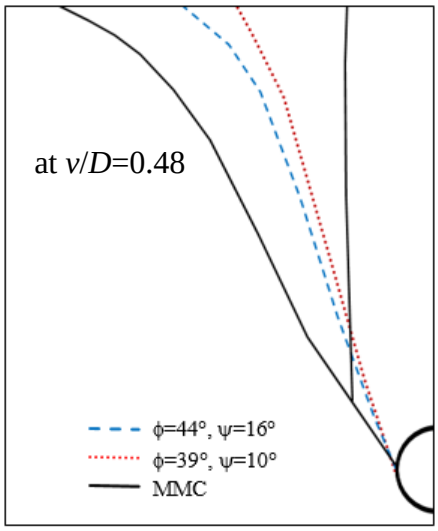

Figure 12. Strain localization for Uplift Loading for MC and MMC: (D=300 mm, H/D=6)

CONCLUSIONS

The pipeline-soil interactions associated with relative movement of the pipeline in the lateral and upward directions are numerically investigated in this study. The FE simulations are performed for two-dimensional plane strain condition. The key features considered in modeling of the behavior of dense sands are: (i) the decrease of peak friction angle with increase in mean effective stress, (ii) an improved stress-strain behavior of dense sand, including the pre-peak hardening and post-peak softening with plastic shear strain; and (iii) plane strain strength parameters. The FE modeling is performed using Abaqus/Explicit FE software.

A comparative study, using the proposed MMC model and built-in MC model in Abaqus, has been performed to examine the force-displacement response and shear band propagation during lateral and vertical loading. Two sets of FE analyses are performed for lateral and upward displacement of the pipe. In the first set, analyses are performed using the built-in MC model in Abaqus (constant angles of internal friction and dilation). In the second set, FE simulations are performed for plane strain condition using the MMC model. The mobilized dilation angle during the initiation of the shear band influences the shape of the failure wedge and thereby the reaction force. As the post-peak softening of stress-strain behavior is not considered, the MC model cannot simulate the degradation of dimensionless force after the peak although it can calculate the peak dimensionless force similar to the MMC model. The MMC model can successfully capture the strain softening behavior of pipeline-soil interaction and hence has significant impact on the soil restraint against pipeline movement.

ACKNOWLEDGMENTS

The work presented in this paper was funded by the Research and Development Corporation (RDC), Newfoundland and Labrador and NSERC Discovery and CRD grants.

REFERENCES

[1] Ahmed, S.M.U. 1973, "A study of the influence of confining pressure on the behaviour of sands", M.Sc. Thesis, McGill University, Montreal, Canada.

[2] ALA (American Lifelines Alliance) retrieved from: www.americanlifelinesalliance.com/pdf/Update061305.pdf

[3] API (American Petroleum Institute), "Recommended Practice for Planning, Designing and Constructing Fixed Offshore Platforms-Working Stress Design, October 2007" Retrieved from: http://www.api.org/

[4] Audibert, J.M.E. & Nyman, K.J. 1978, "Soil restraint against horizontal motion of pipes", *International Journal of Rock Mechanics and Mining Sciences and Geomechanics Abstracts*, vol. 15, no. 2, pp. A29-A29.

[5] Bolton, M. D. 1986, "The strength and dilatancy of sands", *Geotechnique*, vol. 36, no. 1, pp. 65-78.

[6] Byrne, B. W., Schupp, J., Martin, C. M., Oliphant, J., Maconochie, A. & Cathie, D. 2008, "Experimental modeling of the unburial behaviour of pipelines." *Proc. Offshore Technol. Conf.*, Houston, TX, paper OTC-2008-19573.

[7] CEPA (The Canadian Energy Pipeline Association 2013, Retrieved from: http://www.cepa.com/.

[8] Chin, E. L., Craig, W. H., & Cruickshank, M. 2006, "Uplift resistance of pipelines buried in cohesionless soil." *Proc., 6th Int. Conf. on Physical Modelling in Geotechnics*. Ng, Zhang, and Wang, eds., Vol.1, Taylor & Francis Group, London, pp. 723–728.

[9] Cheuk, C. Y., White, D. J. & Bolton, M. D. 2008, "Uplift mechanisms of pipes buried in sand." *J. Geotech. Geoenviron. Engg* 134, No. 2, pp. 154–163.

[10] Daiyan, N., Kenny, S., Phillips, R. & Popescu, R. 2011, "Investigating pipeline–soil interaction under axial–lateral relative movements in sand", *Canadian Geotechnical Journal*, vol. 48, no. 11, pp. 1683-1695.

[11] Dickin, E.A. & Leung, C.F. 1983, "Centrifugal Model Tests on Vertical Anchor Plates", *Journal of Geotechnical Engineering*, vol. 109, no. 12, pp. 1503-1525.

[12] DNV (Det Norske Veritas), DNV-OS-F101, Retrieved from:http://www.dnv.com/industry/oil_gas/industry_assets/subsea/drilling_well/standards_guidelines/

[13] Guo, P. & Stolle, D. 2005, "Lateral pipe-soil interaction in sand with reference to scale effect", *Journal of Geotechnical and Geoenvironmental Engineering*, vol. 131, no. 3, pp. 338-349.

[14] Guo, P. 2005, "Numerical modeling of pipe-soil interaction under oblique loading", *Journal of Geotechnical and Geoenvironmental Engineering*, vol. 131, no. 2, pp. 260-268.

[15] Hansen, J. B. 1961, “The ultimate resistance of rigid piles against transversal forces.” *Bulletin No. 12*, Danish Geotechnical Institute, Copenhagen, Denmark, 5–9.

[16] Jefferies, M. & Been, K. 2006, “Soil liquefaction: a critical state approach”, Taylor & Francis, New York.

[17] Jung, J., O'Rourke, T. & Olson, N. 2013, "Lateral Soil-Pipe Interaction in Dry and Partially Saturated Sand", *Journal of Geotechnical and Geoenvironmental Engineering*, vol. 139, no. 12, pp. 2028-2036.

[18] Jung, J., O'Rourke, T. & Olson, N. 2013, "Uplift soil–pipe interaction in granular soil", *Canadian Geotechnical Journal*, vol. 50, pp. 744-753.

[19] Kouretzis, G.P., Sheng, D. & Sloan, S.W. 2013, “Sand–pipeline–trench lateral interaction effects for shallow buried pipelines”, *Computers and Geotechnics*, 54, 53–59.

[20] Lings, M. L., & Dietz, M. S. 2004, “An Improved Direct Shear Apparatus for Sand.” *Geotechnique*, Vol. 54, No. 4, pp. 245-256.

[21] Loukidis, D. & Salgado, R. 2010, “Effect of relative density and stress level on the bearing capacity of footings on sand”, *Géotechnique,* Volume 61, Issue 2, July 2010, pp 107–119.

[22] O’Rourke, M.J., & Liu, X. 2012, “Seismic design of buried and offshore pipelines”. MCEER Monograph MCEER-12-MN04.

[23] Ovesen, N. K. 1964, “Anchor slabs, calculation methods and model tests.” *Bulletin No. 16*, The Danish Geotechnical Institute, Copenhagen, Denmark.

[24] Palmer, A. C. 2003, “Uplift resistance of buried submarine pipelines: Comparison between centrifuge modelling and full-scale tests.” *Géotechnique*, 53(10), pp. 877–883.

[25] Paulin, M. J. 1998, “An investigation into pipelines subjected to lateral soil loading.” PhD thesis, Memorial Univ. of Newfoundland, St. John’s, Canada.

[26] PIPELINE 101 (an introductory online resource for energy pipeline information), Retrieved from: http://www.pipeline101.com/

[27] Pradhan, T.B.S., Tatsuoka, F. & Horii, N. 1988, "Strength and deformation characteristics of sand in torsional simple shear", *Soils and Foundations*, vol. 28, no. 3, pp. 131-148.

[28] Ranjan, G. & Arora, V. B. 1980, "Model studies on anchors under horizontal pull in clay”, *Proc 3rd Australia-New Zealand Conference on Geomechanics*, Wellington, 12–16 May 1980, vol. 1, pp. 65–70.

[29] Robert, D. J. 2010, “Soil-Pipeline Interaction in Unsaturated Soils”, PhD thesis, University of Cambridge, United Kingdom.

[30] Roy. Kshama.S., Hawlader B.C. & Kenny, S. 2014, “Influence of Low Confining Pressure on Lateral Soil/Pipeline Interaction in Dense Sand”, *33rd International Conference on Ocean, Offshore and Arctic Engineering (OMAE2014)*, San Francisco, California, USA, June 8-13, 2014.

[31] Roy. Kshama.S., Hawlader B.C., Kenny, S. & Moore, I. 2014, “Finite Element Modeling of Uplift Pipeline/Soil Interaction in Dense Sand”, *Geohazards6*, Kingston, Ontario, Canada, June 15-18, 2014.

[32] Scarpelli, G., Sakellariadi, E., & Furlani, G. 1999, "Longitudinal pipeline-soil interaction: results from field full scale and laboratory testing", *Twelfth European Conference on Soil Mechanics and Geotechnical Engineering*, pp. 511.

[33] Schaminée, P. E. L., Zorn, N. F., & Schotman, G. J. M. 1990, “Soil response for pipeline upheaval buckling analyses: full-scale laboratory tests and modeling.” *Proc., 22nd Annual Offshore Technology Conf.*, OTC6486, 563–572.

[34] Schupp, J., Byrne, B. W., Eacott, N., Martin, C. M., Oliphant, J., Maconochie, A., & Cathie, D. 2006, “Pipeline unburial behaviour in loose sand.” *Proc., 25th Int. Conf. on Offshore Mechanics and Arctic Engineering*, Hamburg, Germany, OMAE2006-92541.

[35] Trautmann, C. 1983, “Behavior of pipe in dry sand under lateral and uplift loading”, PhD thesis, Cornell University, Ithaca, NY.

[36] Turner, J.E. 2004, “Lateral force-displacement behavior of pipes in partially saturated sand”, M.S. Thesis, Cornell University, Ithaca, NY.

[37] Vesic, A.S. 1969, “Breakout Resistance of Objects Embedded in Ocean Bottom”, Duke Univ, Durham, NC, USA.

[38] Wang, J., Ahmed, R., Haigh, S. K., Thusyanthan, N. I. & Mesmar, S. 2010, “Uplift resistance of buried pipelines at low cover diameter ratios.” P*roc. Offshore Technol. Conf.*, Houston, TX, paper OTC-2010-20912.

[39] White, D. J., Barefoot, A. J., & Bolton, M. D. 2001, “Centrifuge modeling of upheaval buckling in sand.” *Int. J. Physical Modeling in Geotechnics*, 2(1), pp. 19–28.

[40] Wijewickreme, D., Karimian, H. & Honegger, D. 2009, "Response of buried steel pipelines subjected to relative axial soil movement", *Canadian Geotechnical Journal*, vol. 46, no. 7, pp. 735-735.

[41] Williams, E.S., Byrne, B.W. & Blakeborough, A. 2013, "Pipe uplift in saturated sand: rate and density effects”, *Geotechnique*, vol. 63(11), pp 946–956.

[42] Xie, X. 2008, “Numerical analysis and evaluation of buried pipeline response to earthquake-induced ground fault rupture”, PhD thesis, Rensselaer Polytechnic Institute, New York.

[43] Yimsiri, S., Soga, K., Yoshizaki, K., Dasari, G. & O'Rourke, T. 2004, "Lateral and upward soil-pipeline interactions in sand for deep embedment conditions", *Journal of Geotechnical and Geoenvironmental Engineering*, vol. 130, no. 8, pp. 830-842.

APPENDIX D

Soil Failure Mechanism for Lateral and Upward Pipeline-Soil Interaction Analysis in Dense Sand

This paper has been published and presented in 68th Canadian Geotechnical Conference (GeoQuebec 2015), Quebec City, Quebec, Canada, September 20–23, 2015. Most of the research work presented in this paper was conducted by the first author. He also prepared the draft manuscript. The other authors supervised the research and reviewed the manuscript.

Soil Failure Mechanism for Lateral and Upward Pipeline–Soil Interaction Analysis in Dense Sand

Kshama Roy & Bipul Hawlader
Memorial University of Newfoundland, St. John's, NL, Canada
Shawn Kenny
Carleton University, Ottawa, ON, Canada

GEOQuébec 2015
Challenges from North to South
Des défis du Nord au Sud

ABSTRACT
Finite element (FE) simulation of the response of buried pipelines due to lateral and upward relative displacements is presented in this paper. Analyses are performed using the Arbitrary Lagrangian-Eulerian (ALE) approach available in Abaqus/Explicit FE software adopting a modified Mohr-Coulomb model (MMC) where pre-peak hardening, post-peak softening, density and confining pressure dependent friction and dilation angles are considered. The calculated peak dimensionless force with the MMC model is consistent with the available design guidelines for shallow burial depths. However, at deep burial conditions FE simulations with the Mohr-Coulomb (MC) model give higher peak resistance than the simulations with MMC model. The simulations with the MMC model appeared to be consistent with the trend of model test results. The role of strain-softening on soil resistance and failure pattern is also critically examined.

RÉSUMÉ
Par éléments finis (FE) simulation de la réponse des canalisations enterrées en raison de déplacements relatifs latéraux et au-dessus est présentée dans le présent document. Les analyses sont effectuées en utilisant le (ALE) approche arbitraire Lagrange-Eulerian disponible dans Abaqus / logiciels Explicit FE adoption d'un modèle de Mohr-Coulomb modifié (MMC) où pré-pic durcissement, post-pic ramollissement, la densité et le frottement dépendant de la pression de confinement et des angles de dilatation sont considérés. La force dimension maximale calculée avec le modèle de MMC est conforme aux lignes directrices de conception disponibles pour les profondeurs d'enfouissement peu profondes. Cependant, dans des conditions d'enfouissement profond des simulations avec le modèle FE Mohr-Coulomb (MC) donnent la résistance de pointe plus élevée que les simulations avec le modèle de MMC. Les simulations avec le modèle de MMC semblaient être conforme à la tendance des résultats des tests de modèle. Le rôle de la souche de ramollissement sur la résistance des sols et le motif de l'échec est également un examen critique.

1 INTRODUCTION

With the increasing demand of energy, many major pipeline projects are being pursued by major oil and gas companies to diversify the business and also to add incremental values to existing assets. Key areas of focus for these projects include design of pipelines for transporting large quantities of crude oil over large distances. According to the Canadian Energy Pipeline Association (CEPA), in Canada, a network of approximately 115,000 km of underground energy transmission pipelines operates every day transporting oil and natural gas (http://www.cepa.com/). One of the major concerns for designing pipelines is to ensure very minimum risks to public and the environments. Geohazards and the associated ground movements represent a significant threat to pipeline integrity that may result in pipeline damage and failure (O'Rourke and Liu, 2012). In certain situations, pipelines might pass through a zone of potential ground failures, such as surface faulting, liquefaction-induced soil movements, and landslide induced permanent ground deformation (PGD). These ground movements might cause excessive stresses in pipeline resulting in severe damage.

Several experimental, theoretical and numerical studies have been conducted in the past to estimate the forces acting on pipelines due to relative movement of the soil in specific directions, namely axial, lateral and upward (e.g. Audibert and Nyman, 1978; Dickin and Leung, 1983; Trautmann, 1983; Paulin, 1998; White et al., 2001; Yimsiri et al., 2004; Guo and Stolle, 2005; Chin et al., 2006; Schupp et al., 2006; Byrne et al., 2008; Cheuk et al., 2008; Wijewickreme et al., 2009; Wang et al., 2010; Daiyan et al., 2011; Jung et al., 2013a&b; Williams et al., 2013). Several pipeline design guidelines have been developed on the basis of these extensive research works, (e.g. ALA, 2001; PRCI, 2004; DNV, 2007). Most of the design guidelines focused on the peak force exerted on the pipe. But not only are the peak force, the shape of the force-displacement curves are also significantly influenced by several factors during pipeline-soil interaction.

Continuum finite element (FE) analyses have been performed in the past to simulate lateral and uplift pipeline-soil interaction in sand (e.g. Yimsiri et al., 2004; Jung et al., 2013). The influence of constitutive model of soil on pipeline response has also been examined in some studies (Yimsiri et al., 2004). In the existing guidelines, the resistance of soil against the movement of pipes is quantified using a friction angle of sand. But pre-peak hardening, post-peak softening, density and confining pressure dependent angle of internal friction and dilation angle are the common features observed in laboratory tests on dense sand. The mode of shearing, such as triaxial (TX) or plane strain (PS), also significantly influences the behaviour (Bolton, 1986). All these features of the stress–

strain behaviour of dense sand have not been considered in the available guidelines or FE modeling.

The main objective of the present study is to simulate lateral and upward pipeline–soil interaction using Arbitrary Lagrangian-Eulerian (ALE) approach available in Abaqus/Explicit FE software implementing a modified Mohr-Coulomb (MMC) model for dense sand. FE simulations are compared with experimental and numerical test results available in the literature. Finally, failure mechanisms for both lateral and uplift pipeline–soil interaction for shallow to deep burial conditions are discussed.

2 FINITE ELEMENT FORMULATION

Two-dimensional pipeline–soil interaction analyses are conducted using the Abaqus/Explicit FE software. Typical FE mesh for a 300 mm outer diameter (*D*) pipe subjected to lateral and upward movement is shown in Figs. 1 and 2, respectively. Taking the advantage of symmetry, only half of the domain is modeled for upward loading (Fig. 2). A 4-node bilinear plane strain quadrilateral element (CPE4R) is used for FE modeling of soil. The pipe is modeled as a rigid body. The structured mesh (Figs. 1&2) is generated by Abaqus/cae by zoning the soil domain. Denser mesh is used near the pipe.

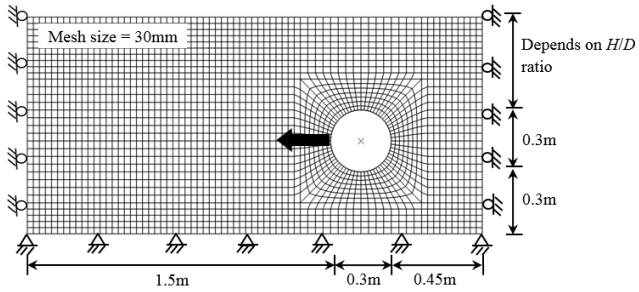

Figure 1. Typical finite element mesh for lateral loading for *D*=300mm and *H*/*D*=2

The bottom of the FE domain is restrained from horizontal and vertical movement, while all the vertical faces are restrained from any lateral movement using roller supports. No displacement boundary condition is applied on the top face and therefore soil can move freely. The centre of the pipe is placed at a distance *H* from the ground surface. The depth of the pipe is measured in terms of *H*/*D* ratio. The thickness of soil above the center of the pipe varies with *H*/*D* ratio. The locations of the bottom and left/right boundaries with respect to the location of the pipe are sufficiently large and therefore boundary effects on predicted lateral and uplift resistance, and soil failure mechanisms are not found.

The interface between pipe and soil is simulated using the contact surface approach available in Abaqus/Explicit. The Coulomb friction model is used for the frictional interface between the outer surface of the pipe and sand. In this method, the friction coefficient (μ) is defined as $\mu=\tan(\phi_\mu)$, where ϕ_μ is the pipe–soil interface friction angle. The value of ϕ_μ depends on the interface characteristics and relative movement between the pipe and soil. The value of μ equal to 0.32 is used in this study.

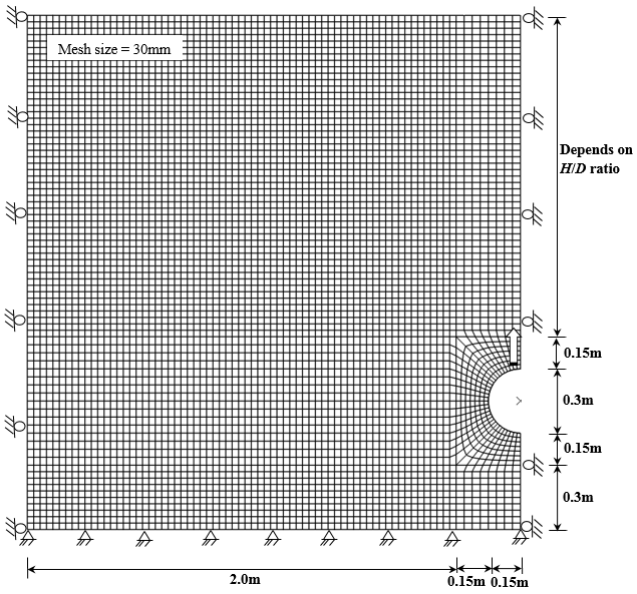

Figure 2. Typical finite element mesh for upward loading for *D*=300mm and *H*/*D*=6

The numerical analysis is conducted in two steps. In the first step, geostatic stress is applied while in the second step, the pipe is displaced in the lateral and upward direction specifying a displacement boundary condition at the reference point of the pipe.

3 MODELING OF SOIL

The Mohr-Coulomb (MC) model in its original form or after some modification has been used by many researchers in the past for pipeline–soil interaction analysis (e.g. Guo and Stolle, 2005; Xie, 2008; Daiyan et al., 2011; Kouretzis et al., 2013). In the present study, analyses are performed using the Mohr-Coulomb model in its original form (MC) and also after some modifications (MMC). In the Mohr-Coulomb model, for a given soil, constant values of angle of internal friction (ϕ') and dilation (ψ) are defined. However, the Modified Mohr-Coulomb Model (MMC) takes into account the effects of pre-peak hardening, post-peak softening, density and confining pressure on angles of internal friction (ϕ') and dilation (ψ) of dense sand. A detailed discussion of the MMC model and estimation of model parameters are available in Roy et al. (2014a&b) and is not repeated here. However, the constitutive equations are summarized in Table 1. The geometry and soil parameters used in the present FE analysis are shown in Table 2.

Abaqus does not have any direct option for modeling stress–strain behavior of the proposed MMC model; therefore, it is implemented using a user subroutine VUSDFLD. The plastic strain increment ($\Delta\gamma^p$) in each time increment is calculated as ($\Delta\gamma^p = \Delta\varepsilon^p_1 - \Delta\varepsilon^p_3$), where $\Delta\varepsilon^p_1$ and $\Delta\varepsilon^p_3$ are the major and minor principal plastic strain

Table 1: Equations for Modified Mohr-Coulomb Model (MMC) (summarized from Roy et al., 2014a&b)

Description	Eq. #	Constitutive Equation	Soil Parameters
Relative density index	(1)	$I_R = I_D(Q - \ln p') - R$	$I_D = D_r(\%)/100$, Q=10, R=1 (Bolton, 1986)
Peak friction angle	(2)	$\phi'_p - \phi'_c = A_\psi I_R$	ϕ'_c, A_ψ
Peak dilation angle	(3)	$\psi_p = \dfrac{\phi'_p - \phi'_c}{k_\psi}$	k_ψ
Strain softening parameter	(4)	$\gamma_c^p = C_1 - C_2 I_D$	C_1, C_2
Plastic strain at ϕ'_p	(5)	$\gamma_p^p = \gamma_c^p (p'/p'_a)^m$	p'_a, m
Mobilized friction angle at Zone-II	(6)	$\phi' = \phi'_{in} + \sin^{-1}\left[\left(\dfrac{2\sqrt{\gamma^p \gamma_p^p}}{\gamma^p + \gamma_p^p}\right)\sin(\phi'_p - \phi'_{in})\right]$	
Mobilized dilation angle at Zone-II	(7)	$\psi = \sin^{-1}\left[\left(\dfrac{2\sqrt{\gamma^p \gamma_p^p}}{\gamma^p + \gamma_p^p}\right)\sin(\psi_p)\right]$	
Mobilized friction angle at Zone-III	(8)	$\phi' = \phi'_c + (\phi'_p - \phi'_c)\exp\left[-\left(\dfrac{\gamma^p - \gamma_p^p}{\gamma_c^p}\right)^2\right]$	
Mobilized dilation angle at Zone-III	(9)	$\psi = \psi_p \exp\left[-\left(\dfrac{\gamma^p - \gamma_p^p}{\gamma_c^p}\right)^2\right]$	
Young's modulus	(10)	$E = K p'_a \left(\dfrac{p'}{p'_a}\right)^n$	K, n

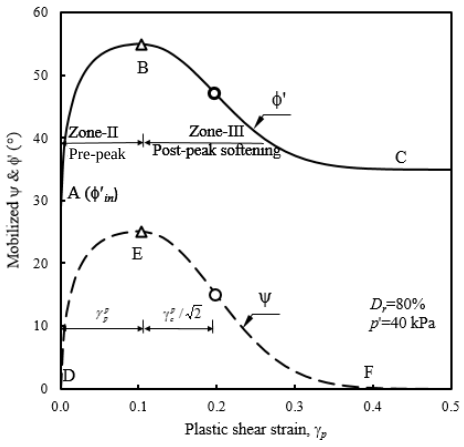

ϕ'_{in} = Initial friction angle, γ^p = Accumulated engineering plastic shear strain

components, respectively. The value of γ^p is calculated as the sum of $\Delta\gamma^p$ over the period of analysis. In the subroutine, γ^p and p' are defined as two field variables FV1 and FV2, respectively. In the input file, using Eqs. (1-9) (Table 1), the mobilized ϕ' and ψ are defined in tabular form as a function of γ^p and p'. During the analysis, the program accesses to the subroutine and updates the values of ϕ' and ψ with field variables.

4 RESULTS

4.1 Validation of FE model

The dashed lines in Figs. 3 and 4 show some experimental test results for the lateral and upward loading, respectively (Trautmann, 1983). The force–displacement curves are presented in normalized form, dimensionless lateral force N_h (=$F/\gamma HD$) with dimensionless lateral displacement u/D (Fig. 3) and dimensionless uplift force N_v (=$F/\gamma HD$) with dimensionless uplift displacement v/D (Fig. 4). Here F is the lateral/uplift force on the pipe per metre length, H is the depth of the centre of the pipe, γ is the unit weight of sand, u and v are the lateral and upward displacements respectively. The peak value of N_h and N_v are defined as N_{hp} and N_{vp}, respectively.

As shown, in both lateral (Fig. 3) and vertical (Fig. 4) loading, the dimensionless force increases with dimensionless displacement to the peak and then decreases. The post-peak decrease of the normalized force is high in the vertical loading as compared to the lateral loading. In order to show the performance of the MMC model, 4 analyses (2 lateral and 2 uplift) are

performed and the results are compared with experimental test results (solid lines in Figs. 3 and 4). To be consistent with experimental tests, D=102 mm is used

Table 2: Parameters used in FE analyses

Parameters		Values MC	Values MMC
Outer diameter of pipe, D (mm)		300	
Parameters for Young's modulus	K	150	
	n	0.5	
	p'_a (kN/m^2)	100	
Poisson's ratio, ν_{soil}		0.2	
Parameters for variation of $\phi'$and ψ	A_ψ	-	5
	k_ψ	-	0.8
	ϕ'_{in}	-	29°
	C_1	-	0.22
	C_2	-	0.11
	m	-	0.25
Critical state friction angle, ϕ'_c		-	35°
Relative density, D_r (%)		80	
Unit weight, γ (kN/m^3)		17.7	
Interface friction coefficient, μ		0.32	
Depth of pipe, H/D		Lateral (2, 4, 10, 15) Uplift (2, 6, 15)	
Friction angle for MC model		44°	-
Dilation angle for MC model		16°	-

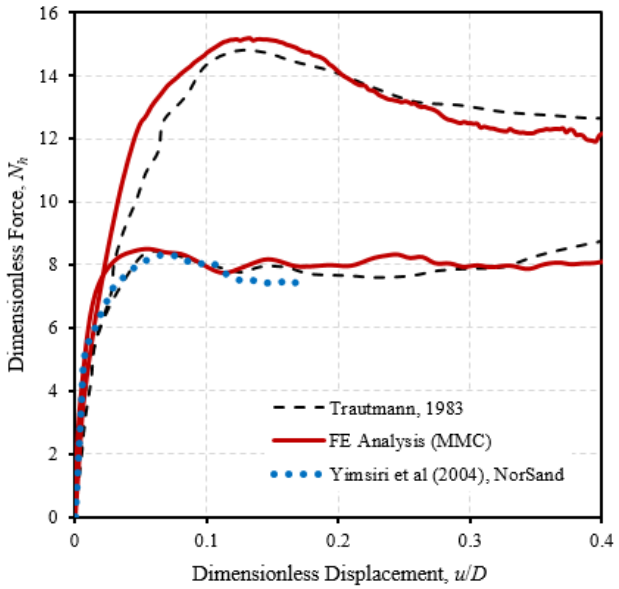

Figure 3. Force-displacement curves for lateral pipe loading tests for D=102mm, redrawn from Trautmann, 1983

in these sets of analyses. The force–displacement curves obtained from the FE analysis with the MMC model match very well for both lateral and upward pipe loading tests. Further details could be found in authors' previous studies (Roy et al., 2014a&b).Two FE analysis results with a complex NorSand soil constitutive model conducted by Yimsiri et al. (2004) are also plotted in Figs. 3 and 4. As shown, the simple MMC model can simulate the force–displacement curves including the post-peak degradation segments.

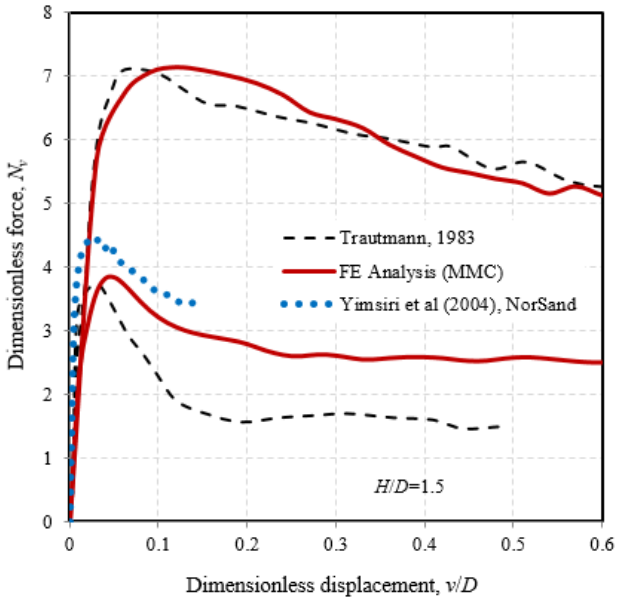

Figure 4. Force-displacement curves for uplift pipe loading tests for D=102mm, redrawn from Trautmann, 1983

4.2 Force–Displacement Behavior

Figure 5 shows the variation of dimensionless lateral force, N_h with dimensionless lateral displacement (u/D) for

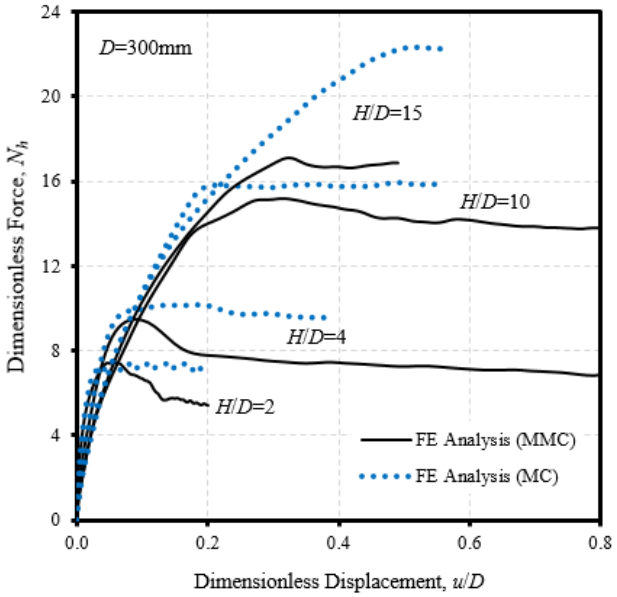

Figure 5. Comparison between MC and MMC for Lateral loading (D=300 mm)

different burial conditions obtained from FE analysis with the MC and MMC models. For shallow burial depths (H/D=2&4), the force–displacement curves with the MMC model show a strain-softening behavior after the peak, while the force–displacement curves with the MC model remains almost horizontal after the peak. This is due to the fact that in the MC model both ϕ' and ψ are constant. As shown in Fig. 3, post-peak degradation of normalized force was observed in the model test (Trautmann, 1983). For shallow to moderate burial depths (H/D=2, 4 & 10), the peak N_{hp} with the MMC model is comparable to the peak N_{hp} with the MC model when ϕ'=44° and ψ=16° is used. However, N_h with the MMC model at relatively large displacements after the peak is not comparable to the N_h with the MC model. This is due to the fact that the mobilized ϕ' and ψ approaches to the critical state in the MMC model, whereas in the MC both ϕ' and ψ remain constant even at large displacement. For a deep burial condition (H/D=15), the peak N_{hp} with the MC model is significantly higher than the N_{hp} with the MMC model. As the MMC model considers the pressure and plastic strain dependent ϕ' and ψ, the peak N_{hp} with the MMC model is lower than the N_{hp} with the MC model. The mean effective stress around the pipe is much higher in deep burial conditions than that in shallow burial condition and hence the peak friction angle is smaller which results lower peak N_{hp}.

Figure 6 shows the force–displacement curves for upward loading. For shallow to moderate burial depths, with the MMC model, N_v increases with vertical

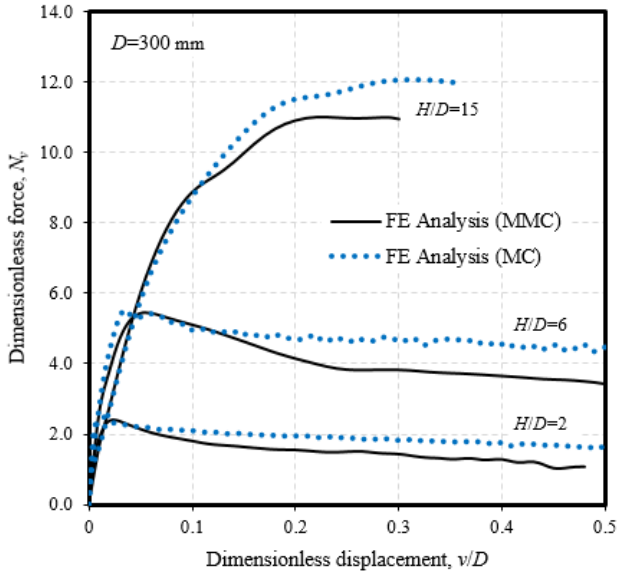

Figure 6. Comparison between MC and MMC for Uplift loading (D=300 mm)

displacement, reaches the peak and then decreases. Similar response (post-peak degradation of normalized force) was observed in the model tests conducted by Trautmann, 1983 (Fig. 4). For the MC model, there is a slight decrease in uplift force after the peak as the burial depth reduces with upward movement of the pipe. For deep burial conditions, the peak uplift force, N_{vp} with the MMC model is lower than the N_{vp} with MC model. This is due to the fact that in the MMC model, both ϕ' and ψ varies with plastic strain and p' whereas, MC model considers only constant ϕ' and ψ values. Therefore, the post-peak stress–strain behaviour of soil needs to be incorporated in the FE analysis for better simulation.

4.3 Peak Dimensionless Force versus Pipe Burial depth

The peak dimensionless force obtained from the present FE analyses for D=102 mm and 300 mm are plotted with H/D ratio in Figs. 7 and 8 for lateral and uplift loadings, respectively. For comparison, the results of experimental tests (Trautmann, 1983) and some design charts (Trautmann and O'Rourke, 1983, Yimsiri et al., 2004 and

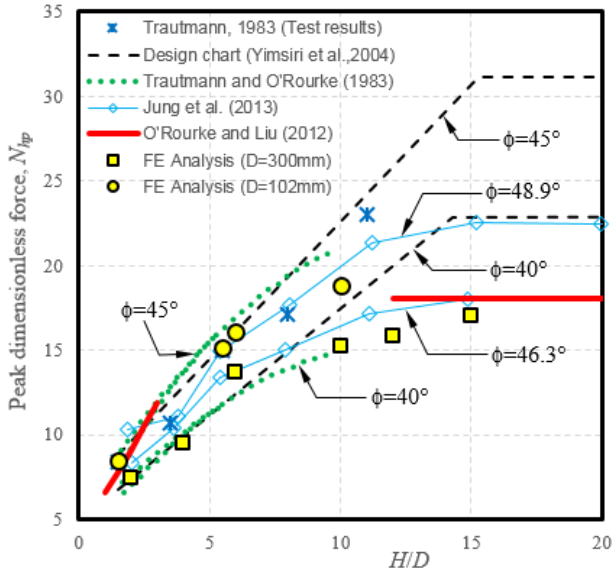

Figure 7. Dimensionless force vs H/D plot (Lateral)

Jung et al., 2013) available in the literature are also plotted on these figures. In Fig. 7, the N_{hp} increases with H/D. Although the curves are plotted as dimensionless force versus dimensionless displacement, they are not straight lines. This is due to the fact that different mechanisms control the behavior for different H/D ratios. The peak dimensionless forces from the present FE analyses at low H/D match well with the available design charts. But at higher H/D ratio, the peak N_{hp} obtained from the present FE analysis is much lower than the values calculated using existing guidelines. The trend of model tests (Trautmann and O'Rourke, 1983) appeared similar to the FE simulation with the MMC model. Jung et al. (2013) also used post-peak softening using a linear variation of angles of ϕ' and ψ with plastic strain, but did not consider the pre-peak hardening in their FE analyses and found smaller values of N_{hp} than Yimsiri et al. (2004) at higher H/D ratio. O'Rourke and Liu (2012) mentioned that for deep burial condition (H/D>12), the peak lateral force, N_{hp} becomes constant (solid line in Fig. 7) and this value can be calculated using a simple empirical equation (N_{hp}=4μ+(1+K_p)(1+μ)-

$1.12(1+K_a)(0.44-0.89\mu)$, where $\mu=\tan\phi'$, K_a and K_p are the Rankine active and passive earth pressure co-efficient, respectively. Their recommended value of N_{hp} is also smaller than that

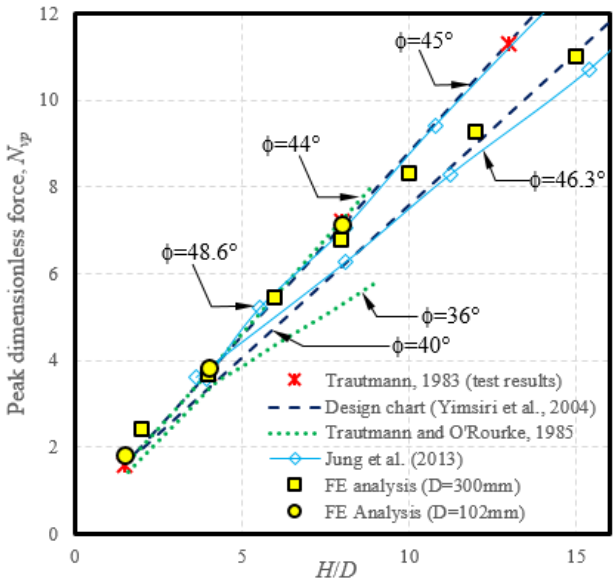

Figure 8. Dimensionless force vs *H*/*D* plot (Uplift)

predicted by the design charts. As discussed before, p' around the pipe increases with depth of burial, and that reduces the mobilized ϕ' and ψ which in turn results in lower N_{hp}. If ϕ' and ψ are independent of p', higher values of N_{hp} could be obtained especially for larger *H*/*D* as shown in Fig. 5 for the MC model (*H*/*D*=15). In the ALA guidelines, the shape of the N_{hp} versus *H*/*D* curves are similar to the Trautmann and O'Rourke (1983) but the values are significantly higher than the value obtained from the present FE analysis with the MMC model. Overestimation of N_{hp} has been also recognized in previous studies (Yimsiri et al., 2004; O'Rourke and Liu, 2012).

The calculated values of N_{vp} with the MMC model are plotted with *H*/*D* ratio in Fig. 8. Experimental results (Trautmann, 1983) and some design charts (Trautmann and O'Rourke, 1983, Yimsiri et al., 2004 and Jung et al., 2013) available in the literature are also plotted in this figure for further comparison. The N_{vp} increases almost linearly with *H*/*D*. The peak dimensionless force obtained from FE analyses compares very well with experimental results and design charts, even with constant values of ϕ'. The effect of pipe diameter is negligible compared to lateral loading as p' around the pipe for uplift loading is lower than that of lateral loading for same *H*/*D* ratio and same displacement. The peak N_{vp} becomes constant at very large *H*/*D* ratios as mentioned by Yimsiri et al. (2004) and Jung et al. (2013); however, in this study, simulations for very large depths are not performed. Although the peak force matches well for both MC and MMC, the failure patterns are different for both cases. For MC model a complete failure plane is developed at a displacement near the peak, and with further displacement, the dimensionless force does not change because ϕ' and ψ on this plane are constant. On the other hand, in MMC model, plastic strains mainly concentrate near the pipe when the peak dimensionless force is mobilized. With further displacement of the pipe, the size of the plastic zone increases and at a large displacement a complete failure plane develops. Details of the comparison in the failure mechanisms of MC and MMC models can be found in Roy et al. (2015).

5 SOIL FAILURE MECHANISM

5.1 Lateral Pipeline-Soil Interaction

Figure 9b shows the instantaneous velocity vectors for lateral loading at peak N_{hp} condition (*u*/*D*=0.05) for a shallow burial depth (*H*/*D*=2 and *D*=300mm). A simplified failure mechanism proposed by O'Rourke and Liu (2012) is also included Fig 9a. The failure mechanism at peak condition matches well with the O'Rourke and Liu (2012). Although it is not presented here, with increase in displacement, three distinct shear bands are formed which gradually reach the ground surface. Details of the shear band propagation pattern (failure mechanism) can be found at Roy et al. (2015).

The soil failure mechanisms for deep burial condition (*H*/*D*=15) are different from failure pattern for *H*/*D*=2. For *H*/*D*=15, a complete below ground zone of soil flow is observed. The plastic shear strain concentration mainly occurs near the pipe instead of reaching the ground surface. O'Rourke and Liu (2012) proposed a simplified four sided rigid block (abcde) failure mechanism for deep burial in sand as shown in Fig. 10a. Instantaneous velocity vectors from the present FE analysis at the peak N_{hp} condition (*u*/*D*=0.2) for deep burial depth (*H*/*D*=15 and *D*=300mm) is also plotted in Fig. 10b. As the pipe moves, the void left by the movement of the pipe is filled by soil following around the block. Fig 10 shows that the simplified failure wedge proposed by O'Rourke and Liu (2012) reasonably matches with the failure wedge from FE analysis with MMC. However, for deep burial condition, a number of shear bands form with increase in lateral displacement. Further studies are required for the failure mechanism at deep burial condition as very limited no of test results are available at deep burial condition.

5.2 Upward Pipeline-Soil Interaction

Figure 11a shows the displacement contours at *u*/*D*=0.2 for shallow burial depth (*H*/*D*=2). A similar failure mechanism for shallow burial condition was found by Ilamparuthi and Muthukrishnaiah (1999) for anchors buried in dense sand (Fig. 11b). For shallow burial depth at the peak resistance, the strain localization is occurred in a small zone of soil near the pipe. With increase in upward displacement, the extent of strain localization increases, and at a relatively large displacement, the shear band reaches the ground surface. Details of the failure pattern developed with MMC model can be found at Roy et al. (2015) and is not repeated here.

For deep burial condition (*H*/*D*=15), the failure mechanism is quite different. Figure 12a shows the

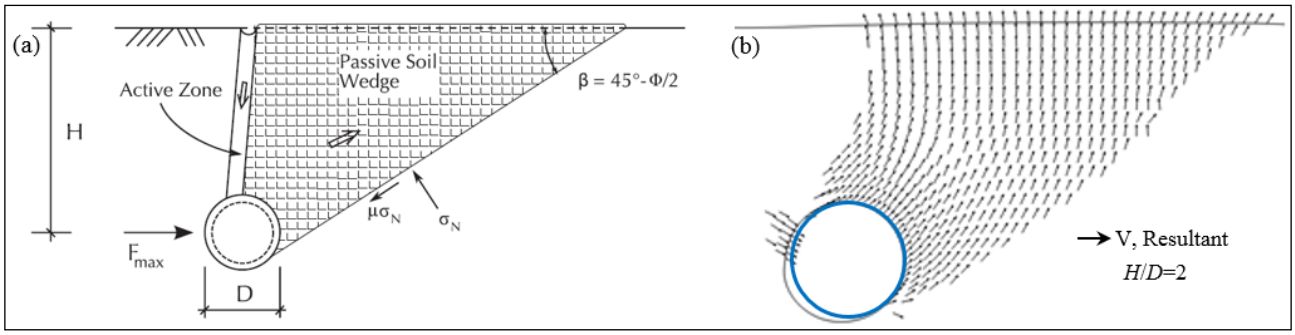

Figure 9. Comparison of failure wedge formation at shallow burial condition with (a) analytical model (O'Rourke and Liu, 2012) and (b) present FE analysis (instantaneous velocity vectors)

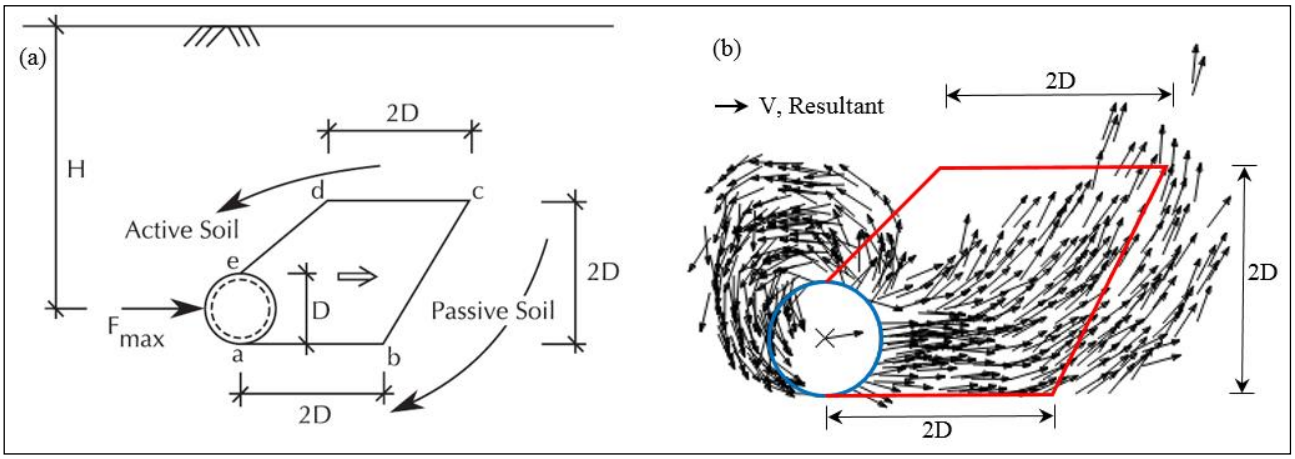

Figure 10. Comparison of failure wedge formation at deep burial condition with (a) analytical model (O'Rourke and Liu, 2012) and (b) present FE analysis (instantaneous velocity vectors)

displacement contours at *u*/*D*=0.2 for deep burial condition (*H*/*D*=15). The soil movement always remain below the ground surface (Fig 12a). The plastic shear strain concentration mainly occurs near the pipe. Similar failure mechanism for deep burial condition was found by Ilamparuthi and Muthukrishnaiah (1999) for anchors buried in dense sand (Fig. 12b).

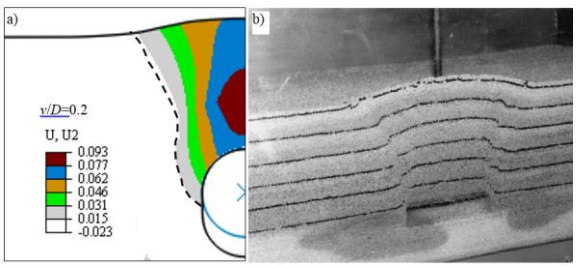

Figure 11. Soil failure mechanism for shallow burial condition: (a) Present FE analysis results (b) Test results for anchor, Ilamparuthi and Muthukrishnaiah (1999)

As pipe moves upward, the void left by the pipe movement is filled by soil following. At moderate to large displacement, large plastic strains accumulate and form several no of below ground zone shear bands. Details of

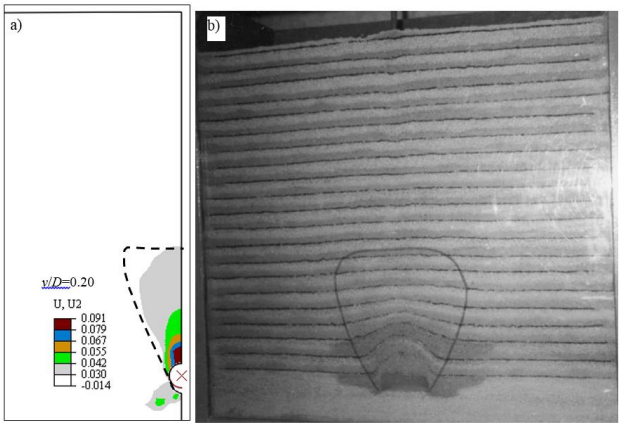

Figure 12. Soil failure mechanism for deep burial condition (Uplift): (a) Present FE analysis results (b) Test results for anchor, Ilamparuthi and Muthukrishnaiah (1999)

the failure pattern developed with MMC model can be found at authors' previous studies, Roy et al. (2015).

6 CONCLUSIONS

The pipeline–soil interactions associated with relative movement of the pipeline in the lateral and upward directions are numerically investigated in this study. The FE simulations are performed in two-dimensional plane strain condition. The key features considered in modeling of the behavior of dense sands are: (i) the decrease of peak friction angle with increase in mean effective stress, (ii) an improved stress–strain behavior of dense sand, including the pre-peak hardening and post-peak softening with plastic shear strain; and (iii) plane strain strength parameters. The FE modeling is performed using Abaqus/Explicit FE software. The FE results with the MMC model are compared with some of the available experimental test results and also with available design charts. Results show the peak dimensionless force vs *H*/*D* curves are consistent with the available design charts for shallow burial condition. However, at deep burial condition, present FE results with the MMC model predict lower peak forces than design guidelines and FE results with MC model. The trend of present FE analysis is similar to the trend of some experimental tests although very limited number of tests are available for deep burial condition. A simplified failure wedge proposed in previous studies is reasonable for shallow burial depth. However, for deep burial condition, a clear wedge does form, but behind the pipe, the plastic shear strains develop in a relatively large zone and sand moves into the gap created by pipe displacements. Further studies are required for proper understanding of failure mechanism at deep burial condition.

ACKNOWLEDGEMENTS

The work presented in this paper was funded by the Research and Development Corporation (RDC), Newfoundland and Labrador and NSERC Discovery and CRD grants.

REFERENCES

American Lifelines Alliance. 2001. Seismic design guidelines for water pipelines. American Lifelines Alliance in partnership with the Federal Emergency Management Agency, Washington, D.C. Available from www.americanlifelinesalliance.org [accessed 4 April 2015].

Audibert, J.M.E., and Nyman, K.J. 1978. Soil restraint against horizontal motion of pipes. International Journal of Rock Mechanics and Mining Sciences and Geomechanics Abstracts, 15(2): A29−A29.

Bolton, M. D. 1986. The strength and dilatancy of sands. Geotechnique, 36(1):65−78.

Byrne, B. W., Schupp, J., Martin, C. M., Oliphant, J., Maconochie, A. and Cathie, D. 2008. Experimental modeling of the unburial behaviour of pipelines. Proc. Offshore Technol. Conf., Houston, TX, paper OTC-2008-19573.

Cheuk, C. Y., White, D. J. and Bolton, M. D. 2008. Uplift mechanisms of pipes buried in sand. Journal of Geotechnical and Geoenvironmental Engineering, 134(2):154–163.

Chin, E. L., Craig, W. H., and Cruickshank, M. 2006. Uplift resistance of pipelines buried in cohesionless soil. Proc., 6th Int. Conf. on Physical Modelling in Geotechnics. Ng, Zhang, and Wang, eds., Vol.1, Taylor & Francis Group, London, pp. 723–728.

Daiyan, N., Kenny, S., Phillips, R., and Popescu, R. 2011. Investigating pipeline–soil interaction under axial–lateral relative movements in sand. Canadian Geotechnical Journal, 48(11):1683−1695.

Dickin, E.A., and Leung, C.F. 1983. Centrifugal model tests on vertical anchor plates. Journal of Geotechnical Engineering, 109(12):1503−1525.

DNV 2007 (Det Norske Veritas). DNV-OS-F101. Available from https://exchange.dnv.com/servicedocuments/dnv/ [accessed 4 April 2015].

Guo, P., and Stolle, D. 2005. Lateral pipe-soil interaction in sand with reference to scale effect. Journal of Geotechnical and Geoenvironmental Engineering, 131(3):338−349.

Honegger, D., and Nyman, D.J. 2004. Guidelines for the seismic design and assessment of natural gas and liquid hydrocarbon pipelines. Pipeline Research Council International, Catalog No. L51927, October.

Ilamparuthi, K. and K. Muthukrishnaiah. 1999. Anchors in sand bed: Delineation of rupture surface. Ocean Eng., 26: 1249-1273.

Jung, J., O'Rourke, T., and Olson, N. 2013. Lateral soil-pipe interaction in dry and partially saturated sand. Journal of Geotechnical and Geoenvironmental Engineering, 139(12): 2028−2036.

Jung, J., O'Rourke, T., and Olson, N. 2013. Uplift soil–pipe interaction in granular soil. Canadian Geotechnical Journal, 50(7):744−753. doi: 10.1139/cgj-2012-0357.

Kouretzis, G.P., Sheng, D., and Sloan, S.W. 2013. Sand-pipeline-trench lateral interaction effects for shallow buried pipelines. Computers and Geotechnics, 54:53-59.

Loukidis, D. and Salgado, R. 2010. Effect of relative density and stress level on the bearing capacity of footings on sand. Géotechnique, 61(2):107–119.

O'Rourke, and M.J., Liu, X. 2012. Seismic design of buried and offshore pipelines. MCEER Monograph, MCEER-12-MN04.

Paulin, M. J. 1998. An investigation into pipelines subjected to lateral soil loading. PhD thesis, Memorial University of Newfoundland, St. John's, Canada.

Roy. Kshama.S., Hawlader B.C., Kenny, S. and Moore, I. 2015. Effect of post-peak softening behavior of dense sand on lateral and upward displacement of buried pipelines. 34th International Conference on Ocean, Offshore and Arctic Engineering (OMAE2015), St. John's, Newfoundland and Labrador, Canada, May 31-June 5, 2015.

Roy. Kshama.S., Hawlader B.C. and Kenny, S. 2014. Influence of Low Confining Pressure on Lateral Soil/Pipeline Interaction in Dense Sand. 33rd International Conference on Ocean, Offshore and Arctic Engineering (OMAE2014), San Francisco, California, USA, June 8-13, 2014.

Roy. Kshama.S., Hawlader B.C., Kenny, S. and Moore, I. 2014. Finite Element Modeling of Uplift Pipeline/Soil Interaction in Dense Sand. Geohazards6, Kingston, Ontario, Canada, June 15-18, 2014.

Schupp, J., Byrne, B. W., Eacott, N., Martin, C. M., Oliphant, J., Maconochie, A., and Cathie, D. 2006. Pipeline unburial behaviour in loose sand. Proc., 25th Int. Conf. on Offshore Mechanics and Arctic Engineering, Hamburg, Germany, OMAE2006-92541.

Trautmann, C. 1983. Behavior of pipe in dry sand under lateral and uplift loading. PhD thesis, Cornell University, Ithaca, NY.

Trautmann, C.H. and O'Rourke, T.D. 1985. Uplift force− displacement response of buried pipe. Journal of Geotechnical Engineering, ASCE, 111(9):1061−1076.

Trautmann, C.H. and O'Rourke, T.D. 1983. Load-Displacement characteristics of a buried pipe affected by permanent earthquake ground movements. Earthquake Behavior and Safety of Oil and Gas Storage Facilities, Buried Pipelines and Equipment, PVP-77, ASME, New York, June, pp. 254-262.

Wang, J., Ahmed, R., Haigh, S. K., Thusyanthan, N. I. and Mesmar, S. 2010. Uplift resistance of buried pipelines at low cover diameter ratios. Proc. Offshore Technol. Conf., Houston, TX, paper OTC-2010-20912.

White, D. J., Barefoot, A. J., and Bolton, M. D. 2001. Centrifuge modeling of upheaval buckling in sand. Int. J. Physical Modeling in Geotechnics, 2(1):19–28.

White, D. J., Cheuk, C. Y., and Bolton, M. D. 2008. The uplift resistance of pipes and plate anchors buried in sand. Geotechnique, 58(10), 771–777.

Wijewickreme, D., Karimian, H., and Honegger, D. 2009. Response of buried steel pipelines subjected to relative axial soil movement. Canadian Geotechnical Journal, 46(7):735−735.

Williams, E.S., Byrne, B.W. and Blakeborough, A. 2013. Pipe uplift in saturated sand: rate and density effects. Geotechnique, 63(11): 946–956.

Xie, X. 2008. Numerical analysis and evaluation of buried pipeline response to earthquake-induced ground fault rupture. PhD thesis, Rensselaer Polytechnic Institute, New York.

Yimsiri, S., Soga, K., Yoshizaki, K., Dasari, G., and O'Rourke, T. 2004. Lateral and upward soil-pipeline interactions in sand for deep embedment conditions. Journal of Geotechnical and Geoenvironmental Engineering, 130(8):830−842.

APPENDIX E

Finite Element Analysis of Strip Anchors Buried in Dense Sand Subjected to Lateral Loading

This paper has been published in 26th International Ocean and Polar Engineering Conference (ISOPE 2016), Rhodes (Rodos), Greece, June 26–July 2, 2016. Most of the research work presented in this paper was conducted by the first author. He also prepared the draft manuscript. The other authors supervised the research and reviewed the manuscript.

Finite Element Analysis of Vertical Strip Anchors Buried in Dense Sand Subjected to Lateral Loading

Kshama Roy[1], *Bipul Hawlader*[1], *Shawn Kenny*[2], *Ian Moore*[3]
[1]Department of Civil Engineering, Memorial University of Newfoundland
St. John's, Newfoundland and Labrador, Canada
[2]Department of Civil and Environmental Engineering, Carleton University
Ottawa, Ontario, Canada
[3]Department of Civil Engineering, Queen's University
Kingston, Ontario, Canada

ABSTRACT

Vertical anchors are widely used to support many structures. In this study, the load–displacement behaviour of a vertical anchor buried in dense sand is modeled numerically. The numerical analyses are performed using Abaqus/Explicit finite element (FE) software adopting two soil models: (i) the elastoplastic Mohr-Coulomb (MC) model and (ii) a Modified Mohr-Coulomb (MMC) model. In the MC model, the two required geotechnical parameters are the constant angles of internal friction (ϕ') and dilation (ψ). However, in the MMC, pre-peak hardening, post-peak softening and the effects of mean effective stress and relative density on stress–strain behaviour of dense sand are considered. Comparison of FE results with physical model test results shows that the MMC model can simulate better the load–displacement response than the MC model. The mechanisms involved in soil deformation are also explained using FE results.

KEY WORDS: Anchors; Soil constitutive model; Mohr-Coulomb model; Modified Mohr-Coulomb model; Finite element analysis; Dense sand; Lateral movement.

INTRODUCTION

Plate anchors are widely used in many onshore and offshore engineering projects, such as transmission towers, utility poles, earth retaining and waterfront structures and mooring of offshore floating platforms. Anchors could be installed in a wide variety of soils at different inclinations, such as horizontal, vertical and inclined. The horizontal pullout capacity of a vertical plate anchor installed in dense sand is the focus of the present study.

A number of researchers studied the behaviour of vertical plate anchors through laboratory experiments, development of analytical methods and numerical analysis (Neely et al., 1973; Das and Seeley, 1975; Akinmusuru, 1978; Rowe and Davis, 1982; Dickin and Leung, 1983; Hoshiya and Mandal, 1984; Basudhar and Singh, 1994; Kumar and Sahoo, 2012; Kame et al., 2012; Bhattacharya and Kumar, 2013). A large number of the available studies on anchors are experimental. Most of the previous studies focused on the ultimate capacity of the anchor, which has been determined from the equilibrium condition of the soil mass above an assumed failure plane inferred from laboratory tests.

Most of the theoretical studies on anchors have been performed based on rigid plastic behaviour of soil (Chattopadhyay and Pise, 1986; Murray and Geddes 1987). Finite element (FE) analyses have also been conducted in the past for modeling lateral load carrying capacity (Rowe and Davis, 1982; Dickin and King, 1993; Bhattacharya and Kumar, 2013). Merifield and Sloan (2006) conducted numerical study to determine the ultimate pullout capacity based on finite element formulation of upper and lower bound theorems of limit analysis. In the above mentioned theoretical and numerical studies, the classical elastoplastic Mohr-Coulomb model has been used for modeling of sand. Sutherland (1988) reported that the FE analyses with an elastoplastic model gives unsatisfactory results for dense sand. Therefore, some researchers suggested that the modeling of progressive development of failure planes in the shear bands would better simulate the response of anchors in dense sands (Tagaya et al., 1983; Abdel Rahman et al. 1992; Sakai and Tanaka 2007). Dickin and Laman (2007) conducted FE analysis using a built-in elastoplastic hyperbolic model described as the Hardening Soil Model (HSM) in PLAXIS and concluded that a more sophisticated soil model is required to simulate uplift resistance of an anchor including the post-peak degradation of resistance as observed in experimental works (e.g. Dickin, 1988). The post-peak degradation of pullout resistance of an anchor in dense sand was observed not only for uplift but also in lateral loading (Neely et al, 1973; Dickin and Leung, 1983). Such post-peak degradation of pullout resistance cannot be

captured using the Mohr-Coulomb model. Moreover, while using the Mohr-Coulomb model, in addition to friction angle, the dilation angle has a significant effect on anchor capacity. Merifield and Sloan (2006) showed that, in extreme cases, the consideration of non-dilatant behaviour of dense sand (zero dilation angle) gave the ultimate lateral capacity approximately half of the capacity with a soil model that satisfies associated flow rule (dilation angle=friction angle). The above mentioned studies clearly show the importance of soil model in numerical modeling of anchor–soil interaction.

The main objective of the present study is to present lateral anchor–soil interaction modeling using Arbitrary Lagrangian-Eulerian (ALE) approach available in Abaqus/Explicit FE software. An advanced soil model, named as modified Mohr-Coulomb (MMC) model, is implemented to simulate the behaviour of vertical plate anchor in dense sand subjected to lateral loading. FE results are compared with experimental results available in the literature. The formation of shearing planes is investigated in order to explain possible mechanisms involved in the force–displacement response observed in laboratory experiments.

PROBLEM DEFINITION

A strip vertical anchor of width B and thickness t buried in dense sand is simulated (Fig. 1). An anchor of finite length (L) can be considered as a strip anchor if the L/B ratio is greater than about 6 (Das and Shukla, 2013). Simulations are performed in two-dimensional plane strain condition. During the installation, the soil in the vicinity of the anchor is usually disturbed. However, the effect of such disturbance on the capacity of anchors is not considered in the present study, instead the simulations are performed for wished-in-place conditions. The dimensions of the anchor is shown in Table 1.

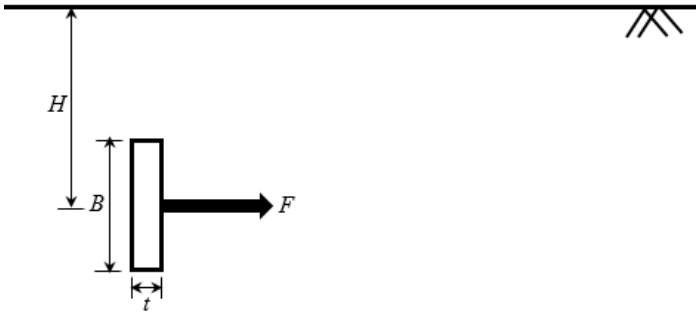

Figure 1: Schematic diagram of the problem considered (vertical anchor)

FINITE ELEMENT FORMULATION

Two-dimensional anchor–soil interaction analyses are conducted using Abaqus/Explicit FE software. A discussion on application of Abaqus/Explicit to pipeline–soil interaction problems could be found in Robert (2010). Figure 2 shows the typical FE model. A 4-node bilinear plane strain quadrilateral, reduced integration, hourglass control element (CPE4R) is used for modeling the soil. The anchor is modeled as a rigid body with a reference point at the center. Abaqus/cae is used to generate a structured finite element mesh. The total number of elements and shape of the element can be defined in the structured mesh, which cannot be done in the auto generated default meshing option in Abaqus. In this study, structured mesh is used because it gives better results, less numerical issues and is computationally more efficient than auto generated mesh.

The bottom of the FE domain is restrained from any horizontal and vertical movements, while all the vertical faces are restrained from any lateral movement using roller supports (Fig. 2). No displacement boundary condition is applied on the top face, and therefore the soil can move freely. The depth of the anchor is measured in terms of H/B ratio. The locations of the bottom and right boundaries (Fig. 2) with respect to the location of the anchor are sufficiently large and therefore boundary effects on predicted lateral resistance, displacement and soil failure mechanisms are not found.

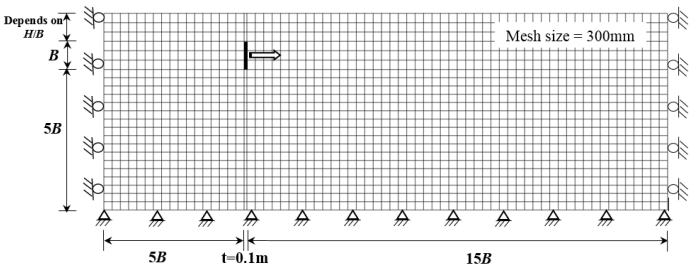

Figure 2: Typical finite element mesh for B=1 m and H/B=1.5

Previous studies on vertical anchors revealed that the anchor interface roughness has an influence on the maximum pullout capacity of vertical anchors (Rowe and Davis, 1982; Merifield and Sloan, 2006). The interface between anchor and soil is simulated using the Coulomb friction model available in Abaqus/Explicit. In this method, the friction coefficient (μ) is defined as $\mu=\tan(\phi_\mu)$, where ϕ_μ is the anchor–soil interface friction angle. The value of ϕ_μ depends on the interface characteristics and relative movement between the anchor and soil (Merifield and Sloan, 2006). The larger value of ϕ_μ represents the characteristics of rough anchors, while the lower values would correspond to relatively smooth anchors. The value of μ equal to 0.4 is used in this study.

The numerical analysis is conducted in two main steps. The first step is a geostatic stress step that accounts for the effects of soil weight and defines the initial stress state in the soil. In the second step, the anchor is moved in the horizontal direction specifying a displacement boundary condition at the reference point of the anchor without any rotational constraint.

MODELING OF SAND

One of the key components that significantly influences the success of FE analyses of anchor–soil interaction is the soil constitutive behaviour (Rowe and Davis, 1982; Merifield and Sloan, 2006; Dickin and Laman, 2007; Sakai and Tanaka, 2007). The Mohr-Coulomb model is one of the simple models that has been used by several researchers in the past for anchor–soil interaction analysis (e.g. Merifield and Sloan, 2006). In the present study, analyses are performed using the Mohr-Coulomb model in its original form (MC) and also after some modifications (MMC). In the Mohr-Coulomb model, constant values of angles of internal friction (ϕ') and dilation (ψ) are defined. The authors of the present study proposed a Modified Mohr-Coulomb Model (MMC) that takes into account the effects of pre-peak hardening, post-peak softening, density and confining pressure on angles of internal friction (ϕ') and dilation (ψ) of dense sand. The model has been successfully used for analysis of response of pipeline in sand for lateral loading (Roy et al., 2015). A detailed discussion of the MMC model and estimation of model parameters are available in Roy et al. (2015) and is not repeated here. However, the constitutive equations of the MMC model are summarized in Table 2. The soil parameters used in the present FE analysis are shown in Table 1.

Abaqus does not have any direct option for modeling stress–strain behaviour using the proposed MMC model; therefore, in this study it is implemented through a user subroutine VUSDFLD. The stress and strain components are called in the subroutine in each time increment. From the stress components, p' is calculated. The strain components are transferred to the principal strain components and stored as state variables. The plastic strain increment ($\Delta\gamma^p$) in each time increment is calculated as $\Delta\gamma^p=\Delta\varepsilon_1^p-\Delta\varepsilon_3^p$, where $\Delta\varepsilon_1^p$ and $\Delta\varepsilon_3^p$ are the major and minor principal plastic strain components, respectively. The value of γ^p is calculated as the sum of increments $\Delta\gamma^p$ over the period of analysis. In the subroutine, γ^p and p' are defined as two field variables FV1 and FV2, respectively. In the input file, using Eqs. (1-9) (Table 2), the mobilized ϕ' and ψ are defined in tabular form as a function of γ^p and p'. During the analysis, the program accesses to the subroutine and updates the values of ϕ' and ψ with field variables.

Table 1. Parameters used in FE analysis

	MC	MMC
Anchor width, B (m)	1.0	
Anchor thickness, t (m)	0.1	
K	250	
n	0.5	
p'_a (kN/m^2)	100	
ν_{soil}	0.2	
A_ψ	-	5
k_ψ	-	0.8
ϕ'_{in} (°)	-	29
C_1	-	0.22
C_2	-	0.11
m	-	0.25
Critical state friction angle, ϕ'_c (°)	-	35
Relative density, D_r (%)	80	
Unit weight, γ (kN/m^3)	16	
Interface friction co-efficient, μ	0.4	
Depth of anchor, H/B	2	
Peak friction angle, ϕ'_p (°)	50, 44, 35	-
Peak dilation angle, ψ_p (°)	25, 19, 16, 0	-
Cohesion[1], c' (kN/m^2)	0.1	
[1]A cohesion value is required for Mohr-Coulomb model in Abaqus. In this study a very small value of 0.1 kN/m^2 is used for dense sand.		

RESULTS

Force–displacement Behaviour

The reaction force at the reference point of the rigid anchor and the displacement of this point are obtained from FE output. The lateral component of the reaction force and displacement are plotted in dimensionless form as N_h ($=F/\gamma HB$) versus u/B. Here, F is the lateral force on the anchor per meter length, H is the depth of the centre of the anchor from soil surface, γ is the unit weight of sand and u is the lateral displacement. The peak value of N_h is defined as N_{hp} and the displacement required to reach to the peak is defined as u_p.

It is to be noted here that, in this study, the depth of the anchor is measured from the ground surface to the centre of the anchor instead of the bottom of the anchor as used by some authors (e.g. Dickin and Leung 1983). Therefore, for a given F, the magnitude of N_h would be higher as compared to those studies.

In order to show the performance of numerical modeling, analysis is performed for the conditions used by Dickin and Leung (1983) in physical modelling. They conducted a series of centrifuge tests to model a continuous strip anchor of 1.0 m width in prototype scale under gravitational acceleration of 40g. One set of tests was conducted in dense sand of relative density 78% for a varying depth of embedment (H/B) ranges between 0.5 and 11.5. Figure 3 shows the force–displacement curve of the test for H/B=1.5. The pullout resistance increases with increase in lateral displacement, reaches the peak and then decreases with further displacement. Post-peak reduction in pullout resistance was observed in all the tests in dense sand and it is more pronounced for deep burial conditions.

FE analysis is performed for the same size of anchor under lateral loading (i.e. B=1.0 m and H/B=1.5). Figure 3 also shows that the force–displacement curve obtained from FE analysis with the MMC model. Similar to experimental results, the lateral resistance increases with displacement, reaches the peak and then decreases. The dimensionless peak resistance (N_{hp}) obtained from FE analyses is consistent with centrifuge test results. However, the lateral displacement required to mobilize the peak (u_p) is lower in FE modeling than the value reported from centrifuge modeling. Palmer et al. (2003) argued that the peak uplift resistance could be obtained from centrifuge modeling; however, the centrifuge modeling gives higher u_p as compared to full-scale tests. They also suggested that strain localization and shear band formation in dense sand might be the cause of this discrepancy in u_p. The present FE modeling with the MMC model also gives similar trend in u_p.

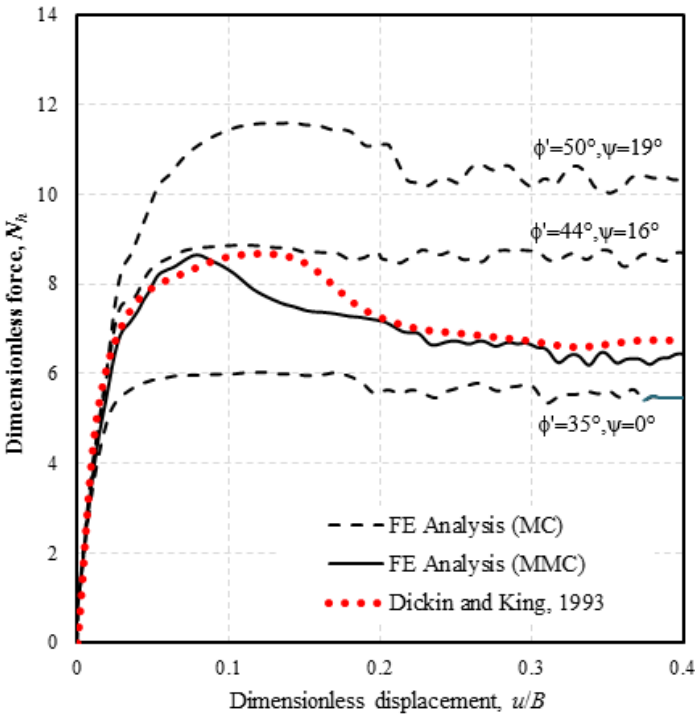

Figure 3: Dimensionless force–displacement curves for lateral loading of vertical anchors (test data from Dickin and Leung, 1983)

FE analysis is also performed using the built-in Mohr-Coulomb model. Two parameters needed for the Mohr-Coulomb model are the friction angle (ϕ') and dilation angle (ψ). The selection of representative values of these two parameters is very difficult because ϕ' and ψ are not constant but varies with a number of factors including shearing strain level as shown in the inset of Table 2. This issue has also been recognized in previous studies. For example, Dickin and Leung (1983) mentioned that a relevant friction angle should be carefully selected in order to calculate the pullout capacity using theoretical models (Neely et al., 1973; Ovesen and Stromann, 1972). They also showed that, if the peak friction angle obtained from laboratory tests is used, the theoretical models significantly overestimate the resistance as compared to model test results. Therefore, although the peak friction angle of the sand they used is greater than 50° in PS condition, they used a representative friction angle of 43.5°–39.4° to calculate the maximum lateral resistance comparable to experimental results. The above mentioned representative friction angles are significantly lower than the peak but higher than the critical state friction angles obtained from element tests (Dickin, 1994). The broken lines in Fig. 3 show the FE results with the built-in Mohr-Coulomb model for three sets of soil parameters: ϕ'=50°, ψ=19°; ϕ'=44°, ψ=16° and ϕ'=35°, ψ=0°. Here the dilation angle is calculated based on Bolton (1986), assuming the PS critical state friction angle equal to 35°. As expected, the simulations using the Mohr-Coulomb model does not show any post-peak degradation, which is consistent with other numerical studies available in the literature (e.g. Dickin and Laman, 2007). Moreover, the lateral resistance decreases with decrease in ϕ' and ψ. If the peak values of friction and dilation angles (ϕ'=50°, ψ=19°) are used, the maximum lateral resistance from FE analysis with the MC model is significantly higher than centrifuge test results (Fig. 3). On the other hand, the use of critical state values (ϕ'=35°, ψ=0°) gives significantly lower resistance.

Therefore, from the comparison shown in Fig. 3, it can be concluded that the modified Mohr-Coulomb model can simulate the force–displacement curve better than the Mohr-Coulomb model.

Table 2: Equations for Modified Mohr-Coulomb Model (MMC) (summarized from Roy et al., 2015)

Description	Eq. #	Constitutive Equation	Soil Parameters
Relative density index	(1)	$I_R = I_D(Q - \ln p') - R$	$I_D = D_r(\%)/100$, Q=10, R=1 (Bolton, 1986)
Peak friction angle	(2)	$\phi'_p - \phi'_c = A_\psi I_R$	ϕ'_c, A_ψ
Peak dilation angle	(3)	$\psi_p = \dfrac{\phi'_p - \phi'_c}{k_\psi}$	k_ψ
Strain softening parameter	(4)	$\gamma_c^p = C_1 - C_2 I_D$	C_1, C_2
Plastic strain at ϕ'_p	(5)	$\gamma_p^p = \gamma_c^p \left(p'/p'_a\right)^m$	p'_a, m
Mobilized friction angle at Zone-II	(6)	$\phi' = \phi'_{in} + \sin^{-1}\left[\left(\dfrac{2\sqrt{\gamma^p \gamma_p^p}}{\gamma^p + \gamma_p^p}\right)\sin\left(\phi'_p - \phi'_{in}\right)\right]$	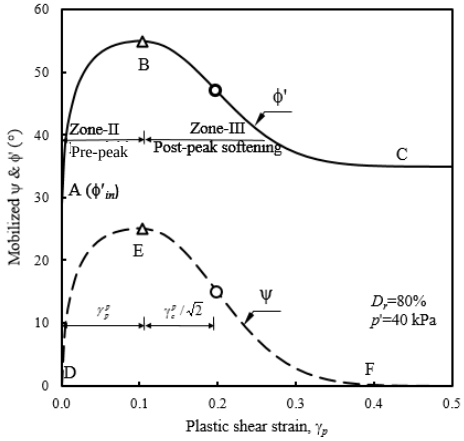
Mobilized dilation angle at Zone-II	(7)	$\psi = \sin^{-1}\left[\left(\dfrac{2\sqrt{\gamma^p \gamma_p^p}}{\gamma^p + \gamma_p^p}\right)\sin\left(\psi_p\right)\right]$	
Mobilized friction angle at Zone-III	(8)	$\phi' = \phi'_c + \left(\phi'_p - \phi'_c\right)\exp\left[-\left(\dfrac{\gamma^p - \gamma_p^p}{\gamma_c^p}\right)^2\right]$	
Mobilized dilation angle at Zone-III	(9)	$\psi = \psi_p \exp\left[-\left(\dfrac{\gamma^p - \gamma_p^p}{\gamma_c^p}\right)^2\right]$	
Young's modulus	(10)	$E = K\, p'_a \left(\dfrac{p'}{p'_a}\right)^n$	K, n

ϕ'_{in} = Initial friction angle, γ^p = Accumulated engineering plastic shear strain

Soil Failure Mechanism

In this section, the soil failure mechanisms are explained using the formation of shear bands with lateral displacements. The mechanisms of shear band formation and their propagation simulated with the MC and MMC models are compared. For this shallow burial depth, the lateral displacement of the anchor in dense sand results in formation of soil wedges, which is commonly known as 'wedge' type failure. Figure 4 shows the plastic shear strains with the MMC model at a lateral displacement of 207 mm (u/B=0.207). Large plastic shear strains develop in some narrow zones which represent the failure planes. As the anchor moves laterally, active failure occurs first behind the anchor which is followed by the failure of passive zone in front of the anchor. Similar pattern of failure for H/B=2.5 was found by Dickin and Leung (1985) in centrifuge test (Fig. 5). The thin lines in Fig. 5 represent the deformed shape of initially horizontal dyed sand layers.

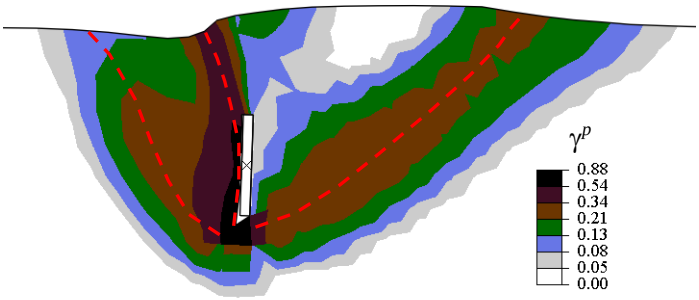

Figure 4: Strain localization for lateral anchor–soil interaction using MMC (B=1m, H/B=1.5, u/B=0.207)

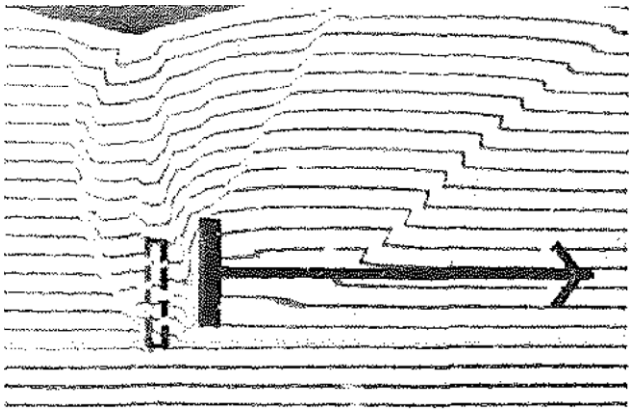

Figure 5: Failure mechanism around shallow anchor for B=1 m and H/B=2.5 (after Dickin and Leung, 1985)

The movement of soil particles could be explained using instantaneous velocity vectors as shown in Fig. 6. The anchor moves slightly upward with lateral displacement. For this shallow burial depth, the displacement of soil elements extents up to the ground surface for this level of lateral displacement of the anchor (u/B=0.207). Heave occurs in front (right side) while settlement occurs behind the anchor. This is again similar to model test results (Fig. 5) and numerical simulations (e.g. Merifield and Sloan, 2006) although the size of the soil wedges is different as discussed below.

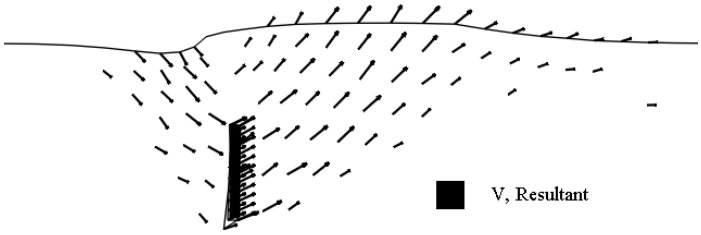

Figure 6: Instantaneous velocity vectors for lateral anchor–soil interaction with MMC (B=1 m, H/B=2, u/B=0.207)

Using digital image correlations in anchor uplift tests, Liu et al. (2012) showed that strain concentration occurs relatively in large areas; however, the highly strain concentration mainly occurs in a narrow zone as shown in Fig. 4. The zone of high plastic shear strain where considerable post-peak softening occurs (see inset of Table 2) represents the shear band. Drawing a line through the shear bands, their location is further examined.

As shown by White et al. (2008) and by the authors of the present study (Roy et al. 2014, 2015) that the location of the shear band is directly related to dilation angle ψ. In other words, dilation angle plays an important role both in ultimate resistance and soil failure mechanisms. To investigate the effect of dilation angle, FE analyses are conducted with the MC model for constant ϕ'=44° but varying ψ (=0°, 16° and 25°). Similar to the dashed line shown in Fig. 4, the location of the shear band is obtained from FE results. Figure 7 shows the location of the shear bands for u/B=0.2. For the passive failure wedge (right side of Fig. 7), the shear band shifts to the right with increase in dilation angle. An opposite trend is found for the active failure zone (left of the anchor). As the lateral resistance of vertical anchor largely depends on the size of passive failure wedge, analysis with ψ=25° gives higher lateral resistance than the analyses with ψ=16° or ψ=0°.

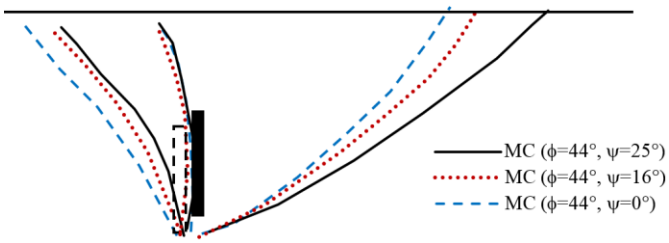

Figure 7: Shear band locations with MC model for different dilation angles (B=1m, H/B=2, u/B=0.2)

In the MMC model, ψ does not remain constant but varies with plastic shear strain (see Eqs. (6)–(9) in Table 2). Strain localization in soil initiates near the bottom of the anchor and then propagates up with increase in lateral displacement of the anchor as shown in Fig. 4. Figure 8 shows the comparison between the location of the shear band with the MMC model and MC model. For this particular case (i.e. geometry and soil properties) the location of the failure plane in the passive side with the MC model (ϕ'=44° and ψ=16°) is almost the same as the one obtained with the MMC model. However, the passive failure plane for ϕ'=35° and ψ=0° creates a shear band further left to the other two cases. The location of the active failure planes in the left side also depends on dilation angle. Note that the lateral pullout resistance mainly depends on the size of the

passive failure wedge and mobilized shear strength along the failure plane. Therefore, higher pullout resistances are obtained for higher values of ψ.

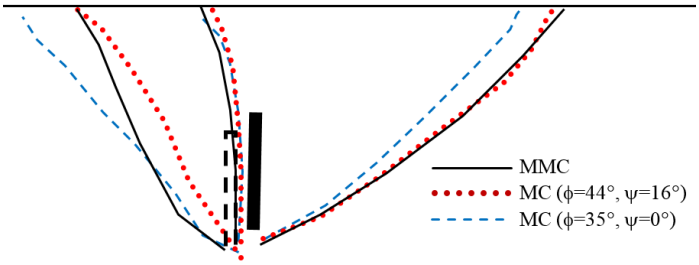

Figure 8: Shear band locations with MC and MMC (*B*=1m, *H*/*B*=1.5, *u*/*B*=0.207)

CONCLUSIONS

Finite element modeling is carried out to simulate the response of a vertical strip anchor in dense sand under lateral loading. Recognizing the fact that constitutive model of sand influences the load-carrying capacity, a comparative study is performed using the built-in Mohr-Coulomb model in Abaqus and a modified Mohr-Coulomb (MMC) model. The progressive formation of shear bands and its relation to the force–displacement response is carefully examined. It is shown that if the mobilized friction angle and dilation angle are modeled as function of plastic shear strain, density, and mean effective stress as the proposed modified Mohr-Coulomb model, the simulation of load–displacement response improves as compared to the simulations with the built-in Mohr-Coulomb model in Abaqus where constant friction and dilation angles are used. The failure mechanisms are also different for the simulations with the Mohr-Coulomb and modified Mohr-Coulomb models. Analysis presented in the paper is only for one geometry and a set of soil properties. Further study on the effects of depth of embedment, size, shape and inclination of the anchor and soil parameters is required.

ACKNOWLEDGEMENTS

The work presented in this paper was funded by the Research and Development Corporation (RDC), Newfoundland and Labrador, Chevron Canada Limited and NSERC Discovery and CRD grants.

REFERENCES

Abdel Rahman, M.A., Othman, M.A. and Edil, T.B. (1992). "Effect of plate flexibility on behaviour of shallow anchors." *Soils and Foundations*, 32(3), 137–143.

Akinmusuru, J.O. (1978). "Horizontally loaded vertical plate anchors in sand." *Journal of Geotechnical Engineering Division*, ASCE, 104(2), 283–286.

Basudhar, P.K., and Singh, D.N. (1994). "A generalized procedure for predicting optimal lower bound break-out factors of strip anchors." *Géotechnique*, 44(2), 307–318.

Bhattacharya, P. and Kumar, J. (2013). "Seismic pullout capacity of vertical anchors in sand." *Geomechanics and Geoengineering*, 8, 191–201.

Bolton, M.D. (1986). "The strength and dilatancy of sands." *Geotechnique*, 36(1), 65−78.

Chattopadhyay, B.C., and Pise, P.J. (1986). "Uplift capacity of piles in sand." *Journal of Geotechnics Engineering*, 112(9), 888–904.

Das, B.M. and Seeley, G.R. (1975). "Load-displacement relationship for vertical anchor plates." *Journal of Geotechnical Engineering Division*, ASCE, 101(7), 711–715.

Das, B.M. and Shukla, S.K. (2013). *Earth Anchors*. 2nd edition, J. Ross Publishing Inc, Florida, USA, ISBN 978-1-60427-077-8.

Dickin, E. and Leung, C.F. (1985). "Evaluation of design methods for vertical anchor plates." *Journal of Geotechnical Engineering*, 111(4), 500–520.

Dickin, E.A. and King, G.J.W. (1993). "Finite element modelling of vertical anchor walls in sand." B.H.V. Topping, (Editor), *Developments in Civil & Construction Engineering Computing*, Civil-Comp Press, Edinburgh, UK, 171–181. doi:10.4203/ccp.15.6.4

Dickin, E.A., and Leung, C.F. (1983). "Centrifugal model tests on vertical anchor plates." *Journal of Geotechnical Engineering*, 109(12), 1503−1525.

Dickin, E.A. 1994, "Uplift resistance of buried pipelines in sand." *Soils and Foundation*, vol. 34, No 2, 41–48.

Dickin, E.A. and Laman, M. (2007). "Uplift response of strip anchors in cohesionless soil." *Advances in Engineering Software*, 38, 618-35.

Dickin, E. (1988). "Uplift behavior of horizontal anchor plates in sand." *Journal of Geotechnical Engineering*, 114(11), 1300–1317.

Kame, G.S., Dewaikar, D.M. and Choudhury, D. (2012). "Pullout capacity of vertical plate anchors in cohesion-less soil." *Geomechanics and Engineering*, 4, 105–120.

Kumar, J. and Sahoo, J.P. (2012). "Upper bound solution for pullout capacity of vertical anchors in sand using finite elements and limit analysis." *International Journal of Geomechanics*, 12, 333–337.

Liu, J., Liu, M., & Zhu, Z. (2012). "Sand deformation around an uplift plate anchor." *Journal of Geotechnical and Geoenvironmental Engineering*, 138(6), 728–737.

Merifield, R. S., and Sloan, S. W. (2006). "The ultimate pullout capacity of anchors in frictional soils." *Canadian Geotechnical Journal*, 43(8), 852–868.

Neely, W.J., Stuart, J.G., and Graham, J. (1973). "Failure loads of vertical anchor plates in sand." *Journal of Soil Mechanics and Foundation Division*, ASCE, 99(9), 669–685.

Ovesen, N. K., & Stromann, H. (1972). "Design method for vertical anchor slabs in sand." *Proc. of Specialty Conf. on Performance of Earth and Earth-Supported Structures*, 1-2, 1418–1500.

Robert, D.J. (2010). "Soil-pipeline interaction in unsaturated soils, Ph.D thesis, University of Cambridge.

Rowe, R.K. and Davis, E.H. (1982). "The behaviour of anchor plates in clay." *Geotechnique*, 31(1), 9–23.

Roy, K.S., Hawlader, B.C., Kenny, S. and Moore, I. (2015). "Finite element modeling of lateral pipeline−soil interactions in dense sand", *Canadian Geotechnical Journal*. doi: 10.1139/cgj-2015-0171.

Roy, K.S., Hawlader, B.C. and Kenny, S. (2015). "Soil failure mechanism for lateral and upward pipeline–soil interaction analysis in dense sand", *GeoQuebec 2015*, Quebec City, Quebec, Canada, September 20–23, 2015.

Roy, K.S., Hawlader, B.C., Kenny, S. and Moore, I. (2014). "Finite element modeling of uplift pipeline/soil interaction in dense sand", *Geohazards6*, Kingston, Ontario, Canada, June 15–18, 2014.

Roy, K.S., Hawlader, B.C., Kenny, S. and Moore, I. (2015). "Effects of post-peak softening behavior of dense sand on lateral and upward displacement of buried pipelines", *34th International Conference on Ocean, Offshore and Arctic Engineering (OMAE 2015)*, St. John's, Newfoundland and Labrador, Canada, May 31–June 5, 2015.

Sakai, T., and Tanaka, T. (2007). "Experimental and numerical study of uplift behavior of shallow circular anchor in two-Layered sand." *Journal of Geotechnical and Geoenvironmental Engineering*, 133(4), 469–477.

Sutherland, H. B. (1988). "Uplift resistance of soils." 28th Rankine

lecture. *Geotechnique*, 38(4), 493-516.
Tagaya, K., Tanaka, A. and Aboshi, H. (1983). "Application of Finite Element Method to Pullout Resistance of Buried Anchor." *Soils and Foundations*, 23(3), 91–104.
White, D. J., Cheuk, C. Y., and Bolton, M. D. (2008). "The uplift resistance of pipes and plate anchors buried in sand." *Geotechnique*, 58(10), 771–777.

APPENDIX F

A Comparative Study between Lateral and Upward Pipe-soil and Anchor-soil Interaction in Dense Sand

This paper has been published and presented in 11th International Pipeline Conference (IPC 2016), Calgary, Alberta, Canada, September 26–30, 2016. Most of the research work presented in this paper was conducted by the first author. He also prepared the draft manuscript. The other authors supervised the research and reviewed the manuscript.

Proceedings of the 2016 11th International Pipeline Conference
IPC2016
September 26-30, 2016, Calgary, Alberta, Canada

IPC2016-64546

A COMPARATIVE STUDY BETWEEN LATERAL AND UPWARD ANCHOR–SOIL AND PIPE–SOIL INTERACTION IN DENSE SAND

Kshama Roy
PhD Candidate
Memorial University of Newfoundland
St. John's, NL, Canada

Bipul Hawlader
Associate Professor
Memorial University of Newfoundland
St. John's, NL, Canada

Shawn Kenny
Associate Professor
Carleton University
Ottawa, ON, Canada

Ian Moore
Professor
Queen's University
Kingston, ON, Canada

ABSTRACT

Buried pipelines are extensively used in onshore and offshore environments for transportation of hydrocarbons. On the other hand, buried anchors have been used for many years to stabilize various structures. In the development of design guidelines for pipelines, theoretical and experimental studies on buried anchors are sometimes used assuming that pipeline–soil and anchor–soil interaction are similar. In the present study, finite element (FE) modeling is performed to simulate the response of pipeline and anchor buried in dense sand subjected to lateral and uplift forces. The similarities and differences between the responses of these two types of structures are examined to justify the application of anchor theory to pipeline behaviour. The stress–strain behaviour of dense sand is modeled using a Modified Mohr-Coulomb (MMC) model, which considers the pre-peak hardening, post-peak softening, density and confining pressure dependent friction and dilation angles. A considerable difference is found between the lateral resistance of pipeline and vertical strip anchor of similar size. Progressive development of shear bands (shear strain concentrated zone) can explain the load–displacement behaviour for both lateral and upward loading.

INTRODUCTION

According to the National energy board of Canada [1], 12% of incidents affecting Canadian regulated pipelines are caused by geohazards. Safe, economic and reliable operation of pipeline transportation systems is the primary goal of pipeline operators and regulatory agencies. Plate anchors have been widely used to stabilize many civil engineering structures. Buried pipelines and anchors might be subjected to loading in different directions. Force–displacement behaviour and associated failure mechanisms is one of the major concerns for current practitioners and designers.

Theoretical, numerical and experimental investigations have been conducted in the past on buried pipelines and its analogue system anchor plates [2-15]. The main focus of most of these studies has been to define the load–displacement relationships, more specifically the maximum resistance and the displacement required to mobilize it, when subjected to axial, lateral and vertical movements. The authors presented a comprehensive literature review on buried pipes and anchors elsewhere [6, 16].

The load–displacement behaviour of buried pipes and anchors is considered to be similar in nature. While there is a large number of studies on buried pipelines and anchors, a limited number of comparative studies are available in the literature that justified the above mentioned similarities. Dickin [18] conducted centrifuge tests on pipelines and anchors of similar size and compared the uplift resistance offered by dense sand. It has been shown that the maximum uplift resistance of buried pipelines is approximately the same as that of an equivalent strip anchor although the displacement required to mobilize this resistance is different. Compiling a large number of model test results (115 tests), White et al. [15] also showed similarities in uplift resistance for pipes and anchors. However, the comparison of the failure mechanisms for anchor–soil and pipe–soil interactions is limited. In addition, further studies on comparison between the lateral resistance of similar sized anchors and pipes are required.

In this paper, a comparative study between the behaviour of similar sized anchors and pipes buried in dense sand is presented. The commercially available Abaqus FE software is used for numerical analysis implementing an advanced soil constitutive model for dense sand. The load–displacement behaviour and failure mechanisms are critically examined to identify the similarities and differences between the response of pipes and anchors.

PROBLEM DEFINITION

Two sets of analyses are performed in this study (Fig. 1). In the first set, a strip anchor of width B and thickness t oriented vertically/horizontally is considered. In the second set, a pipe having diameter (D) same as the width of the anchor (i.e. D=B) is considered. Both anchor and pipe are buried in dense sand at a depth (H) below the ground surface and then subjected to lateral and vertical pullout forces. During installation the soil in the vicinity of the anchor/pipe is usually disturbed. However, the effect of such disturbance on load–displacement behaviour is not considered in the present study, instead the simulations are performed for wished-in-place conditions (i.e. neglecting the effect of installation). The dimensions of the anchor and pipe are shown in Table 1.

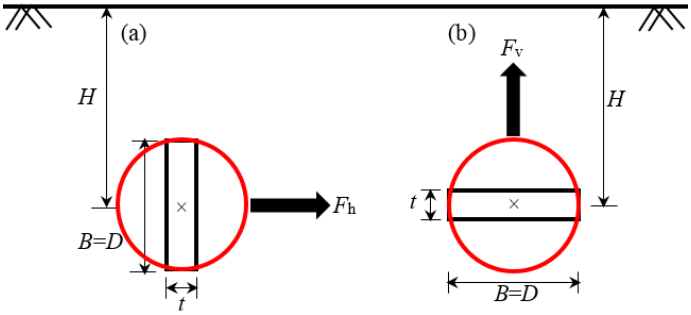

Figure 1: Schematic diagram of the problems: (a) lateral loading; (b) vertical loading

FE MODEL FORMULATION

Anchor/pipe–soil interaction is modeled in plane strain condition using Abaqus/Explicit FE software. Typical FE mesh for a pipe subjected to lateral and upward movement is shown in Figs. 2 and 3, respectively. Similar meshing is considered for anchor–soil interaction. Taking the advantage of symmetry, only half of the domain is modeled for upward loading (Fig. 3).

A 4-node bilinear plane strain quadrilateral element (CPE4R) is used for FE modeling of soil. Both pipe and anchor are modeled as rigid bodies with a reference point at the center. The structured mesh shown in Figs. 2 and 3 is generated by Abaqus/cae by zoning the soil domain.

The bottom of the FE domain is restrained from horizontal and vertical movement, while all the vertical faces are restrained from any lateral movement using roller supports. No displacement boundary condition is applied on the top face and therefore soil can move freely. The center of the anchor/pipe is placed at a distance H from the ground surface. The depth of the anchor/pipe is measured in terms of H/D and H/B ratio for pipe and anchor, respectively, which is termed as "embedment ratio" in this paper. The locations of the bottom and left/right boundaries of the domain with respect to the location of the anchor/pipe are sufficiently large, and therefore boundary effects on predicted lateral and uplift resistance, and soil failure mechanisms are not found.

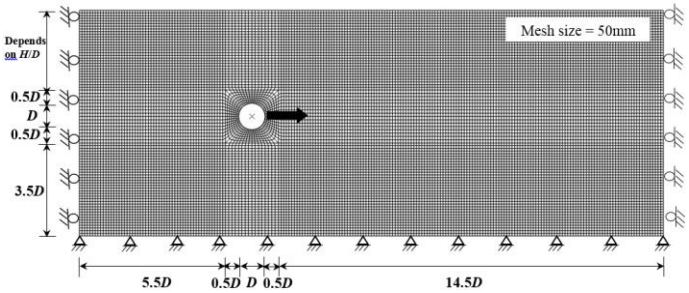

Figure 2. Typical finite element mesh for H/D=4 and D=500 mm under lateral loading

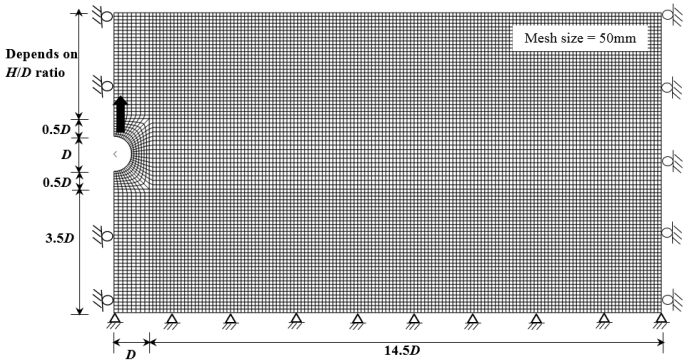

Figure 3. Typical finite element mesh for H/D=4 and D=500 mm for upward loading

The interface between anchor/pipe and soil is simulated using the contact surface approach available in Abaqus/Explicit. The Coulomb friction model is used for the frictional interface between the outer surface of the anchor/pipe and sand. In this method, the friction coefficient (μ) is defined as $\mu=\tan(\phi_\mu)$, where ϕ_μ is the anchor/pipe–soil interface friction angle. The value of ϕ_μ depends on the interface characteristics and relative movement between the anchor/pipe and soil [4, 7]. The value of μ equal to 0.4 is used in this study.

The numerical analysis is conducted in two steps. In the first step, geostatic stress is applied while in the second step, the anchor/pipe is displaced in the lateral and upward direction specifying displacement boundary conditions at the reference point of the anchor/pipe.

MODELING OF SAND

The Mohr-Coulomb (MC) model in its original form or after some modifications has been used by many researchers in the

past for anchor/pipe–soil interaction analysis [e.g. 4, 9, 10, 19, 20]. In the present study, analyses are performed using the modified Mohr-Coulomb model (MMC). In the classical Mohr-Coulomb (MC) model, constant values of angles of internal friction (ϕ') and dilation (ψ) are defined. The MC model is available in Abaqus as a built-in model, and has been used by number of researchers. However, the proposed MMC takes into account the effects of pre-peak hardening, post-peak softening, density and confining pressure on mobilized angles of internal friction (ϕ') and dilation (ψ) of dense sand. A detailed discussion of the MMC model, estimation of model parameters and comparison with the MC models are available in Roy et al. [6] and is not repeated here. However, the constitutive equations are summarized in Table 2. The MMC model is adopted in the analysis developing a user subroutine in Abaqus, which has also been discussed in Roy et al. [6, 17]. The soil parameters used in the present FE analysis are shown in Table 1.

Table 1: Parameters used in FE analyses

Parameters	Value
Anchor width, B (m)	0.5 (1.0)[1]
Anchor thickness, t (m)	0.2 (0.1)[1]
Pipe diameter, D (m)	0.5 (0.102)[1]
K	150
n	0.5
p'_a (kN/m^2)	100
ν_{soil}	0.2
A_ψ	5.0
k_ψ	0.8
ϕ'_{in}	29°
C_1	0.22
C_2	0.11
m	0.25
Critical state friction angle, ϕ'_c	35°
Relative density, D_r (%)	80
Dry unit weight, γ (kN/m^3)	17.7
Interface friction coefficient, μ	0.4
Depth of anchor/pipe, (H/B or H/D)	2, 8 (1.5)[1]
Cohesion (c')[2] (kN/m^2)	0.10

[1]For comparison with model tests D=0.102 m and B=1.0 m, t=0.1m for H/B or H/D=1.5 are used (Fig. 4)
[2]A cohesion value is required to be defined for Mohr-Coulomb model in Abaqus. In this study a very small value of c'=0.10 kN/m^2 is used.

RESULTS

Force–displacement behaviour under lateral loading

In order to show the performance of the present FE modeling, the first set of analysis is performed placing the anchor and pipe at an embedment ratio of 1.5 and then subjected to lateral displacement. As the comparison is performed with physical test results, the diameter of the pipe considered in this set of analysis is 0.102 m as Trautmann's [14] physical model tests. Similarly, for the anchor, B=1.0 m is considered which is same as the width of the anchor in prototype scale used by Dickin and Leung [3] in centrifuge modeling. Both of these model tests were conducted in dense sand having a relative density (D_r) approximately 80%. Moreover, γ=16.0 kN/m^3 is used for anchor only for this simulation as suggested by Dickin and King [2]. Other soil parameters used in FE analyses are listed in Table 1.

In the following sections, the force–displacement curves are presented in normalized forms as N_h (=$F_h/\gamma HB$ or $F_h/\gamma HD$) versus u/B or u/D for lateral loading and N_v (=$F_v/\gamma HB$ or $F_v/\gamma HD$) versus v/B or v/D for vertical loading. Here F_h and F_v are the lateral and upward resistances on the anchor/pipe per meter length, respectively; H is the depth of the center of the anchor/pipe from soil surface, γ is the dry unit weight of soil and u and v are the lateral and upward displacements, respectively. The peak value of N_h and N_v are defined as N_{hp} and N_{vp}, and the displacements required to reach to the peak are defined as u_p and v_p, respectively.

Figure 4 shows the lateral resistance–displacement curves obtained from FE simulations with the MMC model. For comparison, model test results [3, 14] are also plotted in this figure. The resistance increases with increase in lateral displacement, reaches the peak and then decreases with further displacement. There is a post-peak degradation in resistance, although it is more significant in anchor as compared to pipe.

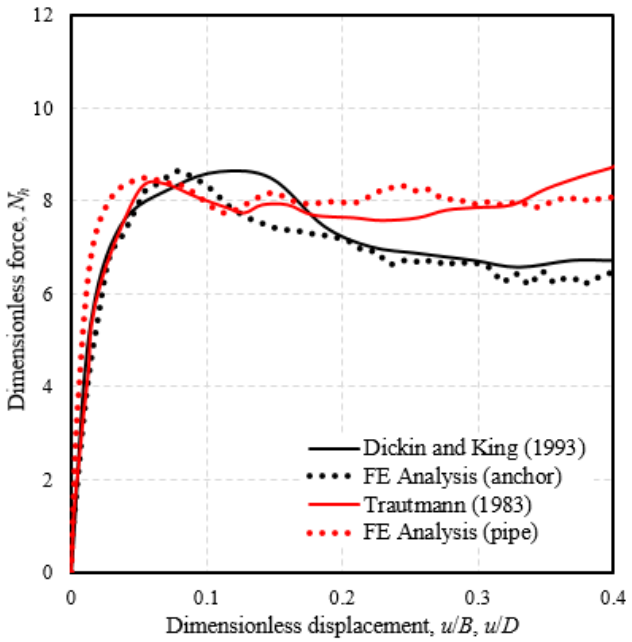

Figure 4. Dimensionless force–displacement curves for lateral loading for embedment ratio of 1.5

As shown, the proposed MMC model can simulate not only the peak resistance but also the post-peak resistance. The shape of the force–displacement curves can be explained using the mobilized angles of internal friction and dilation, as presented by the authors [6]. Note that the classical elastoplastic Mohr-

Coulomb model cannot simulate this post-peak degradation as discussed by the authors elsewhere [6, 16]. For anchor, the dimensionless peak resistance (N_{hp}) obtained from FE analyses is consistent with model test result. However, the lateral displacement required to mobilize the peak (u_p) is lower in FE modeling than centrifuge test result (Fig. 4). It is to be noted here that Palmer et al. [21] argued that the peak uplift resistance could be obtained from centrifuge modeling; however, the centrifuge modeling gives higher u_p as compared to full-scale tests. Strain localization and shear band formation in dense sand might be the cause of this discrepancy in u_p. The present FE modeling with the MMC model also gives similar trend in u_p.

Table 2: Equations for Modified Mohr-Coulomb Model (MMC) (summarized from Roy et al. [6])

Description	Eq. #	Constitutive Equation	Soil Parameters
Relative density index	(1)	$I_R = I_D(Q - \ln p') - R$	$I_D = D_r(\%)/100$, Q=10, R=1 (Bolton [23])
Peak friction angle	(2)	$\phi'_p - \phi'_c = A_\psi I_R$	ϕ'_c, A_ψ
Peak dilation angle	(3)	$\psi_p = \dfrac{\phi'_p - \phi'_c}{k_\psi}$	k_ψ
Strain softening parameter	(4)	$\gamma_c^p = C_1 - C_2 I_D$	C_1, C_2
Plastic strain at ϕ'_p	(5)	$\gamma_p^p = \gamma_c^p (p'/p'_a)^m$	p'_a, m
Mobilized friction angle at Zone-II	(6)	$\phi' = \phi'_{in} + \sin^{-1}\left[\left(\dfrac{2\sqrt{\gamma^p \gamma_p^p}}{\gamma^p + \gamma_p^p}\right)\sin(\phi'_p - \phi'_{in})\right]$	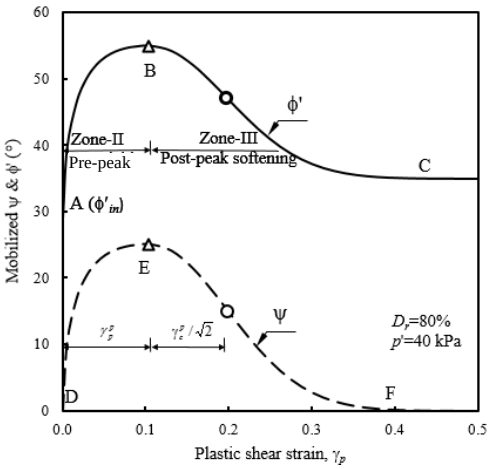
Mobilized dilation angle at Zone-II	(7)	$\psi = \sin^{-1}\left[\left(\dfrac{2\sqrt{\gamma^p \gamma_p^p}}{\gamma^p + \gamma_p^p}\right)\sin(\psi_p)\right]$	
Mobilized friction angle at Zone-III	(8)	$\phi' = \phi'_c + (\phi'_p - \phi'_c)\exp\left[-\left(\dfrac{\gamma^p - \gamma_p^p}{\gamma_c^p}\right)^2\right]$	
Mobilized dilation angle at Zone-III	(9)	$\psi = \psi_p \exp\left[-\left(\dfrac{\gamma^p - \gamma_p^p}{\gamma_c^p}\right)^2\right]$	
Young's modulus	(10)	$E = K p'_a \left(\dfrac{p'}{p'_a}\right)^n$	K, n

ϕ'_{in} = Initial friction angle, γ^p = Accumulated engineering plastic shear strain

Effects of embedment depth

In order to check the effects of embedment ratio, FE simulations are performed for four cases with B=D=500 mm. In the previous cases (Fig. 4), B was different from D because the purpose of those simulations was to compare FE results with physical model test results. However, in these cases, B=D is considered in order to avoid scale effects [3,10]. Figure 5 shows the dimensionless force–displacement curves. The dimensionless force reaches the peak at small u for the shallow burial cases (H/D=2) as compared to deep burial cases (H/D=8). There is a considerable difference between N_{hp} for the anchor and pipe at the same embedment ratio. Note that this difference is not pronounced in Fig. 4 because the diameter of the pipe is smaller than the width of the anchor. A lower width/diameter anchor/pipe

gives higher N_{hp} as recognized also in previous studies [3, 10]. Figure 5 also shows that N_{hp} mobilizes at lower u_p for pipes than anchors.

The post-peak degradation has not been completed in the simulations for embedment ratio of 8. Complete degradation might occur if the simulations were continued for a large displacement. Similar conclusion has been drawn by Dickin and King [2] from experimental results.

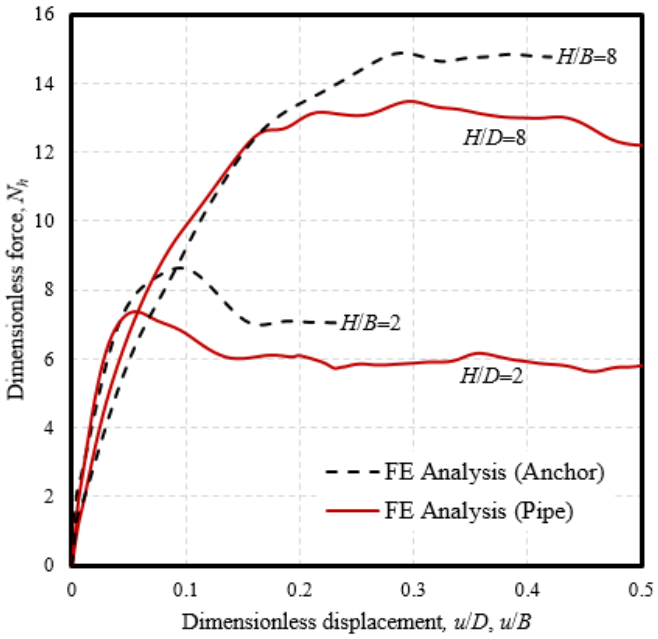

Figure 5. Dimensionless force–displacement curves for lateral loading for different embedment ratio (D=B=500 mm)

Force–displacement behaviour under vertical loading

FE simulations were also performed for vertical loading for embedment ratios of 2 and 8 with B=D=500 mm, similar to the lateral loading as discussed in the previous section. As shown in Fig. 6, N_v increases with vertical displacement, reaches the peak and then decreases in the post-peak zone. The dimensionless upward force–displacement curves for both anchor and pipe are very similar in nature. Similar behaviour was found by Dickin [18] for 25 mm dia pipe and 25 mm wide anchors with some difference in mobilization distance. Further studies are required to investigate the effects of different parameters including the size, roughness and soil parameters.

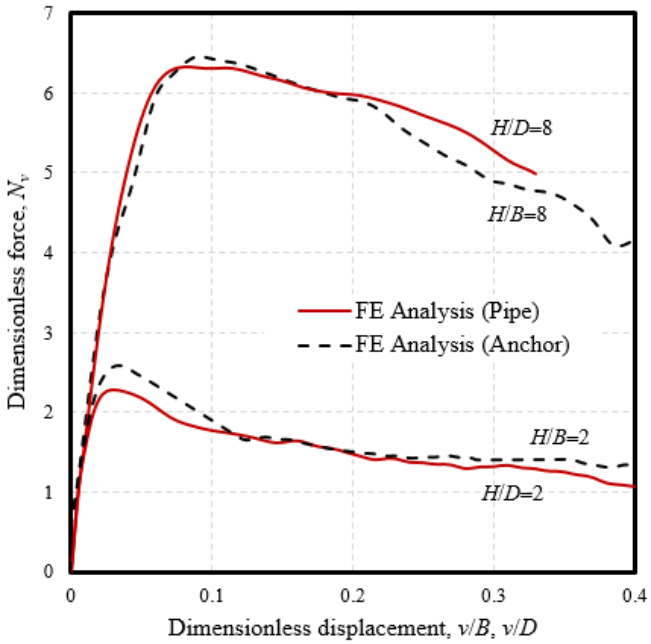

Figure 6. Dimensionless force–displacement curves for upward loading for different embedment ratio (D=B=500 mm)

Soil Failure Mechanisms

In this section, the mechanisms of failure of soil due to lateral and upward displacements of the pipe and anchor are investigated. The mechanisms involved in force–displacement behaviour can be explained using plastic deformation of soil and formation of shear bands (plastic shear strain concentrated zones). Due to space limitation, the failure mechanisms only for the shallow burial conditions are discussed.

The plastic shear strains developed in soil at the displacement when the peak lateral resistance is mobilized is shown in Figs. 7(a) and 7(b) for the pipe and anchor, respectively. The shear band in the passive failure zone (f_1) does not reach the ground surface for the pipe (Fig. 7a) while it reaches the ground surface for the anchor (Fig. 7b). Also the maximum width of the passive failure wedge i.e. the distance from the centre of the anchor/pipe to the point where f_1 reaches the ground surface is 4.5B for the anchor and 4D for the pipe. Note that B=D in this case. Because of this larger size of the passive wedge, the length of the failure plane f_1 is longer for the anchor and therefore gives higher N_{hp} than the pipe of same embedment ratio (Fig. 5). Although it is not presented here, the progressive development of shear bands can also explain the force–displacement curves of embedment ratio of 8 as shown in Fig. 5.

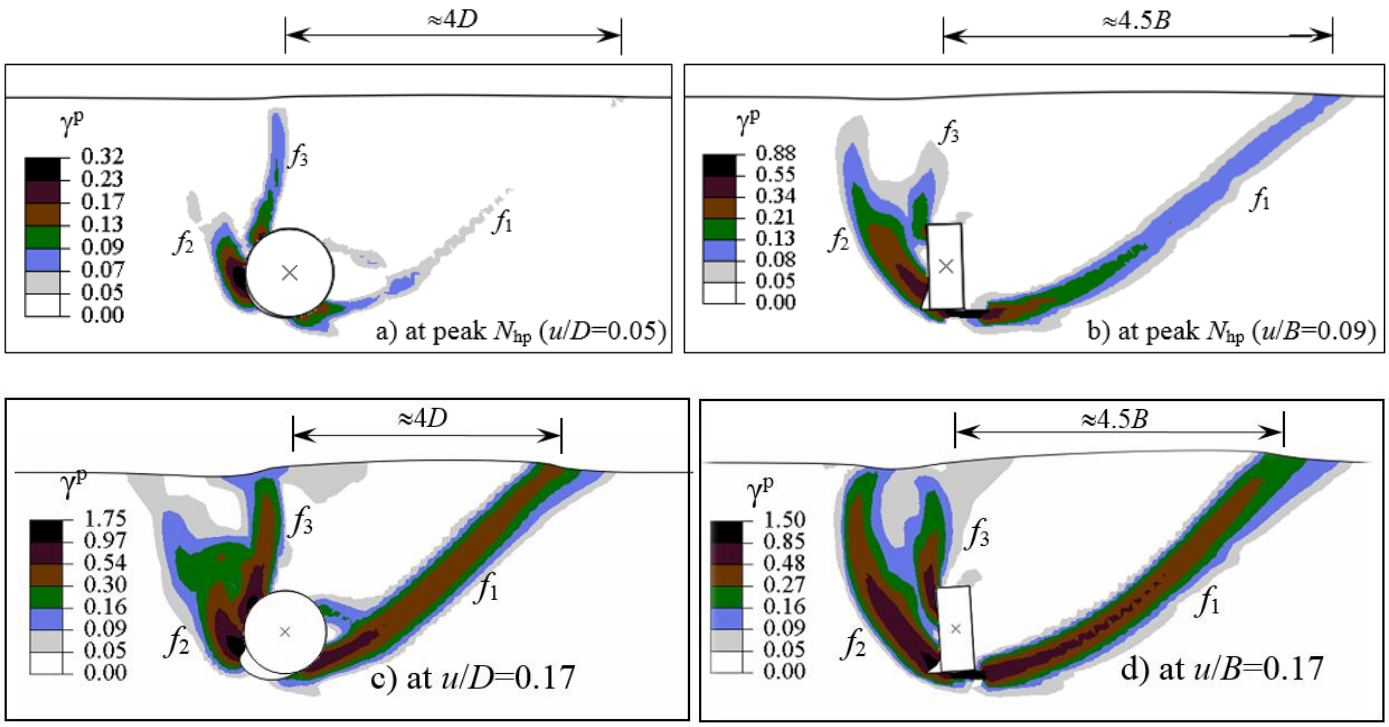

Figure 7. Shear bands under lateral loading for embedment ratio of 2: (a) pipe at the peak, (b) anchor at the peak, (c) pipe at large displacement, (d) anchor at large displacement

Similar to lateral loading, strain localization and shear band formation for the shallow burial case during upward loading is shown in Fig. 8.

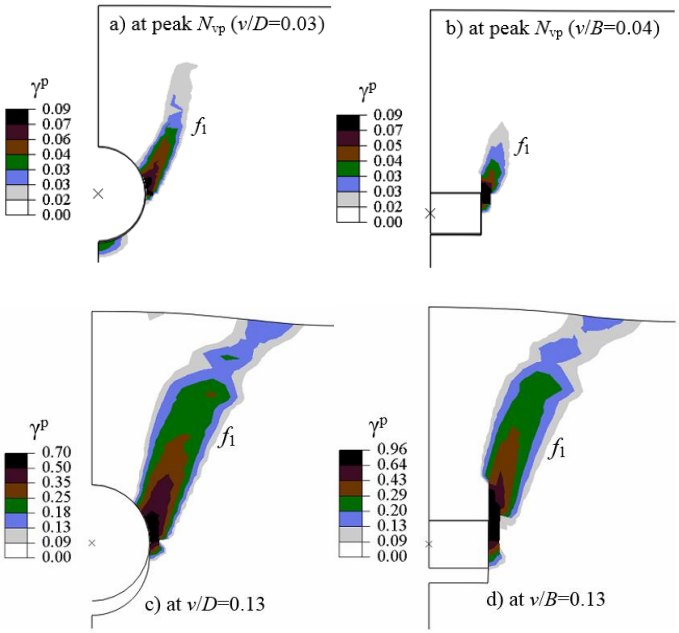

Figure 8. Shear bands under vertical loading for embedment ratio of 2: (a) pipe at the peak, (b) anchor at the peak, (c) pipe at large displacement, (d) anchor at large displacement

At the peak, shear bands do not reach the ground surface (Figs. 8a & 8b). The plastic shear strains mainly concentrate near the anchor/pipe when the peak dimensionless force N_{vp} is mobilized. With further displacement of the anchor/pipe, the size of the plastic zone increases and a complete failure plane develops which curves outward near the ground surface. The shape of the failure plane is similar to physical model test results [15, 22].

CONCLUSIONS

A comparative study of anchor/pipe–soil interactions under lateral and upward loading is presented. Finite element simulations are performed using Abaqus FE software for the plane strain condition using an improved soil model for dense sand. The key features considered in modeling the behaviour of dense sand are: (i) the decrease in peak friction angle with increase in mean effective stress, (ii) variation of mobilized friction and dilation angles as a function of plastic shear strain, including the pre-peak hardening and post-peak softening; and (iii) plane strain shear strength parameters.

The proposed modified Mohr-Coulomb model can simulate the load–displacement behaviour of buried pipes and strip anchors including the post-peak degradation of resistance. A comparative study between the response of 500 mm diameter pipe and 500 mm wide strip anchor shows that strip anchors can offer higher peak lateral resistance than a pipe of similar diameter. However, no significant difference is found between the maximum vertical uplift resistance of the pipe and the strip

anchor. The formation of shear bands and their propagation can explain the force–displacement behaviour.

While this study shows performance of the MMC model, a comprehensive parametric study is required for different pipe and anchor sizes (diameter and width), interface behaviour, soil parameters, and burial depths.

ACKNOWLEDGMENTS

The work presented in this paper was funded by the Research and Development Corporation (RDC), Newfoundland and Labrador, Chevron Canada Limited and NSERC Discovery and CRD grants.

REFERENCES

[1] National Energy Board of Canada. 2003, Focus on safety, a comparative analysis of pipeline safety performance.

[2] Dickin, E.A. and King, G.J.W. 1993, "Finite element modelling of vertical anchor walls in sand." B.H.V. Topping, (Editor), *Developments in Civil & Construction Engineering Computing*, Civil-Comp Press, Edinburgh, UK, 171–181. doi:10.4203/ccp.15.6.4.

[3] Dickin, E.A., and Leung, C.F. 1983, "Centrifugal model tests on vertical anchor plates." *Journal of Geotechnical Engineering*, 109(12), 1503−1525.

[4] Merifield, R. S., and Sloan, S. W. 2006, "The ultimate pullout capacity of anchors in frictional soils." *Canadian Geotechnical Journal*, 43(8), 852–868.

[5] Kame, G.S., Dewaikar, D.M. and Choudhury, D. 2012, "Pullout capacity of vertical plate anchors in cohesion-less soil." *Geomechanics and Engineering*, 4, 105–120.

[6] Roy, K.S., Hawlader, B.C., Kenny, S. and Moore, I. 2016, "Finite element modeling of lateral pipeline−soil interactions in dense sand", *Canadian Geotechnical Journal*, 53(3), 490–504. doi: 10.1139/cgj-2015-0171.

[7] Yimsiri, S., Soga, K., Yoshizaki, K., Dasari, G., and O'Rourke, T. 2004, "Lateral and upward soil-pipeline interactions in sand for deep embedment conditions." *Journal of Geotechnical and Geoenvironmental Engineering*, 130(8), 830−842.

[8] Cheuk, C. Y., White, D. J. and Bolton, M. D. 2008, "Uplift mechanisms of pipes buried in sand." *Journal of Geotechnical and Geoenvironmental Engineering*, 134(2), 154–163.

[9] Daiyan, N., Kenny, S., Phillips, R., and Popescu, R. 2011, "Investigating pipeline–soil interaction under axial–lateral relative movements in sand." *Canadian Geotechnical Journal*, 48(11), 1683−1695.

[10] Guo, P., and Stolle, D. 2005, "Lateral pipe-soil interaction in sand with reference to scale effect." *Journal of Geotechnical and Geoenvironmental Engineering*, 131(3), 338−349.

[11] Jung, J., O'Rourke, T., and Olson, N. 2013, "Lateral soil-pipe interaction in dry and partially saturated sand." *Journal of Geotechnical and Geoenvironmental Engineering*, 139(12), 2028−2036.

[12] Jung, J., O'Rourke, T., and Olson, N. 2013, "Uplift soil–pipe interaction in granular soil." *Canadian Geotechnical Journal*, 50(7), 744−753. doi: 10.1139/cgj-2012-0357.

[13] O'Rourke, and M.J., Liu, X. 2012, "Seismic design of buried and offshore pipelines." MCEER Monograph, MCEER-12-MN04.

[14] Trautmann, C. 1983, "Behavior of pipe in dry sand under lateral and uplift loading." PhD thesis, Cornell University, Ithaca, NY.

[15] White, D. J., Cheuk, C. Y., and Bolton, M. D. 2008, "The uplift resistance of pipes and plate anchors buried in sand." *Geotechnique*, 58(10), 771–777.

[16] Roy, K.S., Hawlader, B.C., Kenny, S. and Moore, I. 2016, "Finite element analysis of strip anchors buried in dense sand subjected to lateral loading", *26th International Ocean and Polar Engineering Conference (ISOPE 2016)*, Rhodes, Greece. June 26-July 2, 2016. (under review)

[17] Roy, K.S., Hawlader, B.C., Kenny, S. and Moore, I. 2014, "Finite element modeling of uplift pipeline/soil interaction in dense sand", *Geohazards6*, Kingston, Ontario, Canada, June 15–18, 2014.

[18] Dickin, E.A. 1994, "Uplift resistance of buried pipelines in sand." *Soils and Foundation*, 34(2), 41–48.

[19] Kouretzis, G.P., Sheng, D., and Sloan, S.W. 2013, "Sand-pipeline-trench lateral interaction effects for shallow buried pipelines." *Computers and Geotechnics*, 54, 53–59.

[20] Xie, X. 2008, "Numerical analysis and evaluation of buried pipeline response to earthquake-induced ground fault rupture." PhD thesis, Rensselaer Polytechnic Institute, New York.

[21] Palmer, A., et al. 2003, "Uplift resistance of buried submarine pipelines: Comparison between centrifuge modelling and full-scale tests." *Géotechnique*, 53(10), 877–883.

[22] Liu, J., Liu, M., and Zhu, Z. 2012, "Sand deformation around an uplift plate anchor."*Journal of Geotechnical and Geoenvironmental Engineering*, 10.1061/(ASCE)GT.1943-5606.0000633, 728–737.

[23] Bolton, M. D. 1986, "The strength and dilatancy of sands." *Geotechnique*, 36(1), 65−78.

APPENDIX G

Additional Details of Finite Element Modelling and Modified Mohr-Coulomb Model

G.1 Introduction

The purpose of this Appendix is to provide further details on finite element modelling and the Modified Mohr–Coulomb (MMC) model, which are not discussed in Chapters 3–6 and Appendixes A–F. Each of these chapters has been submitted as a manuscript to journals and conferences.

G.2 Finite Element Modelling

Abaqus/Explicit finite element (FE) program is used in the present study for numerical analysis. This is a special-purpose FE analysis that uses an explicit dynamic FE formulation. Although Abaqus/Explicit is developed for high speed dynamic events, it can effectively be used for modelling pipe–soil or anchor–soil interaction, as presented in this study, by maintaining quasi-static condition. Some of the key features of the present FE modelling are discussed in the following sections.

One of the main advantages of analyzing pipe–soil and anchor–soil interactions using Abaqus/Explicit is that it controls mesh distortions that result from large deformations of soil due to large displacements of the pipe and anchor. The Arbitrary Lagrangian Eulerian (ALE) adaptive meshing technique available in Abaqus/Explicit is used in the present study. This technique is based on small strain Lagrangian increments together with frequent mesh regeneration, keeping the mesh topology unchanged. In this technique, the nodes in the specified adaptive domain (e.g. Zone–A in Fig. 4.2) are frequently adapted to maintain minimal element distortion during the movement of the pipe or anchor. However, the number of elements and their connectivity are not altered. For example, the FE mesh around the pipe for the simulation presented in Fig. 4.3 are shown in Fig. G-1 for four levels of displacement of the pipe. For comparison, the same problem is simulated without adaptive meshing. As shown in Fig. G-1 that at a small displacement of the pipe (e.g. v/D=0.06), no significant distortion occurs in both cases. With an

increase in displacement of the pipe, the soil elements around the pipe is significantly distorted in the simulation without adaptive meshing. However, with adaptive meshing, new mesh generates that maintains the mesh in acceptable shape (Fig. G-1).

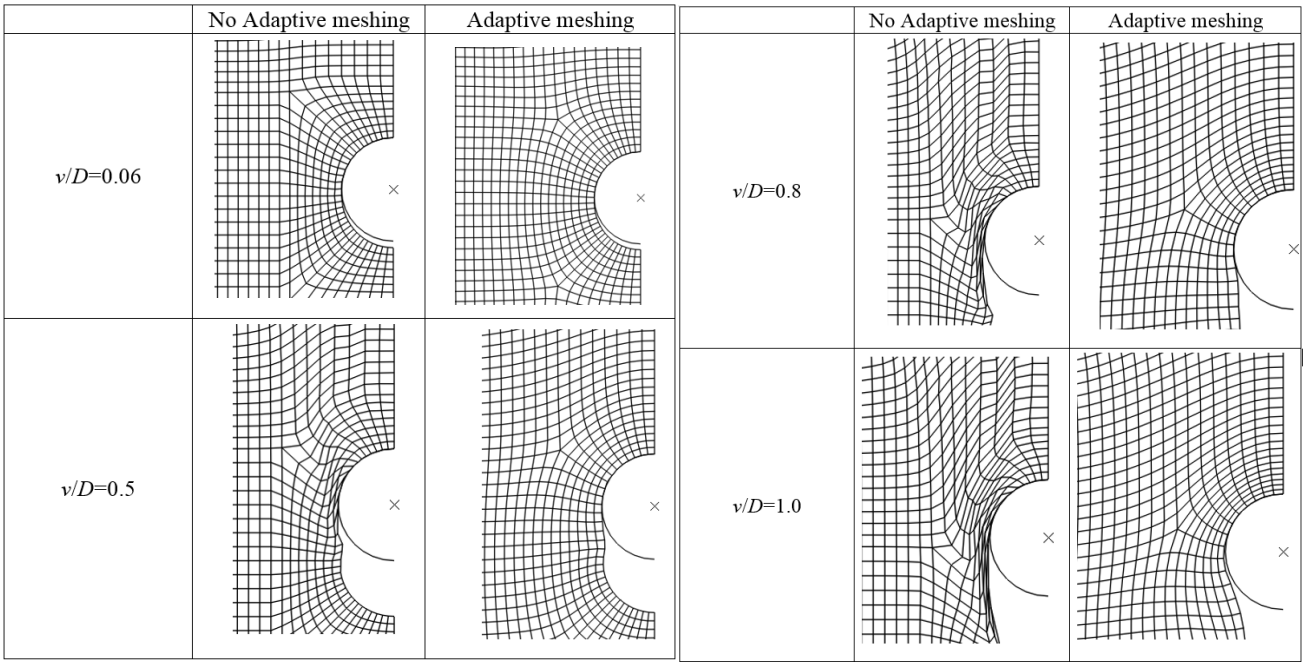

Fig. G-1: FE mesh at different displacement of the pipe

In the present study, the pipeline and anchor are moved slowly such that the inertial force is negligible, in order to maintain quasi-static condition. The automatic time incrementation scheme available in Abaqus/Explicit is used where the code accounts for changes in the stability limit and therefore requires no user intervention. The quasi-static condition is also checked by plotting the components of energy in the system with time. As an example, Fig. G-2 shows the components of energy for the simulation presented in Fig. 4.3. As shown, the kinetic energy (ALLKE) and energy absorbed by viscous dissipation (ALLVD) stay a very low fraction of the internal energy (ALLIE), which ensures that the quasi-static condition is satisfied (Dassault Systèmes 2010).

It is also to be noted here that, in physical modelling, the pipes or anchors are generally pulled slowly in order to ensure drained condition (Bransby and Ireland 2009) or to capture soil failure mechanisms (Cheuk et al. 2008). For example, Cheuk et al. (2008) pulled the pipe at an upward velocity of 10 mm/hr that allowed regular photography of soil deformation using digital cameras (Fig. 4.3). However, in FE modelling, the pipe is pulled at a velocity of 10 mm/s maintaining a quasi-static condition. Simulations are also performed for slower rates (1 and 5 mm/s); however, no significant difference is found in load–displacement behaviour. In the present FE modelling, drainage is not an issue because the soil is modelled based on stress–strain behaviour in drained condition.

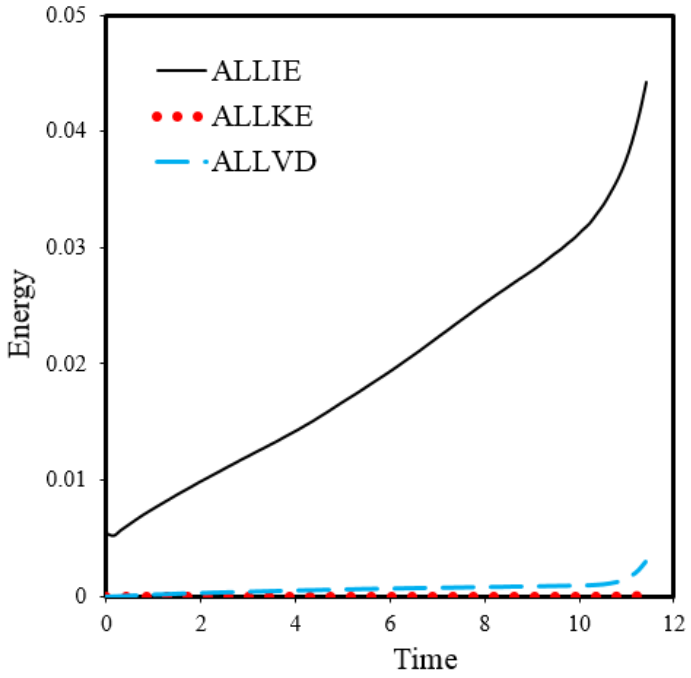

Figure G-2: Energy components in FE analysis ($\widetilde{H}$=3 and D=100 mm)

G.3 Modified Mohr–Coulomb Model

The modified Mohr–Coulomb (MMC) developed in this study is based on experimental results on dense sand available in the literature. While there are some differences in stress–strain behaviour of dense

sand depending upon physical properties (e.g. angularity, grain size), laboratory tests show some common features, which are briefly discussed in the following sections.

The shear strength of sand at a given relative density (D_r) is generally calculated using the angle of internal friction (ϕ'). Similarly, the volume change behaviour is modelled using the dilation angle (ψ). However, laboratory tests show than ϕ' and ψ are not constant but varies with mean effective stress and level of shear strain. Typical variation of ϕ' and ψ of dense sand obtained from an improved direct shear apparatus is shown in Fig. G-3 (Lings and Dietz 2004). In these figures, v_x represents the horizontal shear displacement and ϕ'_{ds} represents the direct shear friction angle. As shown, the peak friction (ϕ'_p) and the peak dilation (ψ_p) angles increase with a decrease in normal stress. The horizontal shear displacement required to mobilize ϕ'_p and ψ_p increases with an increase in normal stress. At a large shear displacement (v_x>7 mm), ϕ' remains almost constant and ψ becomes zero. Moreover, the variation of ϕ' and ψ with v_x is nonlinear having a pre-peak hardening followed by a post-peak softening. Similar response was found in triaxial tests (Hsu and Liao 1998; Suzuki and Yamada 2006). The modified Mohr–Coulomb model proposed in the present study can capture these behaviour (see Chapter 3 for further details).

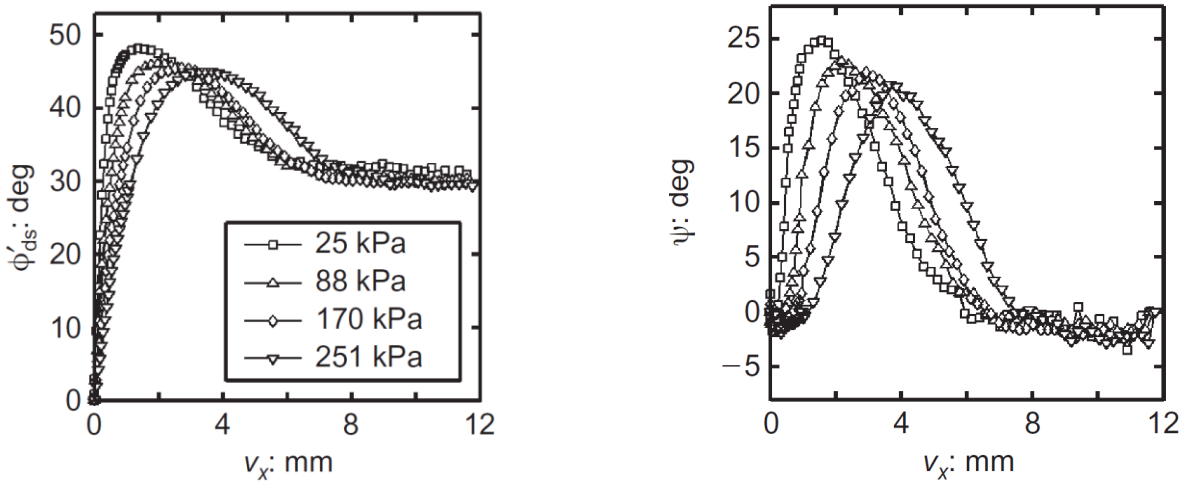

Figure G-3: Mobilized ϕ' and ψ obtained from direct shear test, (D_r=90%) (Lings and Dietz 2004)

Although Fig. G-3 shows that ϕ' starts to mobilize from zero at a very small shear displacement, previous studies suggested that the strain at the start of loading is primarily elastic (Mair 1993; Atkinson 2000). There exists an elastic boundary beyond which plastic deformation occurs. In this study, the elastic zone is defined by using an initial friction angle (ϕ'_{in}). In other words, if the stress in a soil element is inside the initial yield surface, defined by ϕ'_{in}, the strain increment due to loading is elastic. Rowe (1962) and Mitchell and Soga (2005) suggested that ϕ' represents the sum of the contributions of four components: interparticle friction, effect of dilation, rearrangement of particles (fabric) and crushing. The effect of soil particle crushing at the low stress level, considered in this study, is not significant. Figure G-3 shows that the dilation is almost zero at small displacements. Based on typical contributions of each component presented in Mitchell and Soga (2005), ϕ'_{in}=29° is used in this study.

In addition to mean effective stress p' (normal stress in direct shear tests in Fig. G-3), the shear strain required to mobilize the peak friction angle (γ_p^p) depends on relative density. In the proposed modified Mohr–Coulomb model, Eqs. 4.4 and 4.5 are used to capture this behaviour. These equations show that the higher the relative density the lower the γ_p^p. Moreover, γ_p^p increases with mean effective stress. The parameters required to model this behaviour (C_1, C_2 and m) are obtained by calibrating the model against laboratory test results, as presented in Chapter 3.

Although laboratory tests show that the mobilized friction angle varies with shear strain, the design guidelines for pipelines (e.g. ALA 2005) recommended to use a constant value of ϕ' depending upon the density of soil. However, the progressive formation of shear plane, as discussed in this study, has a significant influence on load–displacement behaviour. This recommended value of ϕ' can be considered as an equivalent friction angle (ϕ'_e), which should be less than ϕ'_p. Rowe (1969) recognized the importance

of deformation on failure of soil mass and suggested a progressivity index. Assuming the progressivity index equal to 0.5, Dickin (1994) showed that $\phi'_e = (\phi'_p + \phi'_c)/2$ can reasonably calculate the measured peak uplift resistance of pipe buried in dense sand. The importance of progressive formation of slip planes has also been recognized for other buried structures. For example, Loukidis and Salgado (2010) proposed $\phi'_e = \phi_c'^{TX} + \left\{\left[17.6\left(\frac{D_R}{100}\right) - 8.8\right] - 2.44\ln\left(\frac{B\gamma'}{p'_a}\right)\right\}$ to calculate the bearing capacity of strip footing, where $\phi_c'^{TX}$ is the critical state friction angle in triaxial compression and *B* is the width of the footing.

In the present study, ϕ'_e=45° is used in the limit equilibrium solution (Eq. 5.12) to calculate the peak uplift resistance. Similarly, ϕ'_e=44° is used in the empirical equation (Eq. 6.14) proposed by O'Rourke and Liu (2012) to calculate the peak lateral resistance.

G.4 Implementation of the Modified Mohr–Coulomb Model

The modified Mohr–Coulomb model is implemented in Abaqus/Explicit via a user defined subroutine VUSDFLD written in FORTRAN. In the subroutine, the mean effective stress (*p*') and accumulated plastic shear strain (γ^P) are calculated for each time increment, which are defined as two field variables (f_1 and f_2) and then transfer to Abaqus input file. Based on the values of f_1 and f_2, updated values of mobilized ϕ' are ψ are used for the next time increment. Figure G-4 shows the steps followed in the development of the subroutine.

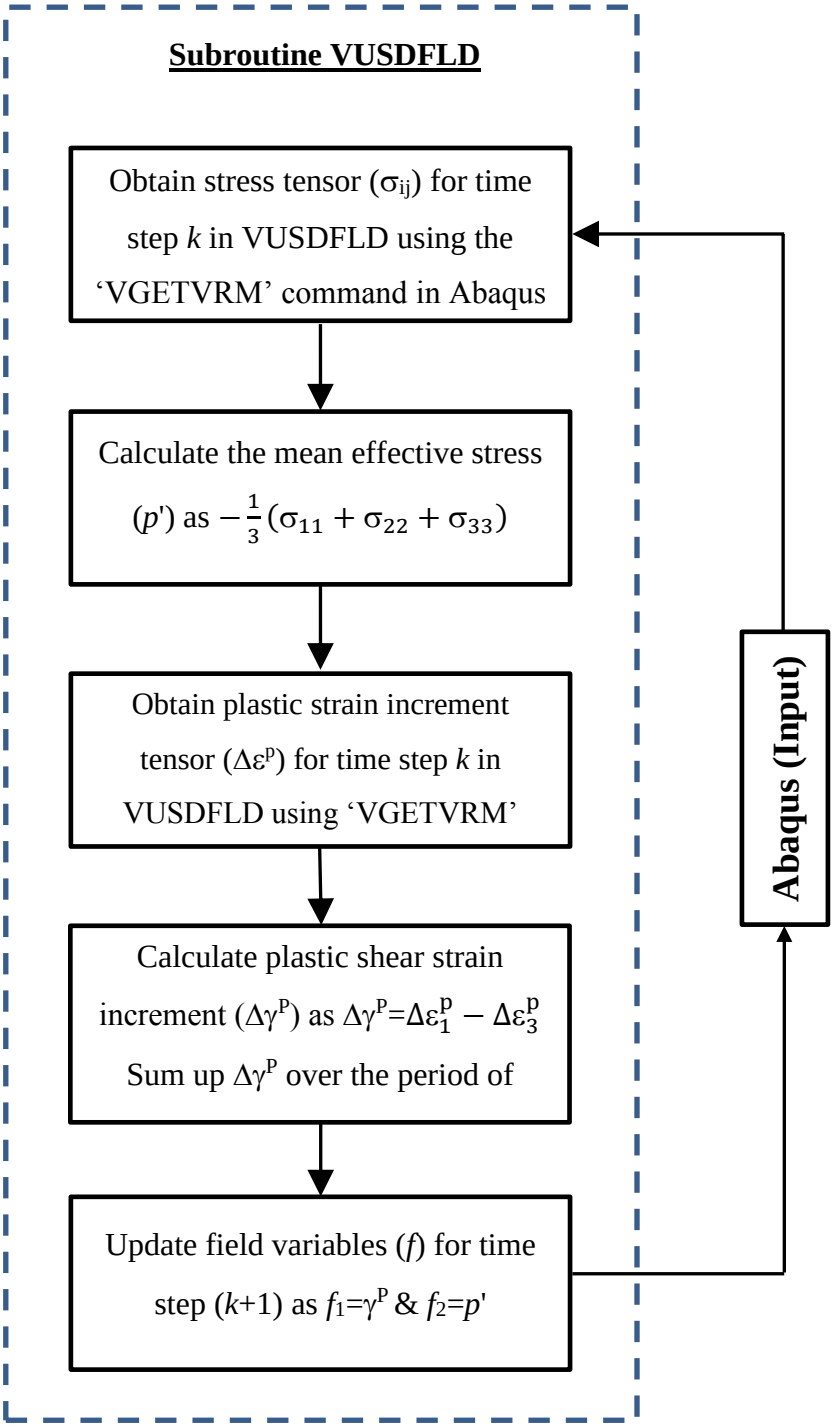

Figure G-4. VUSDFLD subroutine flowchart for updating field variables